Micro- and Nano- Fabrication and Replication Techniques

Why do we have to write thing small and replicate fast ?

Plenty of Room at the Bottom

Richard P. Feynman, December 1959

How do we *write* it? We have no standard technique to do this now. But let me argue that it is not as difficult as it first appears to be. We can reverse the lenses of the electron microscope in order to demagnify as well as magnify. A source of ions, sent through the microscope lenses in reverse, could be focused to a very small spot. We could write with that spot like we write in a TV cathode ray oscilloscope, by going across in lines, and having an adjustment which determines the amount of material which is going to be deposited as we scan in lines. **This method might be very slow** because of space charge limitations. There will be more rapid methods. We could first make, perhaps by some **photo process**, a screen which has holes in it in the form of the letters. Then we would strike an arc behind the holes and draw metallic ions through the holes; then we could again use our system of lenses and make a small image in the form of ions, which would deposit the metal on the pin.

Plenty of Room at the Bottom

Richard P. Feynman, December 1959

A simpler way might be this (though I am not sure it would work): We take light and, through an optical microscope running backwards, we focus it onto a very small photoelectric screen. Then electrons come away from the screen where the light is shining. These electrons are focused down in size by the electron microscope lenses to impinge directly upon the surface of the metal. Will such a beam etch away the metal if it is run long enough? I don't know. If it doesn't work for a metal surface, it must be possible to find some surface with which to coat the original pin so that, where the electrons bombard, a change is made which we could recognize later.

Plenty of Room at the Bottom

Richard P. Feynman, December 1959

There is no intensity problem in these devices---not what you are used to in magnification, where you have to take a few electrons and spread them over a bigger and bigger screen; it is just the opposite. The light which we get from a page is concentrated onto a very small area so it is very intense. The few electrons which come from the photoelectric screen are demagnified down to a very tiny area so that, again, they are very intense. **I don't know why this hasn't been done yet!**

Fabrication of Nanomaterials

- Top-down
  - Begin with bulk materials that are reduced into nanoparticles
- Bottom-up
  - Begin with atoms and molecules that can grown into zero, one, two an three-dimensional nanostructures
- Hybrid

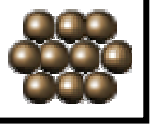

Top-down

- Mechanical energy
  - Ball milling, polishing, grinding
- Thermal
  - Annealing, evaporation, pyrolysis
- High energy
  - Arch, laser, ion milling, reactive ion etching
- Chemical
  - Chemical etching, CMP, electropolishing, anodizing
- Lithographic
  - Photo, e-beam, EUV, X-ray, μ-cp, NIL, Nanosphere
- Nature
  - Erosion, decomposition, digestion

Bottom-up

- Gas
  - Chemical vapor deposition, atomic layer deposition, MOCVD, MBE, ion implantation
- Liquid
  - Self-assembly, supermolecule, reduction, template synthesis
- Lithographic
  - Dip-pen, block co-polymer, STM writing
- Biological
  - Protein, nuclear acid, crystal formation

Ancient Patterning

"This is the Elks' land". A greeting at the mouth of Dalbergsaa, Southern Dal.

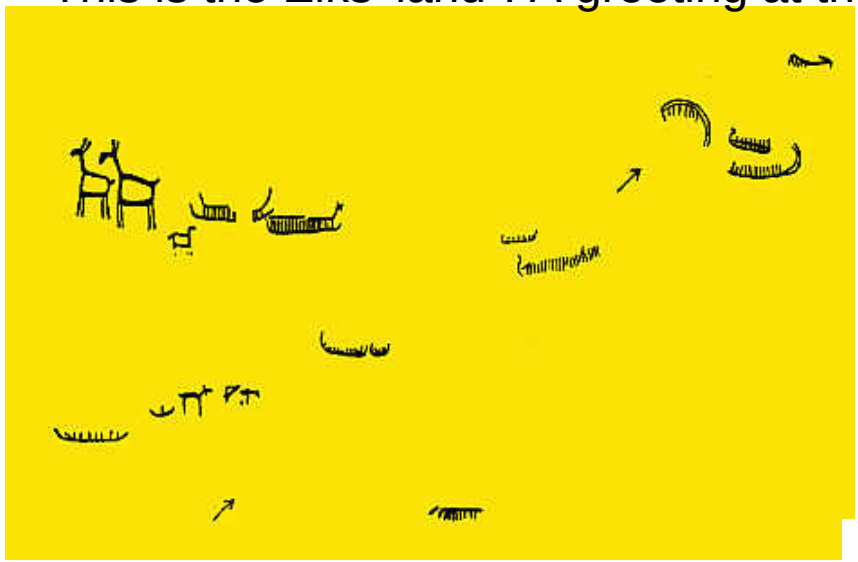

It seems that the carvings of Northern Scandinavia's including Kola Peninsula are the oldest.
Large figures of ritual animals characterise the Mesolithic period mostly before c.4200 BC

Writing by Inks

Writing Brush ~2000 Ys

Quill Pen ~1000 Ys

Chinese Replication

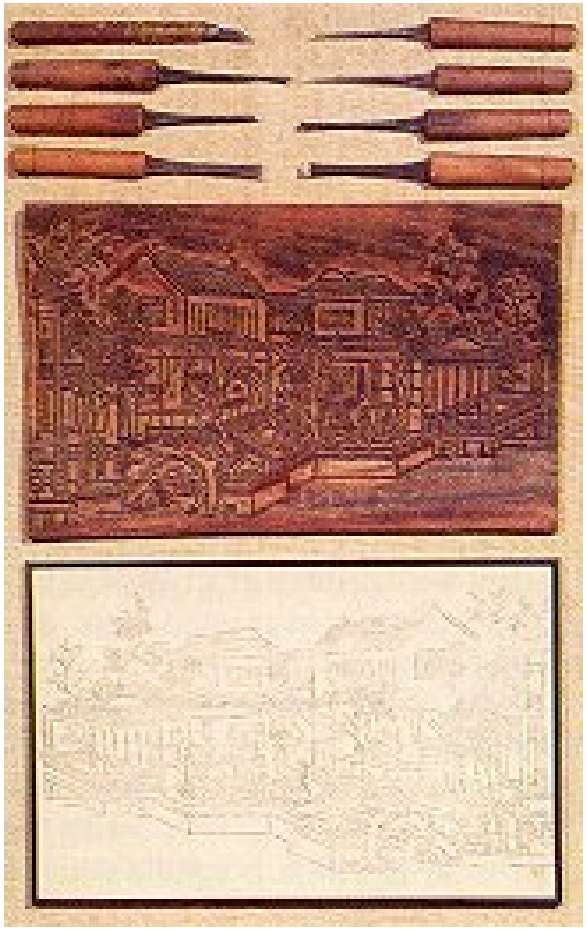

868

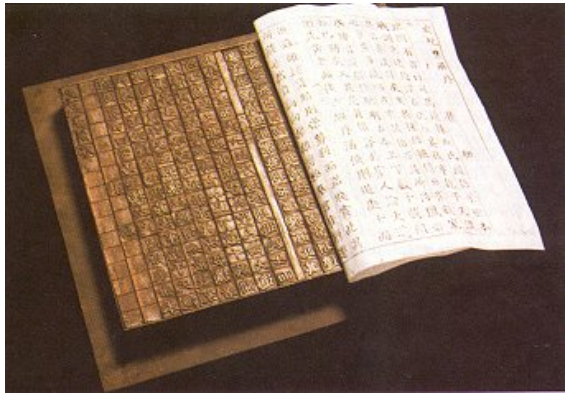

1041 and 1048

Western Replication

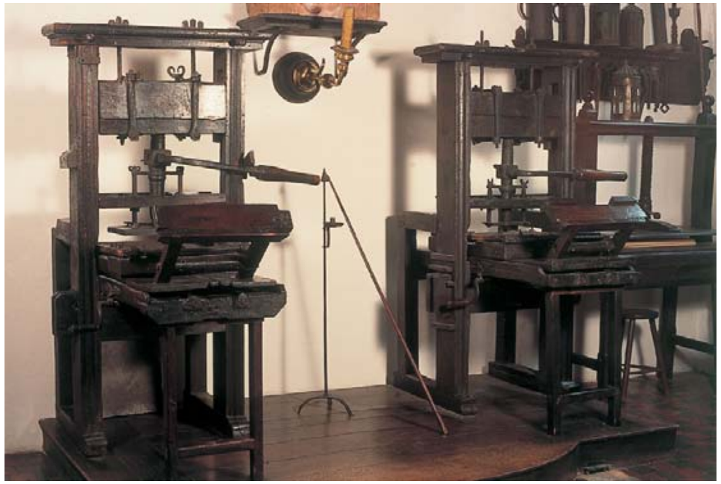

1543 - 1610

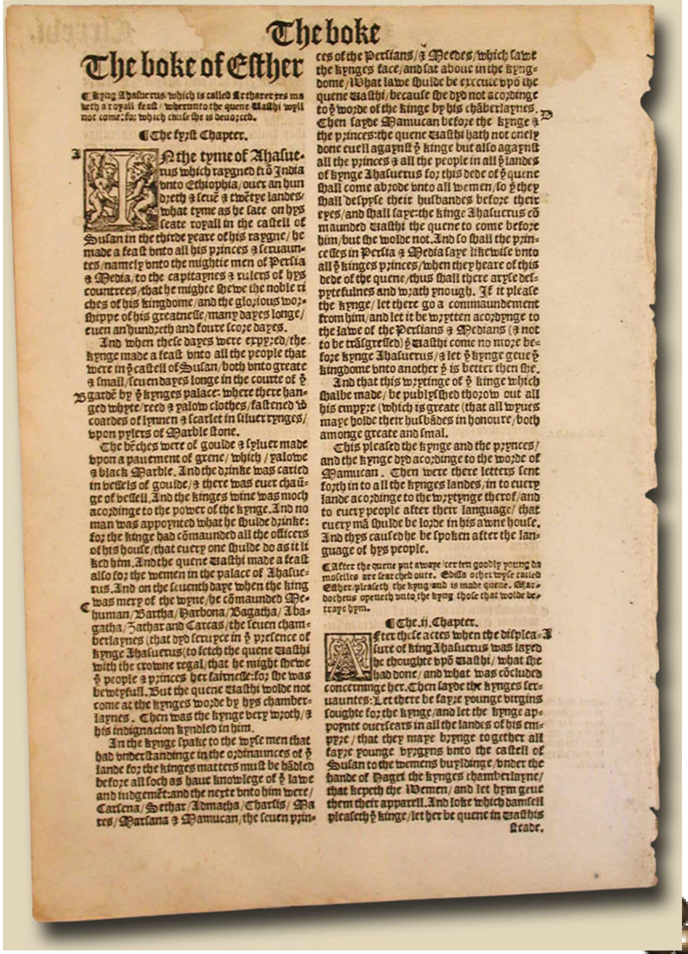

The boke

The boke of Esther

Kyng Ahasuerus which is called Artharerres maketh a royall feast / wherunto the quene Vasthi wyll not come: for which cause she is devorced.

The fyrst Chapter.

A In the tyme of Ahasuerus which raygned frō India unto Ethiopia / over an hundreth & seuē & twētye landes / what tyme as he sate on hys seate royall in the castell of Susan in the thirde yeare of his raygne / he made a feast unto all his princes & seruauntes / namely unto the mightie men of Persia & Media / to the capitaynes & rulers of hys countrees / that he mighte shewe the noble riches of his kingdome / and the glorious worshippe of his greatnesse / many dayes longe / euen an hundreth and foure score dayes.

And when these dayes were expyred / the kynge made a feast unto all the people that were in ẏ castell of Susan / both unto greate & small / seuen dayes longe in the courte of ẏ

B gardē by ẏ kynges palace: where there hanged whyte / reed & yalow clothes / fastened wᵗ coardes of lynnen & scarlet in siluer rynges / upon pylers of Marble stone.

The bēches were of goulde & syluer made upon a pauement of grene / which / yalowe & black Marble. And the drinke was caried in vessels of goulde / & there was euer chaūge of vessell. And the kinges wine was moch acordinge to the power of the kynge. And no man was appoynted what he shulde drinke: for the kinge had cōmaunded all the officers of his house / that euery one shulde do as it liked him. And the quene Vasthi made a feast also for the wemen in the palace of Ahasuerus. And on the seuenth daye when the king

C was mery of the wyne / he cōmaunded Mehuman / Bartha / Harbona / Bagatha / Abagatha / Zathar and Carcas / the seuen chamberlaynes (that dyd seruyce in ẏ presence of kynge Ahasuerus) to fetch the quene Vasthi with the crowne regal / that he might shewe ẏ people & princes her fairnesse: for she was bewtyfull. But the quene Vasthi wolde not come at the kynges worde by hys chamberlaynes. Then was the kynge very wroth / & his indignacion kyndled in him.

And the kynge spake to the wyse men that had understandinge in the ordinaunces of ẏ lande for the kinges matters must be hādled before all soch as haue knowlege of ẏ lawe and iudgemēt: and the nexte unto him were / Carsena / Sethar / Admatha / Tharsis / Mares / Marsana & Mamucan / the seuen princes of the Persians / & Medes / which sawe the kynges face / and sat aboue in the kyngdome / What lawe shulde be executte upō the quene Vasthi / because she dyd not acordinge to ẏ worde of the kinge by his chāberlaynes.

D Then sayde Mamucan before the kynge & the princes: the quene Vasthi hath not onely done euell agaynst ẏ kinge but also agaynst all the princes & all the people in all ẏ landes of kynge Ahasuerus for this dede of ẏ quene shall come abrode unto all wemen / so ẏ they shall despyse their husbandes before their eyes / and shall saye: the kinge Ahasuerus cōmaunded Vasthi the quene to come before him / but she wolde not. And so shall the princesses in Persia & Media saye likewise unto all ẏ kinges princes / when they heare of this dede of the quene / thus shall there aryse despytefulnes and wrath ynough. If it please the kynge / let there go a commaundement from him / and let it be wrytten acordynge to the lawe of the Persians & Medians (& not to be trāsgressed) ẏ Vasthi come no more before kynge Ahasuerus / & let ẏ kynge geue ẏ kingdome unto another ẏ is better then she.

And that this wrytinge of ẏ kinge which shalbe made / be publyshed thorow out all his empyre (which is greate (that all wyues maye holde their husbādes in honoure / both amonge greate and smal.

This pleased the kynge and the prynces / and the kynge dyd acordinge to the worde of Mamucan. Then were there letters sent forth in to all the kynges landes / in to euery lande acordinge to the wrytynge therof / and to euery people after their language / that euery mā shulde be lorde in his awne house. And thys caused he be spoken after the language of hys people.

After the quene put awaye / certen goodly young damoselles are searched oute. Edissa other wyse called Esther / pleaseth the kyng / and is made quene. Mardocheus openeth unto the kyng those that wolde betraye hym.

The .ij. Chapter.

A After these actes when the displeasure of king Ahasuerus was layed he thoughte upō Vasthi / what she had done / and what was cōcluded concernynge her. Then sayde the kynges seruauntes: Let there be fayre younge virgins soughte for the kynge / and let the kynge appoynte ouersears in all the landes of his empyre / that they maye brynge together all fayre younge virgyns unto the castell of Susan to the wemens buyldinge / under the hande of Hagei the kynges chamberlayne / that kepeth the Wemen / and let hym geue them their apparell. And loke which damsell pleaseth ẏ kinge / let her be quene in Vasthis steade.

Building a computer

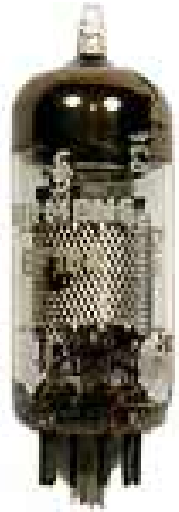

First Integrated Circuit

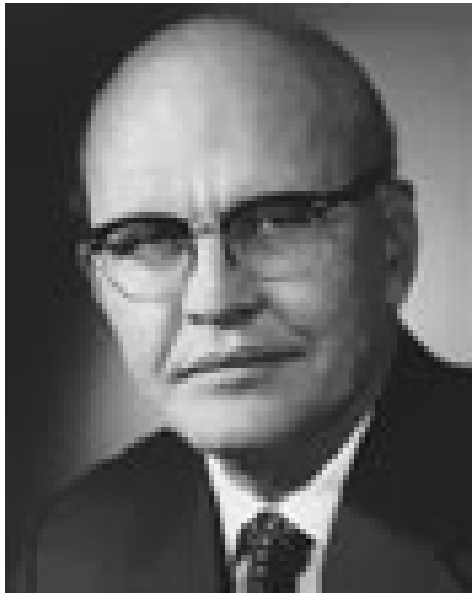

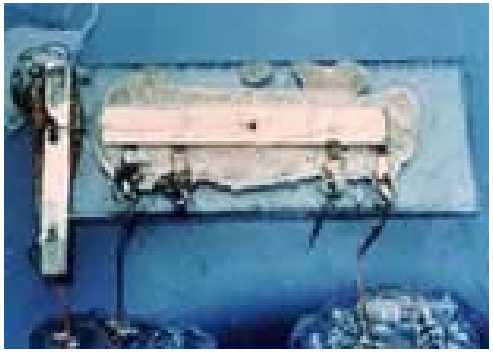

"What we didn't realize then was that the integrated circuit would reduce the cost of electronic functions by a factor of a million to one, nothing had ever done that for anything before" - Jack Kilby 2000 Nobel Prize

1958 Texas Instruments

metal-oxide-semiconductor field-effect transistor (MOSET)

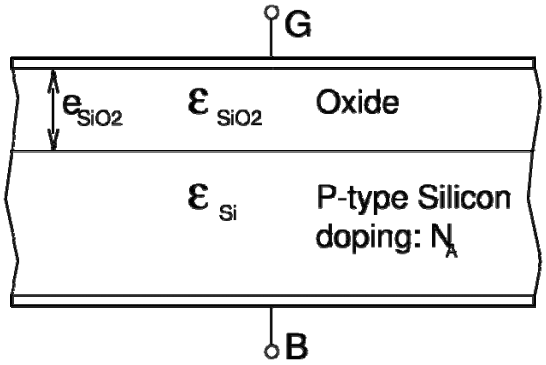

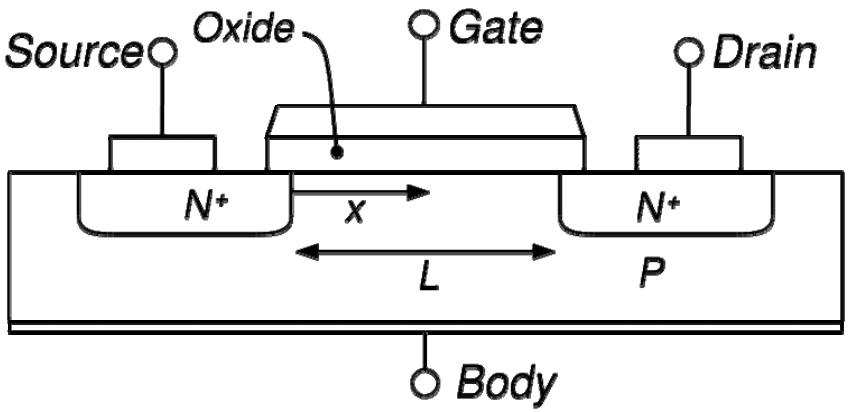

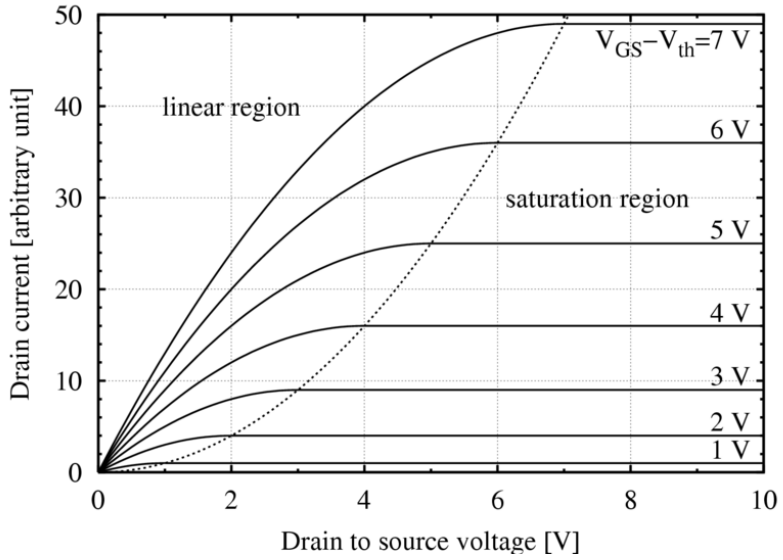

Moore's Law

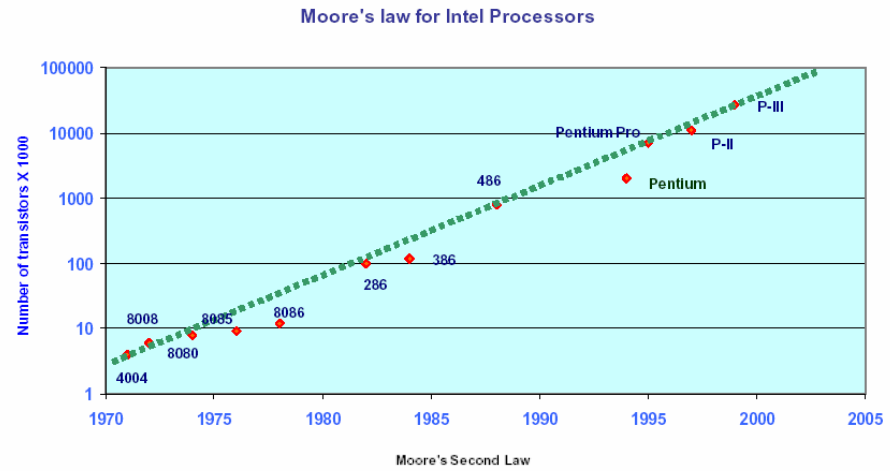

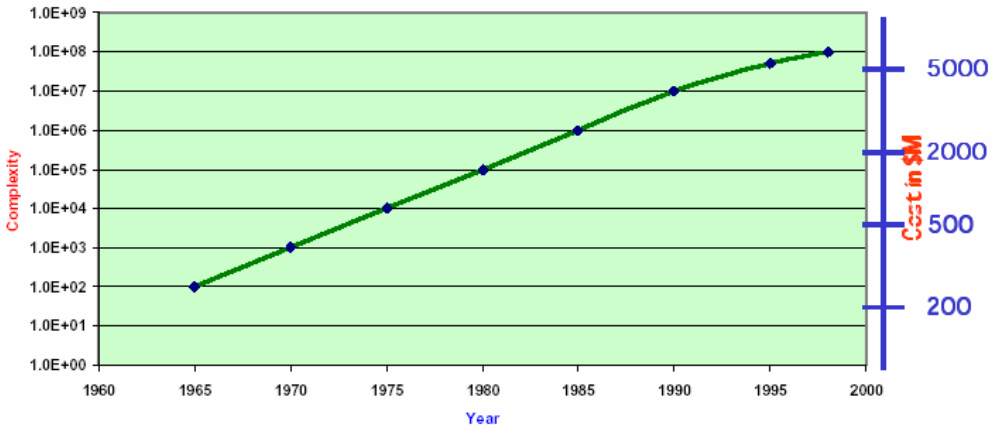

Moore's Laws

First Law: Number of components in a chip (IC) will double roughly every 18 months (1965, in *Electronics*). This has held true more or less since then.

Second Law: Facility costs increase on a semilog scale (terminology due to Eugene Meieran, Intel Fellow). Fab costs double approximately every four years.

Tool Cost

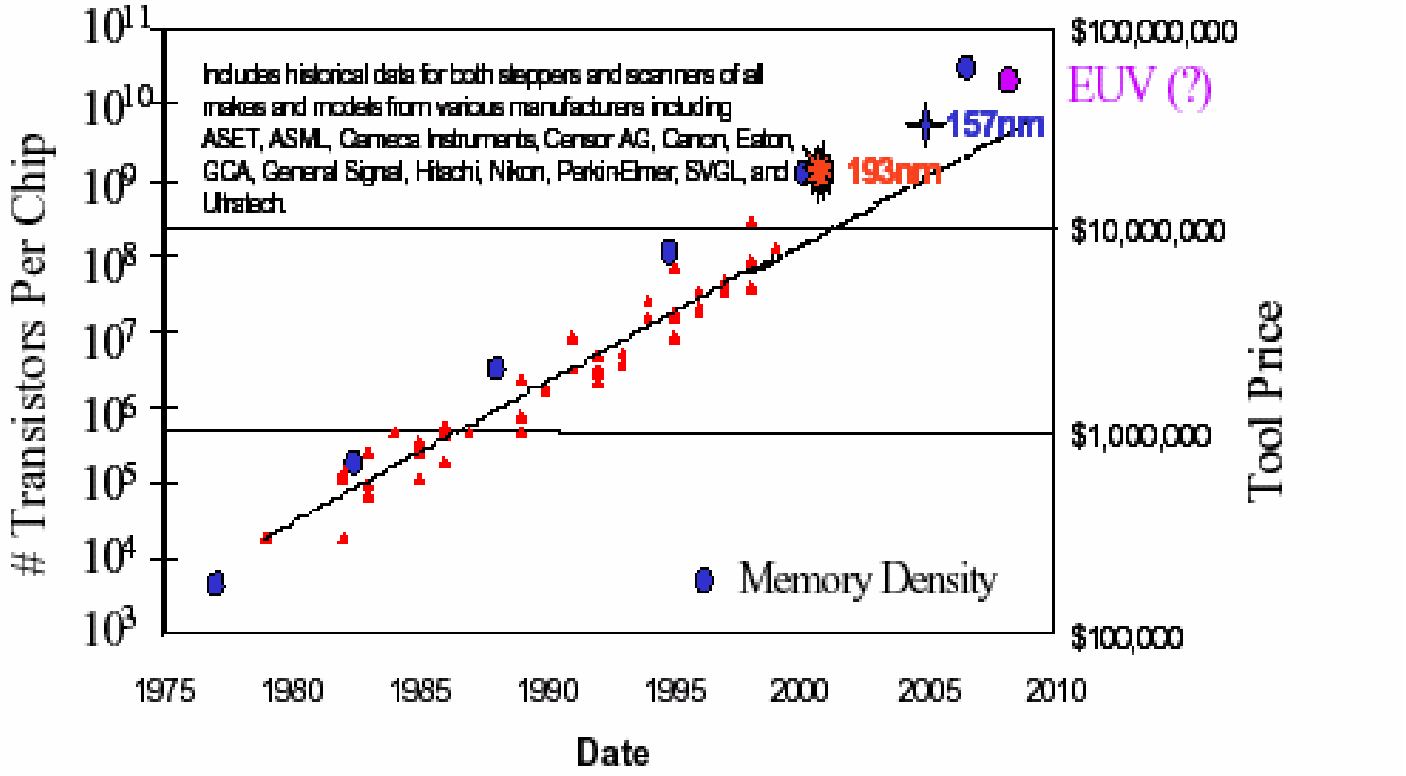
Includes historical data for both steppers and scanners of all makes and models from various manufacturers including ASET, ASML, Cameca Instruments, Censor AG, Canon, Eaton, GCA, General Signal, Hitachi, Nikon, PerkinElmer, SVGL, and Ultratech.
157nm
193nm
EUV (?)
Memory Density
Transistors Per Chip
Tool Price
Date
10^{11}
10^{10}
10^{9}
10^{8}
10^{7}
10^{6}
10^{5}
10^{4}
10^{3}
$100,000,000
$10,000,000
$1,000,000
$100,000
1975
1980
1985
1990
1995
2000
2005
2010

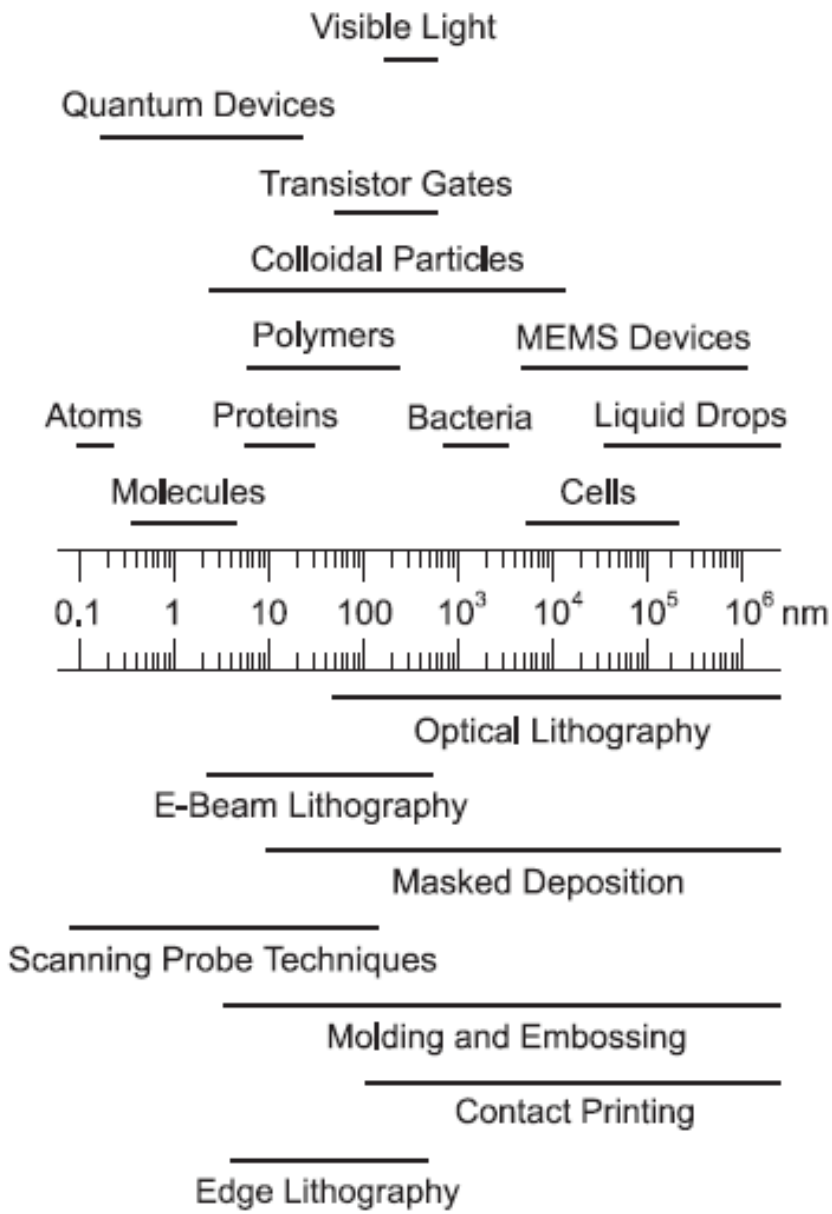
Visible Light
Quantum Devices
Transistor Gates
Colloidal Particles
Polymers
MEMS Devices
Atoms
Proteins
Bacteria
Liquid Drops
Molecules
Cells
0.1
1
10
100
10^3
10^4
10^5
10^6 nm
Optical Lithography
E-Beam Lithography
Masked Deposition
Scanning Probe Techniques
Molding and Embossing
Contact Printing
Edge Lithography

Industrial Process

- Lithography
- Deposition
- Etching
- Planization
- Packaging

Optical Microscope

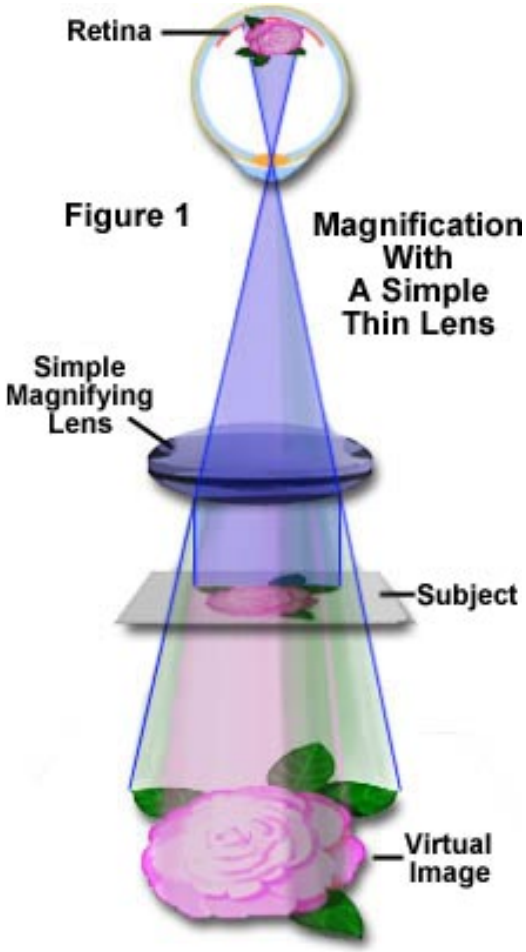

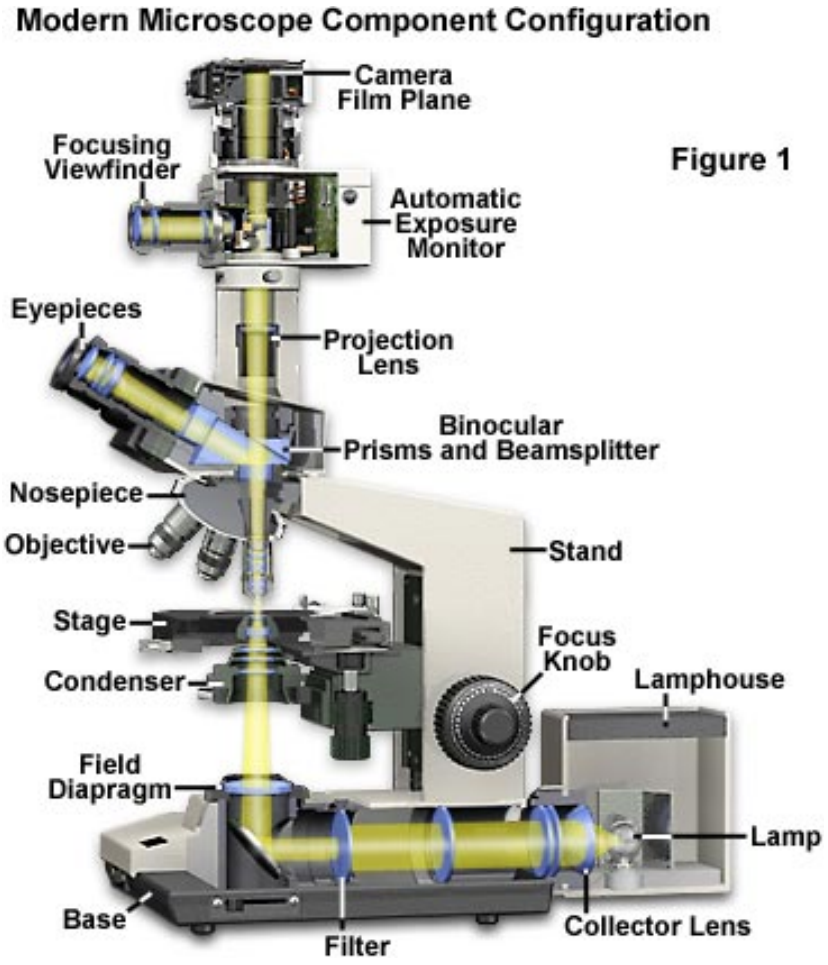

Limit of Photolithography

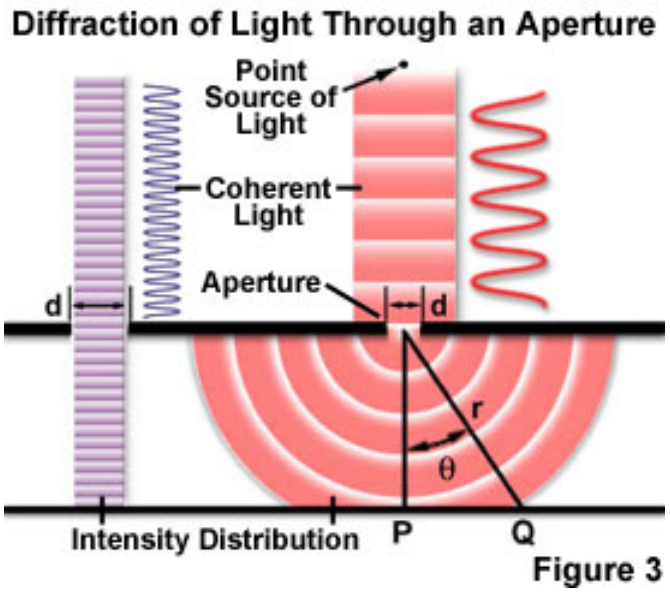

Figure 3

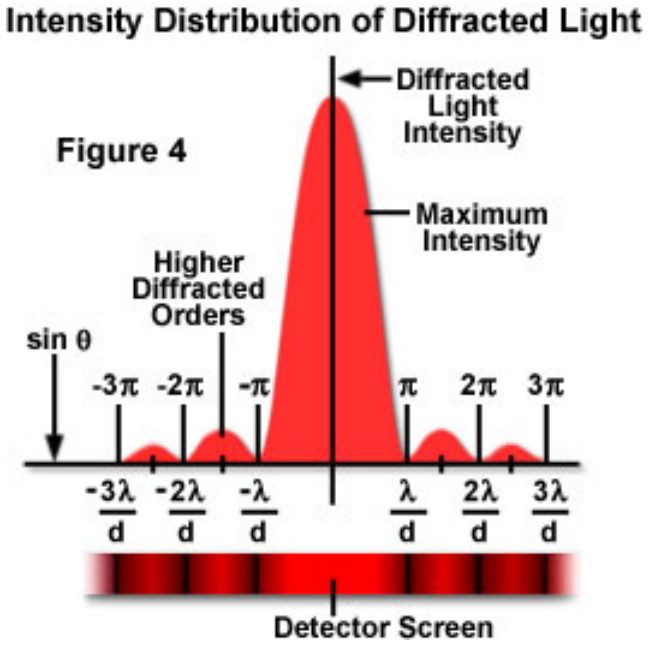

Figure 4

r = 1.22 x λ/(2 x N.A.)

N.A. = n x sin(θ)

Diffraction Limit

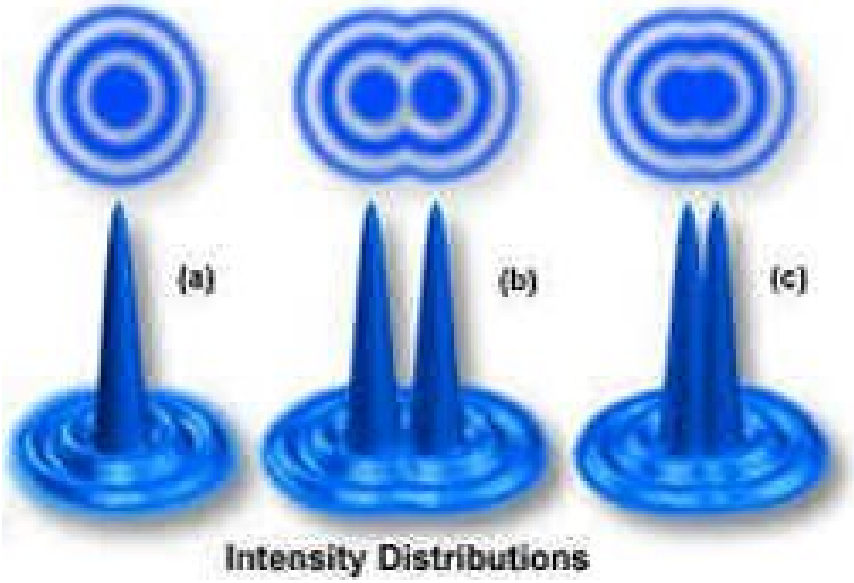

Resolution = K x λ/(N.A.)

Depth of Focus = λ/(N.A.)^2

K = 0.61

Methods of Photolithography

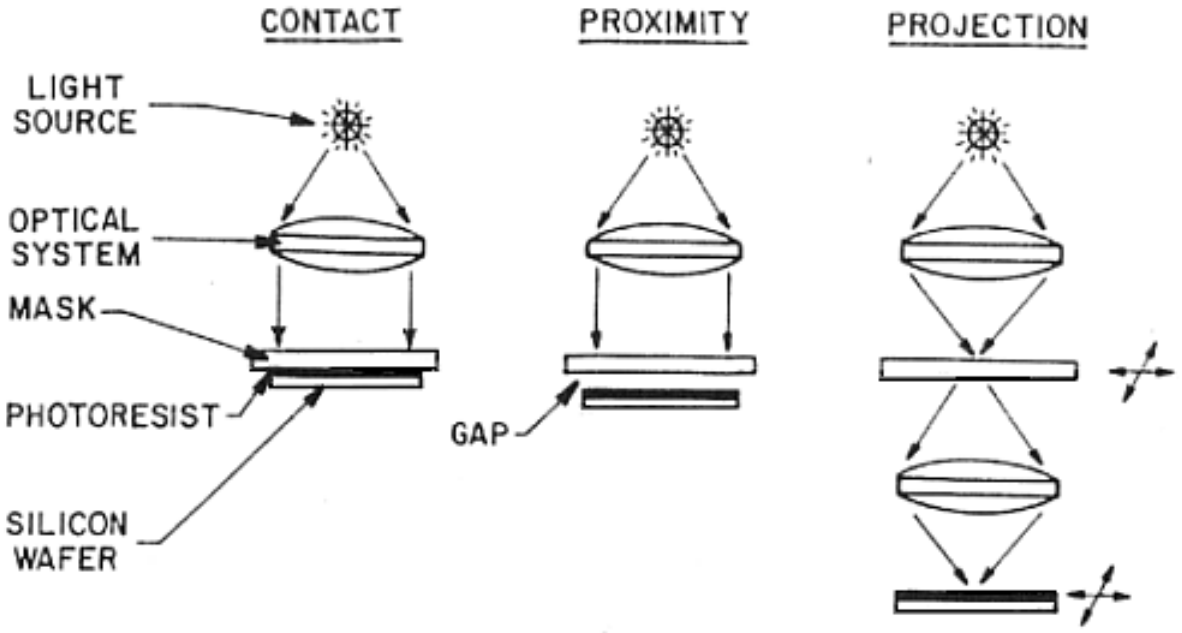

$W_{min} = k_1 \text{ sqrt}(\lambda d)$

$W_{min} = k_1 \lambda/NA$

Photolithography

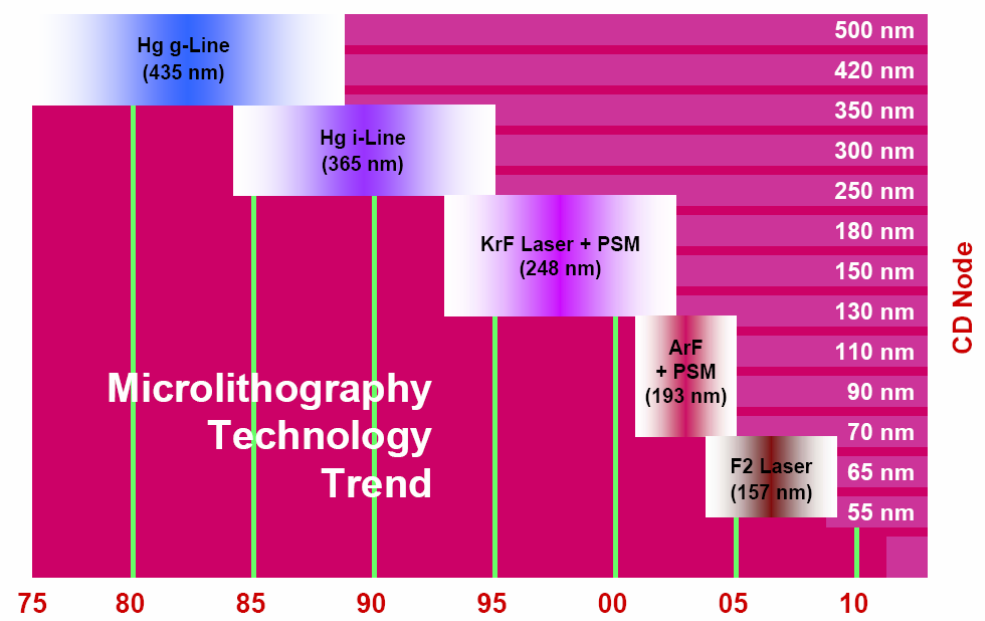

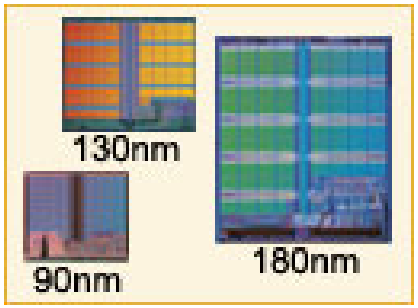

UV Wavelength (nm)	Wavelength Name	UV Emission Source
436	g-line	Mercury arc lamp
405	h-line	Mercury arc lamp
365	i-line	Mercury arc lamp
248	Deep UV (DUV)	Mercury arc lamp or Krypton Fluoride (KrF) excimer laser
193	Deep UV (DUV)	Argon Fluoride (ArF) excimer laser
157	Vacuum UV (VUV)	Fluorine (F_2) excimer laser

Year	Linewidth (nm)	Wavelength (nm)
1986	1,200	436
1988	800	436/365
1991	500	365
1994	350	365/248
1997	250	248
1999	180	248
2001	130	248
2003	90	248/193
2005 (fcst)	65	193
2007 (fcst)	45	193

Water Immersion Lithography

Year	Linewidth (nm)	Wavelength (nm)
1986	1200	436 g-line mercury lamp
1988	800	436/365
1991	500	365 i-line mercury lamp
1994	350	365/248
1997	250	248 KrF excimer laser
1999	180	248
2001	130	248
2003	90	248/193
2005	65	193 ArF excimer laser
2007	45	193/157

Resolution (R) = K x λ/(N.A.)
K = 0.25, NA ~1.4, λ = 193
R = 35 nm

Air n= 1.0003
Water n = 1.437

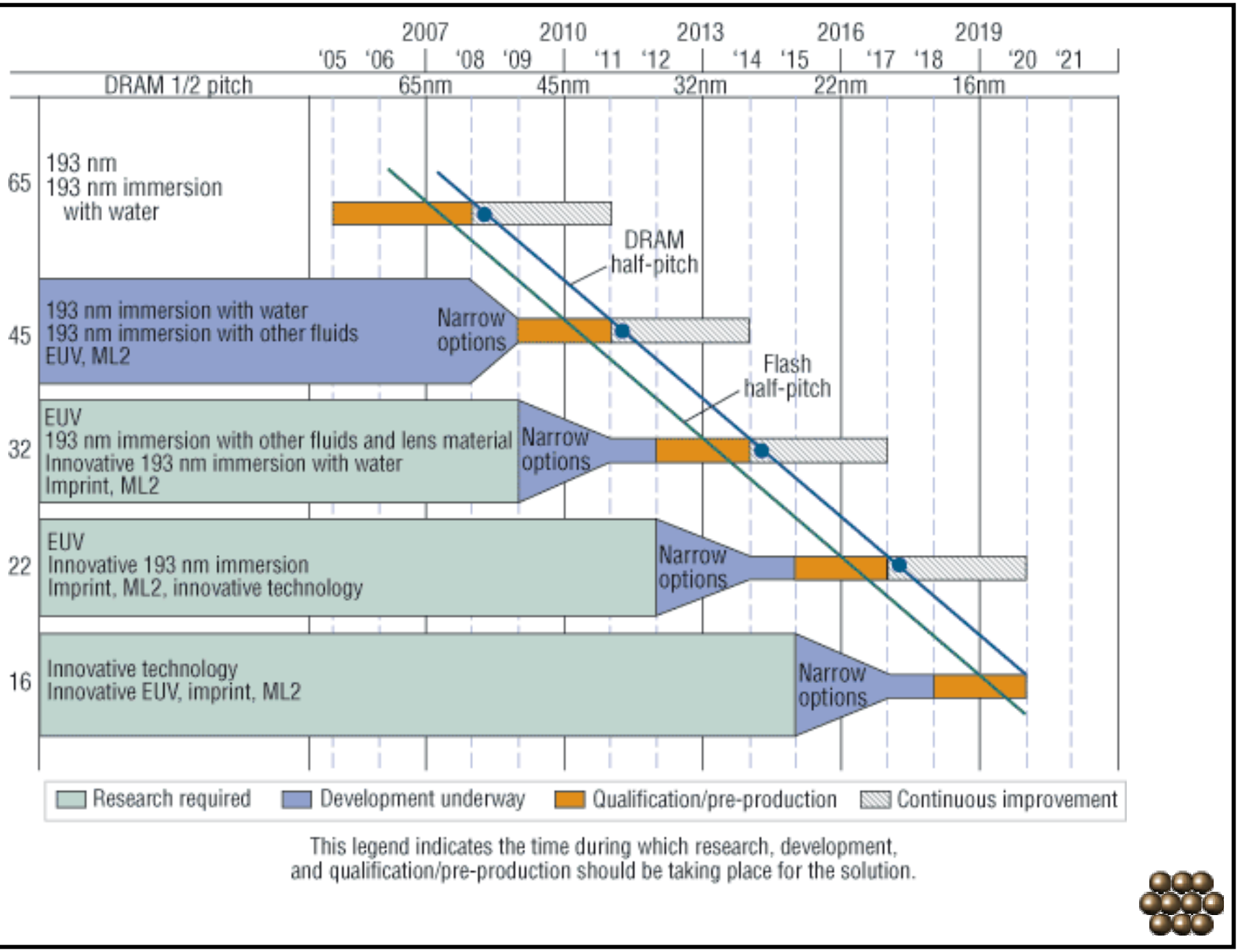

This legend indicates the time during which research, development, and qualification/pre-production should be taking place for the solution.

Photolithography Process

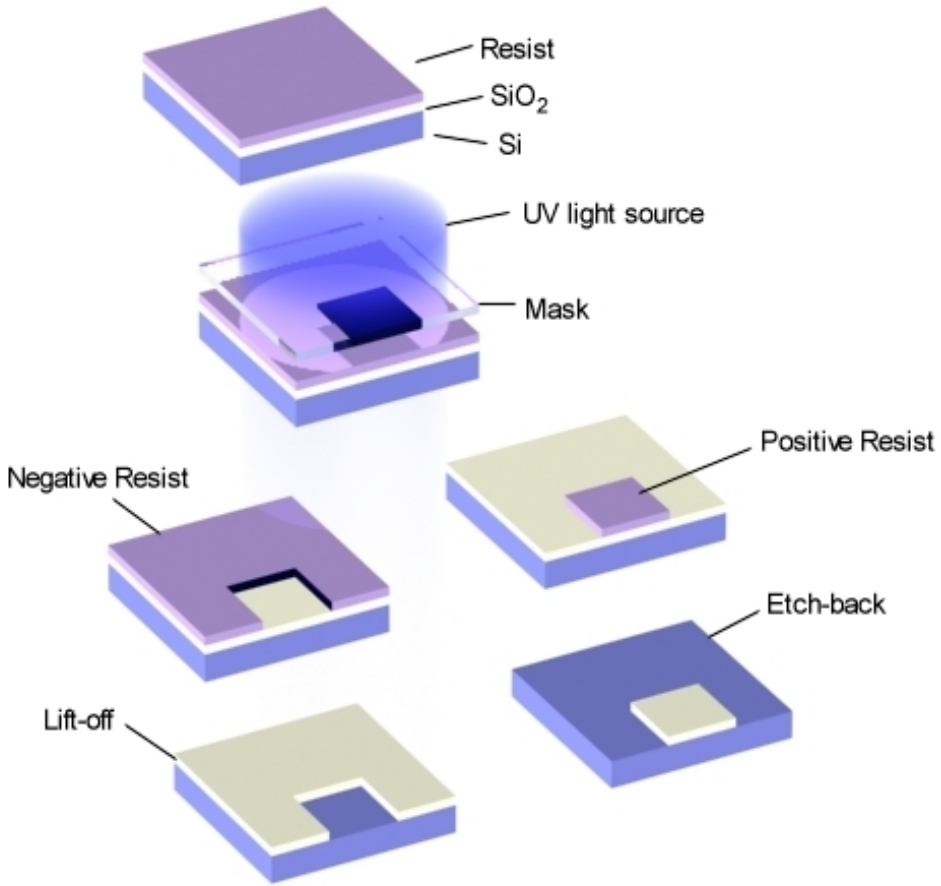

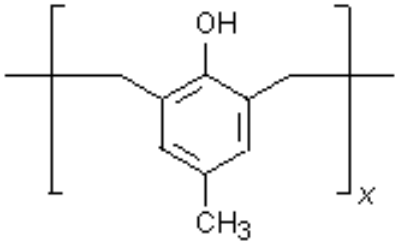

Novolak

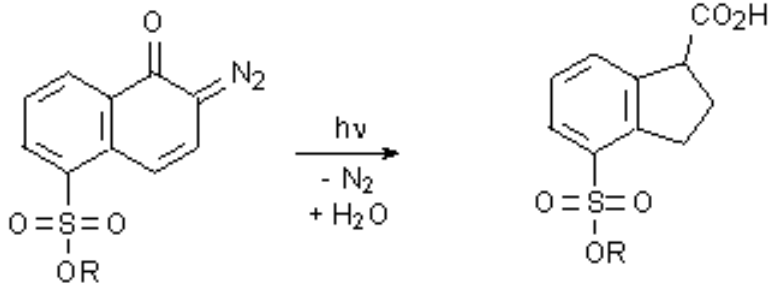

Diazonaphthaquinone additive

Positive tone

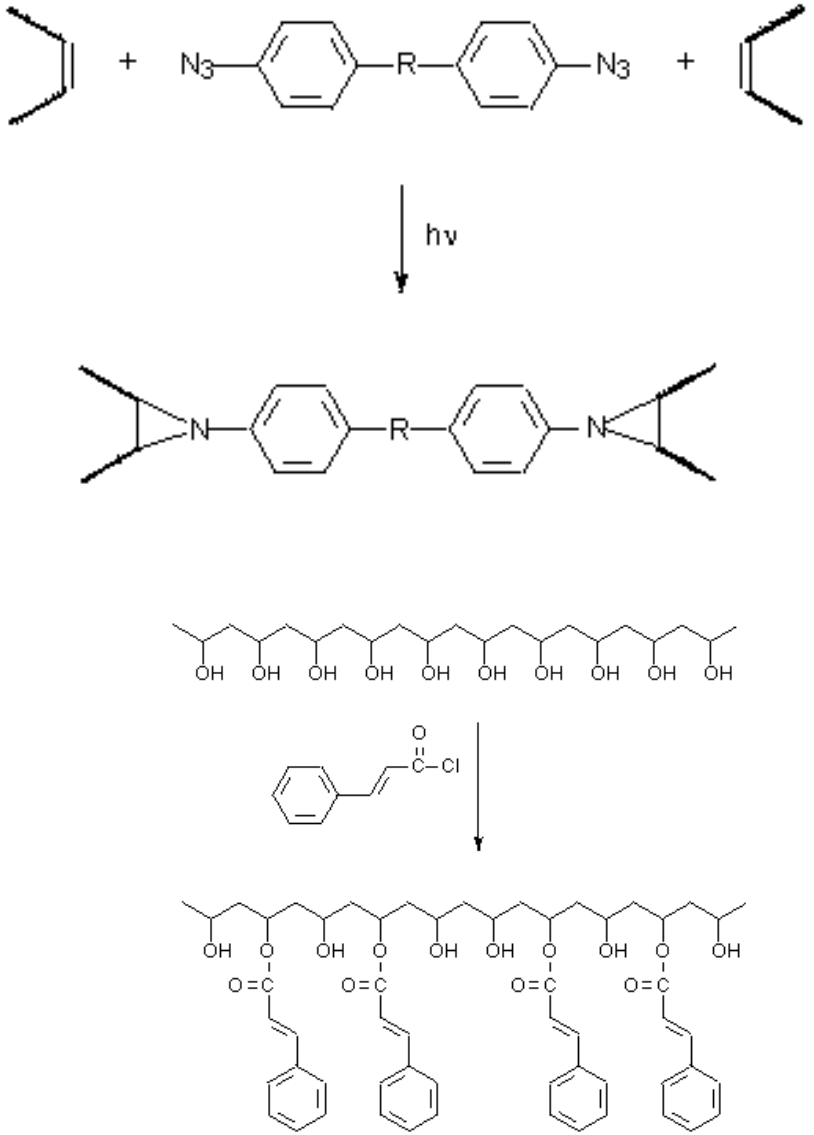

Negative tone

RCA Cleaning (By Radio Corporation of America in 1965)

Chemicals	Volume ratio	Procedure Time (min)	Operation Temperature	Function
Trichlorothane		5	Room T	Dissolve Organic
Acetone		5	Room T	Dissolve Organic
DI Water		5	Room T	Washing
H_2SO_4 (98%)-H_2O_2 (30%) (Piranha Solution)	3:1	10-20	～90℃	Oxide and Dissolve Organic and Metals
DI Water		5	Room T	Washing
HF(49 wt %)-H_2O	～2:100	10-20	Room T	Dissolve surface $Si0_2$
NH_4OH(29%)-H_2O_2(30%)-H_2O	1:1:5	10-20	～90℃	Oxide and Dissolve Metals
DI Water		5	Room T	Washing
HCl(37%)- H_2O_2(30%)-H_2O	1:1:5	10-20	～90℃	Oxide and Dissolve Metals
DI Water		5	Room T	Washing
Spin Dry (In lad – N_2 blow)				

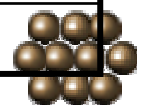

Spin Coating Photoresist on Wafer

1

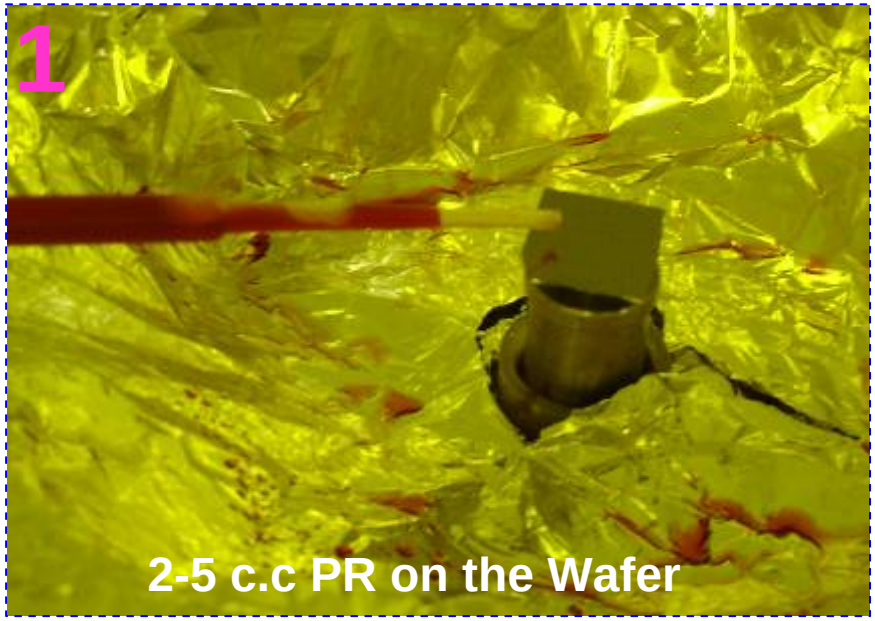

2-5 c.c PR on the Wafer

2

Wait for 5 to 15 second

3

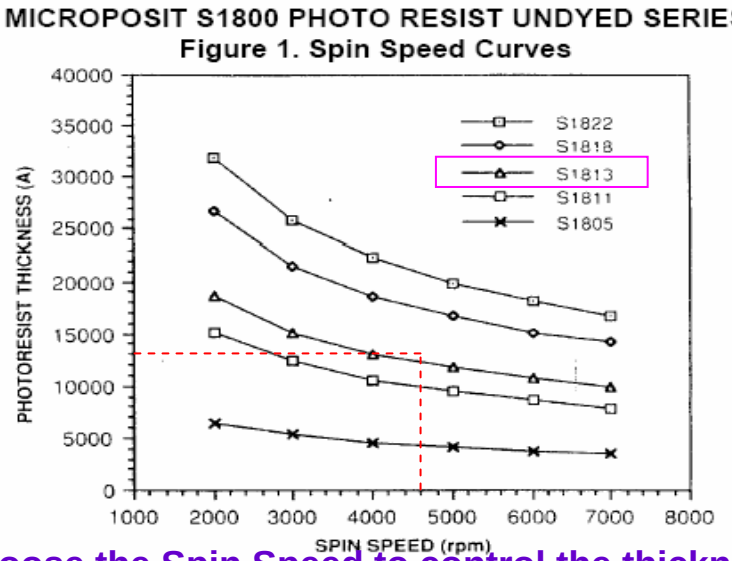

Choose the Spin Speed to control the thickness

- Photo resist：Shipley **1813**
- **Spin： 2000 rpm 5 s**
  4500 rpm 15 s
- Soft Bake：110℃ 60 s
- Exposure：7 s
- Developed：MF319 for 15 s

Standard Mask Size: 5” x 5”

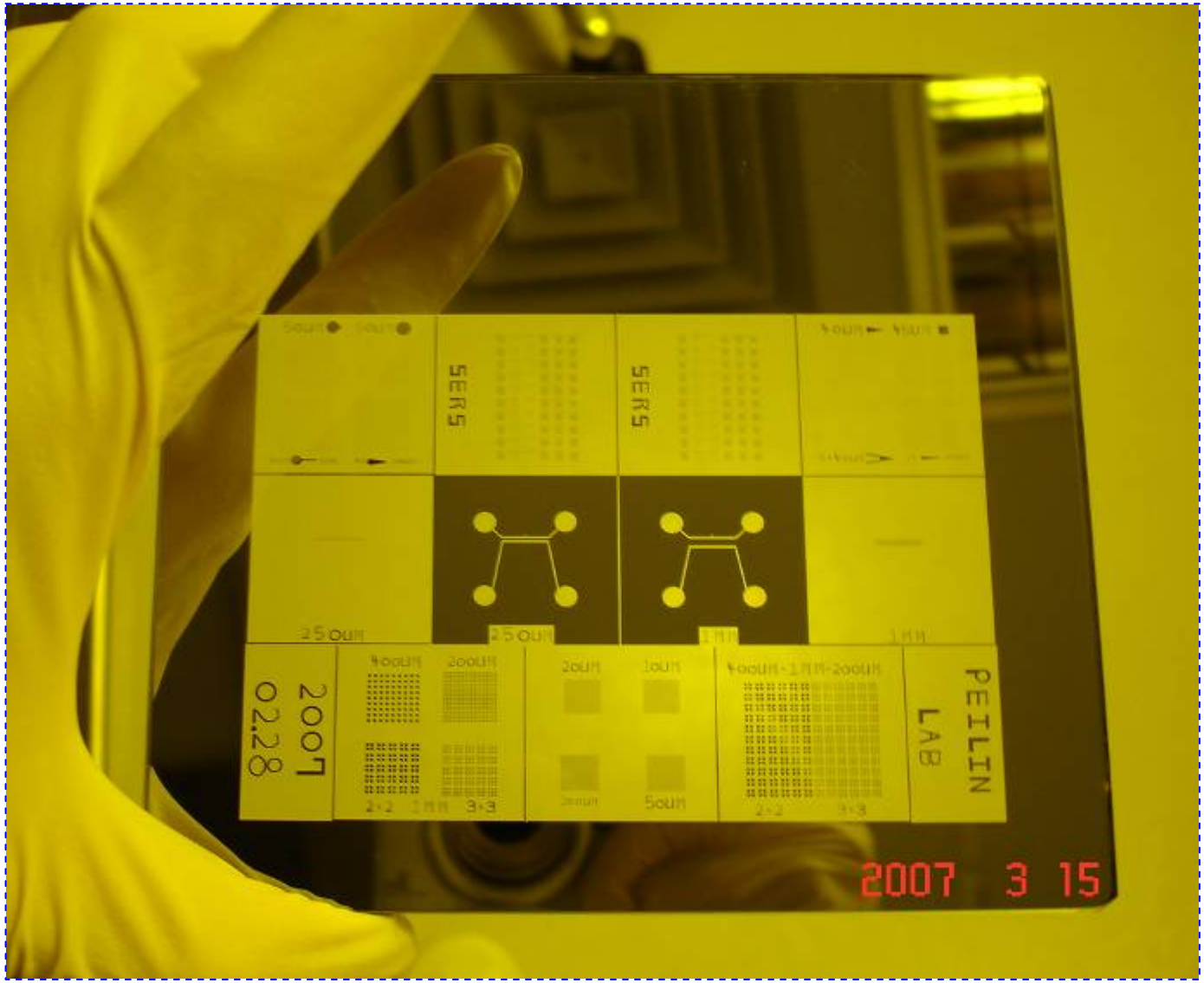

Align the pattern and Exposure

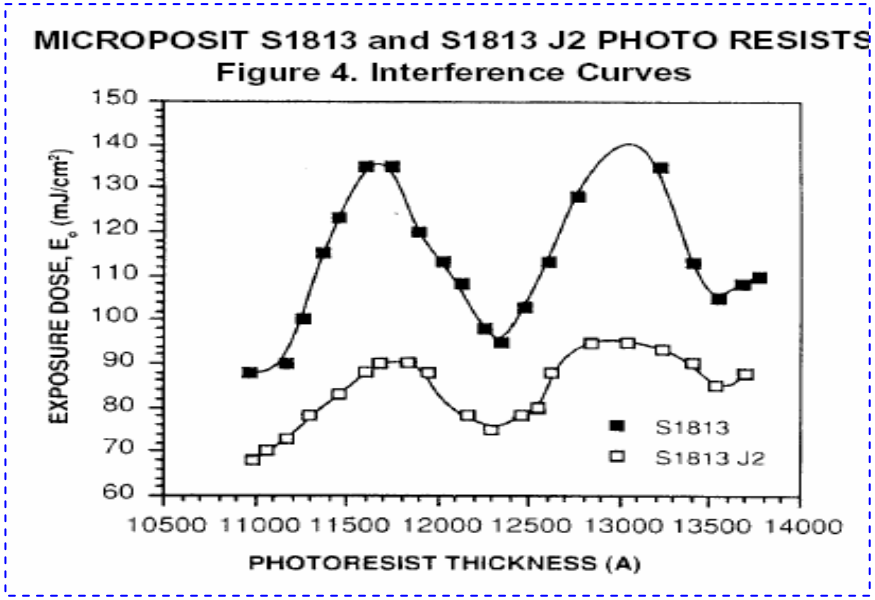

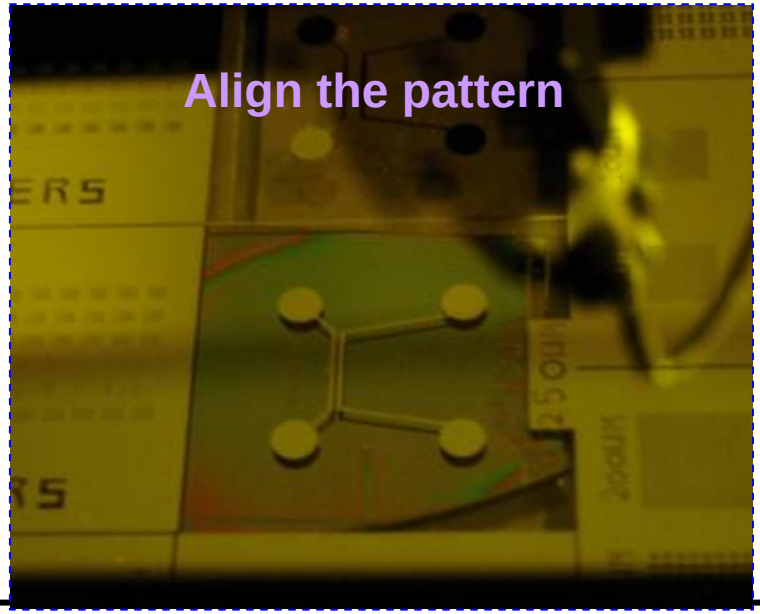

Some Photoresist Need PEB (post exposure Bake)

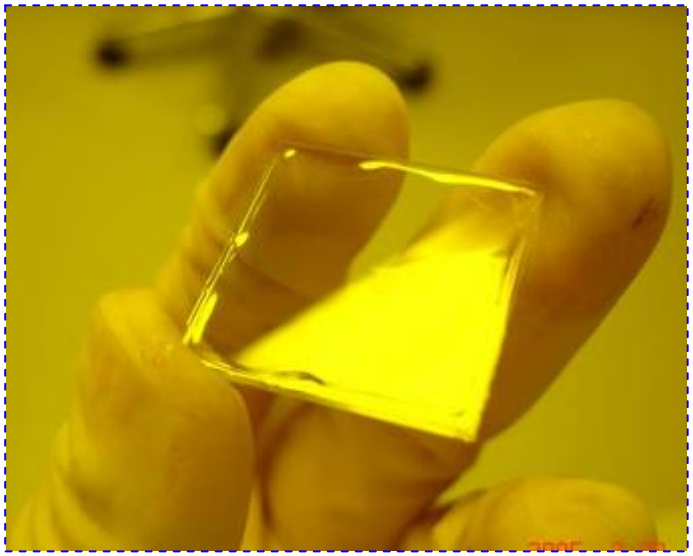

SU-8 2015

65 ℃, 60 s

95 ℃, 60 s

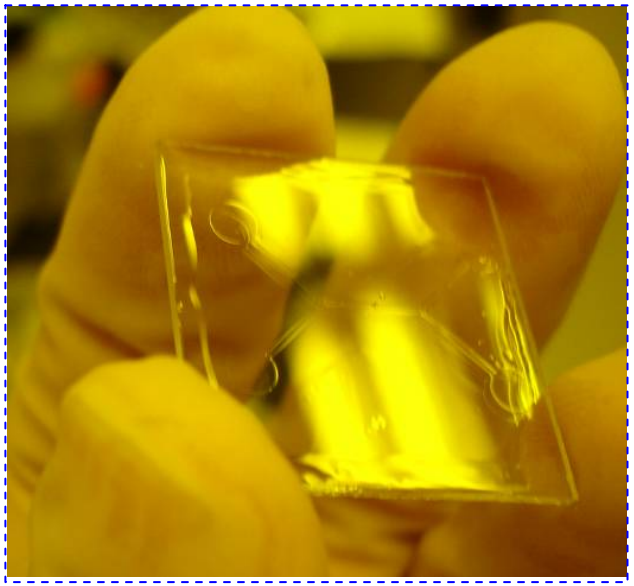

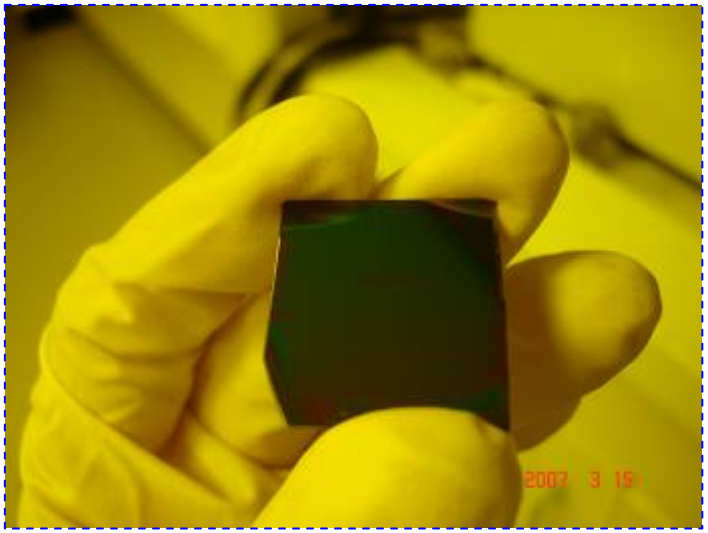

SPR 510A

90 ℃, 90 s

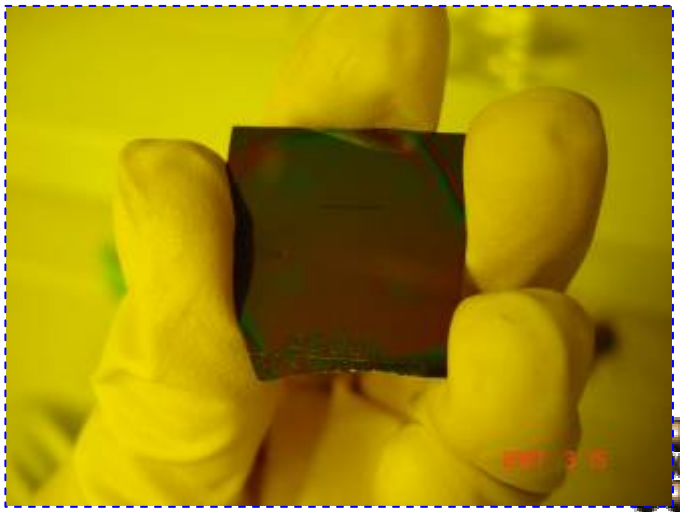

Develop the Photoresist

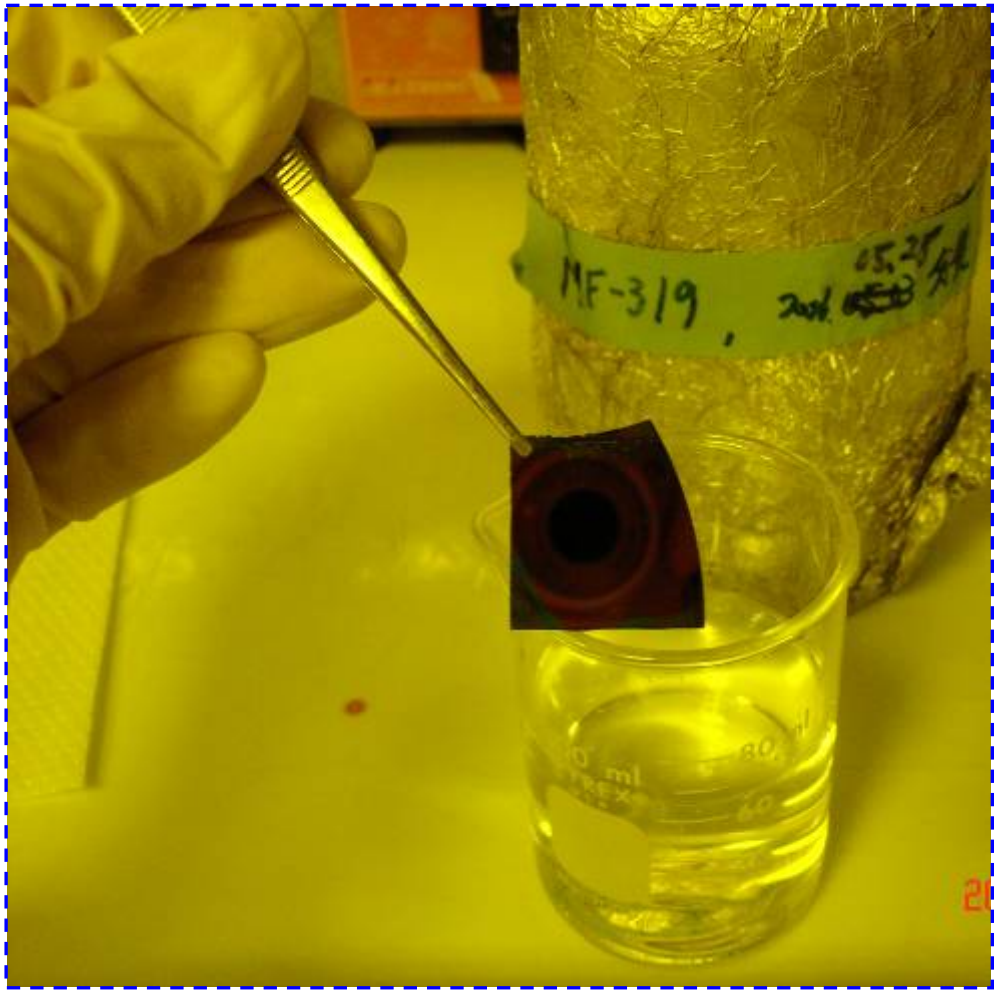

- Photo resist：Shipley **1813**
- Spin： 2000 rpm 5 s
  4500 rpm 15 s
- Soft Bake：110℃ 60 s
- Exposure：7 s
- **Developed：MF319 for 15 s**

黃光室的黃光是很重要的

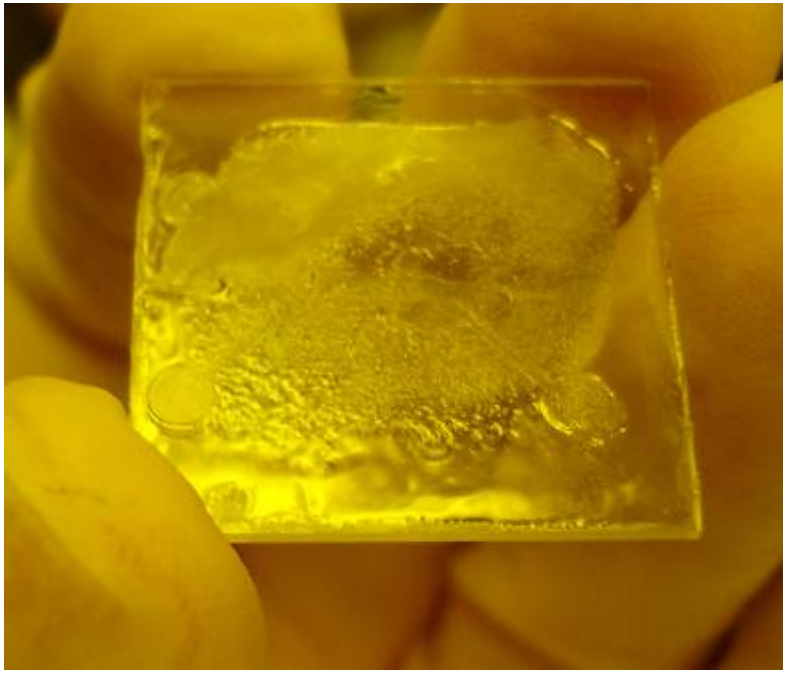

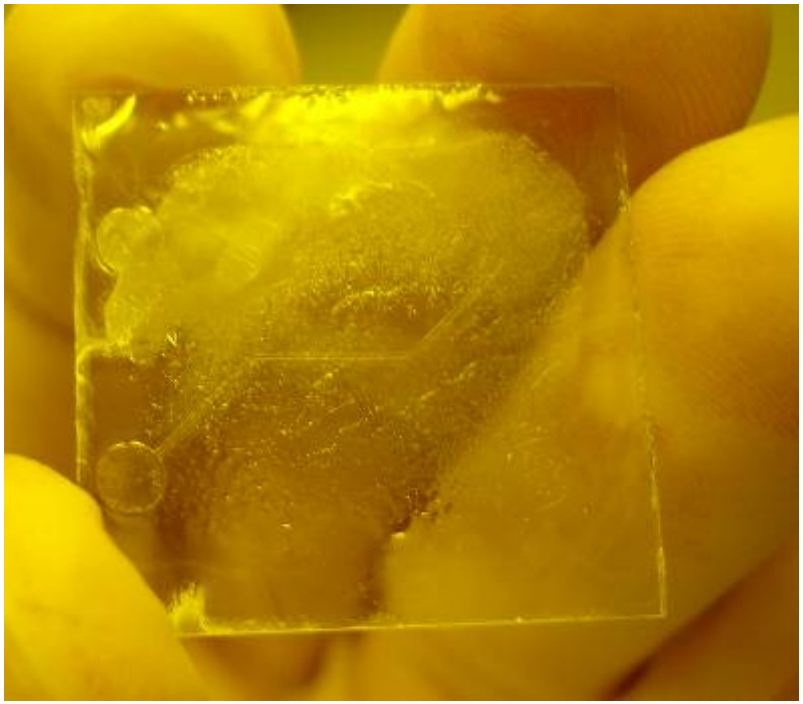

Lift OFF PROCESS BY ACETONE

Thermal Evaporator

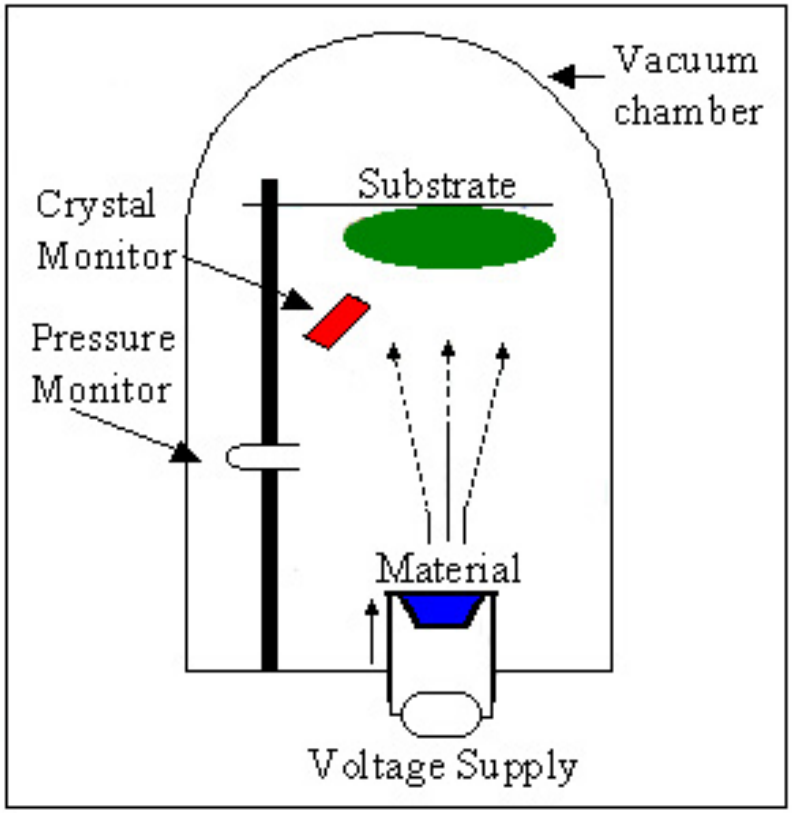

Sputter

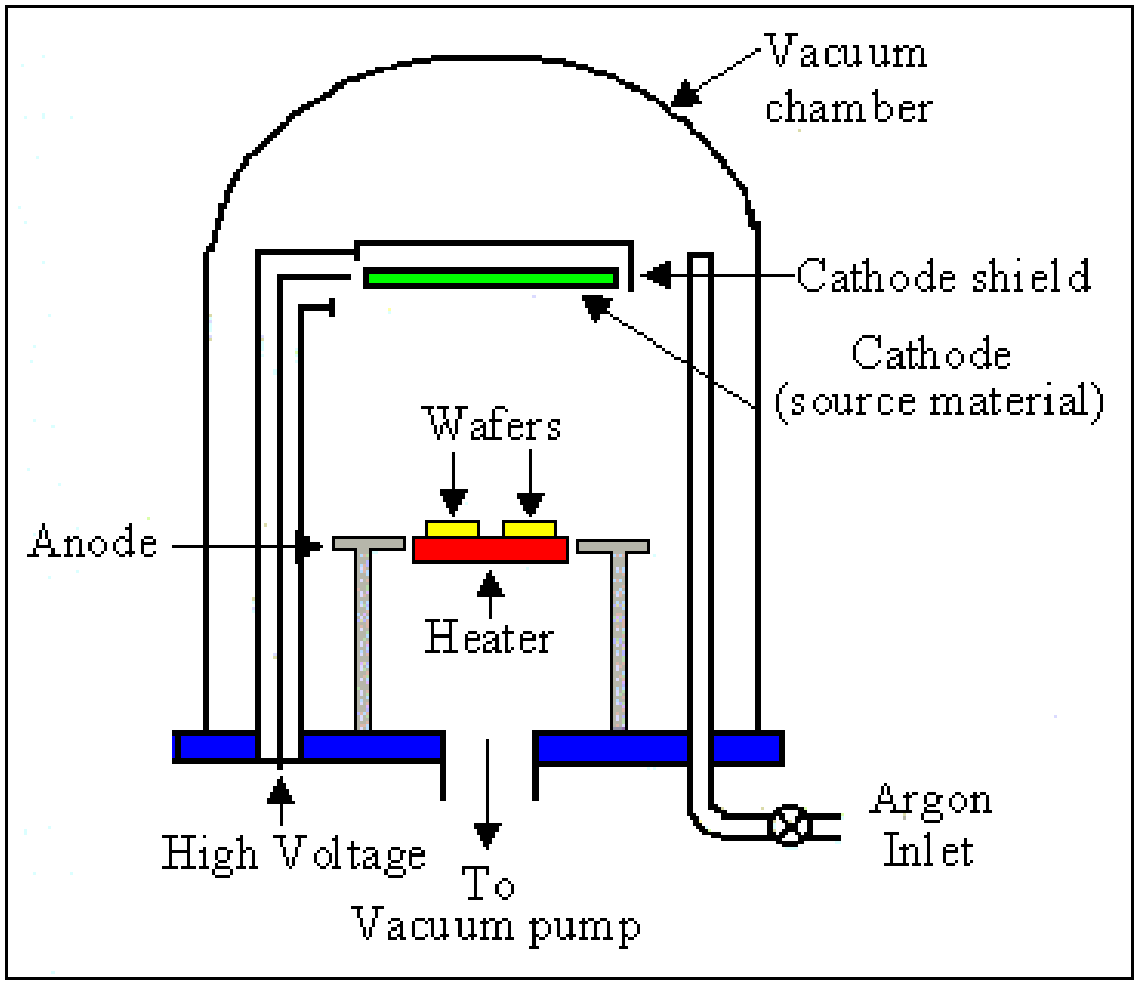
Vacuum chamber
Cathode shield
Cathode (source material)
Wafers
Anode
Heater
High Voltage
To Vacuum pump
Argon Inlet

E-beam Evaporator

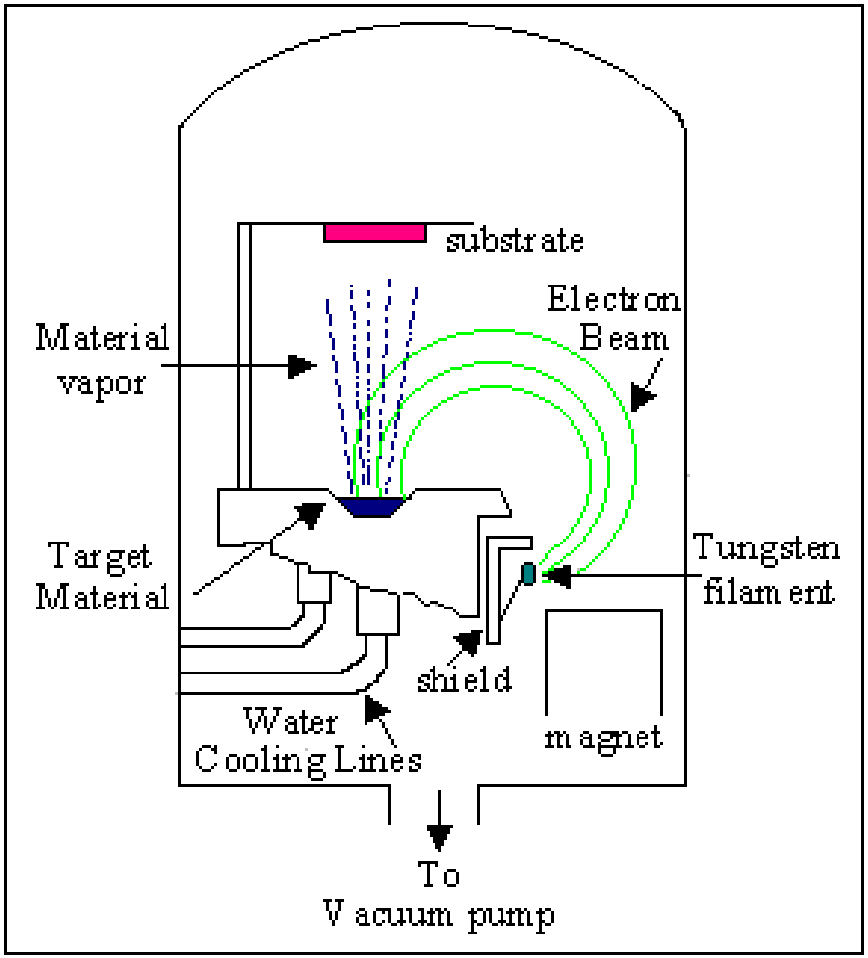

RCAS E-Beam Evaporator

一儀器名稱

中文名稱：電子束蒸鍍系統

英文名稱：E-Beam

二. 儀器廠牌、型號及儀器購置年限

廠牌：聚昌科技 AST

儀器購置年限：民國92年7月

三. 重要規格

蒸鍍金屬: Ni、Ti、 Au、Al、 Pt 、Cr

回儀器配置圖

TI 50 nm

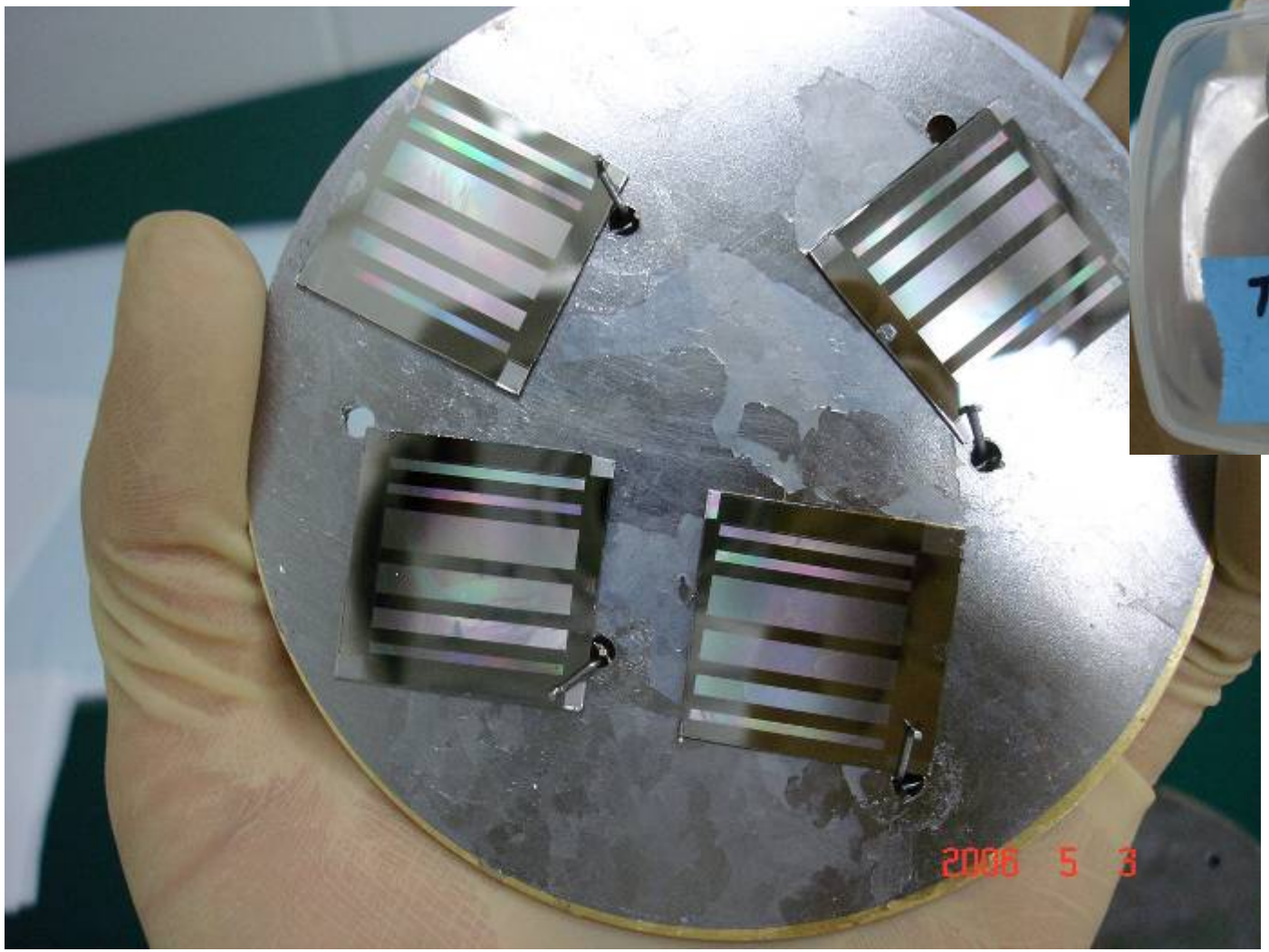

SEM image of Ti 50 nm on Si wafer

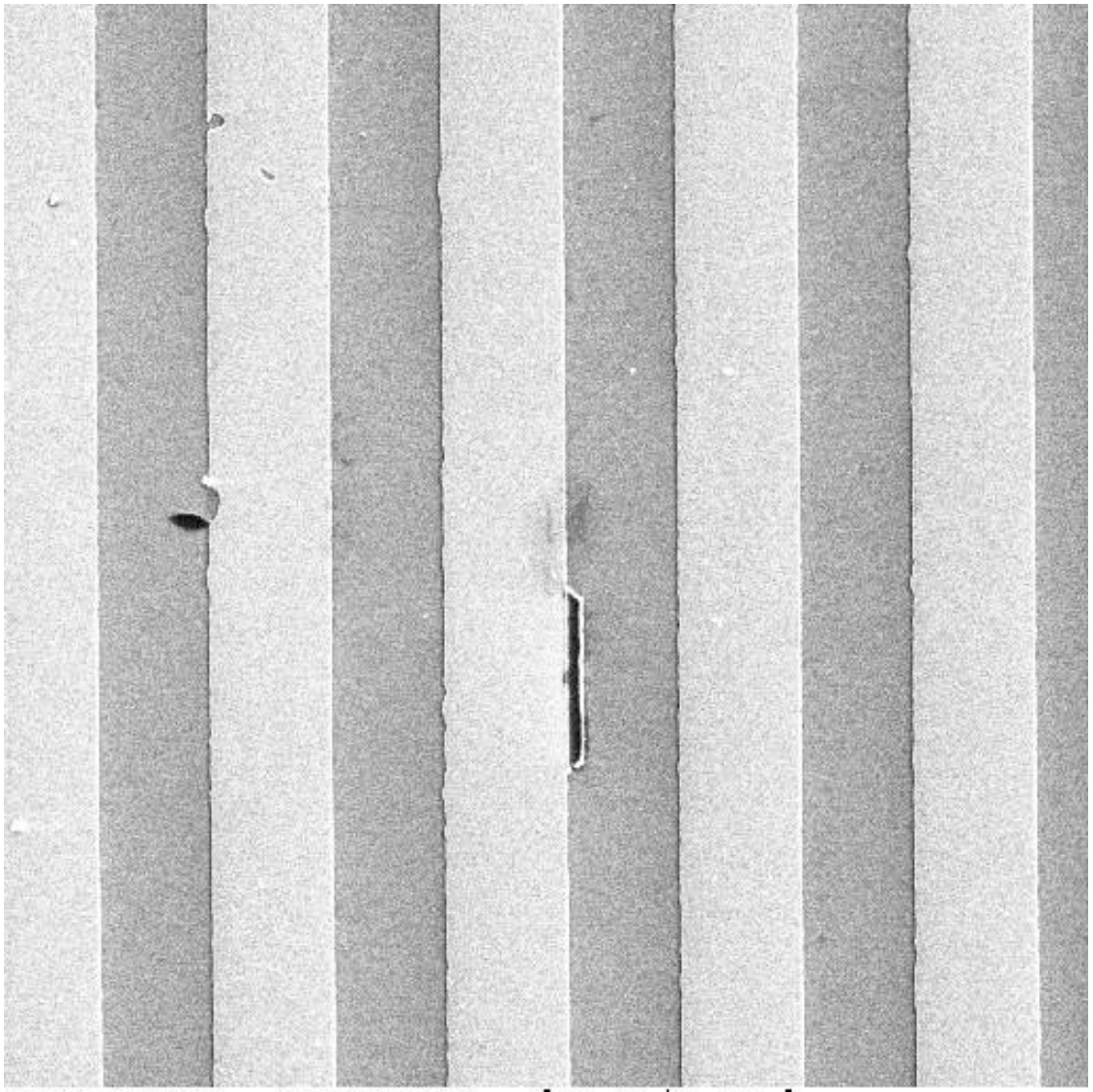

Ti 50 nm

LIFT OFF

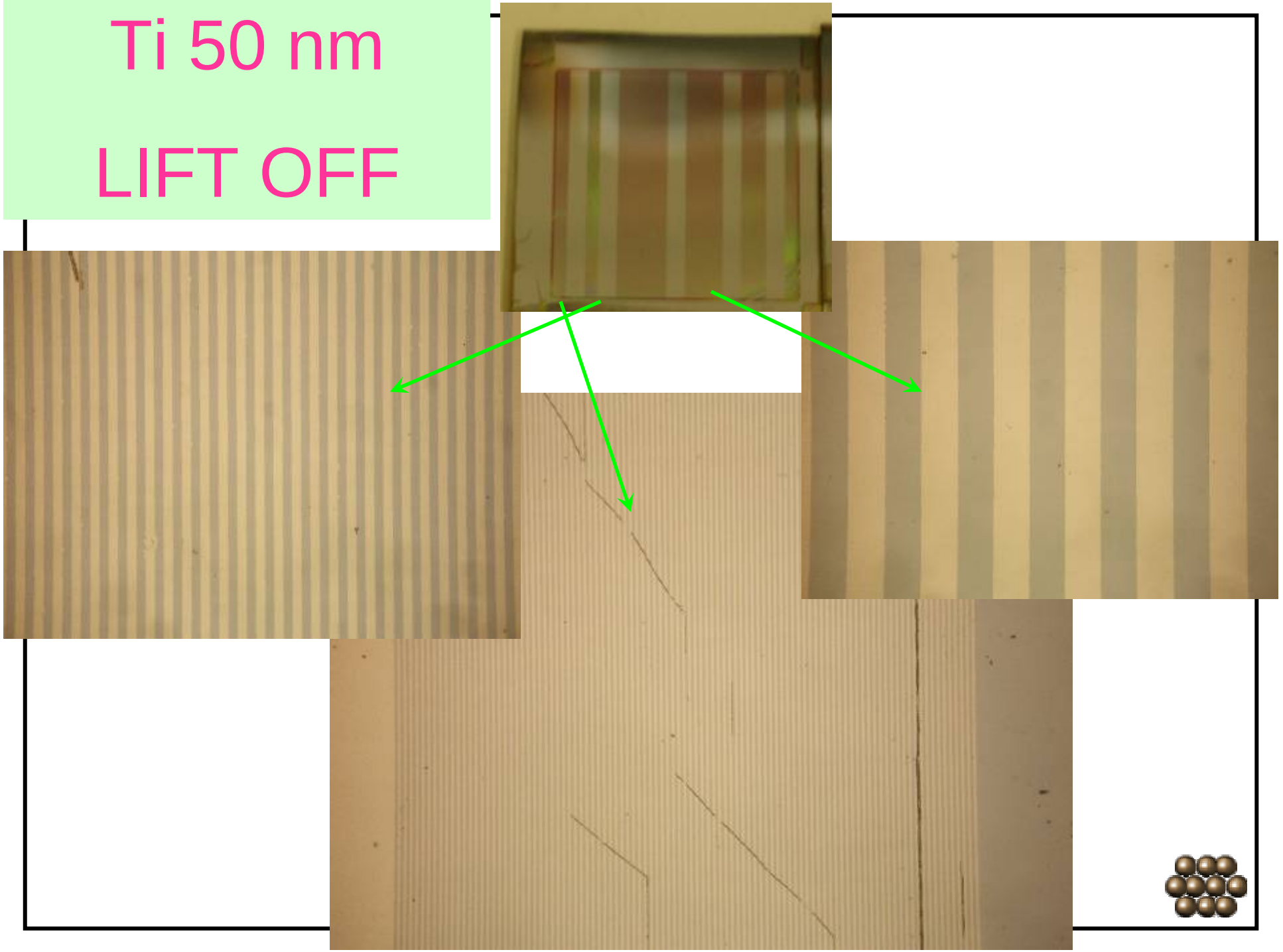

Ti 50 nm on Si 20 um

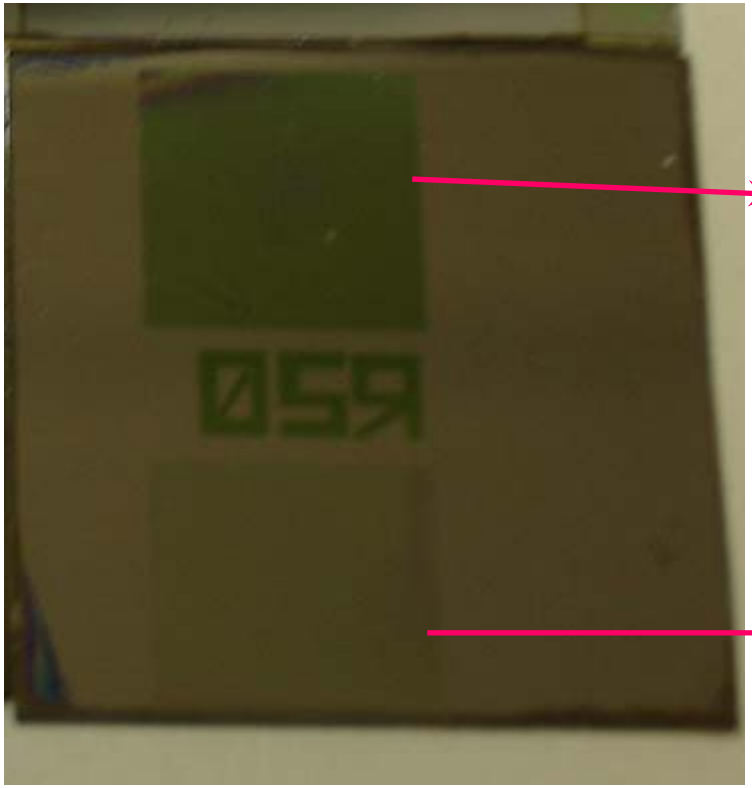

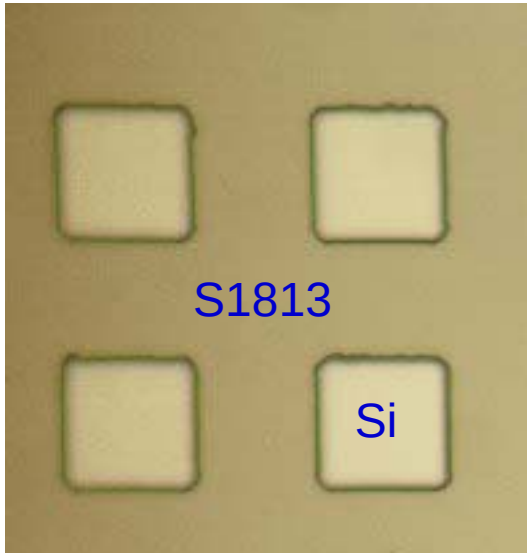

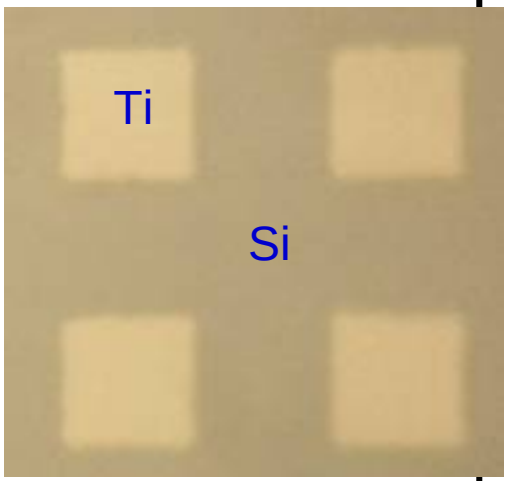

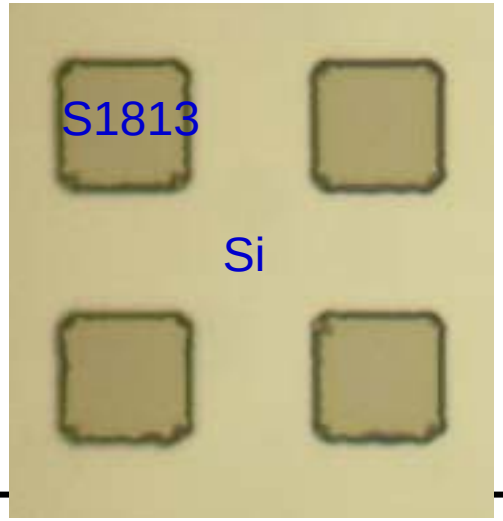

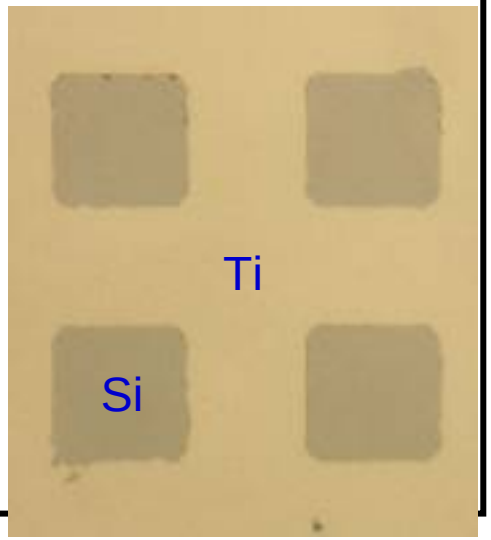

Ti 50 nm on Si 5 um

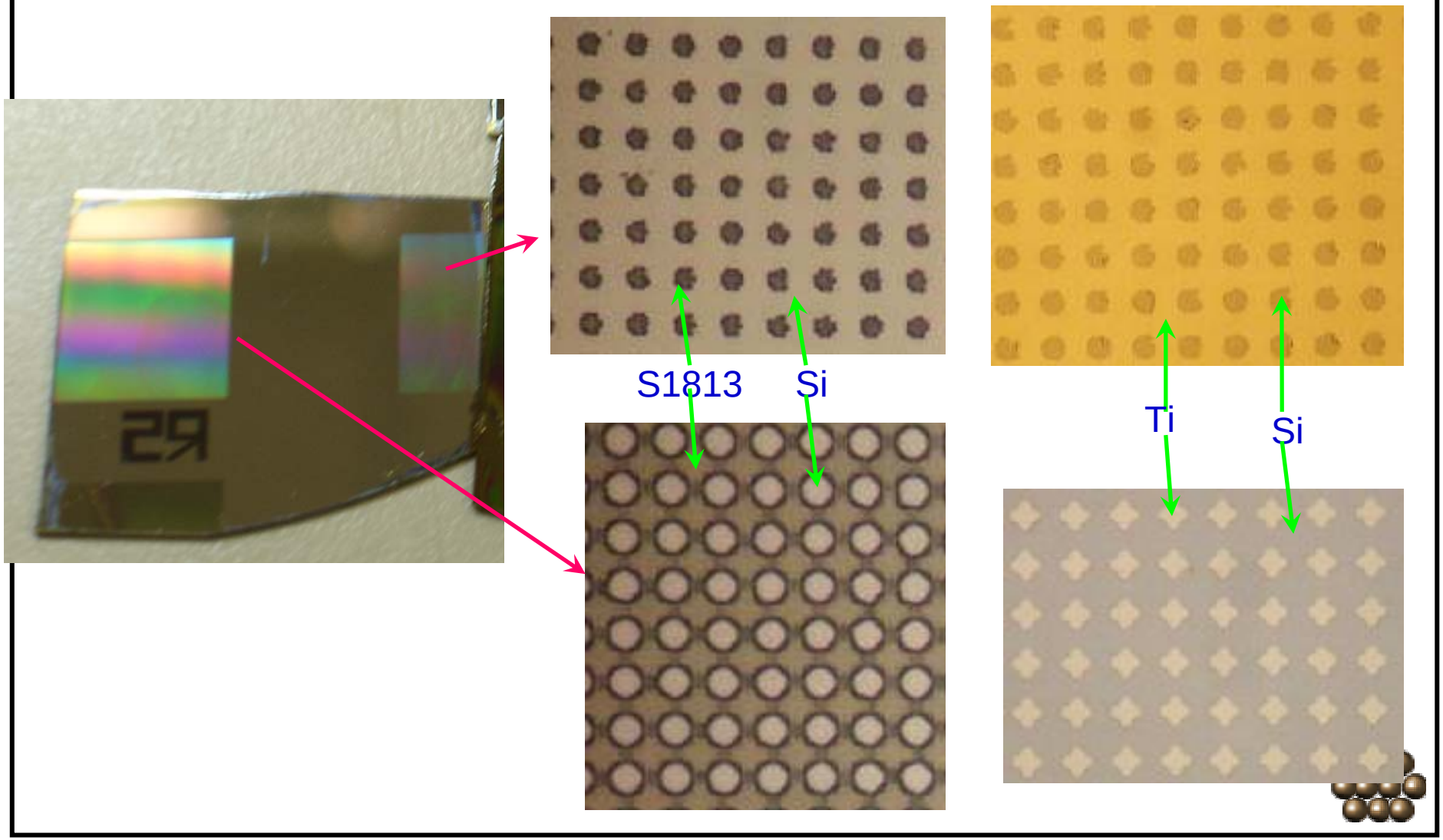

Reactive Ion Etching

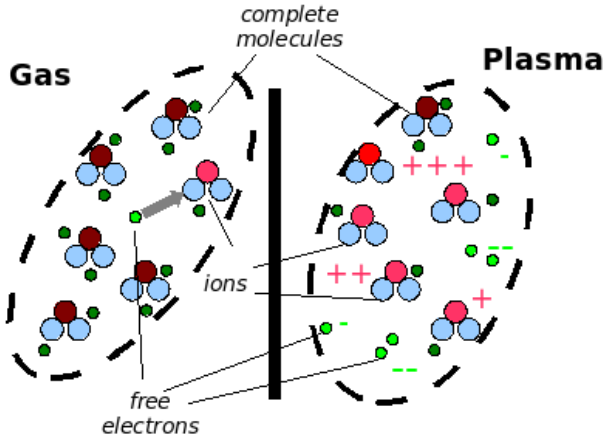

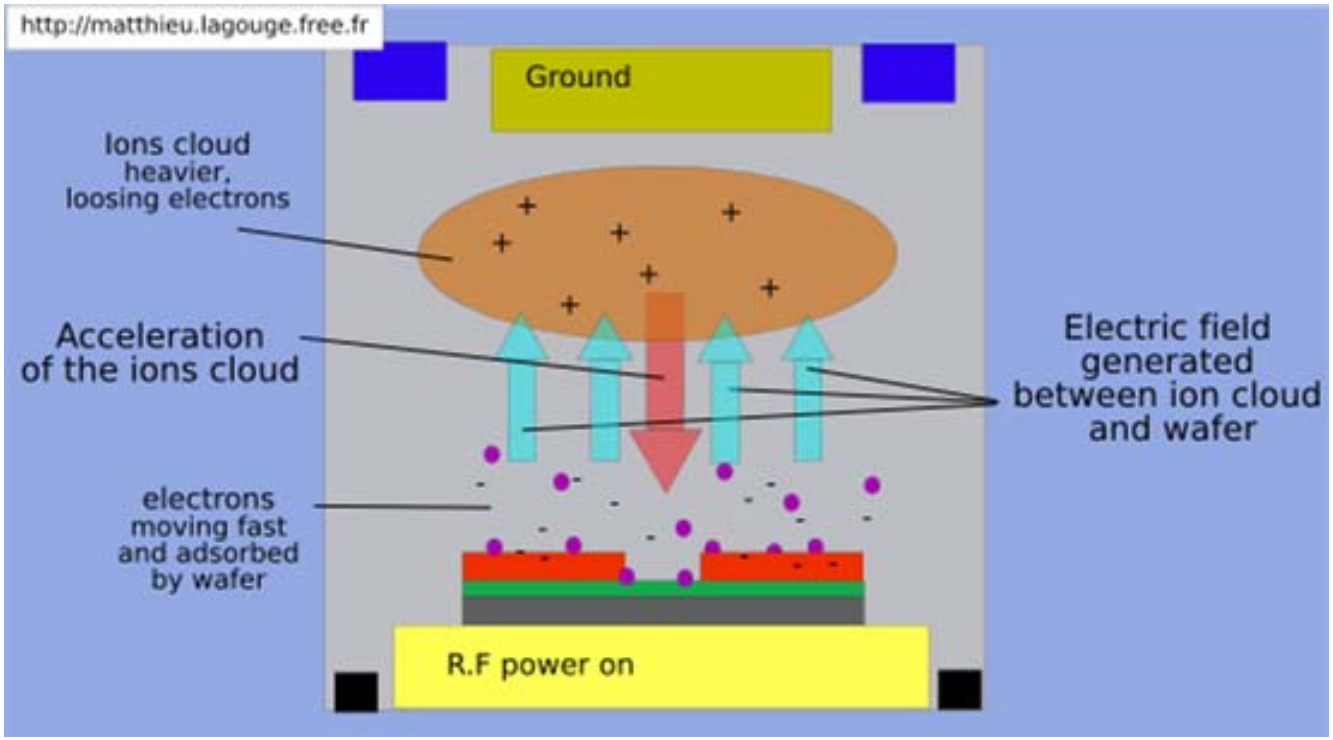

Reactive Ion Etching

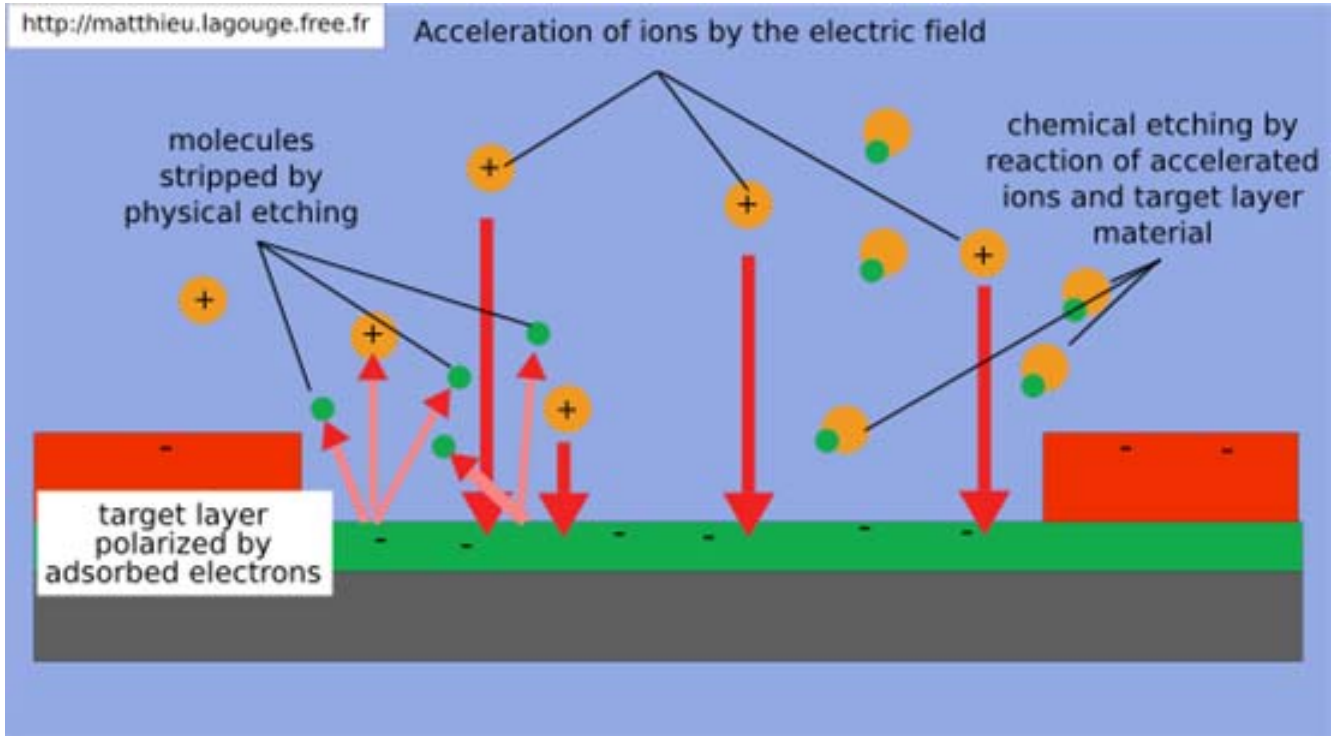

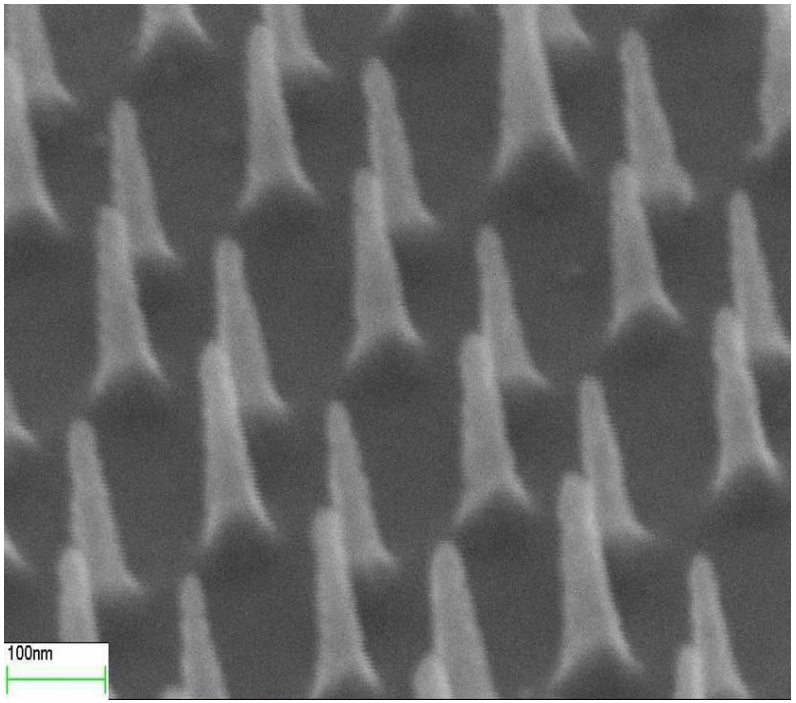
100nm

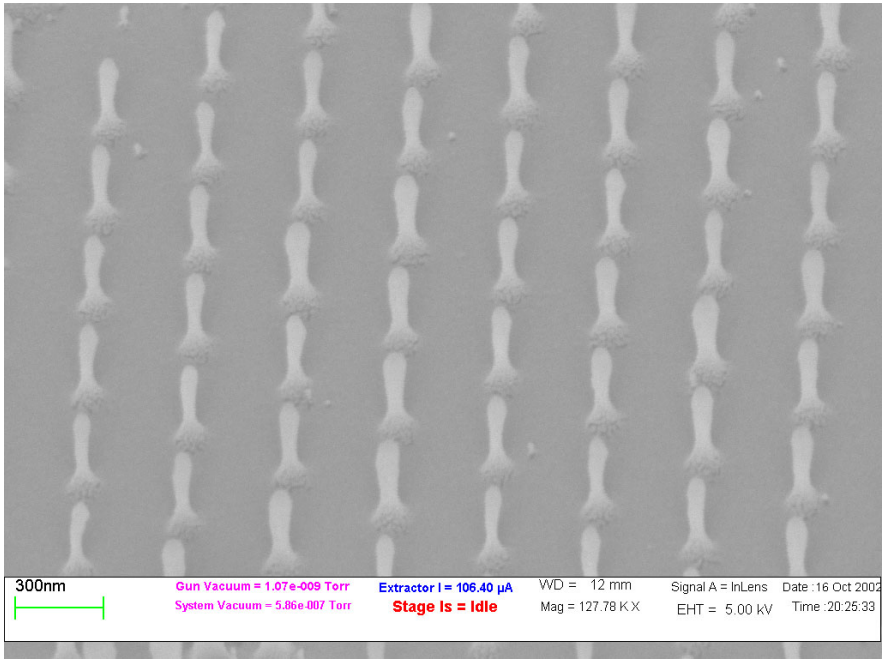
300nm
Gun Vacuum = 1.07e-009 Torr
System Vacuum = 5.86e-007 Torr
Extractor I = 106.40 µA
Stage Is = Idle
WD = 12 mm
Mag = 127.78 K X
Signal A = InLens
EHT = 5.00 kV
Date :16 Oct 2002
Time :20:25:33

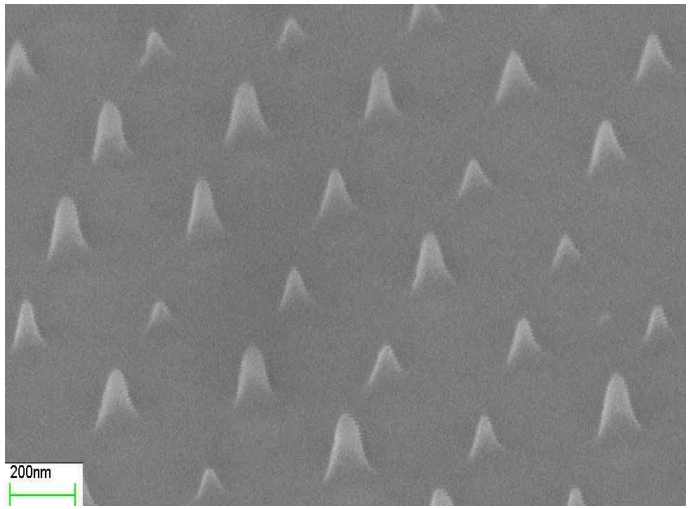
200nm

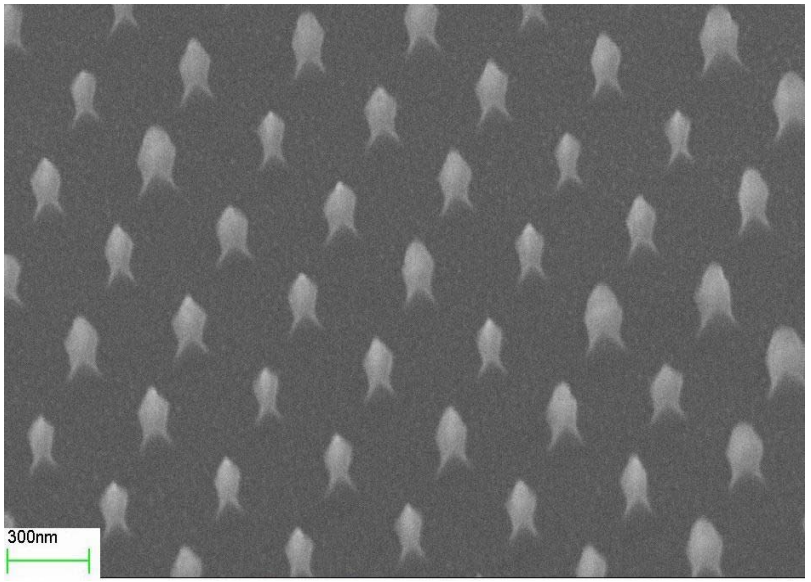
300nm

ICP- “BOSCH” Recipe
Etching & Sidewall Passivation Cycle

(a) Etch Step

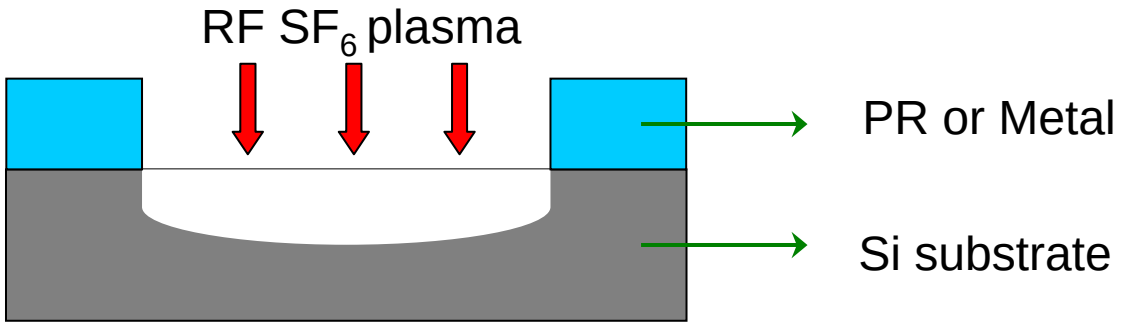

(b) Passivate Step

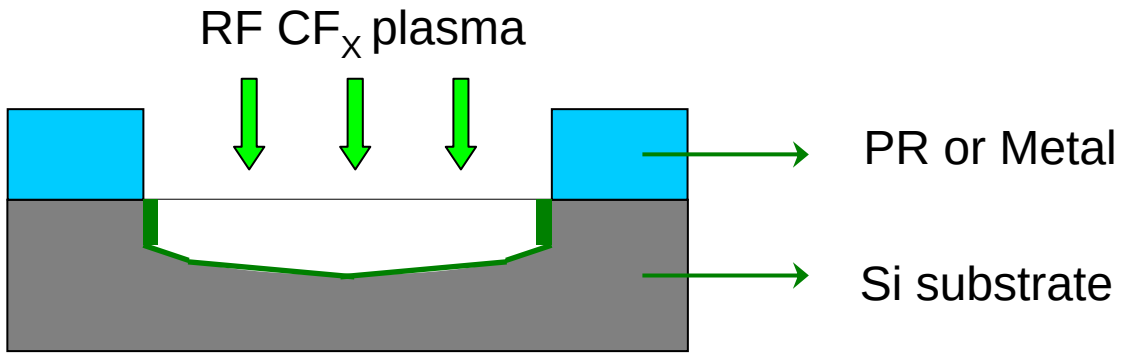

(a’) Etch Step

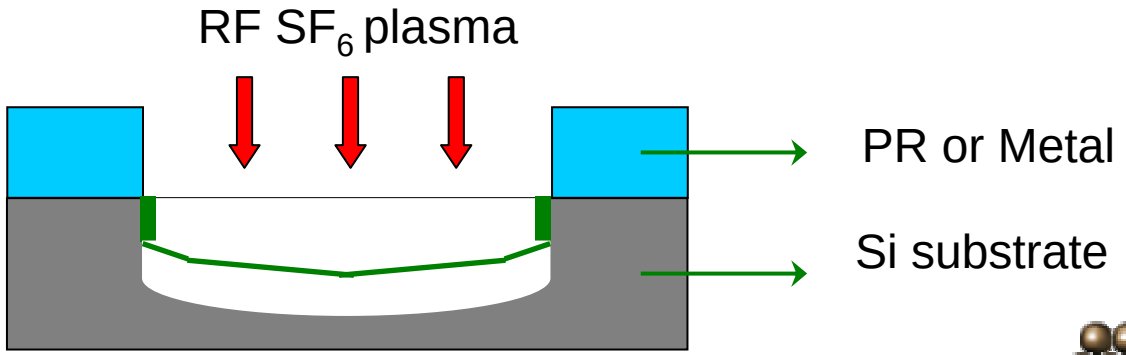

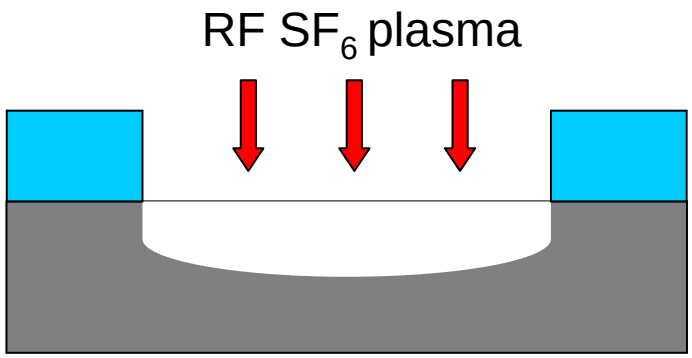

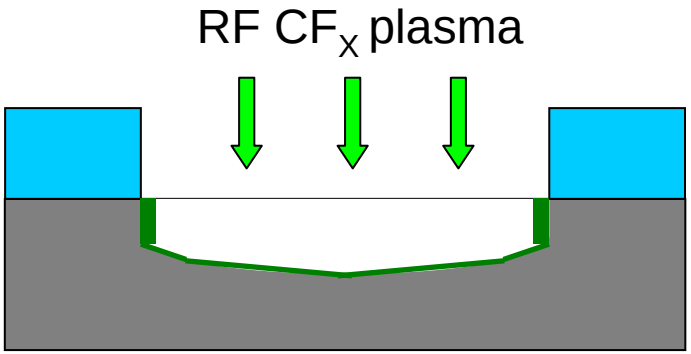

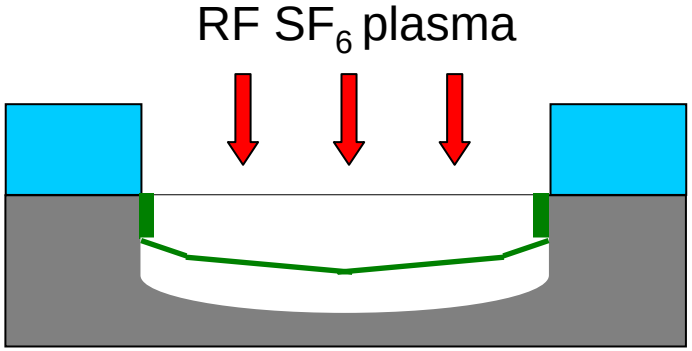

The gases in RCAS

C_4F_8, CF_4, CHF_3, Ar, O_2

SAMCO ICP (RECIPE)

Si etching CF_4 / O_2= 30 / 10

SiO_2 (on Si) CHF_3 / Ar = 15 / 30

The gases in NEMSRC

SF_6, C_4F_8, CF_4, O_2

RECIPE

	TIME	
Etch:	11.5 s	SF_6(130sccm) O_2(13sccm)
Passivate:	7s	C_4F_8(85sccm)

NEMSRC ICP

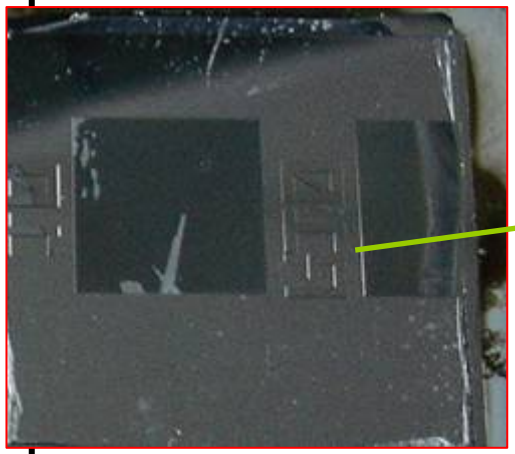

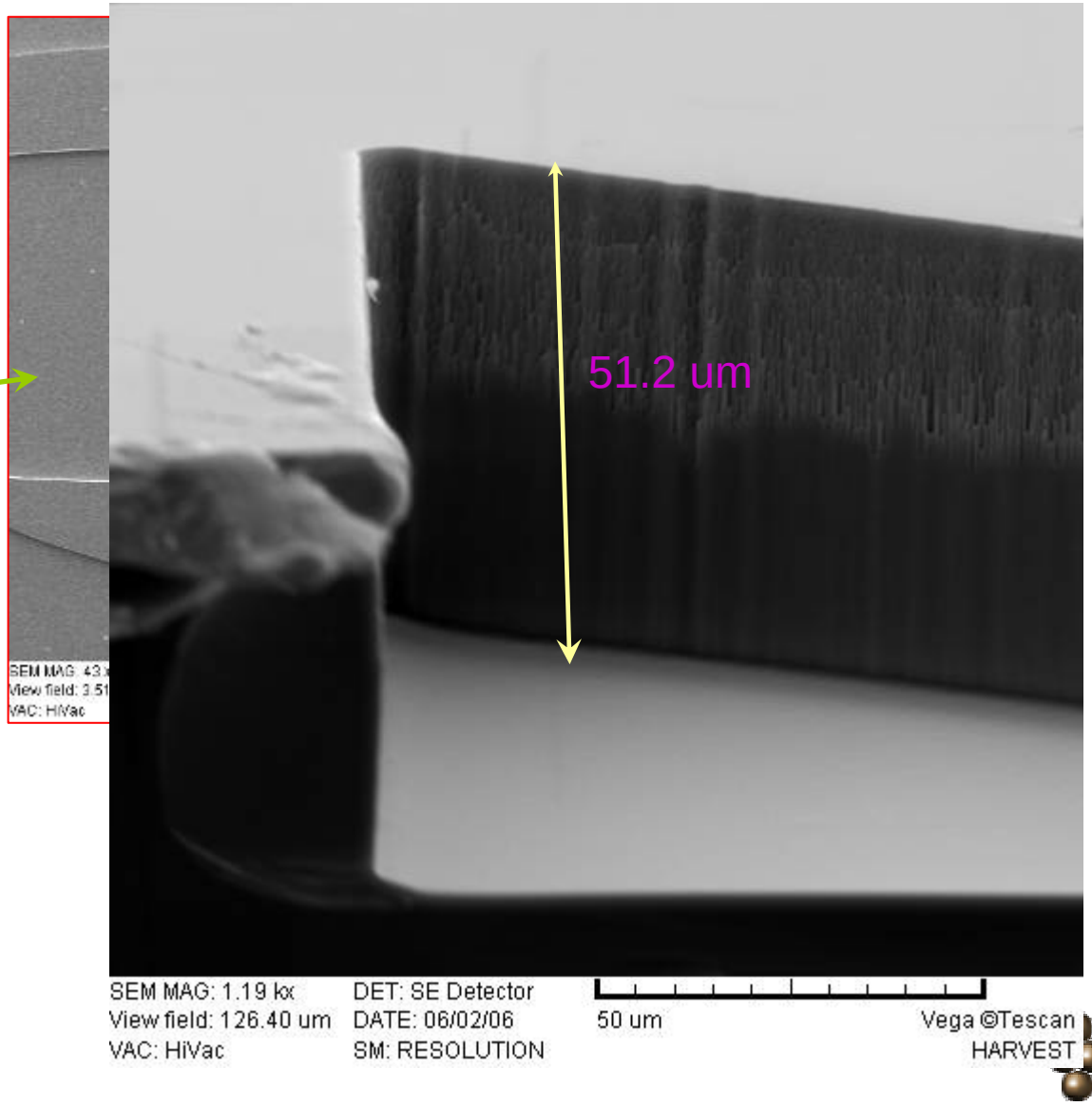
51.2 um
SEM MAG: 1.19 kx
View field: 126.40 um
VAC: HiVac
DET: SE Detector
DATE: 06/02/06
SM: RESOLUTION
50 um
Vega ©Tescan
HARVEST

Si ---S1813---ICP

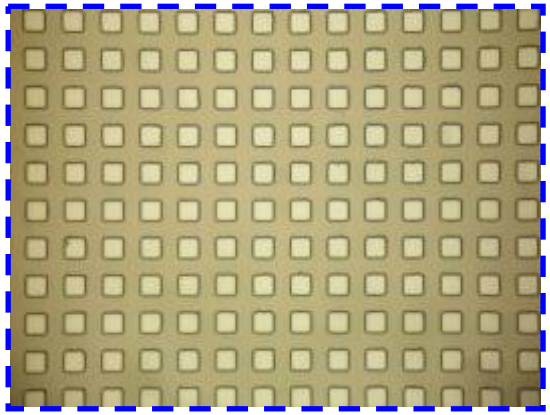

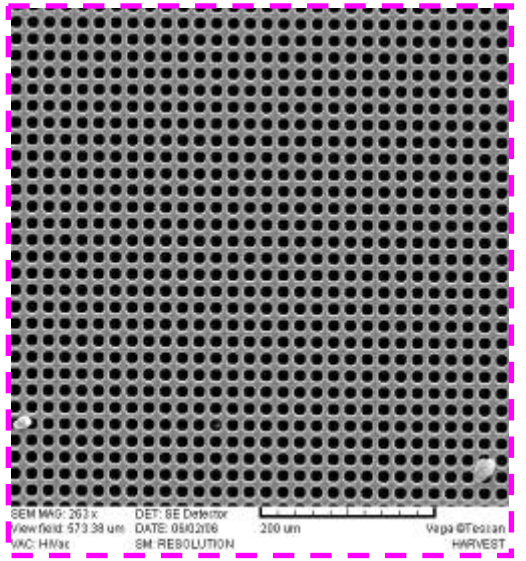

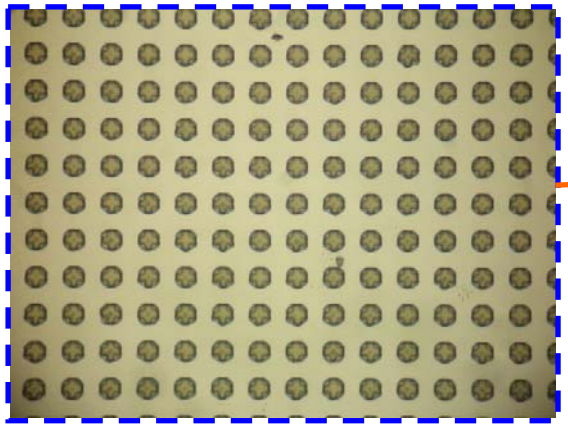

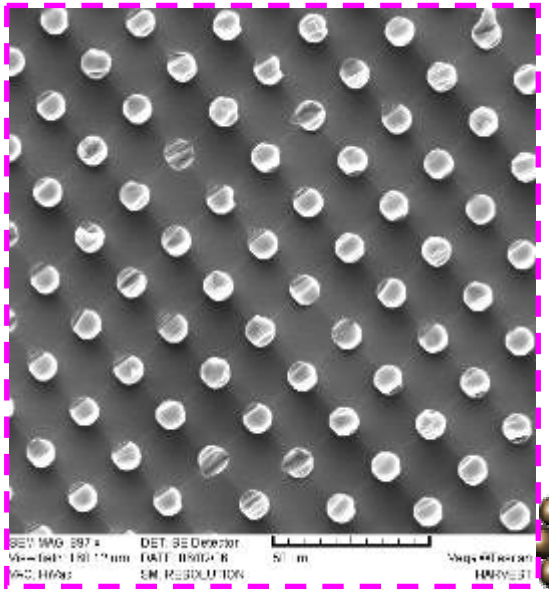

NEMSRC ICP ：S1813 on Si

The gases in NEMSRC

SF_6, C_4F_8, CF_4, O_2

RECIPE

	TIME		
Etch:	11.5 s	SF_6(130sccm)	O_2(13sccm)
Passivate:	7s	C_4F_8(85sccm)	

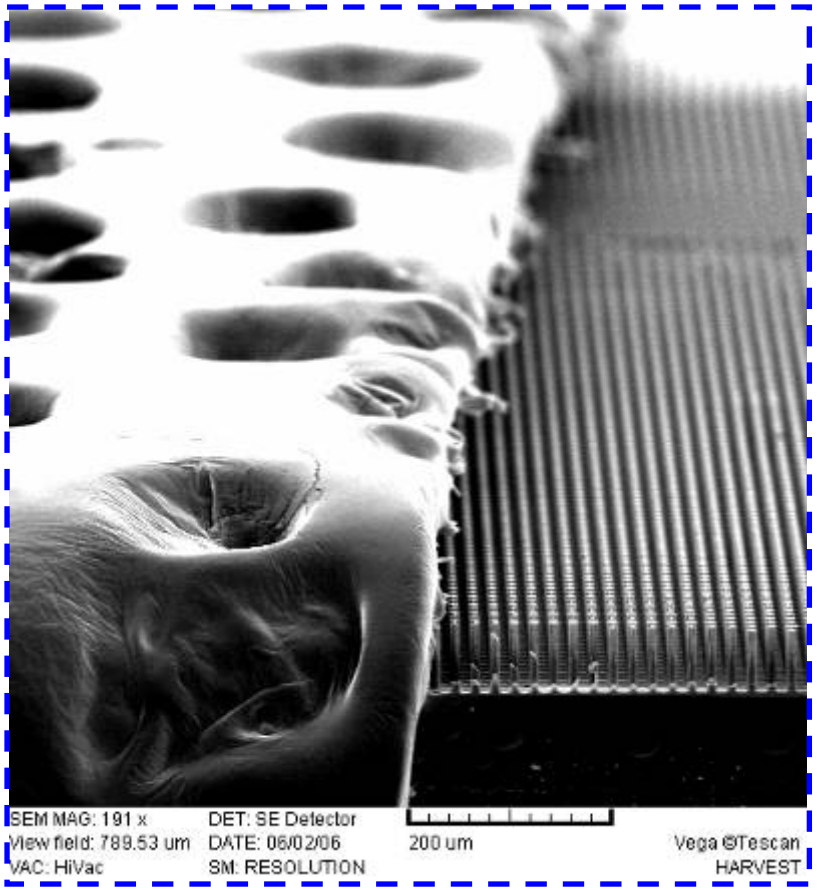

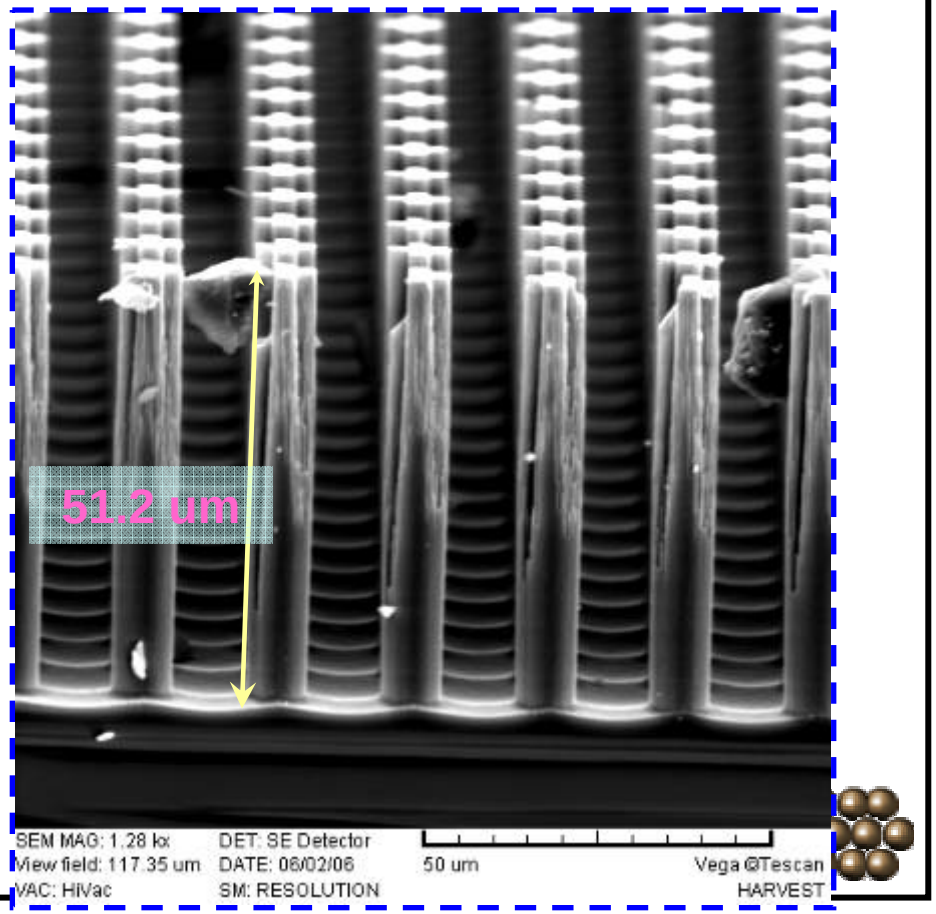

NEMSRC ICP ：S1813 on Si --20 μm array

The gases in NEMSRC

SF_6, C_4F_8, CF_4, O_2

RECIPE

	TIME		
Etch:	11.5 s	SF_6(130sccm)	O_2(13sccm)
Passivate:	7s	C_4F_8(85sccm)	

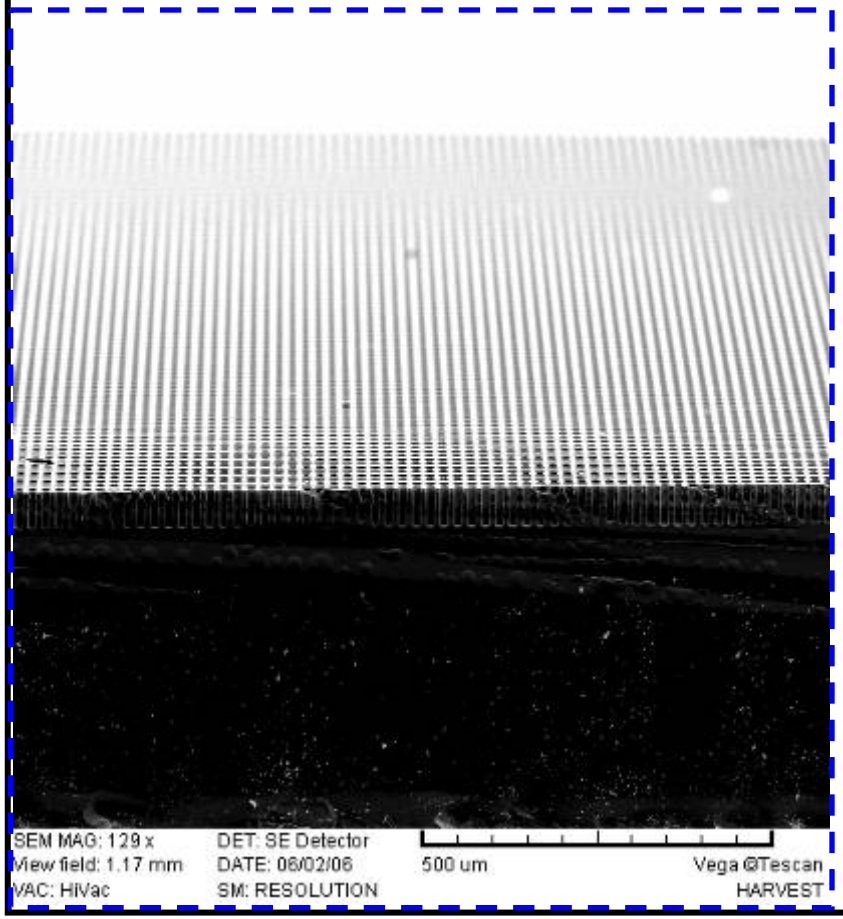

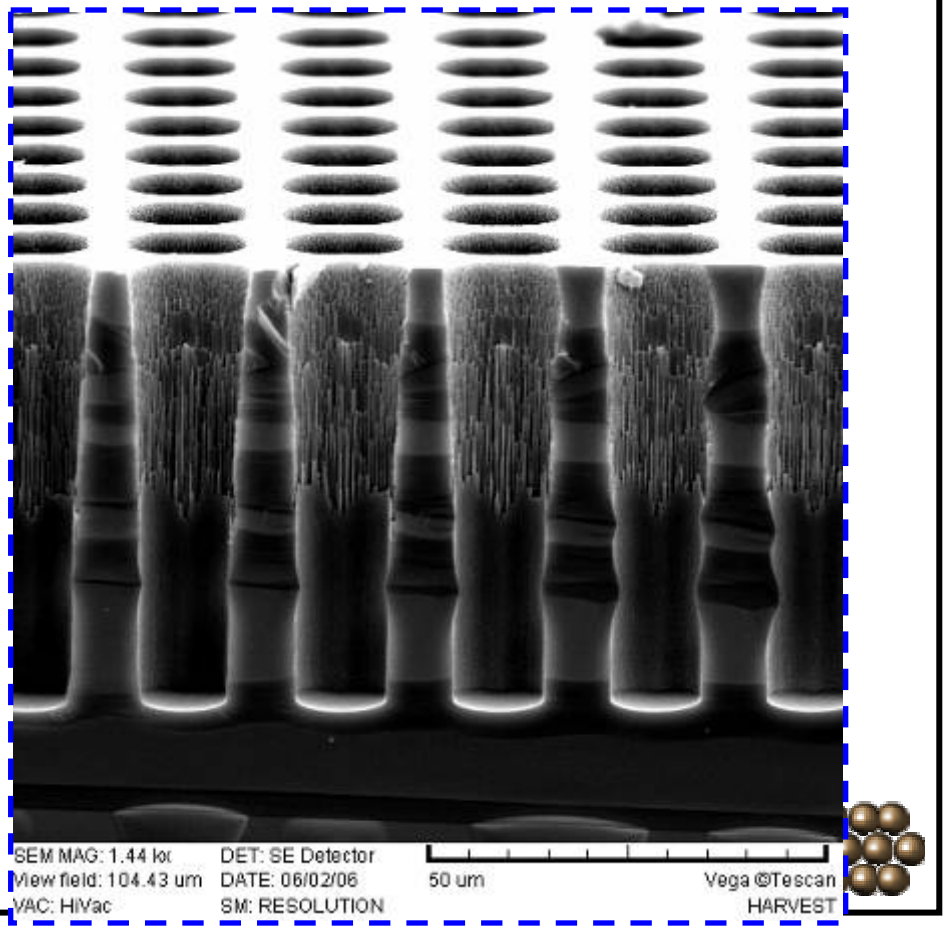

NEMSRC ICP

Si 10 um Line

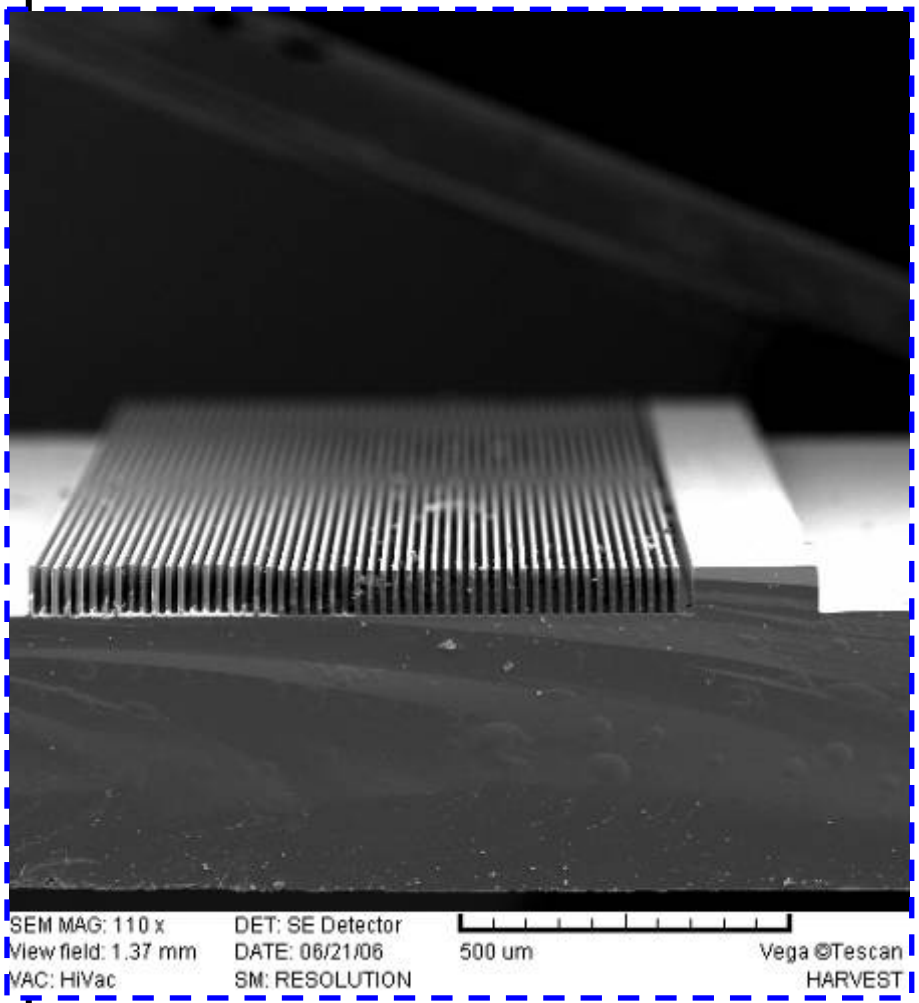

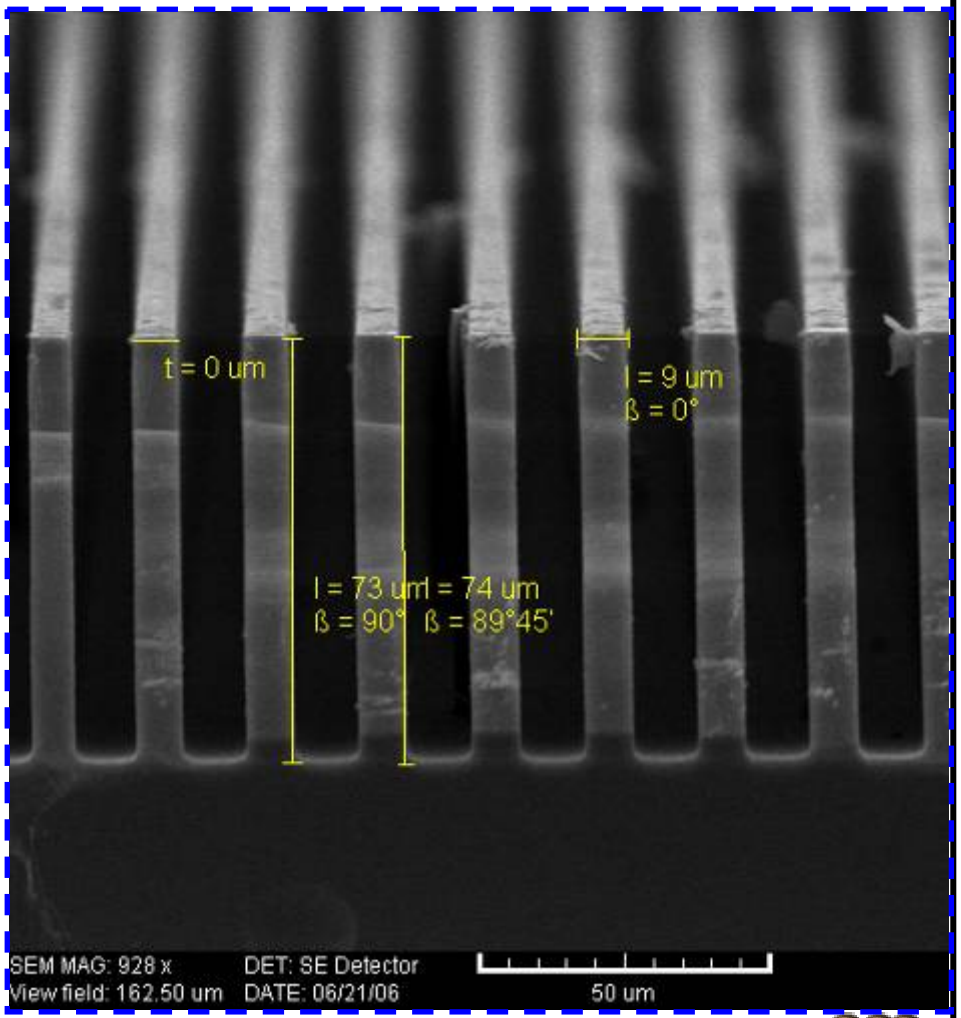

NEMSRC ICP

Si 10 um pillar

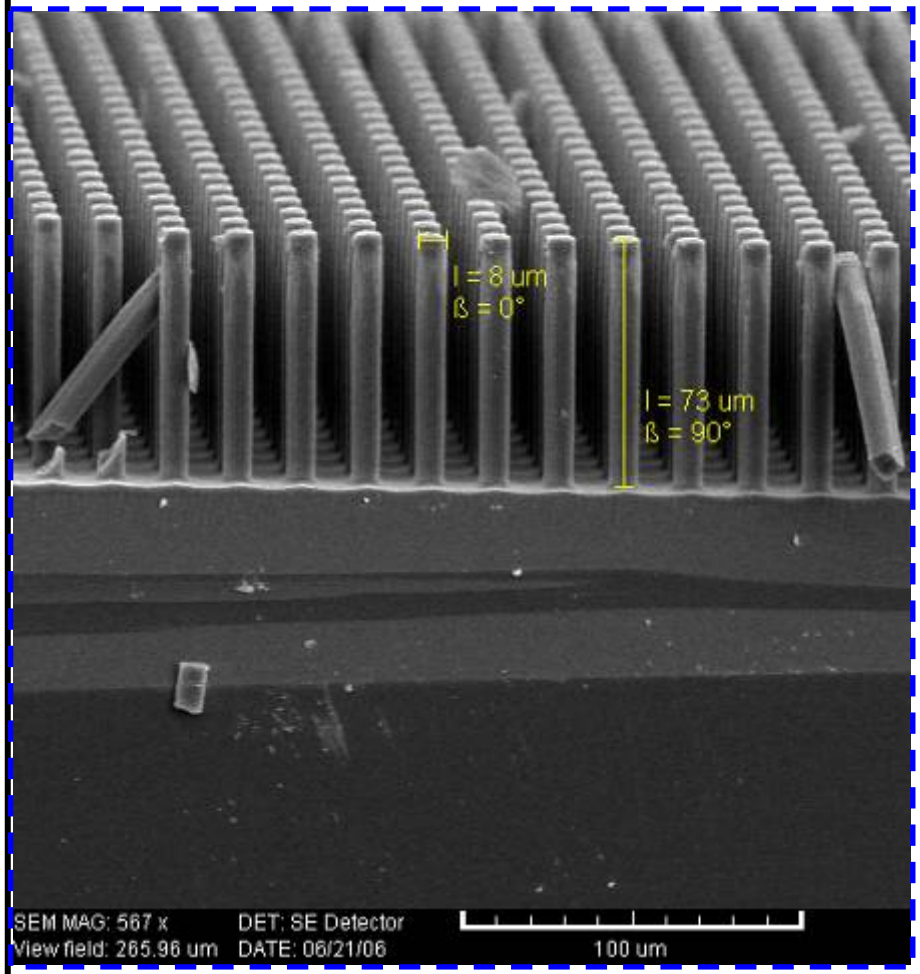

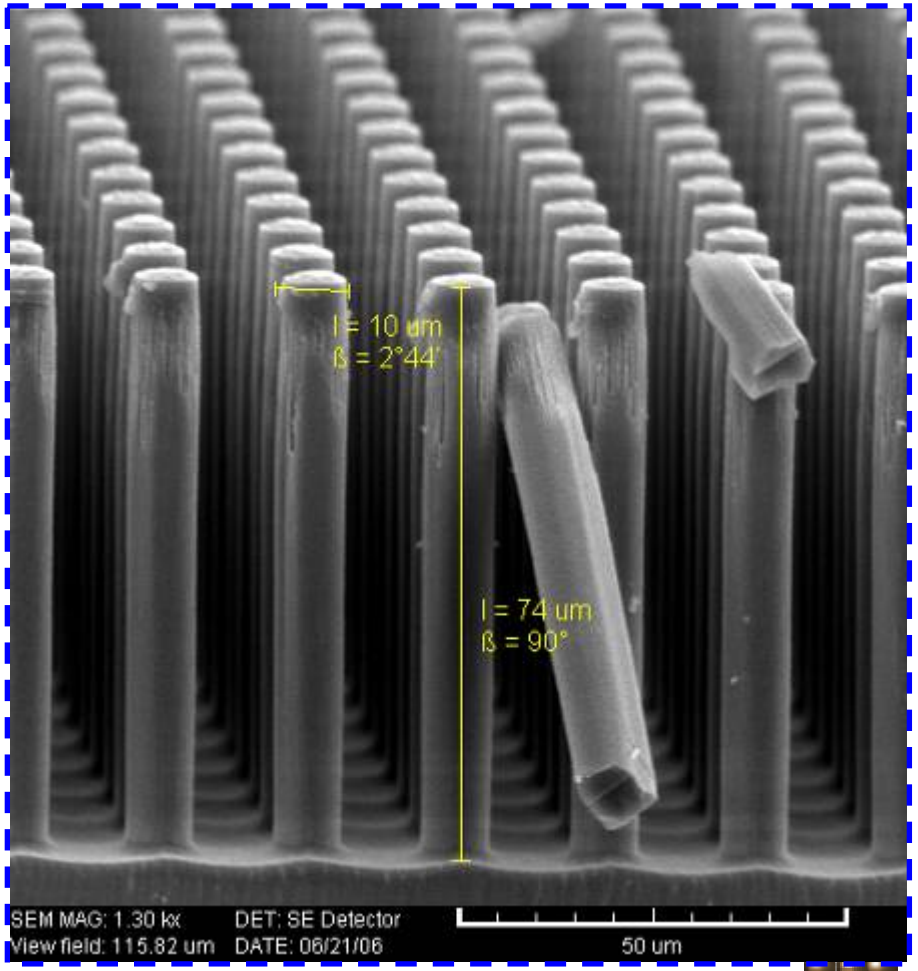

Si 5um Line

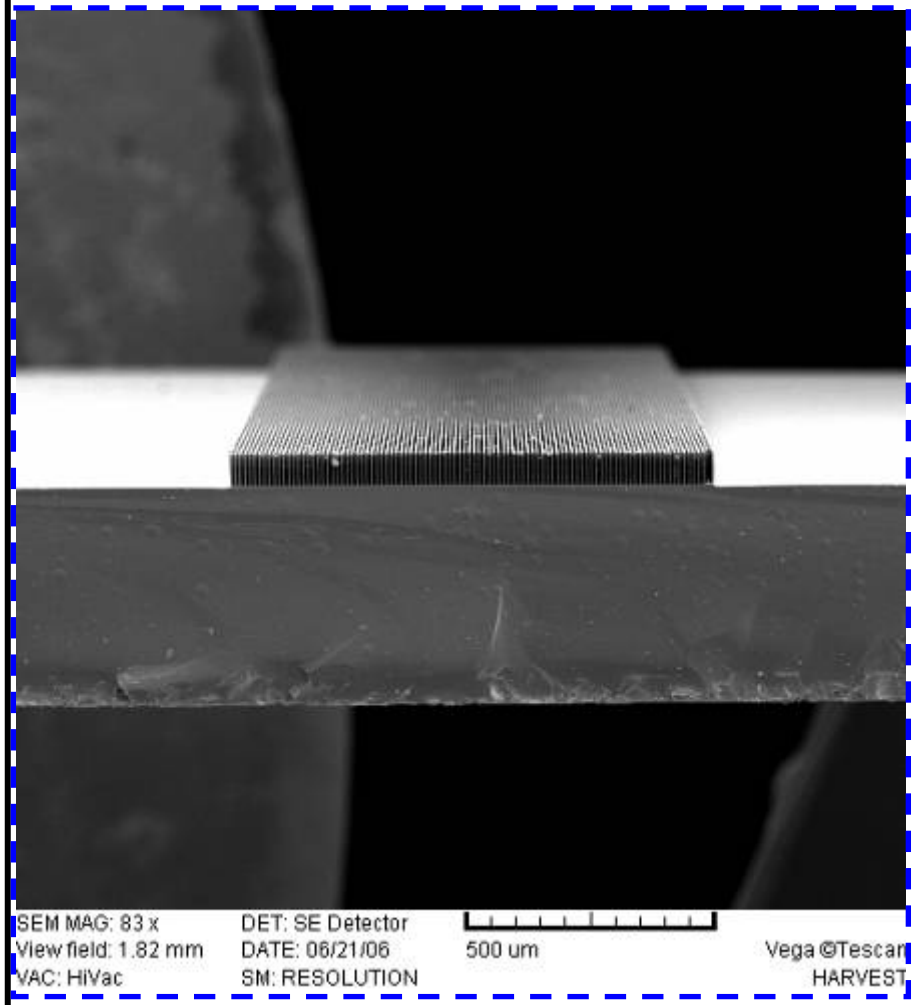
SEM MAG: 83 x
View field: 1.82 mm
VAC: HiVac
DET: SE Detector
DATE: 06/21/06
SM: RESOLUTION
500 um
Vega ©Tescan
HARVEST

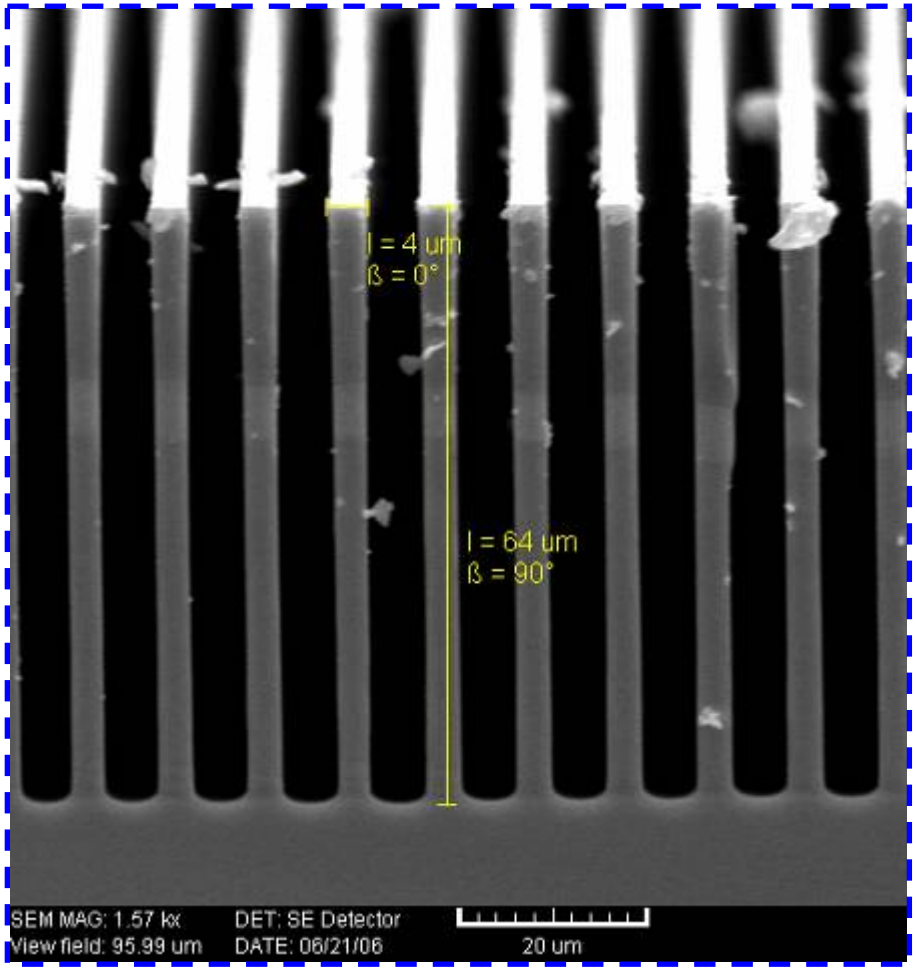
l = 4 um
ß = 0°
l = 64 um
ß = 90°
SEM MAG: 1.57 kx
View field: 95.99 um
DET: SE Detector
DATE: 06/21/06
20 um

NEMSRC ICP ：S1813 on Si

5 um pillar

The gases in NEMSRC

SF_6, C_4F_8, CF_4, O_2

RECIPE

TIME

Etch: 11.5 s SF_6(130sccm) O_2(13sccm)

Passivate: 7s C_4F_8(85sccm)

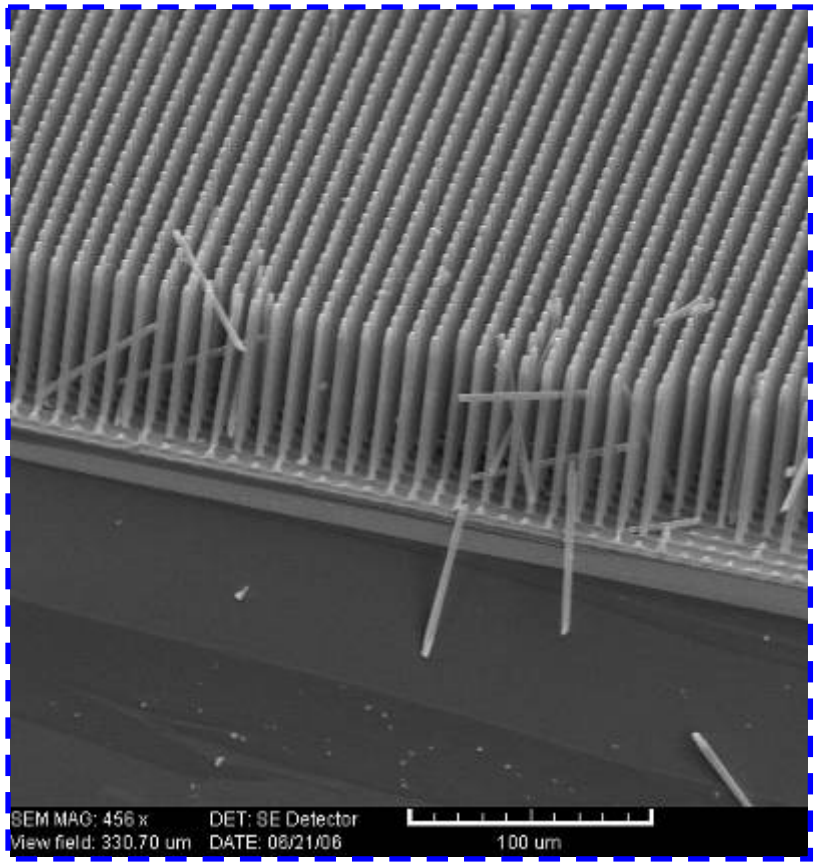

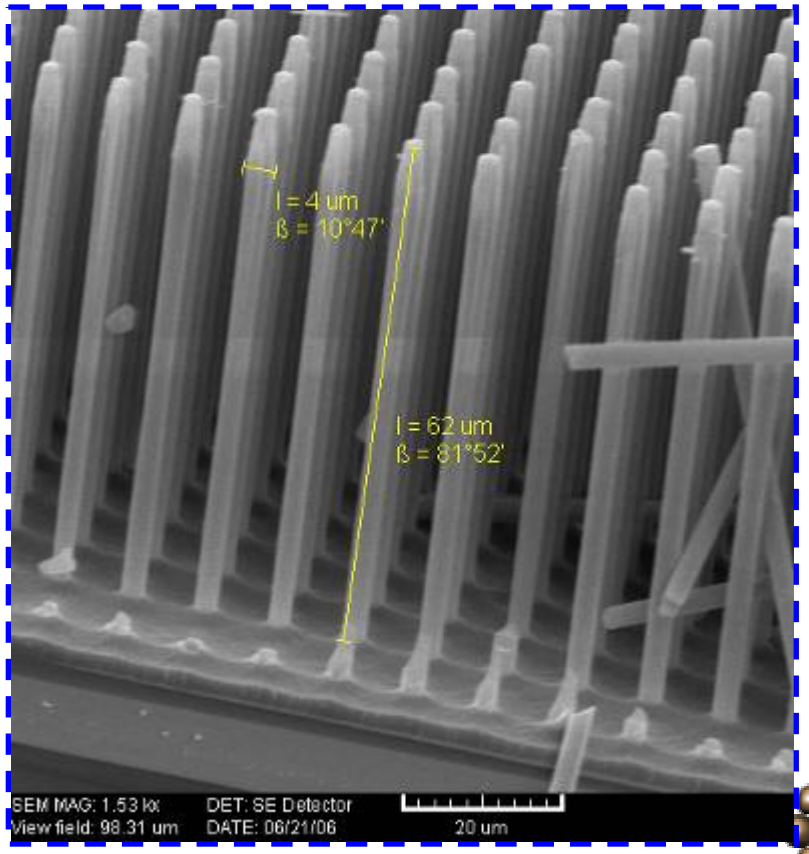

Electron Microscope

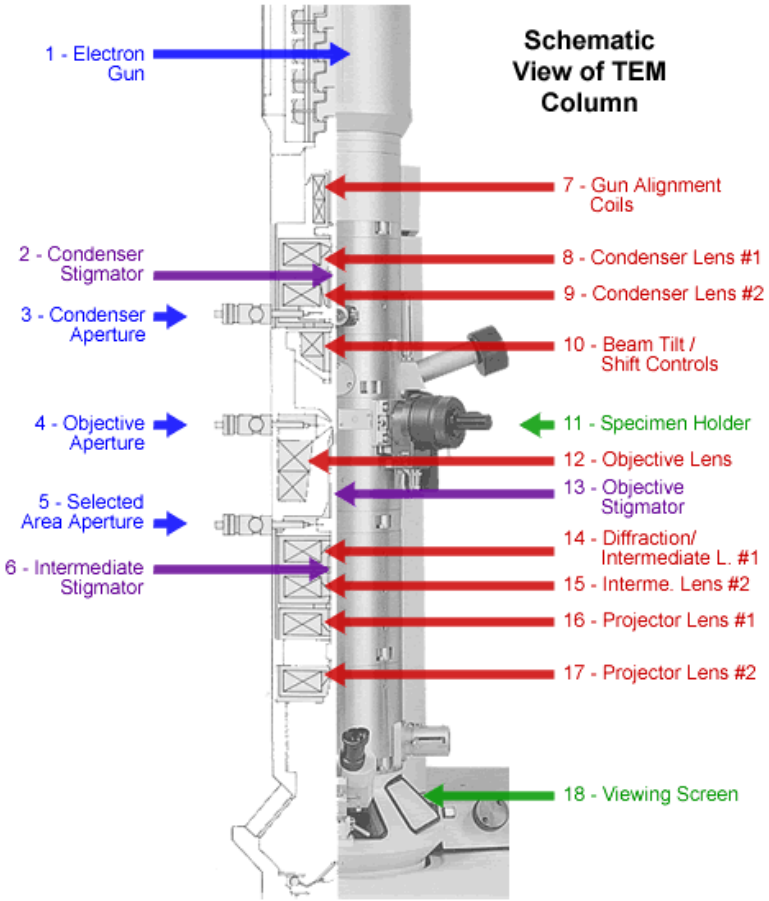

TEM Image

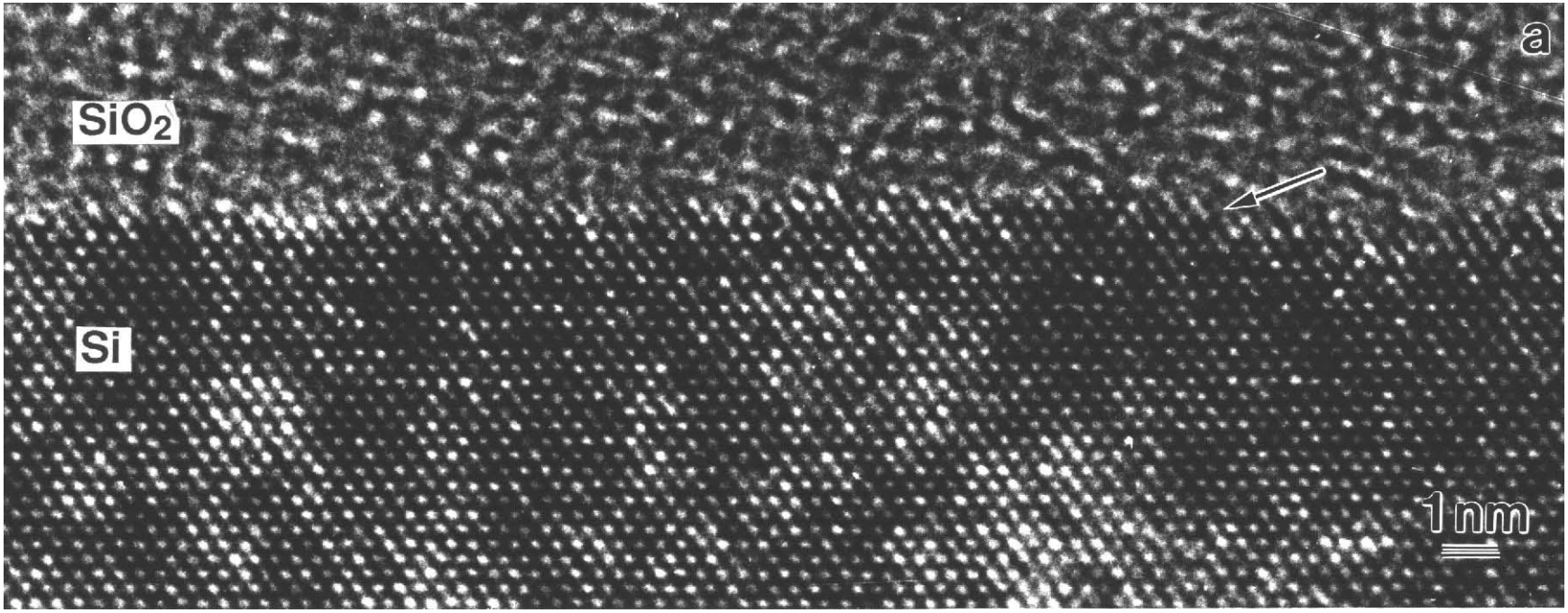

100 kV = 0.00388 nm

$\lambda = h/p = h/mv$ h /sqrt(2 meV)

E-Beam Lithography

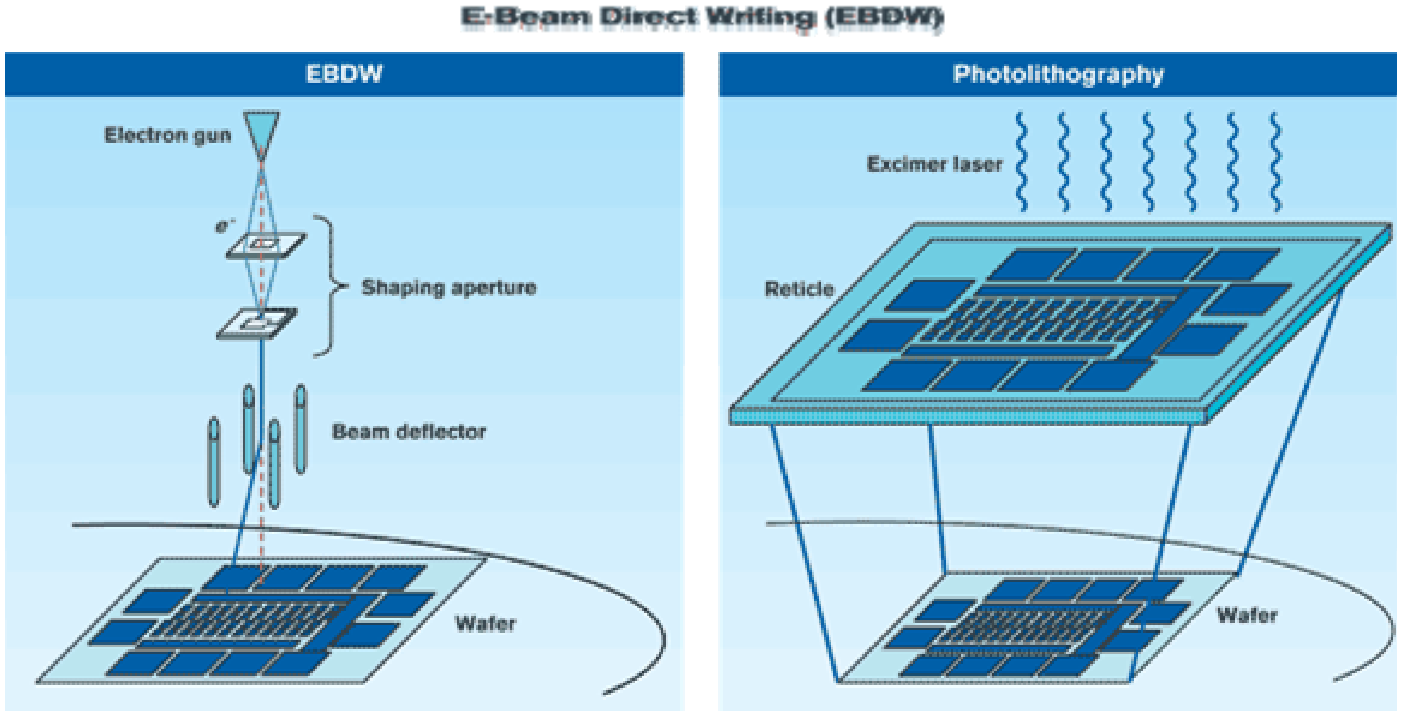

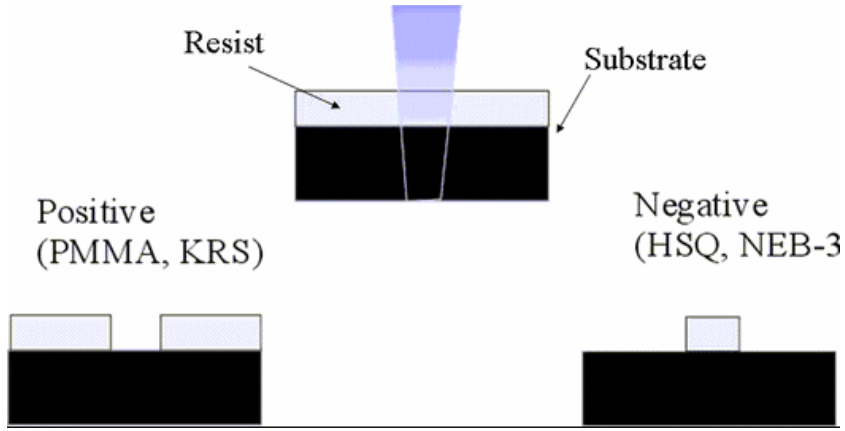

E-Beam Lithography

Resolution:

2 nm @ 20 KeV

2 nm @ 1.0 KeV

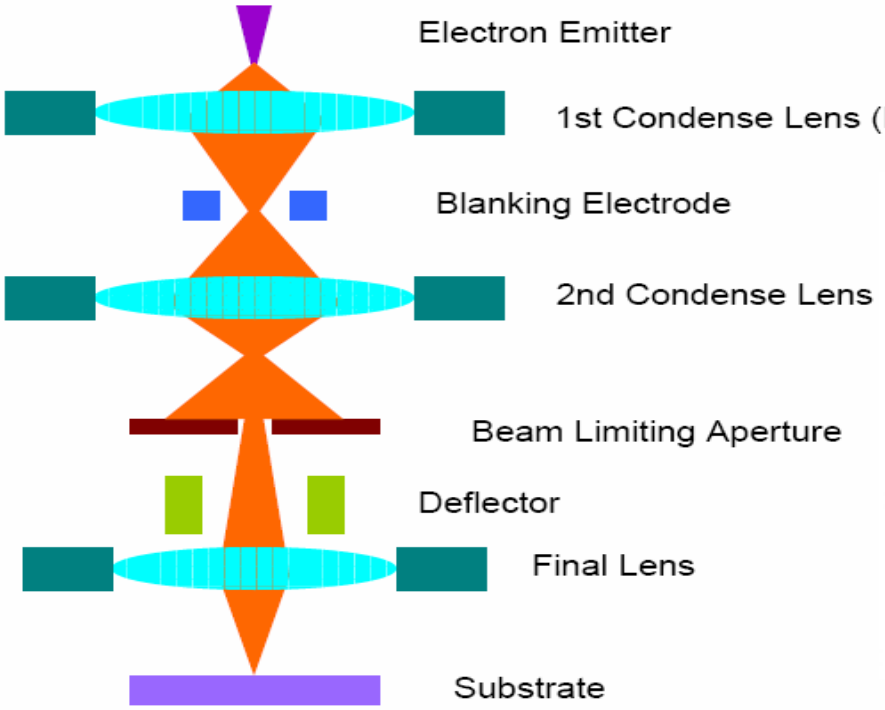

E-beam Writer

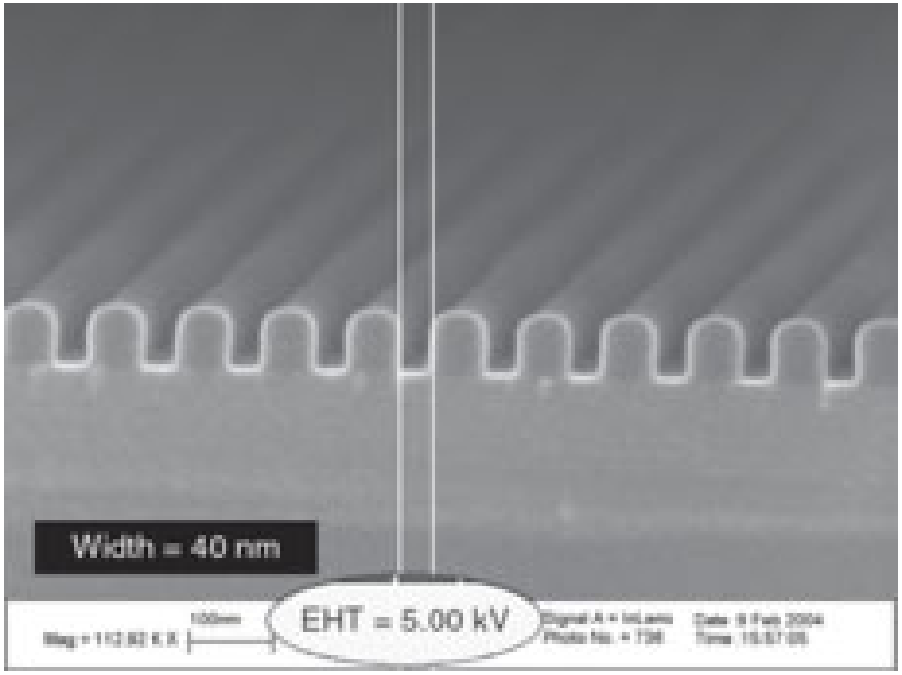

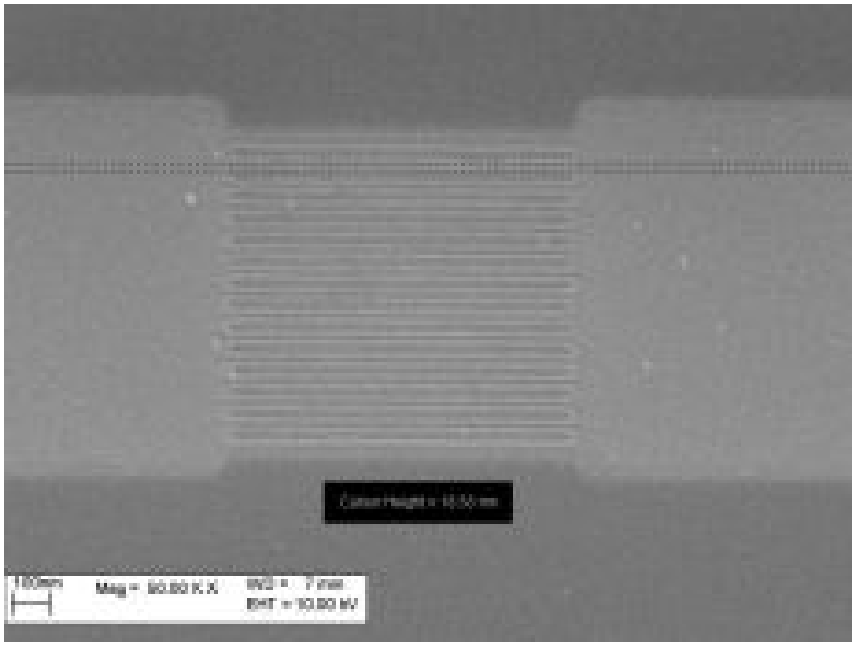

Better than 10 nm lines over 4 inch wafer

EUV System

EUV Source

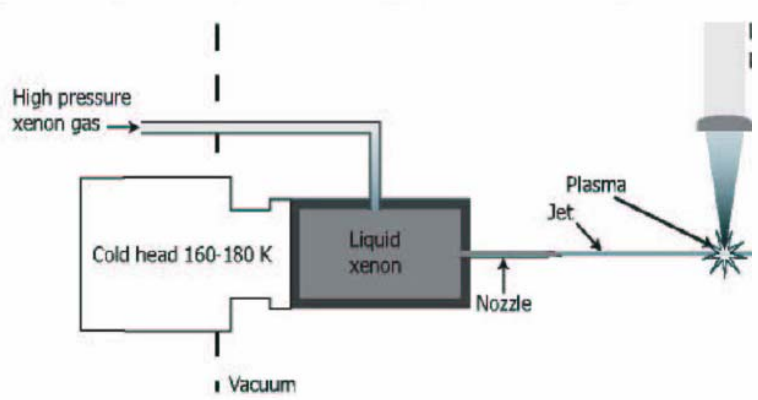

1. 13.4nm source.
2. Laser-produced plasma

Reflective Optics for EUV

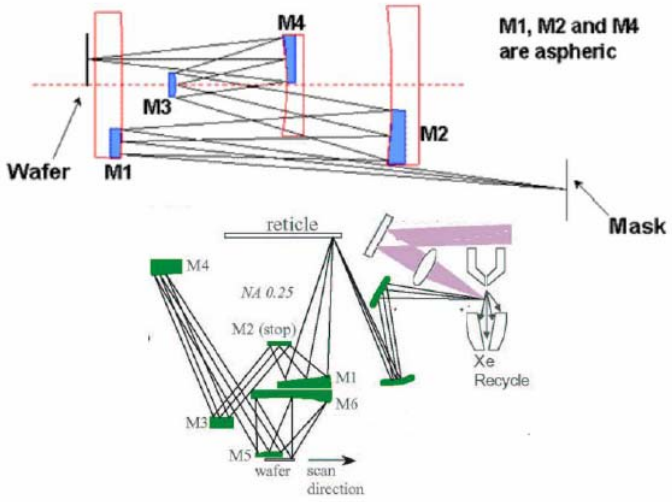

EUV light (< 100nm) is absorbed by almost all materials -> No lens.

Laser Writing

	write head				
	2mm	**4mm**	**10mm**	**20mm**	**40mm**
min. structure size [µm]	0.6	1.0	2.5	5.0	10.0
address resolution [nm]	20	40	100	200	400
writing speed [mm²/min]	1.5	5.7	36	119	416
line width uniformity, 3σ [nm]	80	100	220	440	880
edge roughness, 3σ [nm]	60	80	120	180	280

Two Photon Writing

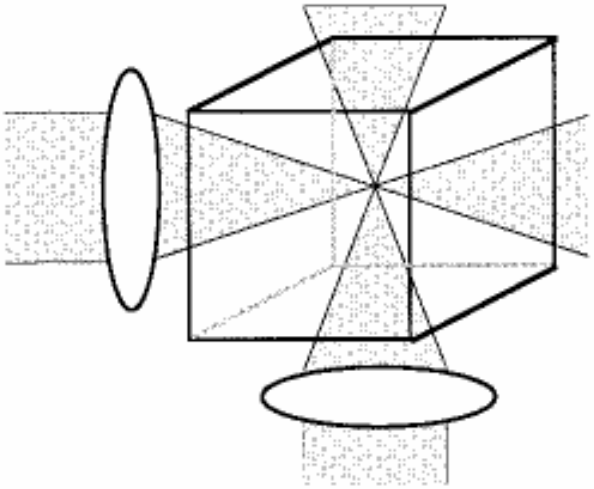

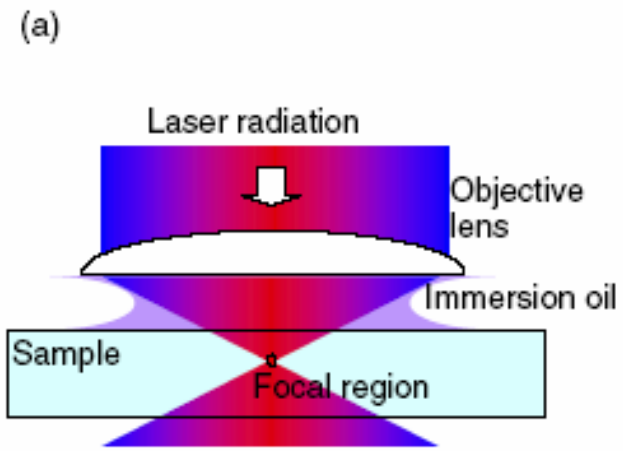

$$D(r) = w_0\sqrt{2\ln\left(\frac{I(r)}{I_{\text{th}}}\right)\frac{1}{N}},$$

$$L(z) = 2z_{\text{R}}\sqrt{\left(\frac{I(z)}{I_{\text{th}}}\right)^{\frac{1}{N}} - 1},$$

Two Photon Writing

NATURE | VOL 412 | 16 AUGUST 2001 |

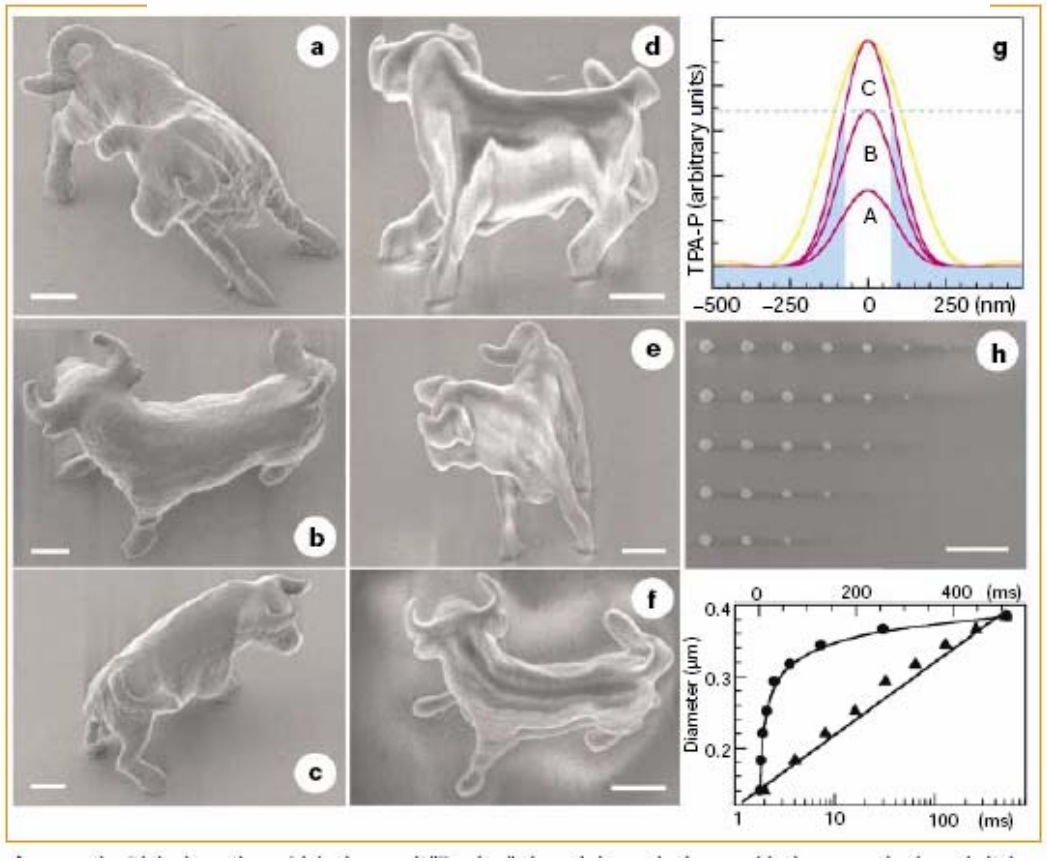

Two Photon Writing

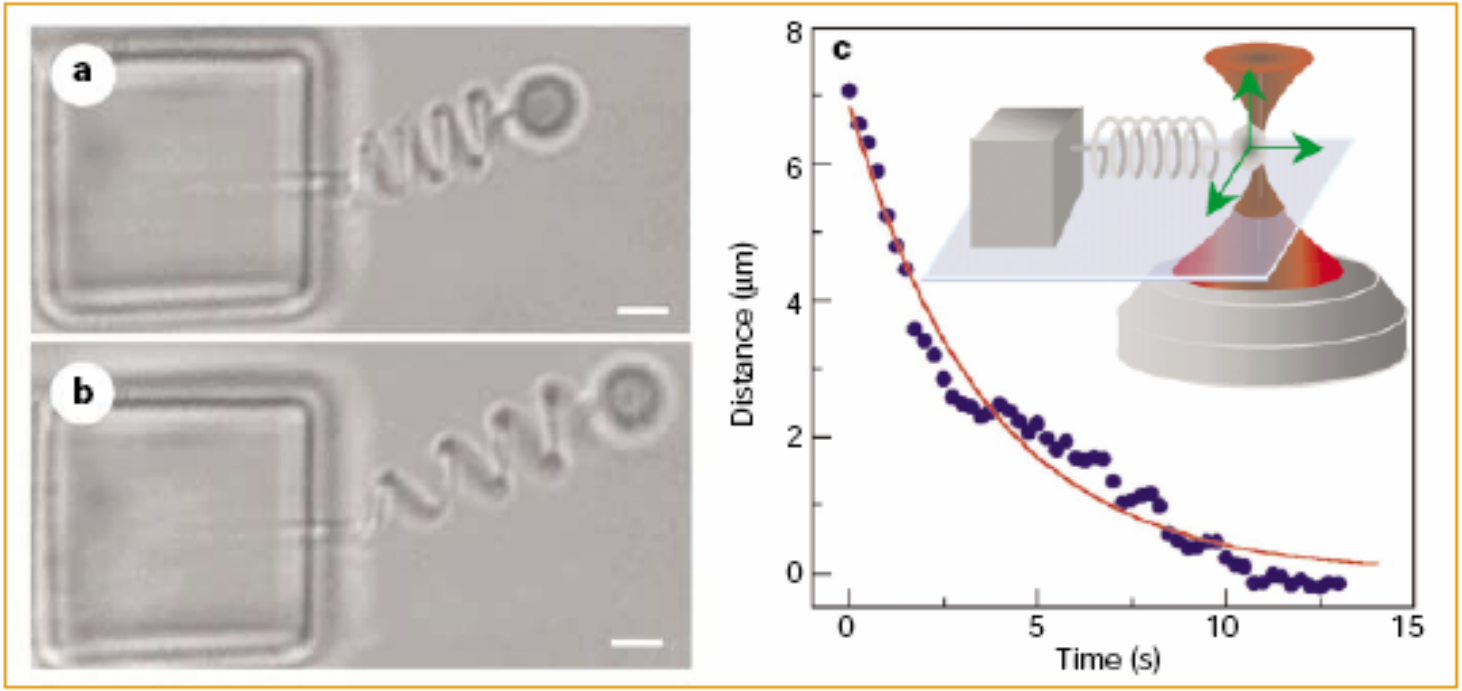

Figure 2 Functional micro-oscillator system, in which not only the spring but also the cubic anchor and the bead were produced using our two-photon absorption system. The oscillator was kept in ethanol so that the buoyancy would balance gravity and eliminate bead–substrate friction. **a**, **b**, The spring in its original (**a**) and extended (**b**) states. Scale bars, 2 μm. **c**, Restoring curve of the damping oscillation; inset, diagram showing driving of the oscillator by using laser trapping.

Interference

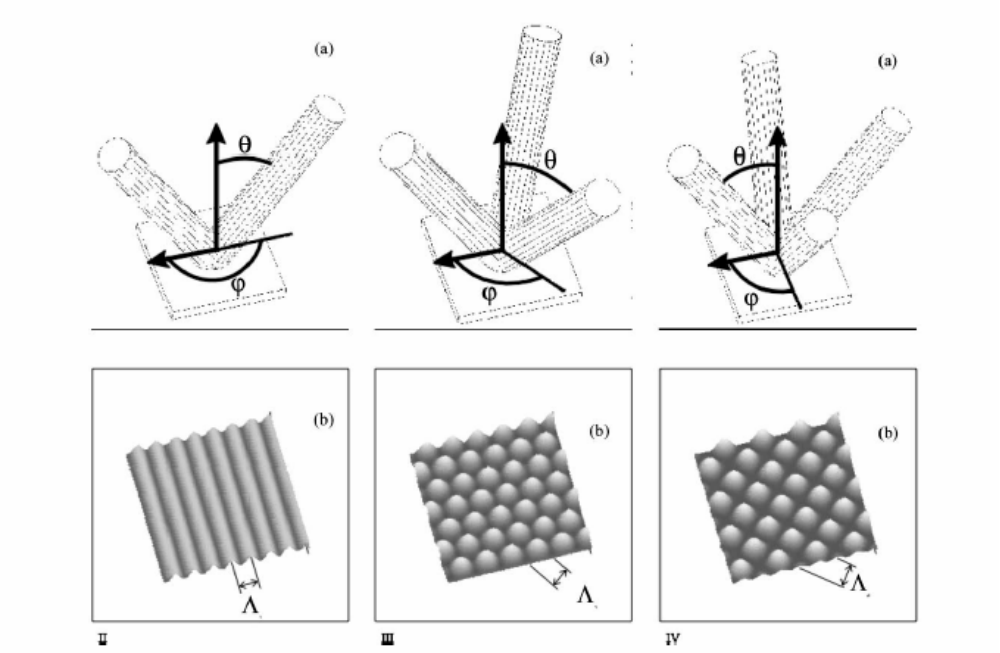

Fig. 1. The orientation of the two (left column), three (middle column) and four (right column) incident beams: (a) and the resulting interference patterns (b).

1. Two beams

$$I_2' = I_1 + I_2 + 2\cos(k(R_2 - R_1))$$

2. Three beams

$$I_3' = I_1 + I_2 + I_3 + 2[\cos(k(R_2 - R_1)) + \cos(k(R_3 - R_1)) + \cos(k(R_3 - R_2))]$$

3. Four beams

$$I_4' = I_1 + I_2 + I_3 + I_4 + 2[\cos(k(R_2 - R_1)) + \cos(k(R_3 - R_1)) + \cos(k(R_3 - R_2)) + \cos(k(R_4 - R_1)) + \cos(k(R_4 - R_2)) + \cos(k(R_4 - R_3))]$$

Interference

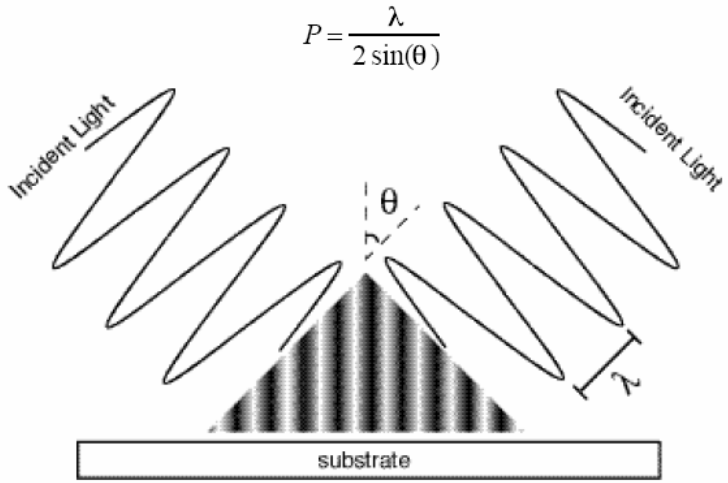

Figure 2.1: *Two-beam interference forms a standing wave.*

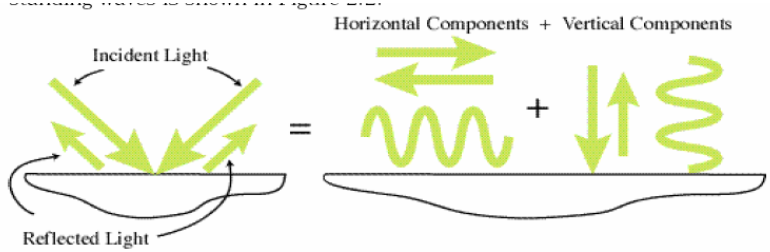

Figure 2.2: *The horizontal and vertical components combine separately to create the desired horizontal standing wave and the undesired vertical standing wave*

Interference Lithography

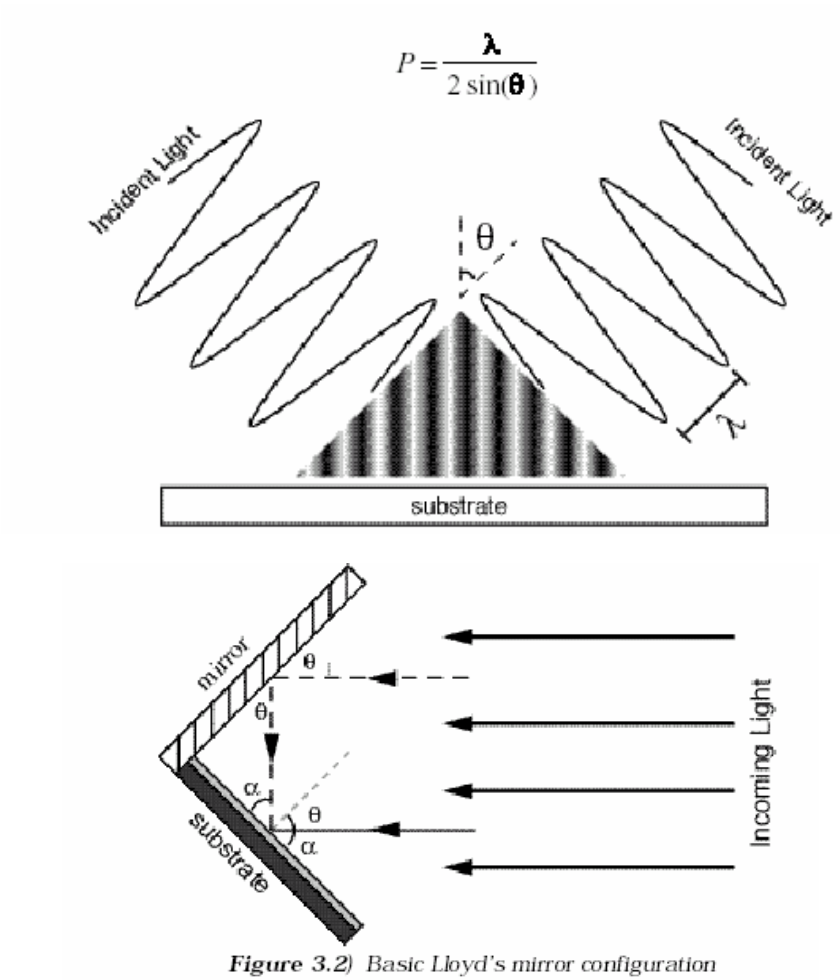

Figure 3.2) Basic Lloyd's mirror configuration

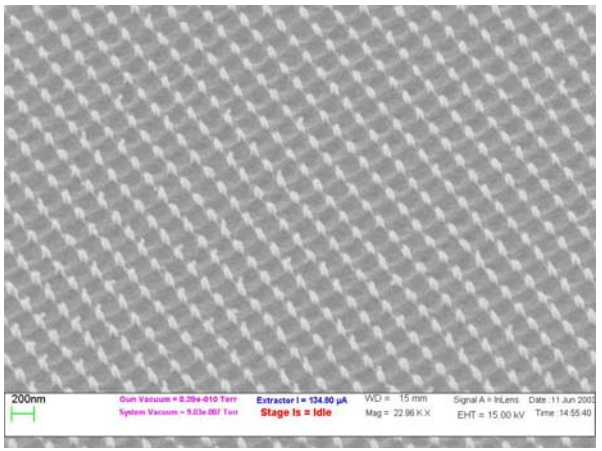

Holographic

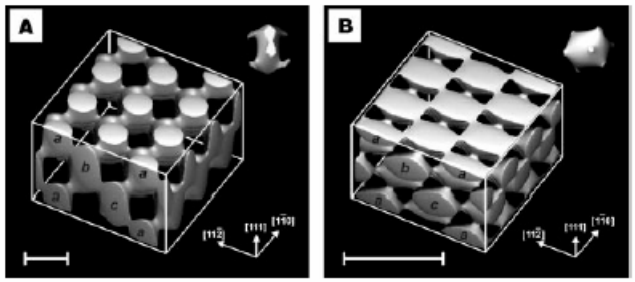

Figure 1 Calculated constant-intensity surfaces in four-beam laser interference patterns designed to produce photonic crystals for the visible spectrum from photoresist. The primitive basis (contents of a Wigner-Seitz unit cell) is shown inset in each case. **A**, f.c.c. pattern with lattice constant 922 nm, used to produce the structures shown in Fig. 3a–d and 4. The close-packed layers of the f.c.c. lattice are indicated on one side of the cube. **B**, f.c.c. pattern with lattice constant 397 nm. Scale bars, 500 nm.

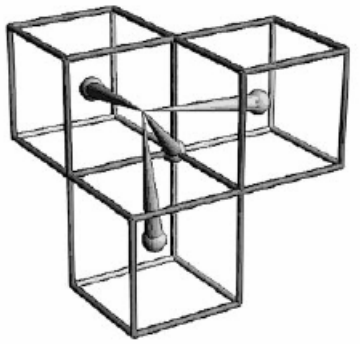

Figure 2 Beam geometry for an f.c.c. interference pattern. The wavevectors of the four laser beams are drawn as cones originating from lattice points in a b.c.c reciprocal lattice. The differences between the central beam wavevector $\mathbf{k}_0$, which originates from the common point of the three cubes shown, and the three wavevectors $\mathbf{k}_{1-3}$ originating from body-centre lattice points, are the primitive set of reciprocal lattice vectors $2\pi/d\langle\bar{1}11\rangle$.

Holographic

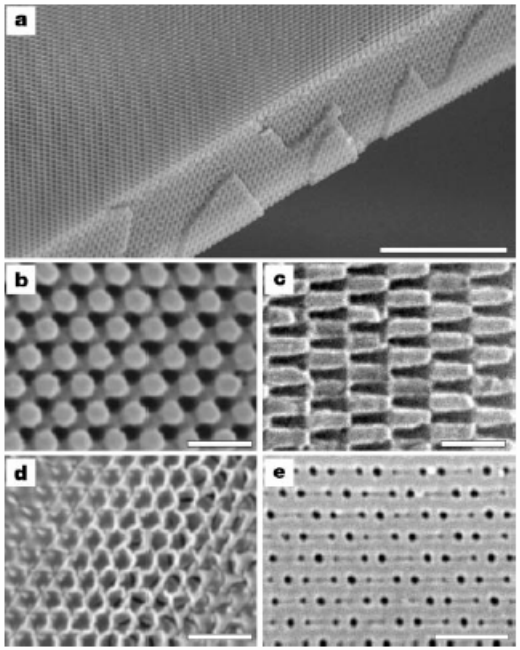

Figure 3 SEM images of photonic crystals generated by holographic lithography. **a**, Polymeric photonic crystal generated by exposure of a 10-μm film of photoresist to the interference pattern shown in Fig. 1A. The top surface is a (111) plane; the film has been fractured along the (11$\bar{1}$) cleavage planes. Scale bar, 10 μm. **b**, Close-up of a (111) surface. Scale bar, 1 μm. **c**, Close-up of a (11$\bar{1}$) surface. Scale bar, 1 μm. **d**, Inverse replica in titania made by using the polymeric structure as a template. The surface is slightly tilted from the (111) plane. Scale bar, 1 μm. **e**, ($\bar{1}$02) surface of a b.c.c. polymeric photonic crystal. Scale bar, 1 μm.

PDMS

Table 1. Physical and Chemical Properties of PDMS

property	characteristic	consequence
optical	transparent; UV cutoff, 240 nm	optical detection from 240 to 1100 nm
electrical	insulating; breakdown voltage, 2×10^7 V/m [71]	allows embedded circuits; intentional breakdown to open connections[43]
mechanical	elastomeric; tunable Young's modulus, typical value of ~750 kPa [24]	conforms to surfaces; allows actuation by reversible deformation;[24] facilitates release from molds
thermal	insulating; thermal conductivity, 0.2 W/(m·K); coefficient of thermal expansion, 310 μm/(m·°C)[71]	can be used to insulate heated solutions;[64] does not allow dissipation of resistive heating from electrophoretic separation
interfacial	low surface free energy ~ 20 erg/ cm^2 [20]	replicas release easily from molds; can be reversibly sealed to materials
permeability	impermeable to liquid water; permeable to gases and nonpolar organic solvents	contains aqueous solutions in channels; allows gas transport through the bulk material; incompatible with many organic solvents
reactivity	inert; can be oxidized by exposure to a plasma; $Bu_4N^+F^-$((TBA)F)	unreactive toward most reagents; surface can be etched; can be modified to be hydrophilic and also reactive toward silanes;[20] etching with (TBA)F can alter topography of surfaces[59]
toxicity	nontoxic.	can be implanted in vivo; supports mammalian cell growth[57,59]

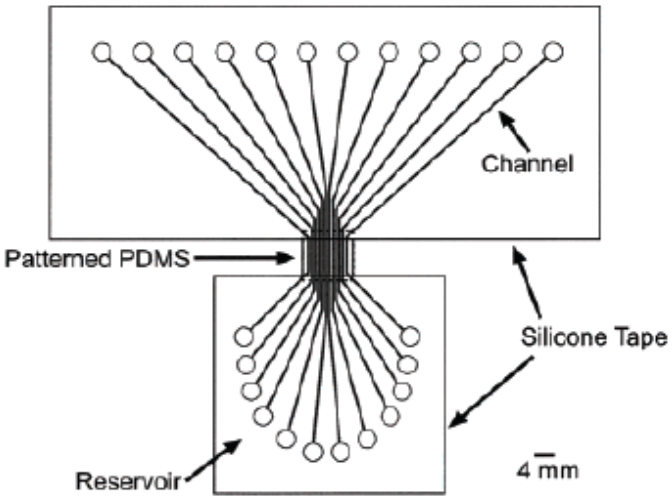

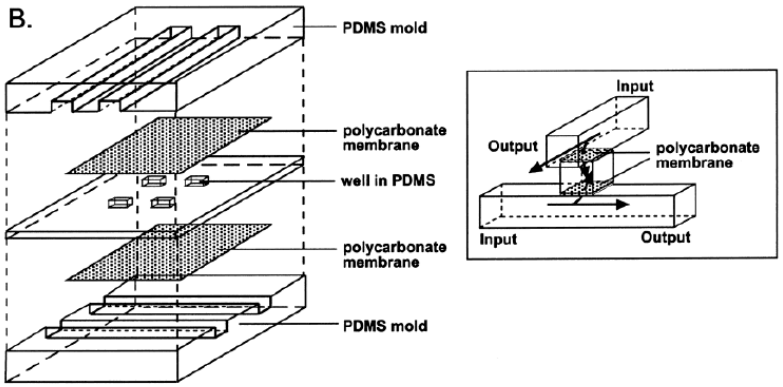

Solvent Compatibility of Poly(dimethylsiloxane)-Based Microfluidic Devices

Anal. Chem. **2003,** *75,* 6544−6554

solvent	δ^a	S^b	μ (D)
perfluorotributylamine	5.6	1.00	0.0
perfluorodecalin	6.6	1.00	0.0
pentane	7.1	1.44	0.0
poly(dimethylsiloxane)	7.3	∞	0.6−0.9
diisopropylamine	7.3	2.13	1.2
hexanes	7.3	1.35	0.0
n-heptane	7.4	1.34	0.0
triethylamine	7.5	1.58	0.7
ether	7.5	1.38	1.1
cyclohexane	8.2	1.33	0.0
trichloroethylene	9.2	1.34	0.9
dimethoxyethane (DME)	8.8	1.32	1.6
xylenes	8.9	1.41	0.3
toluene	8.9	1.31	0.4
ethyl acetate	9.0	1.18	1.8
benzene	9.2	1.28	0.0
chloroform	9.2	1.39	1.0
2-butanone	9.3	1.21	2.8
tetrahydrofuran (THF)	9.3	1.38	1.7
dimethyl carbonate	9.5	1.03	0.9
chlorobenzene	9.5	1.22	1.7
methylene chloride	9.9	1.22	1.6
acetone	9.9	1.06	2.9
dioxane	10.0	1.16	0.5
pyridine	10.6	1.06	2.2
N-methylpyrrolidone (NMP)	11.1	1.03	3.8
tert-butyl alcohol	10.6	1.21	1.6
acetonitrile	11.9	1.01	4.0
1-propanol	11.9	1.09	1.6
phenol	12.0	1.01	1.2
dimethylformamide (DMF)	12.1	1.02	3.8
nitromethane	12.6	1.00	3.5
ethyl alcohol	12.7	1.04	1.7
dimethyl sulfoxide (DMSO)	13.0	1.00	4.0
propylene carbonate	13.3	1.01	4.8
methanol	14.5	1.02	1.7
ethylene glycol	14.6	1.00	2.3
glycerol	21.1	1.00	2.6
water	23.4	1.00	1.9

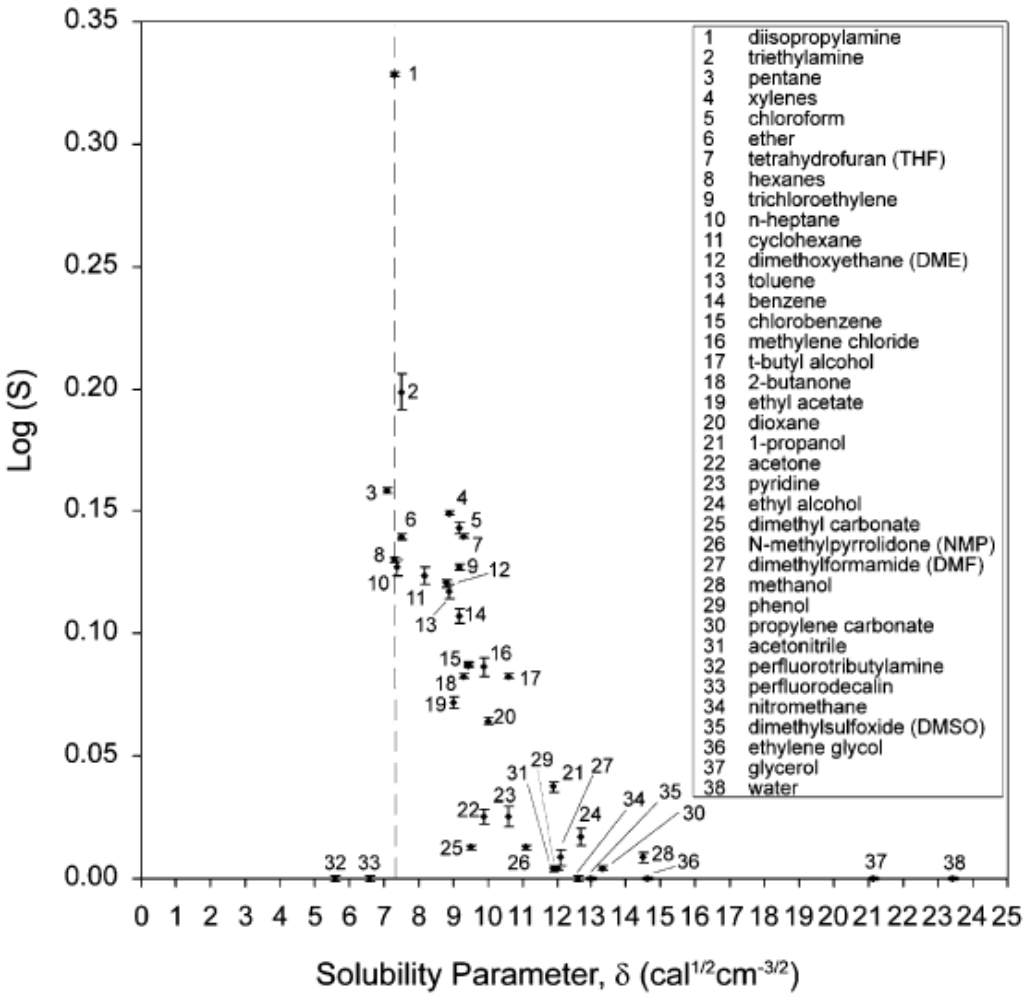

Microfluidics by Soft Lithography

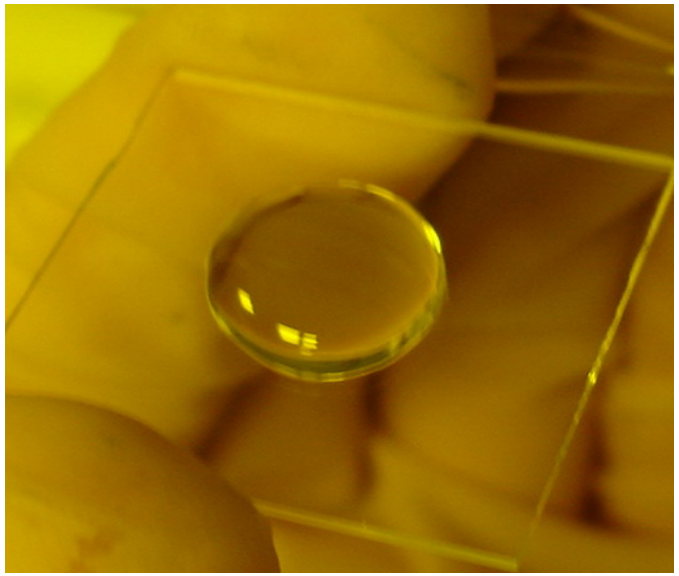

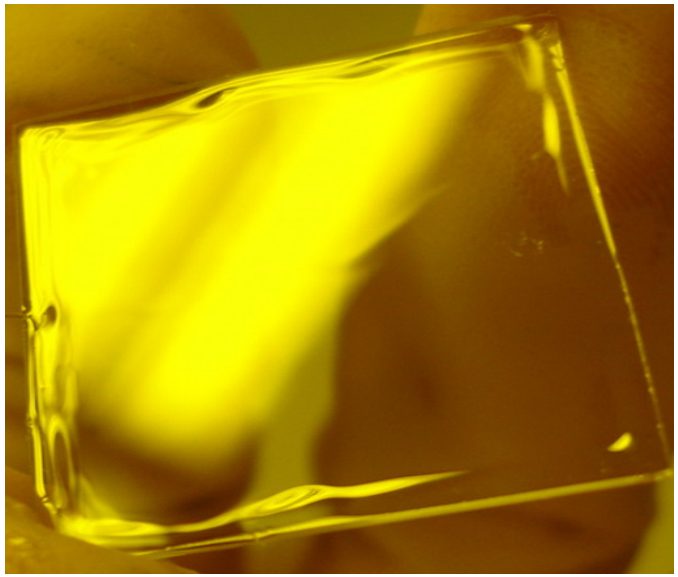

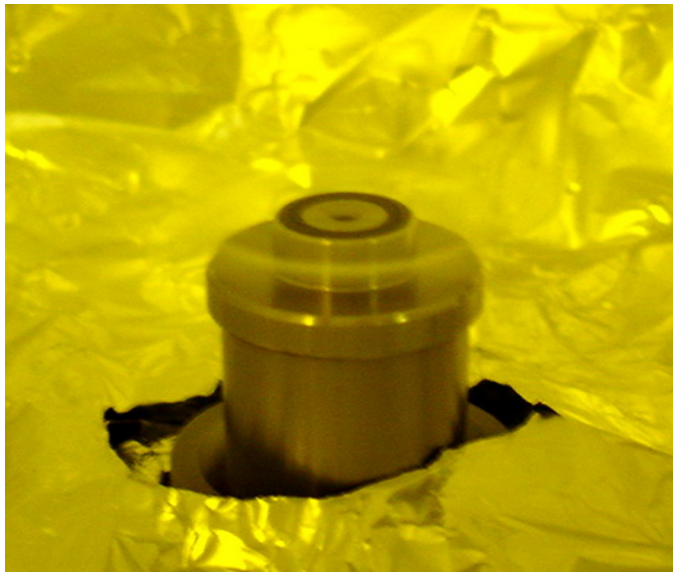

Microfluidics by Soft Lithography

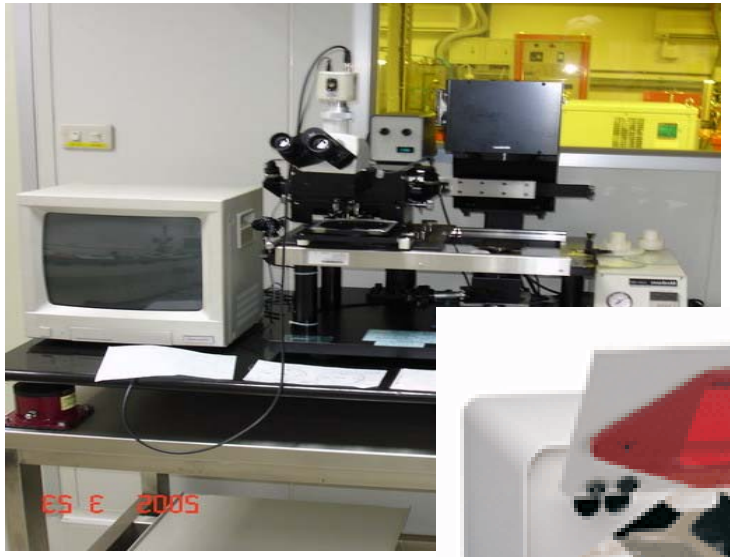

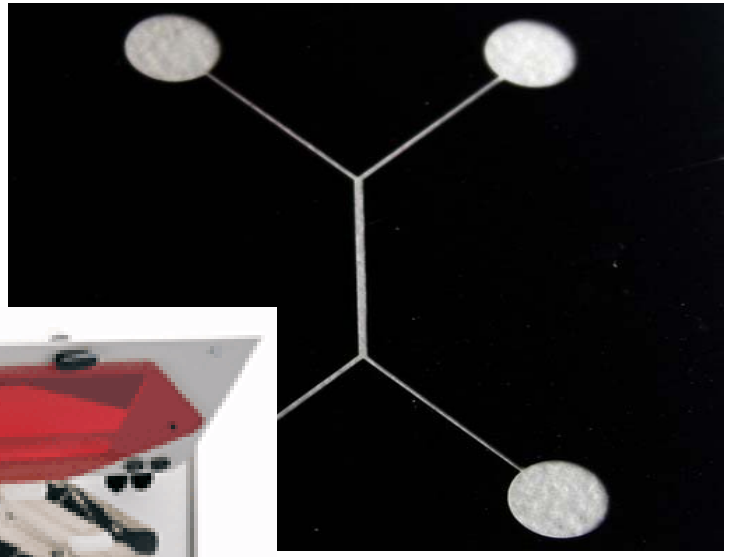

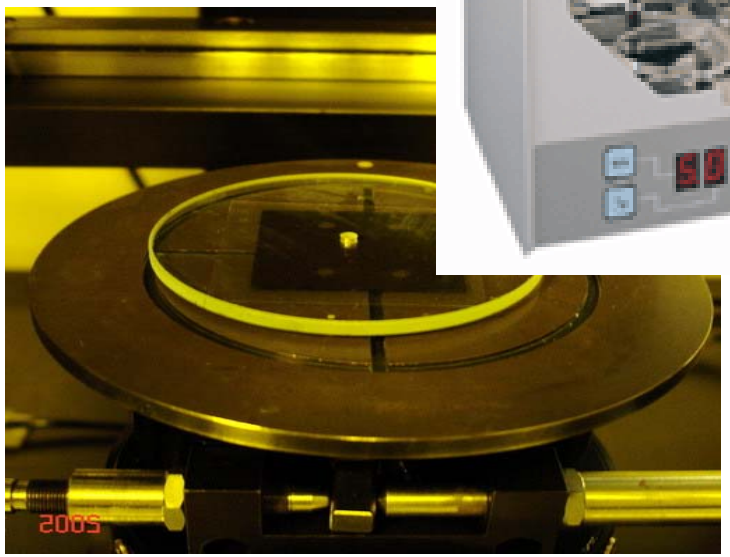

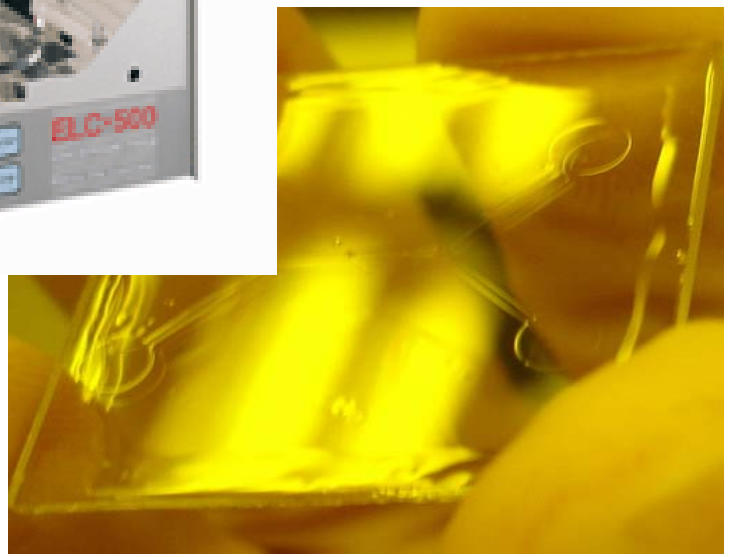

Microfluidics by Soft Lithography

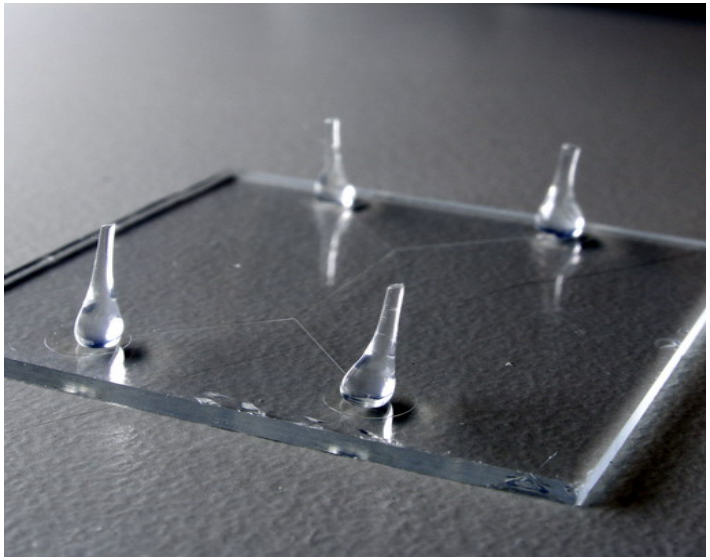

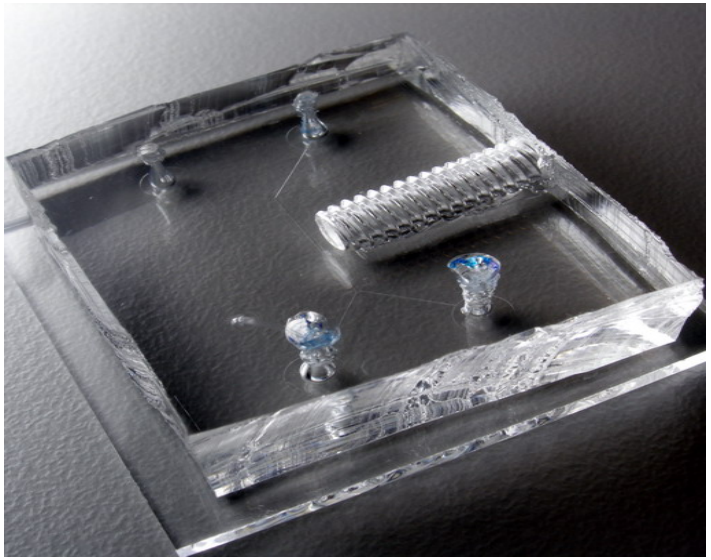

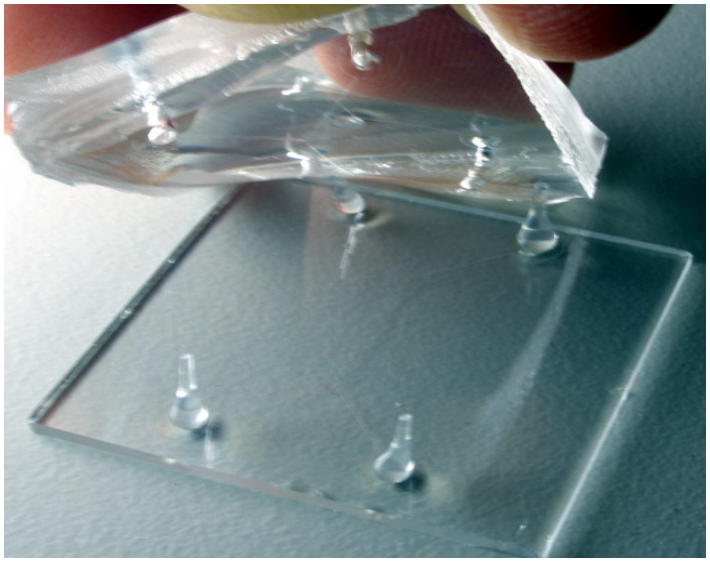

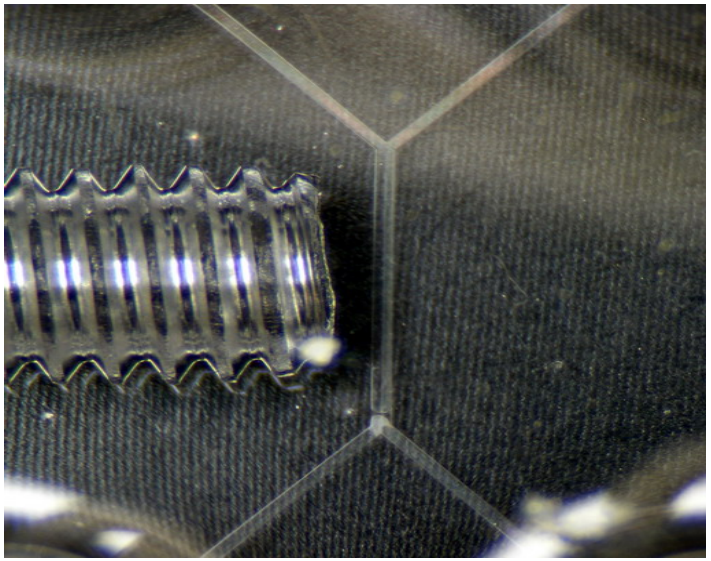

Microfluidics by Soft Lithography

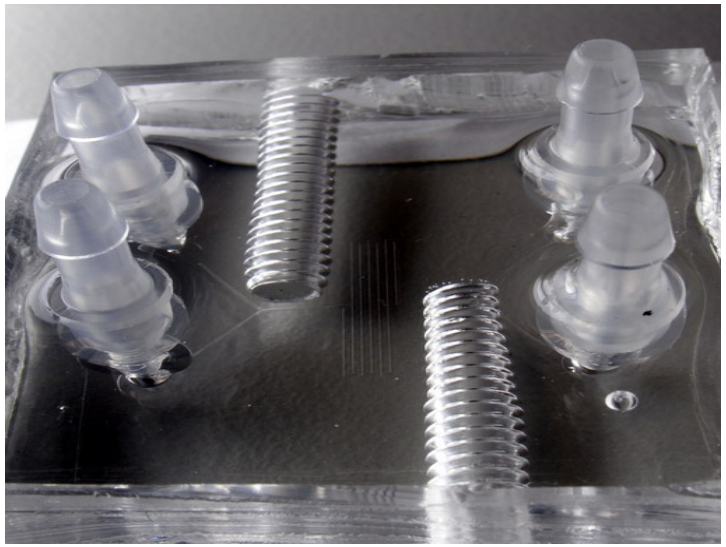

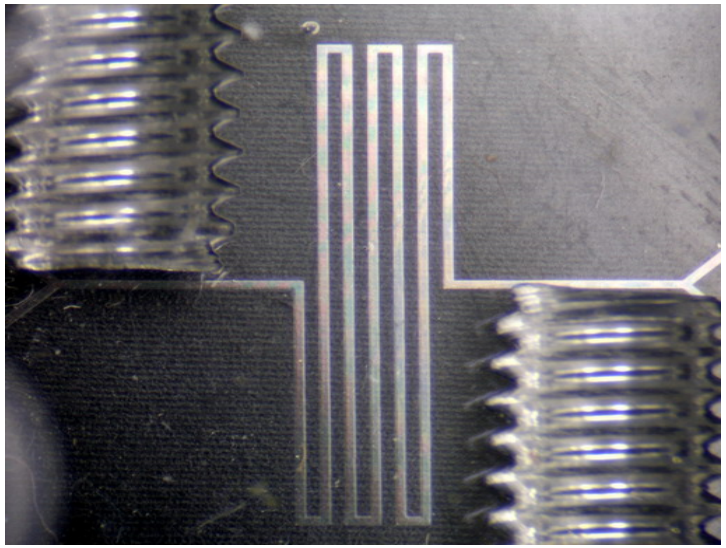

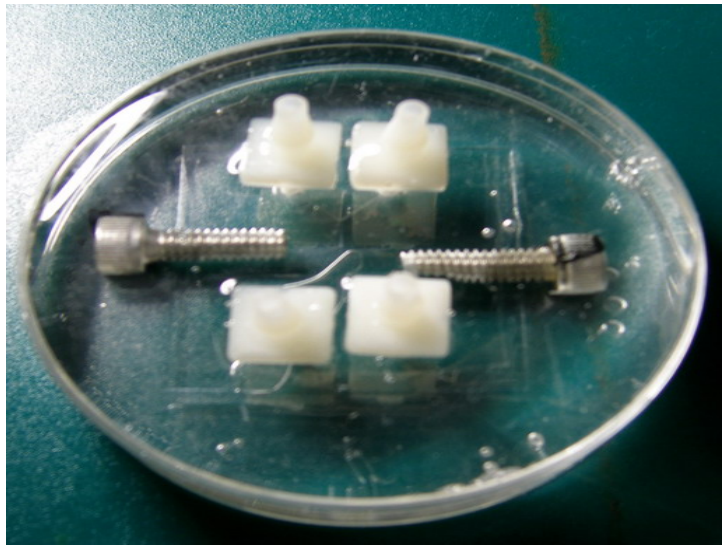

Monolithic Microfabricated Valves and Pumps by Multilayer Soft Lithography

SCIENCE VOL 288 7 APRIL 2000

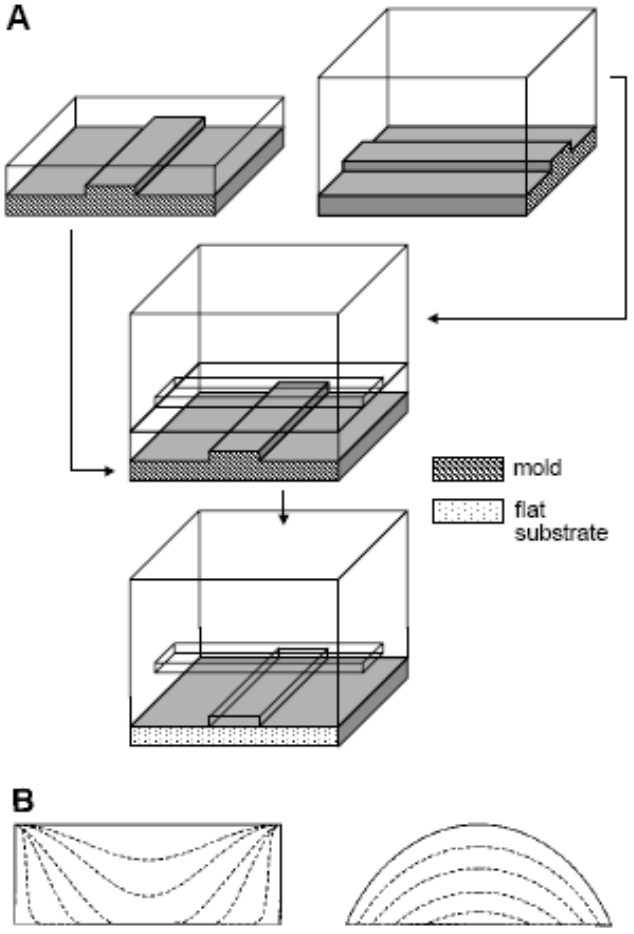

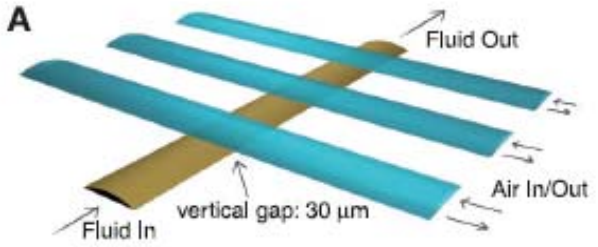

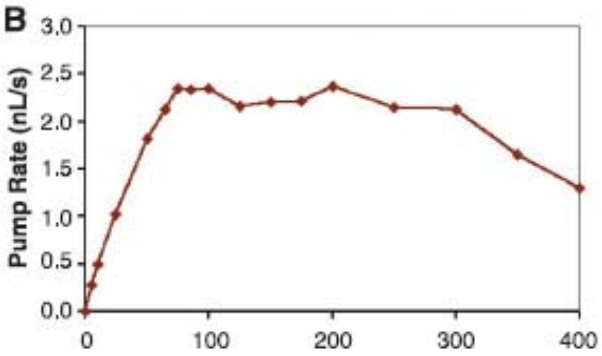

Microfluidic Large-Scale Integration

18 OCTOBER 2002 VOL 298 SCIENCE

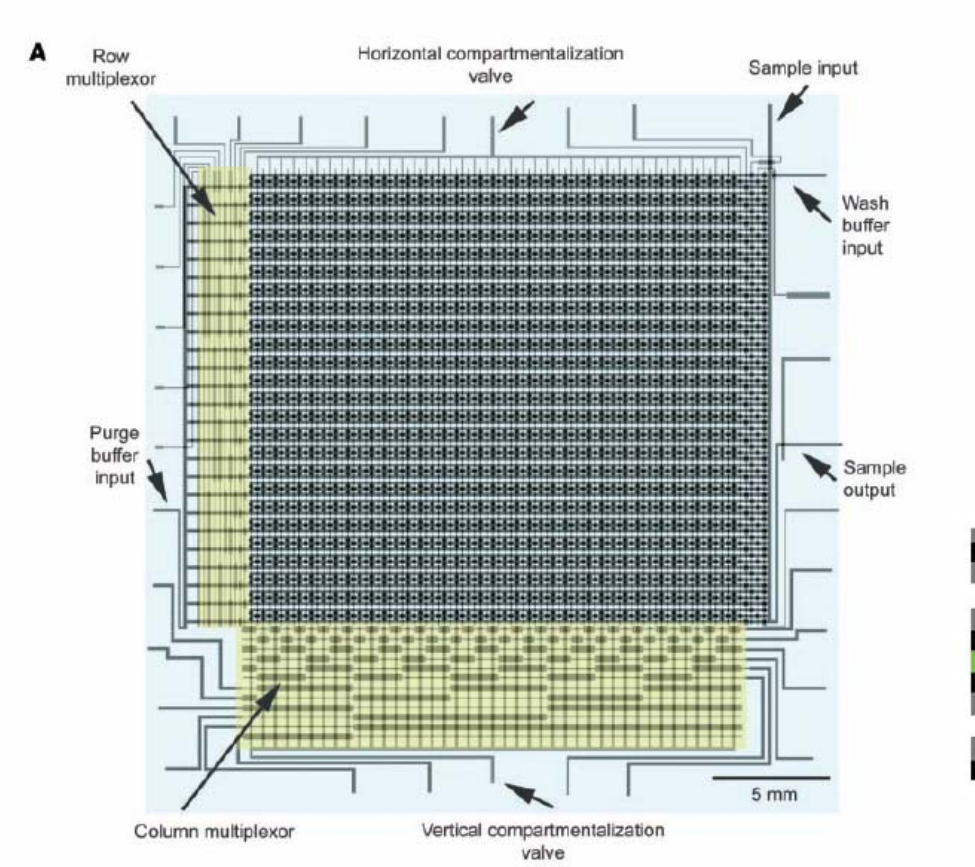

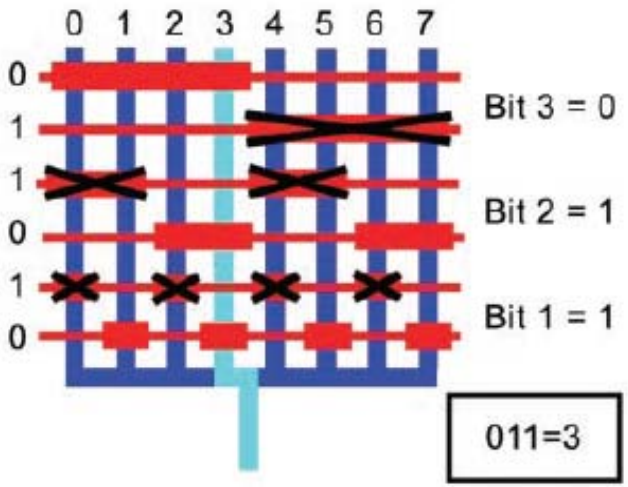

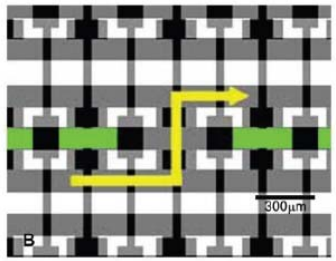

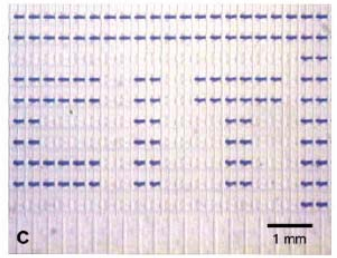

- $2 \log_2 n$ control channels.

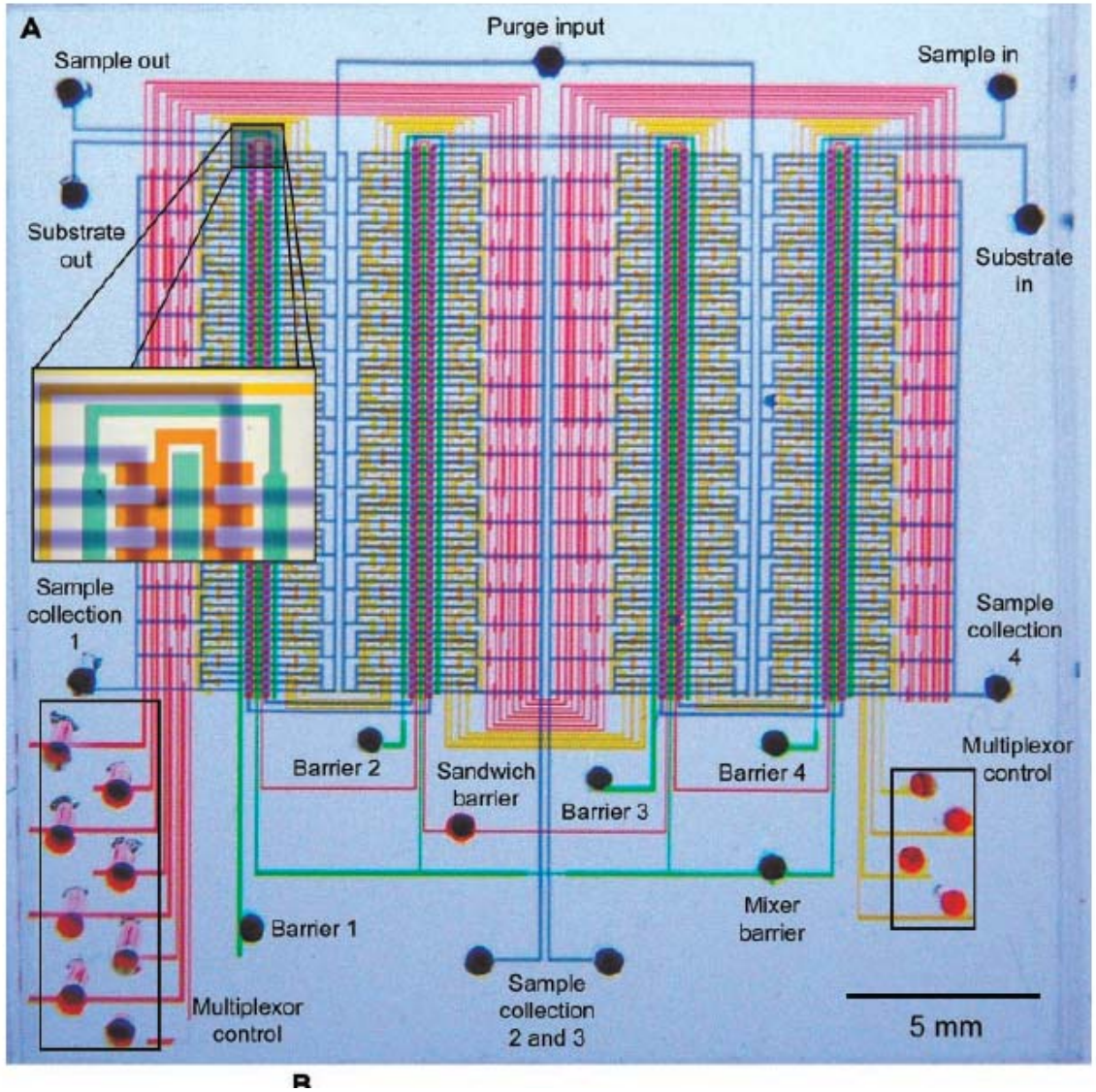
A
Purge input
Sample out
Sample in
Substrate out
Substrate in
Sample collection 1
Sample collection 4
Barrier 2
Sandwich barrier
Barrier 3
Barrier 4
Multiplexor control
Barrier 1
Mixer barrier
Multiplexor control
Sample collection 2 and 3
5 mm
B

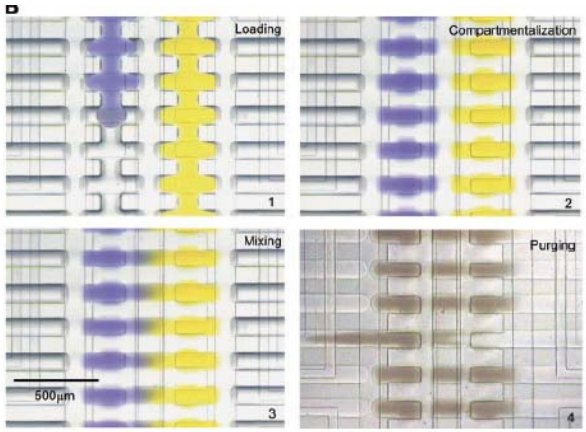
Loading
Compartmentalization
Mixing
Purging
500 µm
1
2
3
4

Microfabricated Fluidic System by Soft Lithography

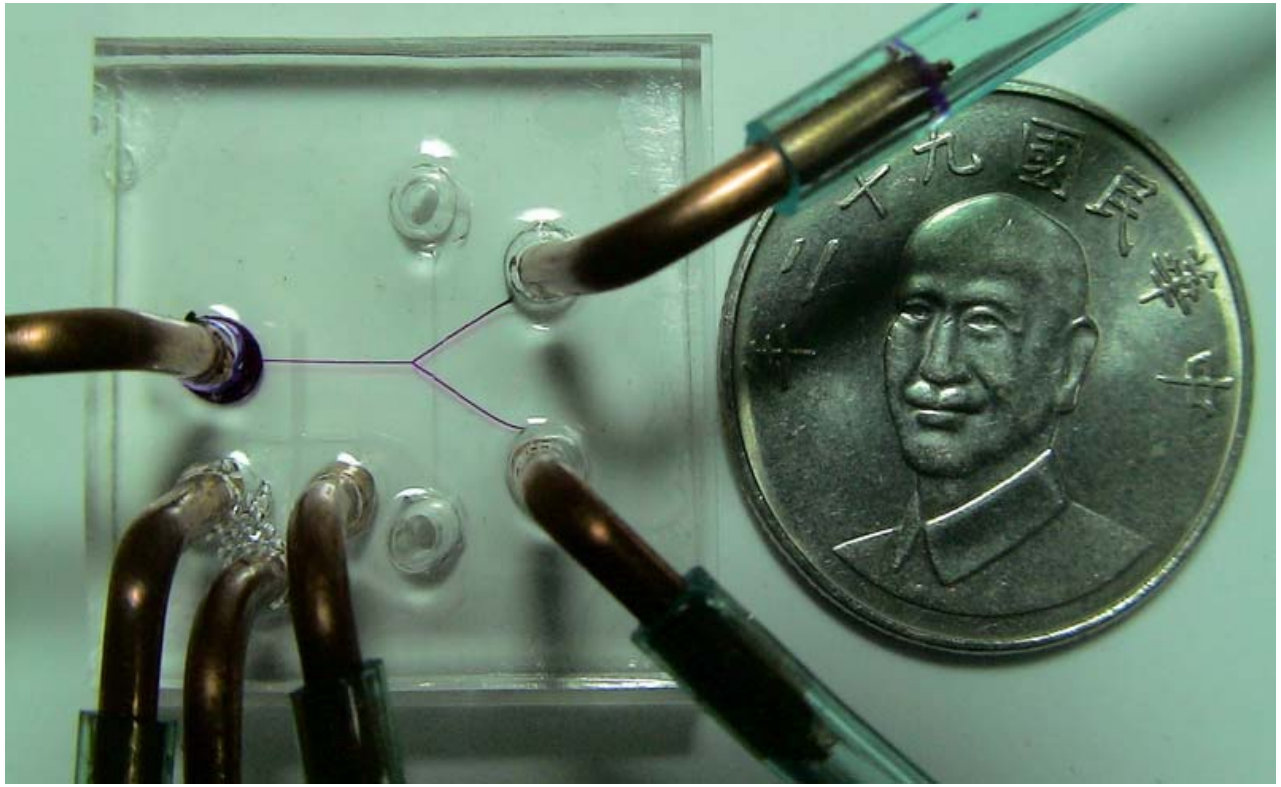

Integrated Detection System in Microchannel

fluidic channel + microlens + fiber

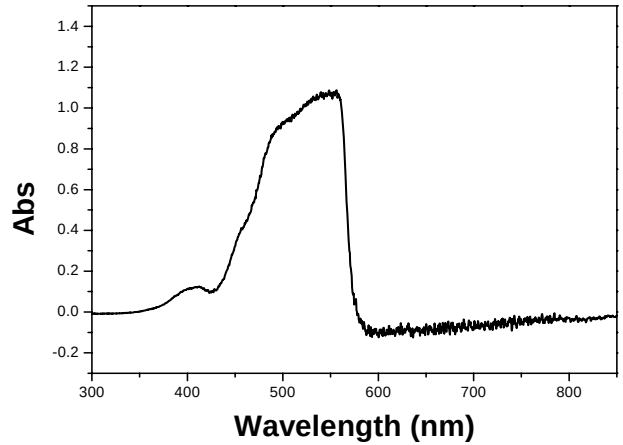

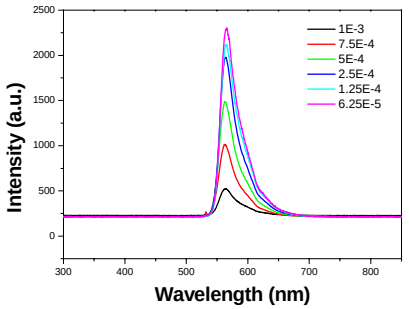

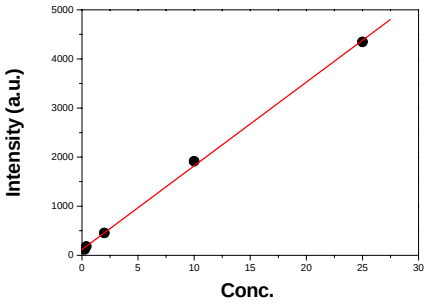

Introduction To Scanning Probe Microscopy

General features of SPM

The first scanning probe microscope was invented in 1981 by Gerd Binnig and Heinrich Rohrer at the IBM laboratory in Zurich. Since that time, a vast family of scanning probe microscopes has been spawned, a few of which are represented in this family tree. Despite the huge number of types of SPM and modes in which they can be operated, the underlying operation is the same for them all. Each different type of SPM is **characterized by the nature of the local probe and its interaction with the sample surface.**

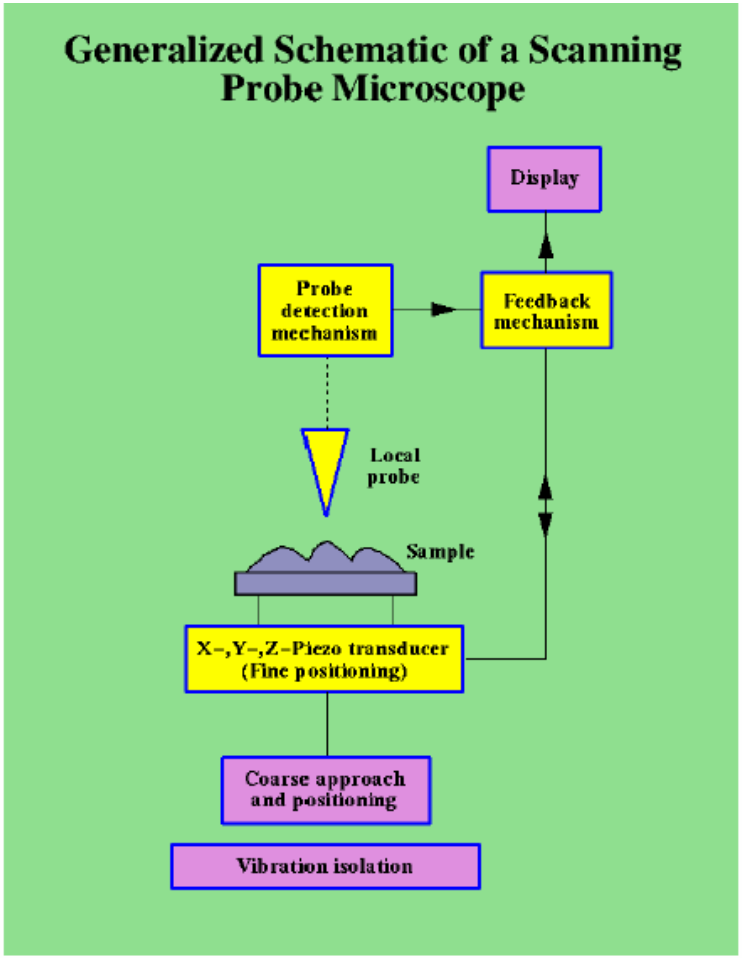

Scanning Probe Family

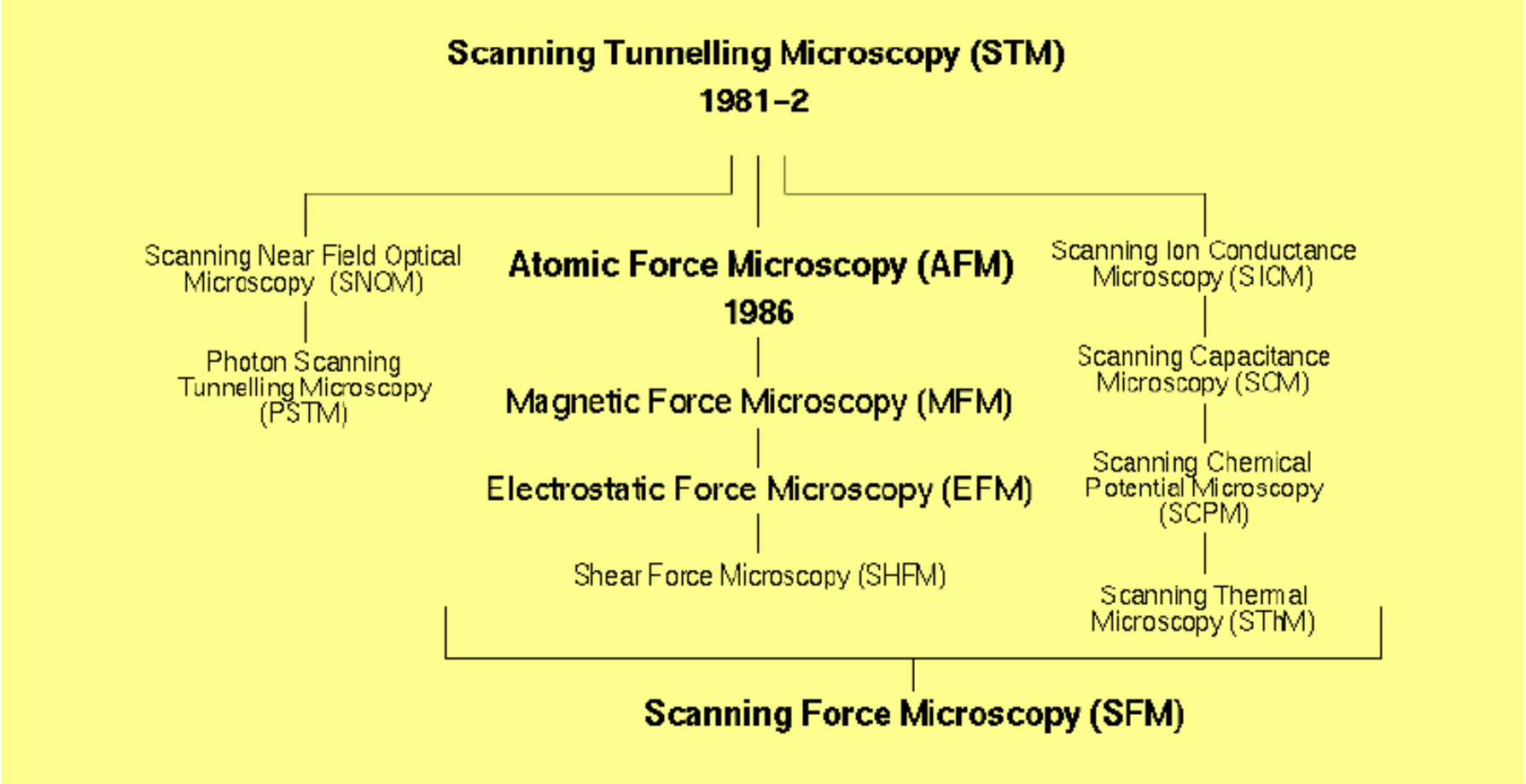

Scanning Tunneling Microscopy

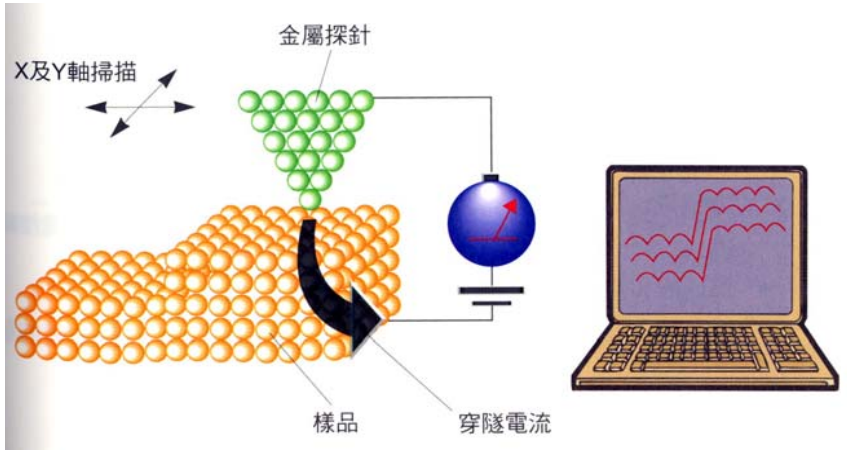

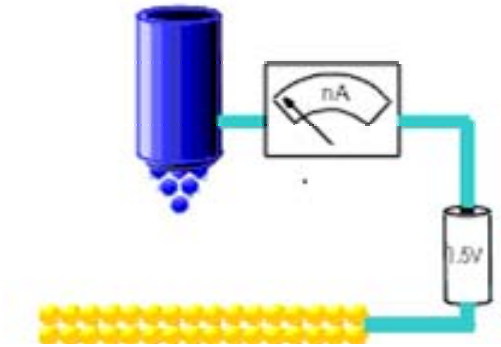

Tunneling Current

$$\Psi(d) = \Psi(0)e^{-\kappa d} \qquad \text{where} \quad \kappa = \frac{\sqrt{2m(\Phi - E)}}{\hbar}$$

$$W(d) = |\Psi(d)|^2 = |\Psi(0)|^2 e^{-2\kappa d}$$

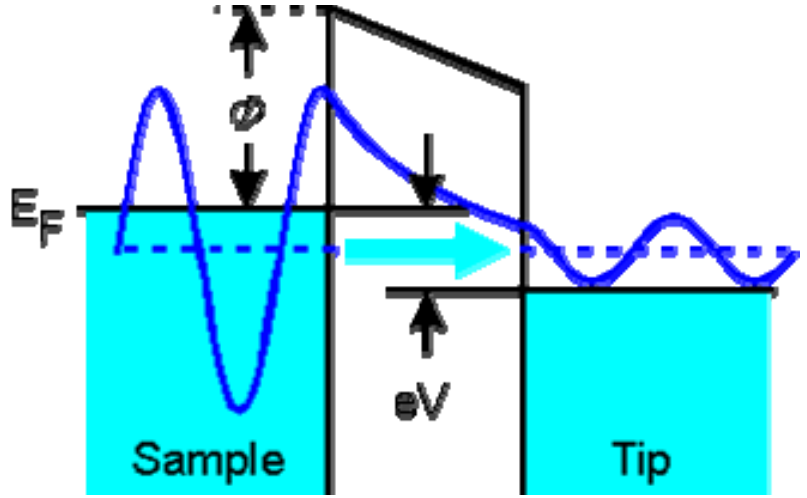

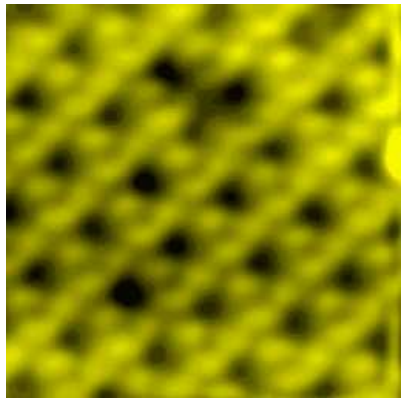

$$I \propto V\rho_{ss}(0, E_F)e^{-2\kappa d} \qquad (*)$$

$$\propto V\rho_{ss}(0, E_F)e^{-1.025\sqrt{\Phi}d} \quad \text{where} \quad [d] = \text{Å}; \; [\Phi] = \text{eV};$$

STM

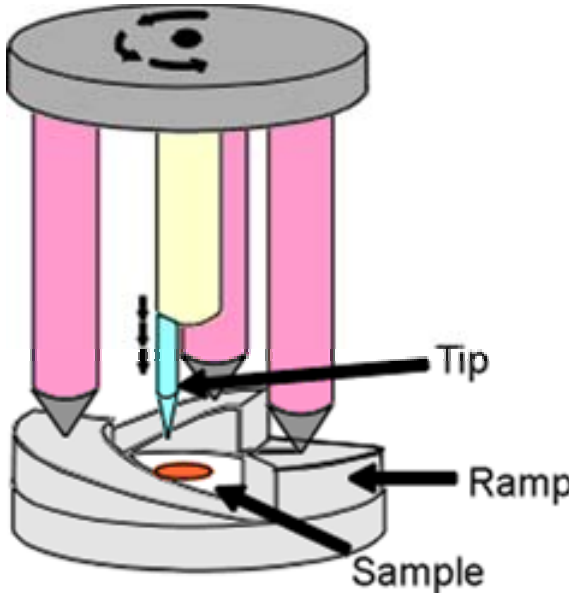
Tip
Ramp
Sample

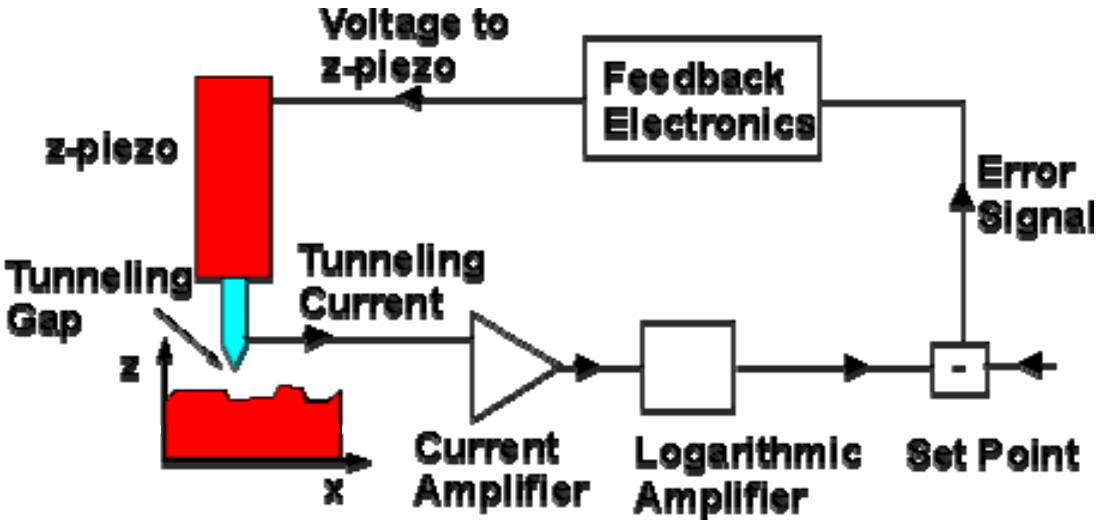
Voltage to z-piezo
Feedback Electronics
z-piezo
Error Signal
Tunneling Gap
Tunneling Current
z
x
Current Amplifier
Logarithmic Amplifier
Set Point

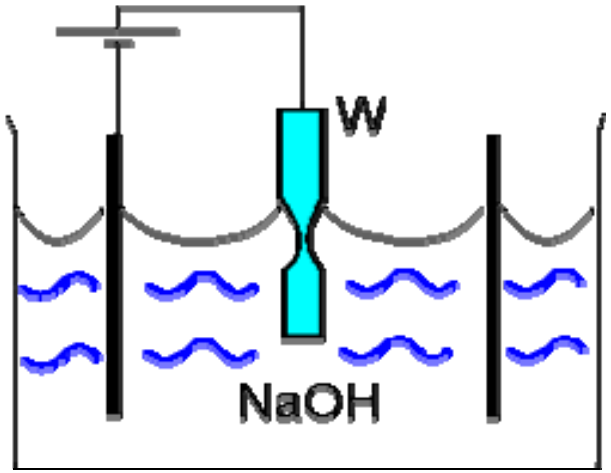
W
NaOH

STM

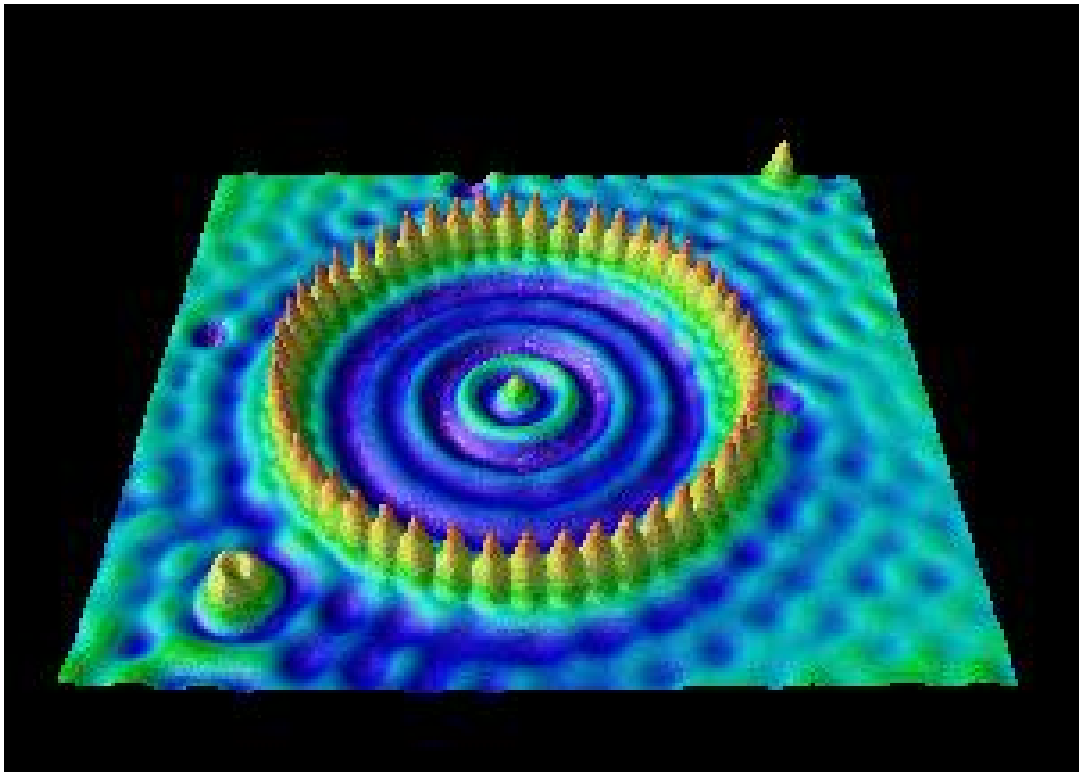

STM

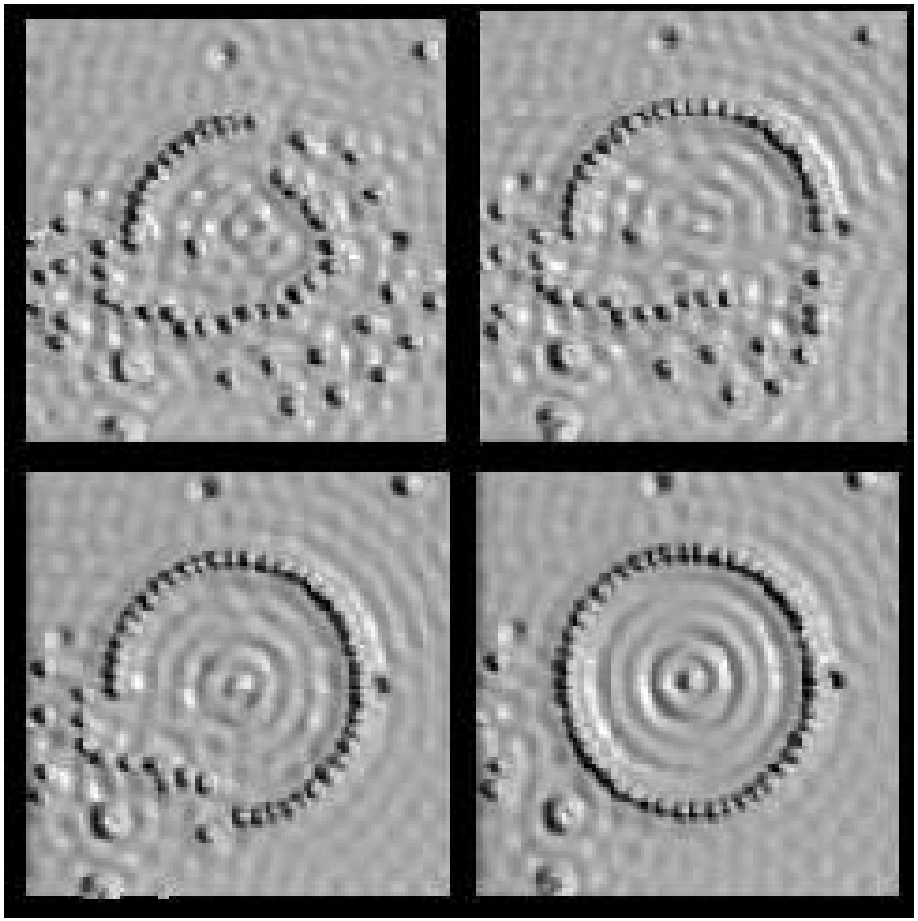

Atomic Force Microscopy

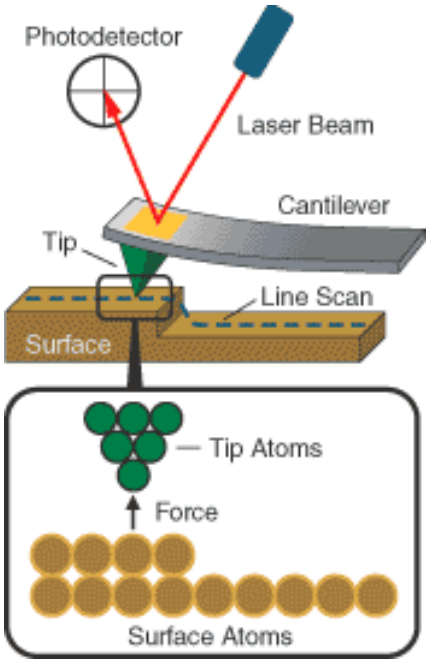

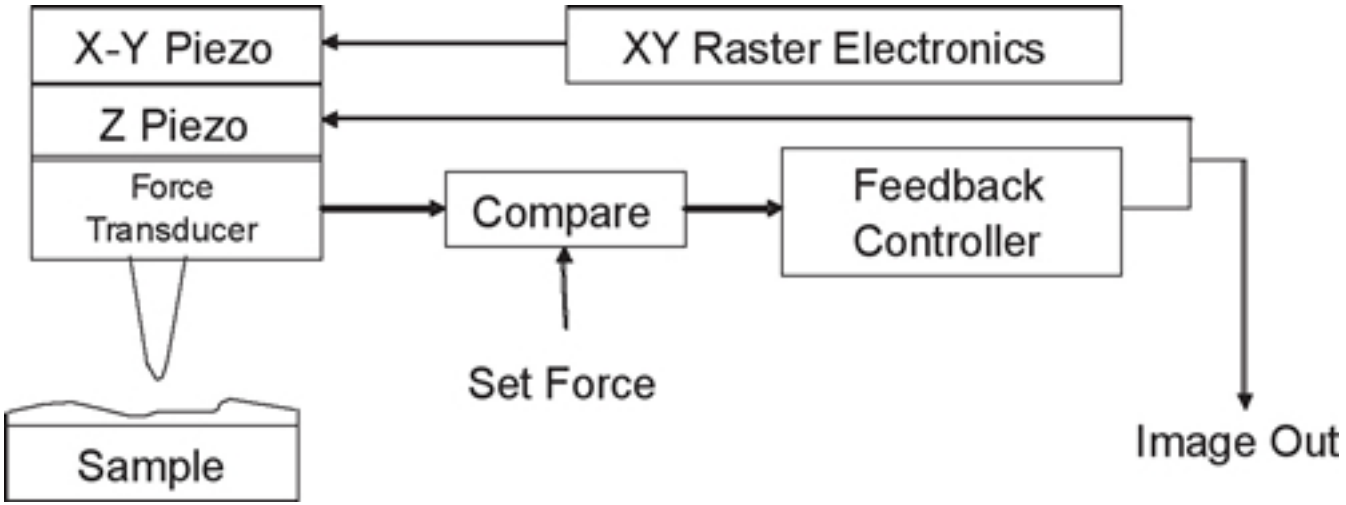
X-Y Piezo
XY Raster Electronics
Z Piezo
Force Transducer
Compare
Feedback Controller
Set Force
Image Out
Sample

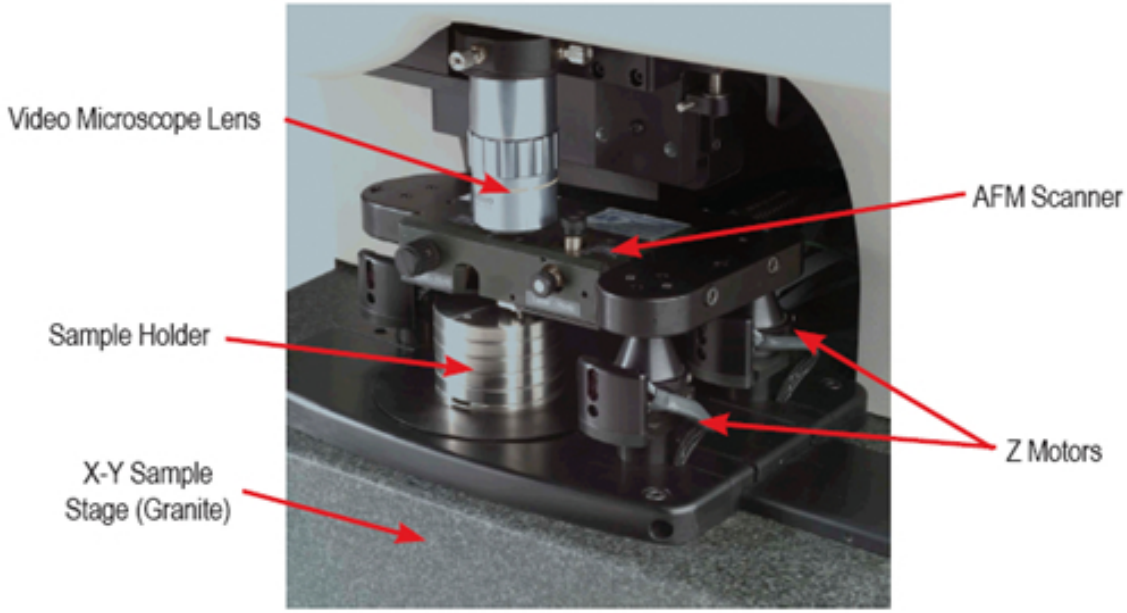
Video Microscope Lens
AFM Scanner
Sample Holder
Z Motors
X-Y Sample Stage (Granite)

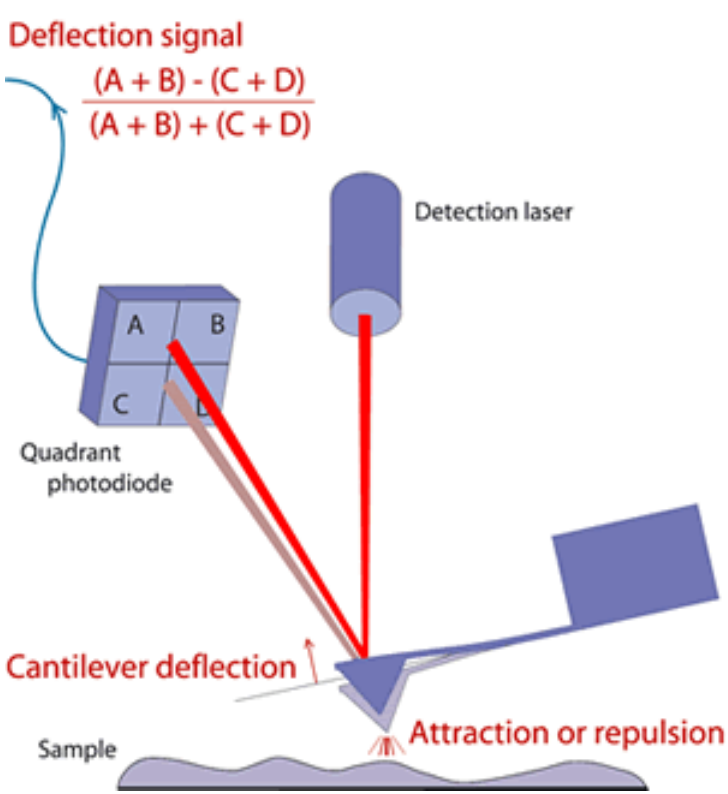
Deflection signal
(A + B) - (C + D)
(A + B) + (C + D)
Detection laser
A
B
C
D
Quadrant photodiode
Cantilever deflection
Attraction or repulsion
Sample

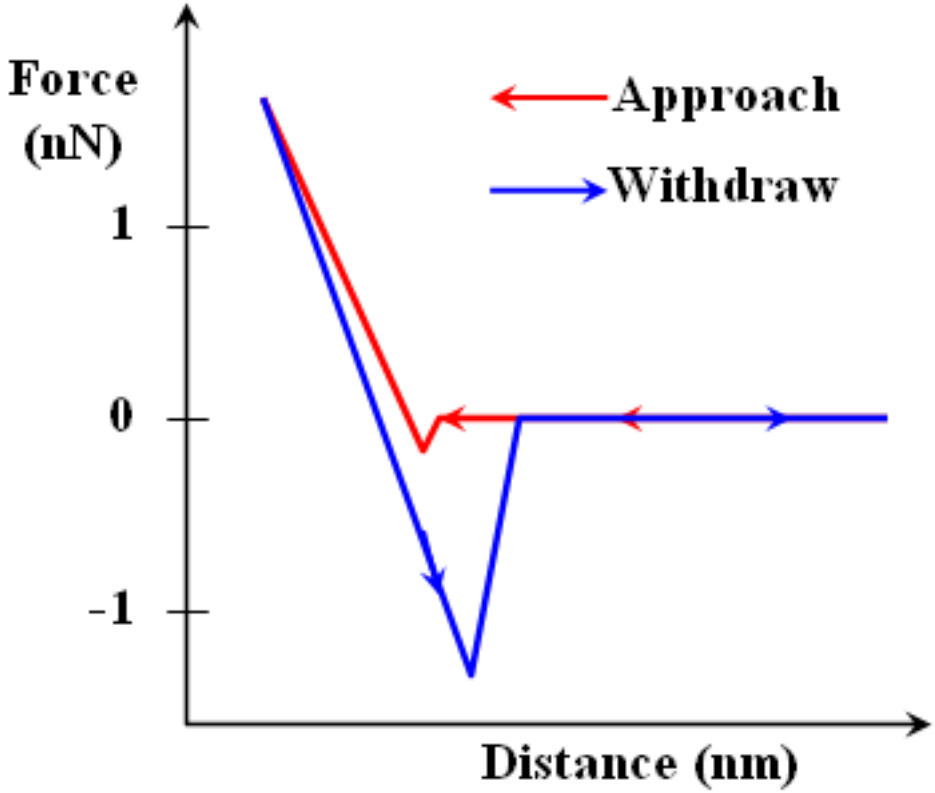
Force (nN)
1
0
-1
Approach
Withdraw
Distance (nm)

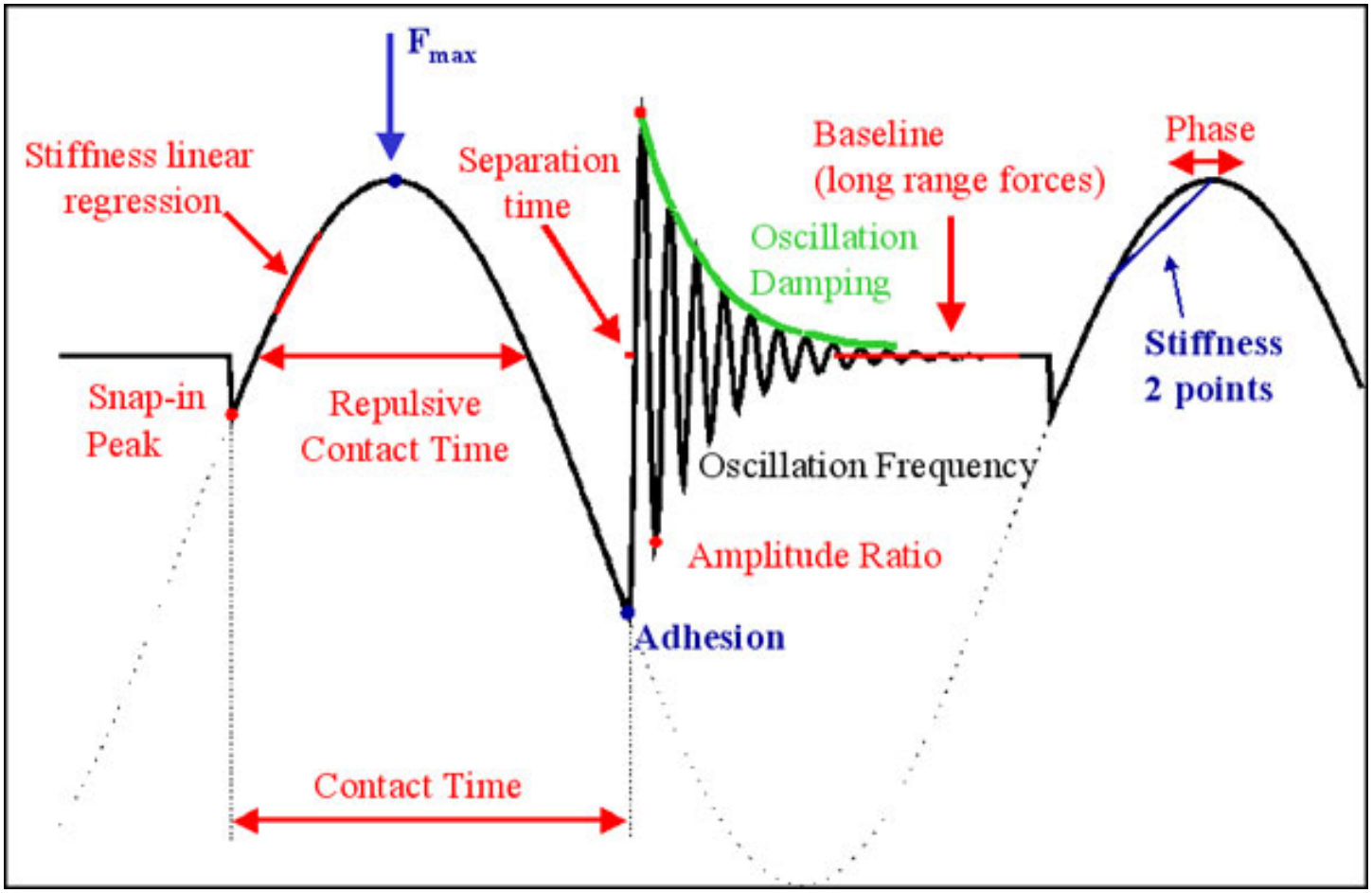
F_{max}
Stiffness linear regression
Separation time
Baseline (long range forces)
Phase
Oscillation Damping
Snap-in Peak
Repulsive Contact Time
Stiffness 2 points
Oscillation Frequency
Amplitude Ratio
Adhesion
Contact Time

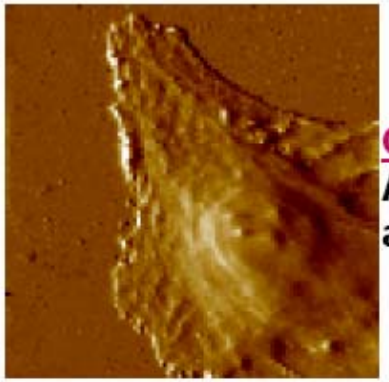

Cell surface imaging
AFM imaging of living and fixed animal cells

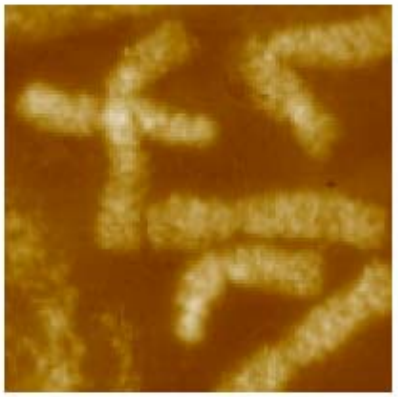

Chromosomes
A large selection of work on both human and plant chromosomes

Scanning Probe Microscope

DNA
AFM images of double-stranded DNA and of some special single-double-stranded DNA constructs

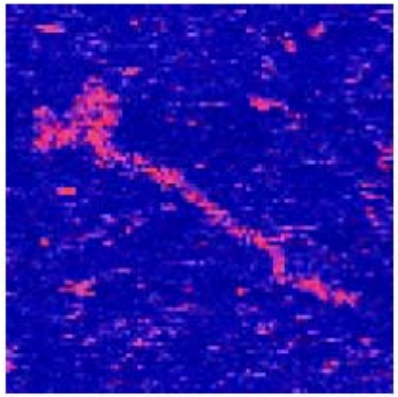

Muscle Proteins
High resolution AFM images of myosin and titin

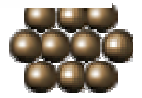

AFM Images

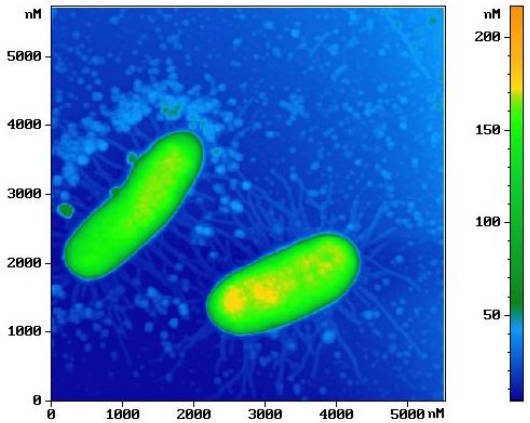

E Coli

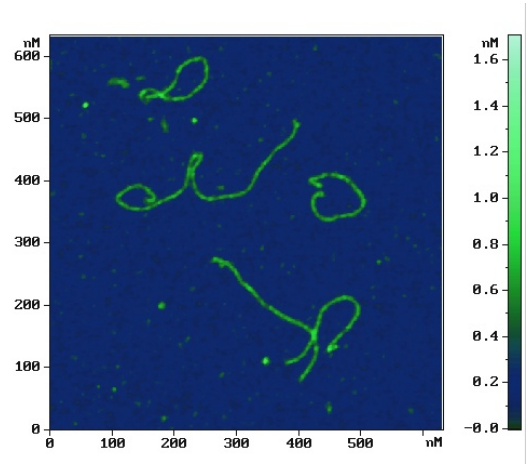

Protein

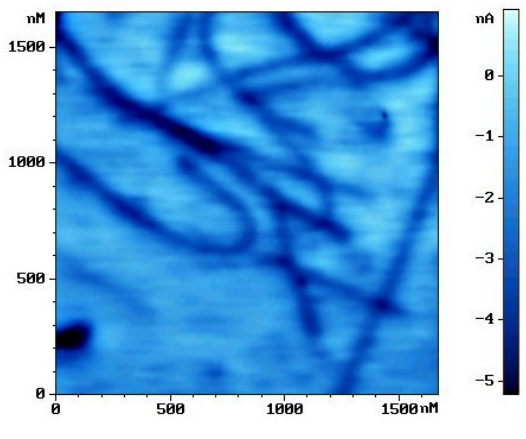

Nanotubes

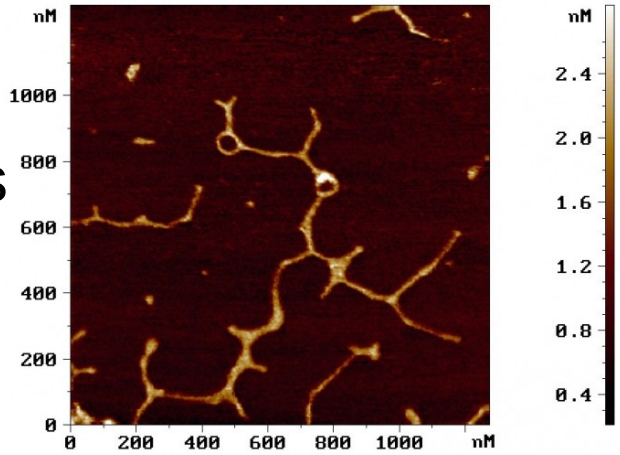

DNA

STM Lithography

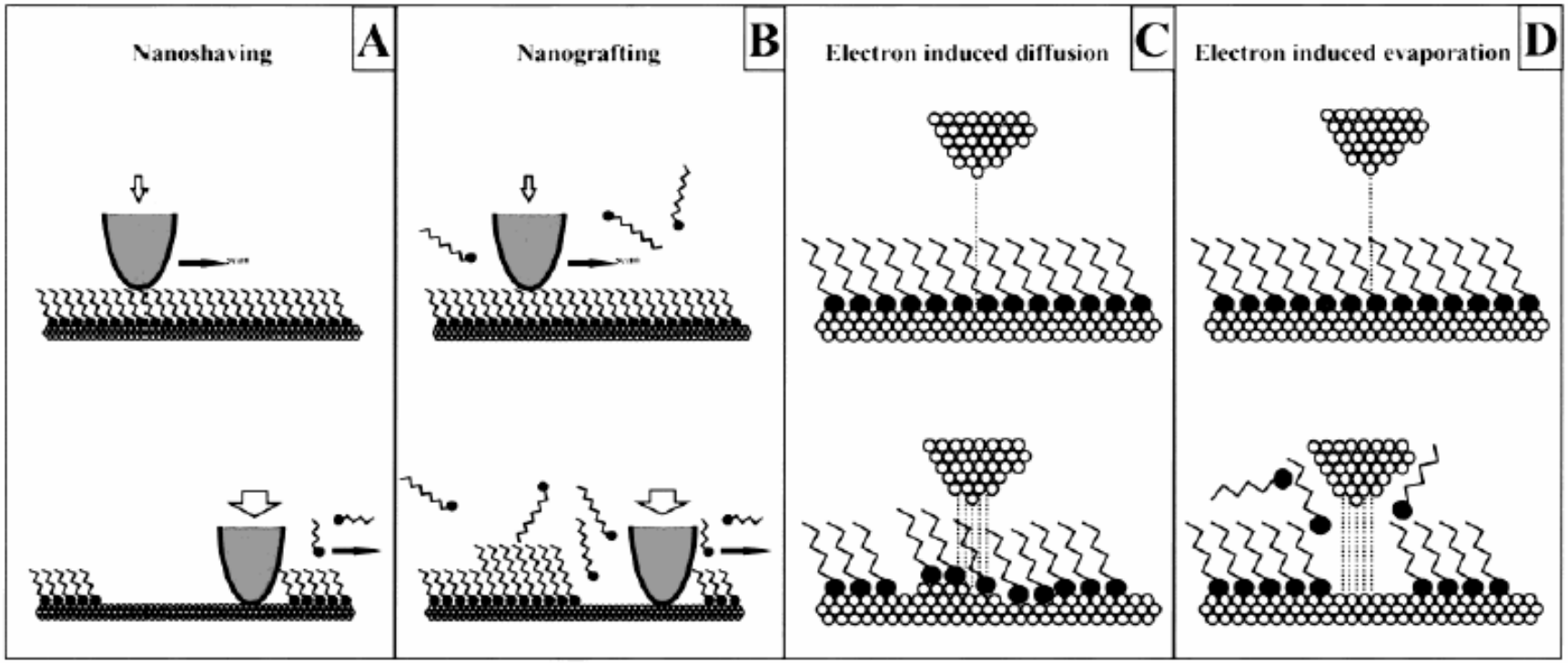

Resist: Thiol

STM Lithography

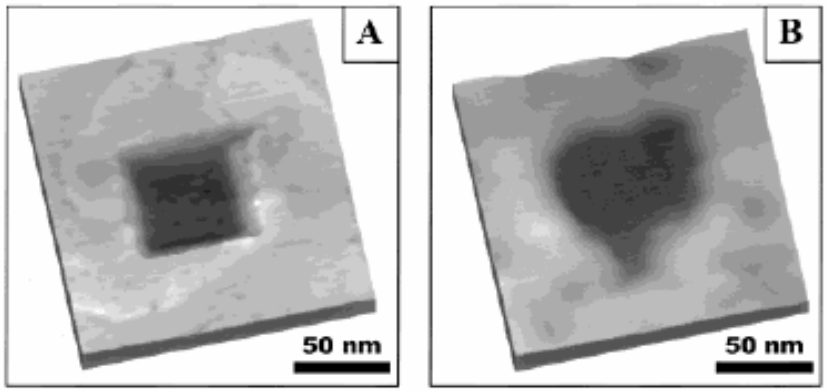

FIGURE 3. (A) 160 × 160 nm² topographic images of $C_{18}S$/Au(111) with the thiols shaved away from the central 50 × 50 nm² square. (B) 160 × 160 nm² topographic images of OTE/mica containing a heart-shaped pattern produced using nanoshaving.

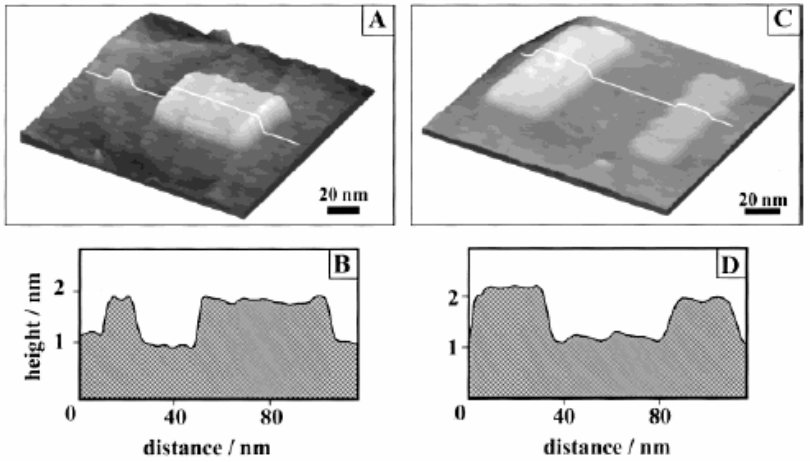

Oxidation Lithography

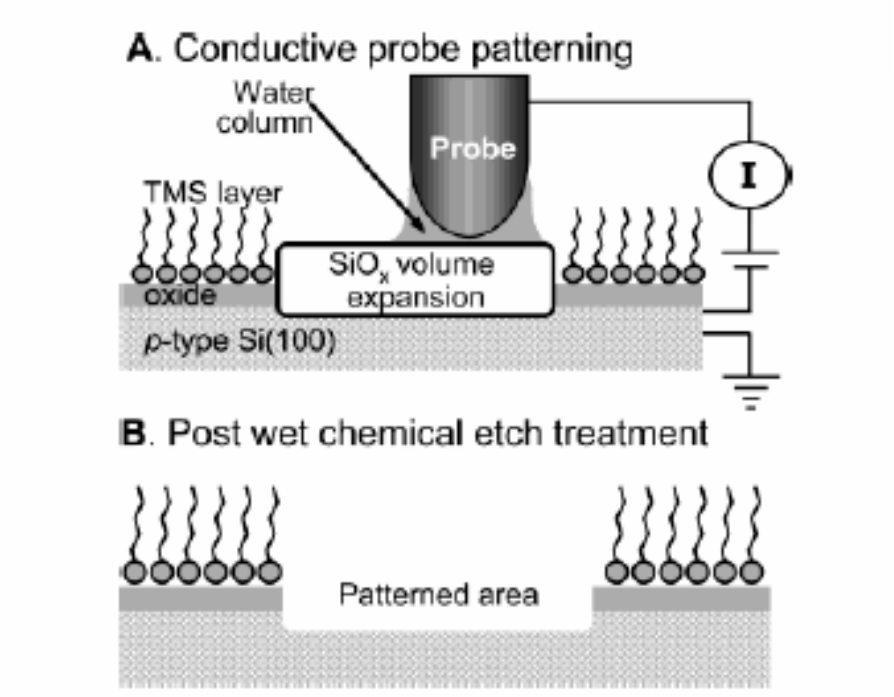

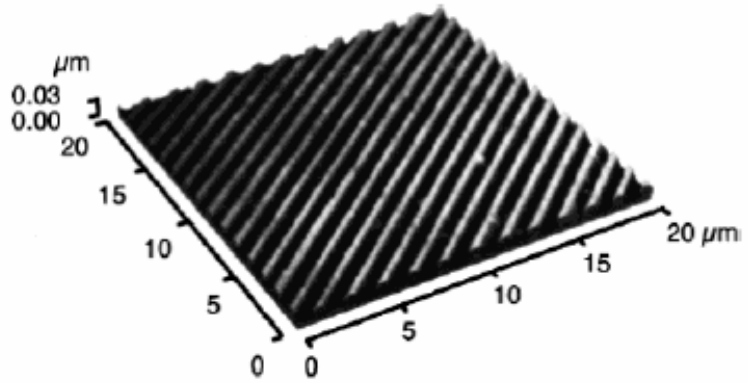

Figure 8. AFM images showing the results of AFM anodic oxidation and wet etching of a pattern in an ODS-SAM on a multilayer resist: scan speed, 10 μm/s; probe current, 5 nA; etching steps with 0.5 wt % hydrofluoric acid (0.5 min) and 25 wt % tetraammonium hydroxide (3 min). Reprinted with permission from ref 111. Copyright 1999 Society of the American Institute of Physics.

AFM Lithography

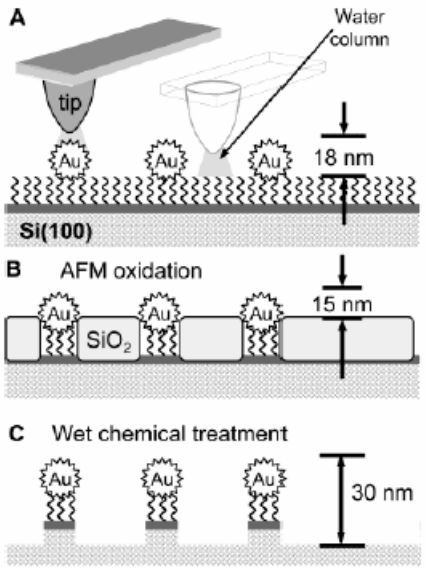

Figure 10. Schematic diagram of (A) selective anodization of the silicon regions not masked by nanoparticles. (B) The volume expansion of the silicon led to a decreased height contrast between the particles and the substrate. (C) After a wet etching step, silicon columns capped with a nanoparticle were formed.

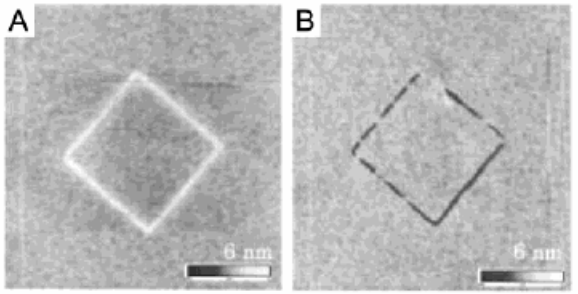

Figure 12. AFM images showing a lithographically defined pattern in a palmitic acid LB layer adsorbed to a SiO_N/Si substrate. Diamond pattern with protruding lines was written with −10 V applied tip bias (A), and that with grooves, with +10 V applied tip bias (B) (*z*-scale: 6 nm). Reprinted with permission from ref 123. Copyright 2002 American Institute of Physics.

Substitution Lithography

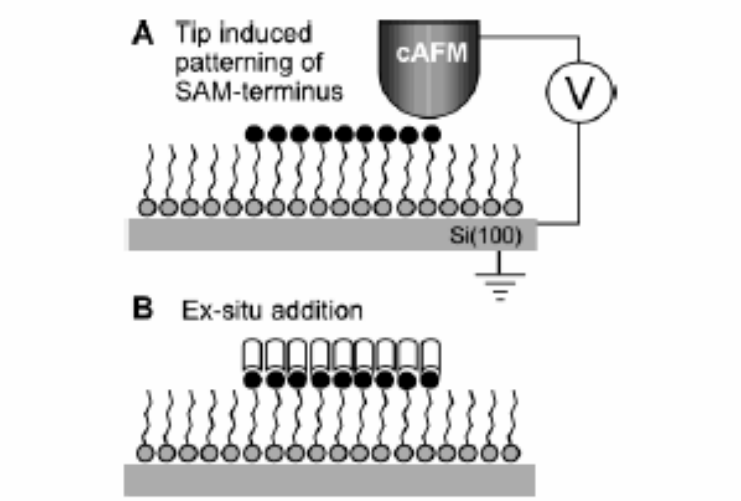

Figure 39. Schematic diagram of substitution lithography through the headgroup modification under an applied bias: (A) conductive AFM tip scanned under an applied bias voltage across a SAM and modified the headgroup without changing the structural integrity of the SAM; (B) altered functionality used for the subsequent binding of a second self-assembly molecule.

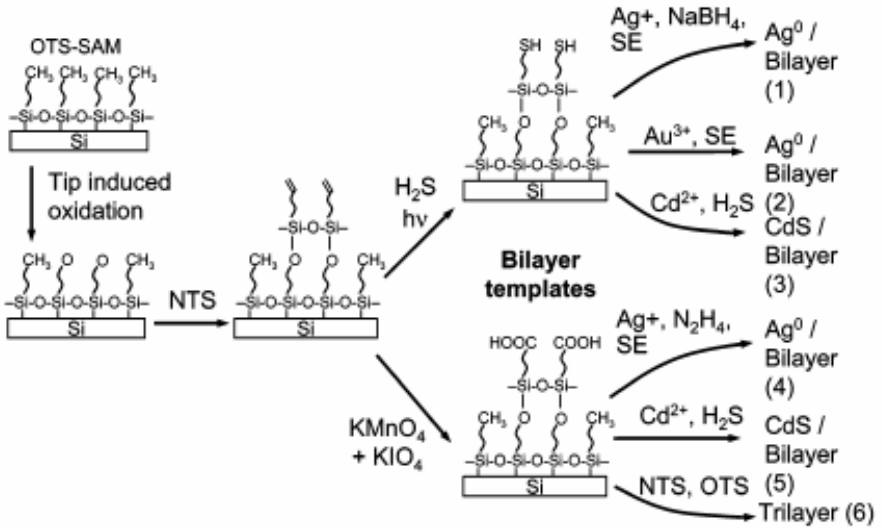

Dip-Pen Lithography

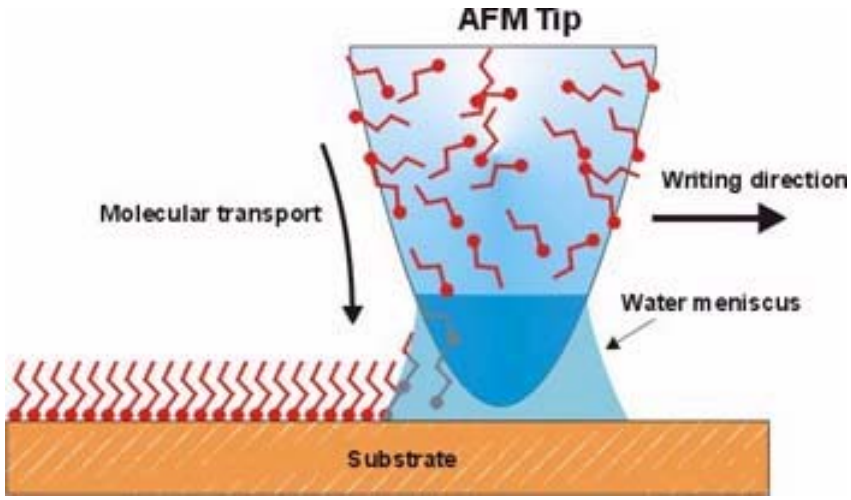

Conducting Polymers

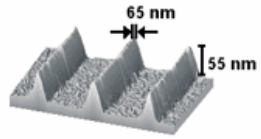

Silicon Nanostructures

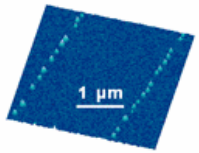

Single Nanoparticle Lines

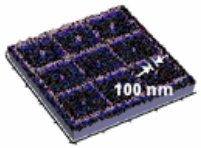

Protein Nanoarrays

Dip-Pen Nanolithograpy

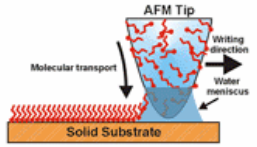

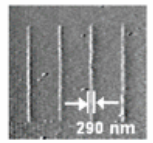

Sol Gel Templates

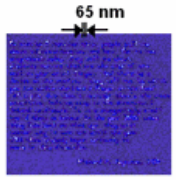

Small Organic Molecules

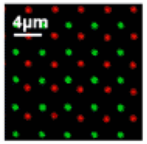

Ultrahigh Density DNA Arrays

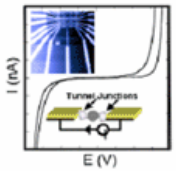

Single Particle Devices

"Dip-Pen" Nanolithography

Richard D. Piner, Jin Zhu, Feng Xu, Seunghun Hong,
Chad A. Mirkin*

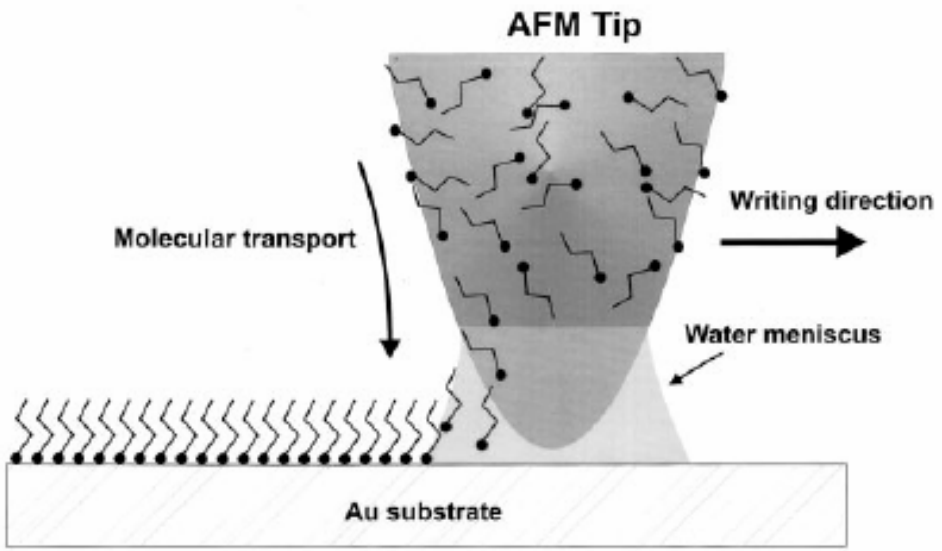

Fig. 1. Schematic representation of DPN. A water meniscus forms between the AFM tip coated with ODT and the Au substrate. The size of the meniscus, which is controlled by relative humidity, affects the ODT transport rate, the effective tip-substrate contact area, and DPN resolution.

SCIENCE VOL 283 29 JANUARY 1999

Dip-Pen Lithography

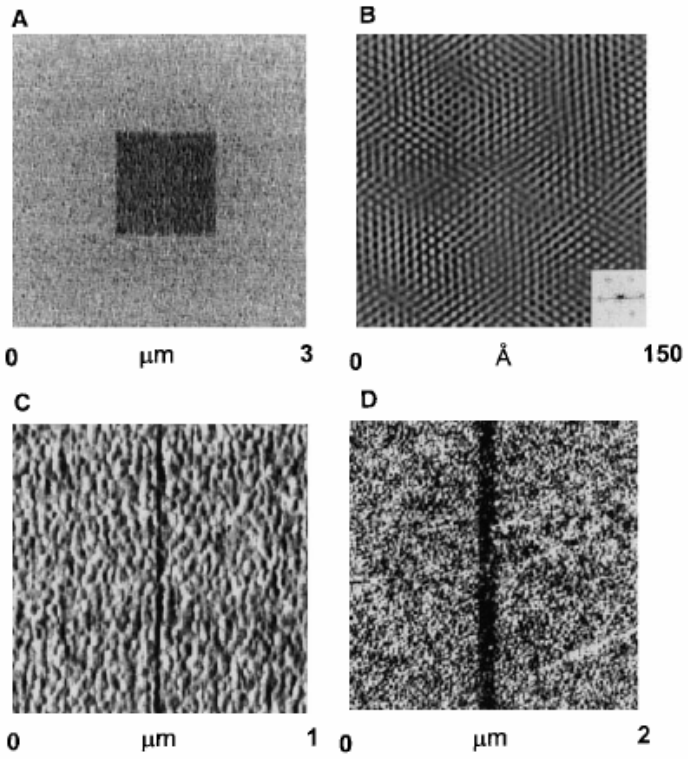

Fig. 2. (A) Lateral force image of a square of ODT measuring 1 µm by 1 µm, deposited onto a Au substrate by DPN. This pattern was generated by scanning the 1-μm^2 area at a scan rate of 1 Hz for a period of 10 min at a relative humidity of 39%. Then the scan size was increased to 3 µm, and the scan rate was increased to 4 Hz while the image was recorded. The faster scan rate prevents ODT transport. (B) Lattice-resolved, lateral force image of an ODT SAM deposited onto Au(111)/mica by DPN. The image has been filtered with a fast Fourier transform (FFT), and the FFT of the raw data is shown in the lower right insert. The monolayer was generated by scanning a 1000 Å square area of the Au(111)/mica five times at a rate of 9 Hz at 39% relative humidity. (C) Lateral force image of a 30-nm-wide line (3 µm long) deposited onto Au/mica by DPN. The line was generated by scanning the tip in a vertical line repeatedly for 5 min at a scan rate of 1 Hz. (D) Lateral force image of a 100-nm line deposited on Au by DPN. The method of depositing this line is analogous to that used to generate the image in (C), but the writing time was 1.5 min. In all images, darker regions correspond to areas of relatively lower friction.

Dip-Pen Lithography

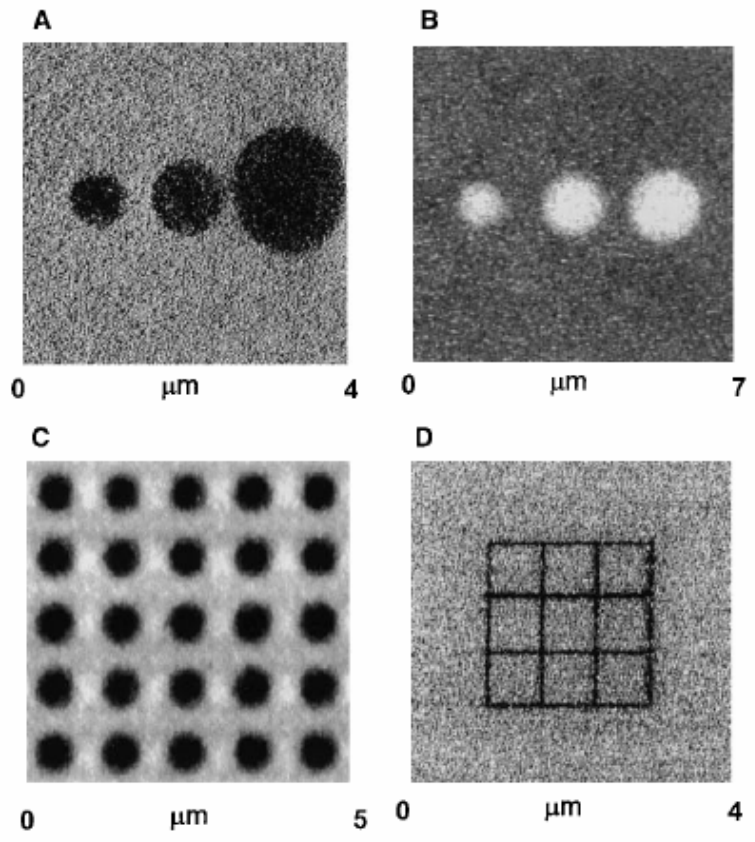

Fig. 3. (A) Lateral force image of an Au substrate after an AFM tip, which was coated with ODT, had been in contact with the substrate for 2, 4, and 16 min (left to right); the relative humidity was held constant at 45%, and the image was recorded at a scan rate of 4 Hz. (B) Lateral force image of dots of 16-mercaptohexadecanoic acid on a Au substrate. To generate the dots, an AFM tip coated with 16-mercaptohexadecanoic acid was held on the Au substrate for 10, 20, and 40 s (left to right). The relative humidity was 35%. The images show that the transport properties of 16-mercaptohexadecanoic acid and of ODT differ substantially. (C) Lateral force image of an array of dots generated by DPN. Each dot was generated by holding an ODT-coated tip in contact with the surface for ~20 s. Writing and recording conditions were the same as in (A). (D) Lateral force image of a molecule-based grid. Each line is 100 nm in width and 2 μm in length and required 1.5 min to write.

Dip-pen Lithography

SCIENCE VOL 288 9 JUNE 2000

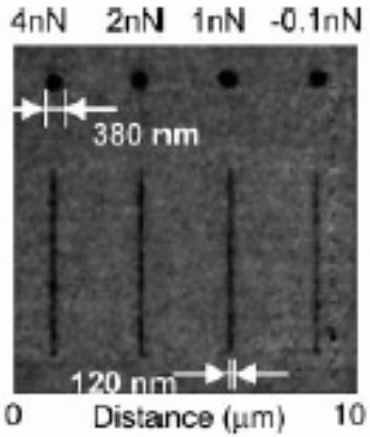

Fig. 1. Lateral force microscopy (LFM) images of ODT monolayer nanodot and line features on gold generated by the same tip but under different tip-substrate contact forces. Feature sizes vary less than 10%.

Fig. 4. LFM images of eight identical patterns generated with one imaging tip and eight writing tips coated with ODT molecules.

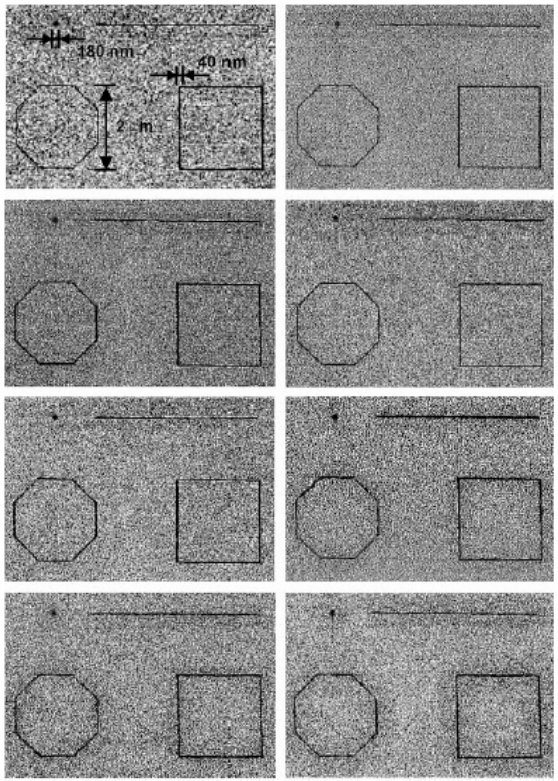

Protein Nanoarrays Generated By Dip-Pen Nanolithography

Ki-Bum Lee,[1] So-Jung Park,[1] Chad A. Mirkin,[1]* Jennifer C. Smith,[2] Milan Mrksich[2]*

1 MARCH 2002 VOL 295 SCIENCE

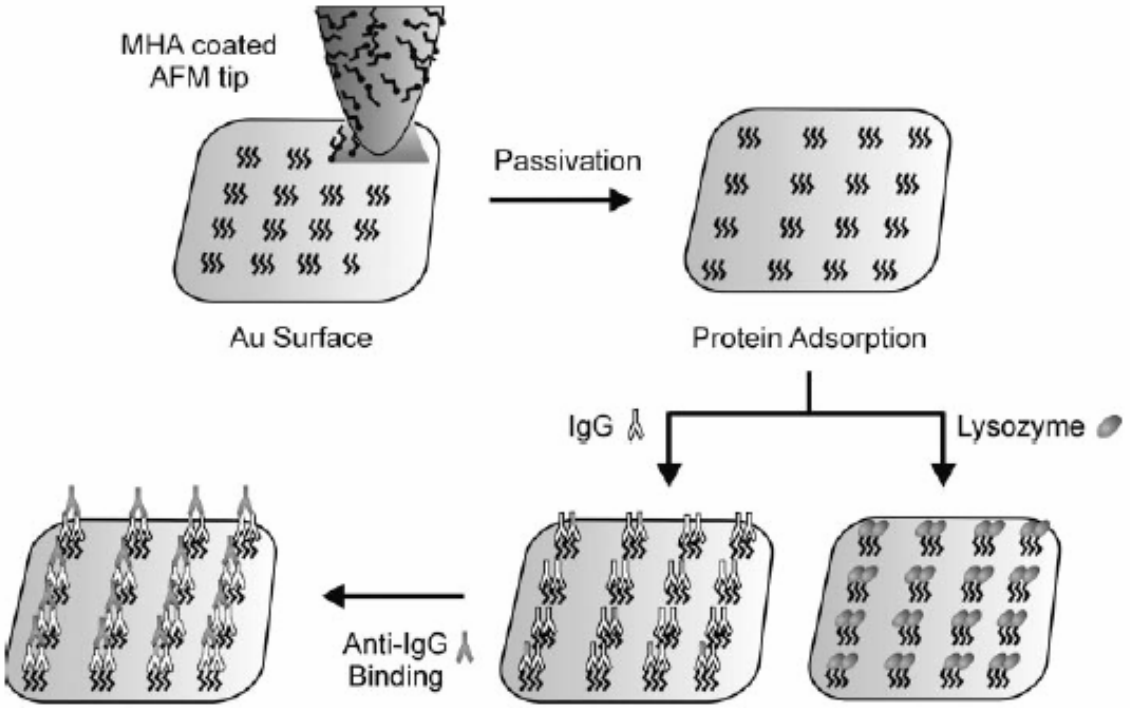

Fig. 2. Diagram of proof-of-concept experiments, in which proteins were absorbed on preformed MHA patterns. The resulting protein arrays were then characterized by AFM.

Protein Nanoarrays Generated By Dip-Pen Nanolithography

Ki-Bum Lee,[1] So-Jung Park,[1] Chad A. Mirkin,[1]* Jennifer C. Smith,[2] Milan Mrksich[2]*

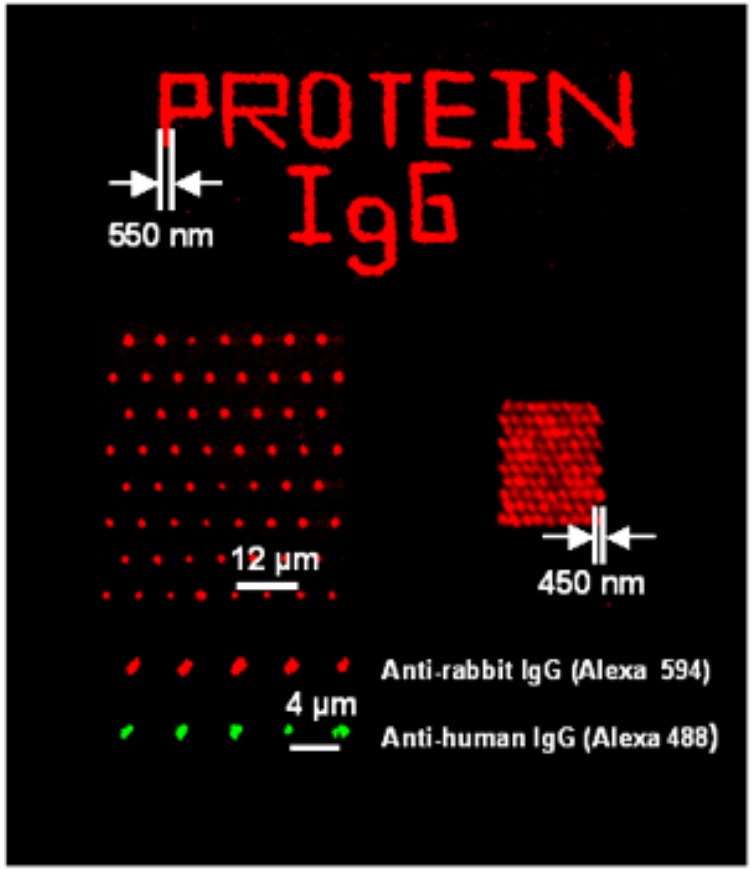

Protein Nanoarrays Generated By Dip-Pen Nanolithography

Ki-Bum Lee,[1] So-Jung Park,[1] Chad A. Mirkin,[1]* Jennifer C. Smith,[2] Milan Mrksich[2]*

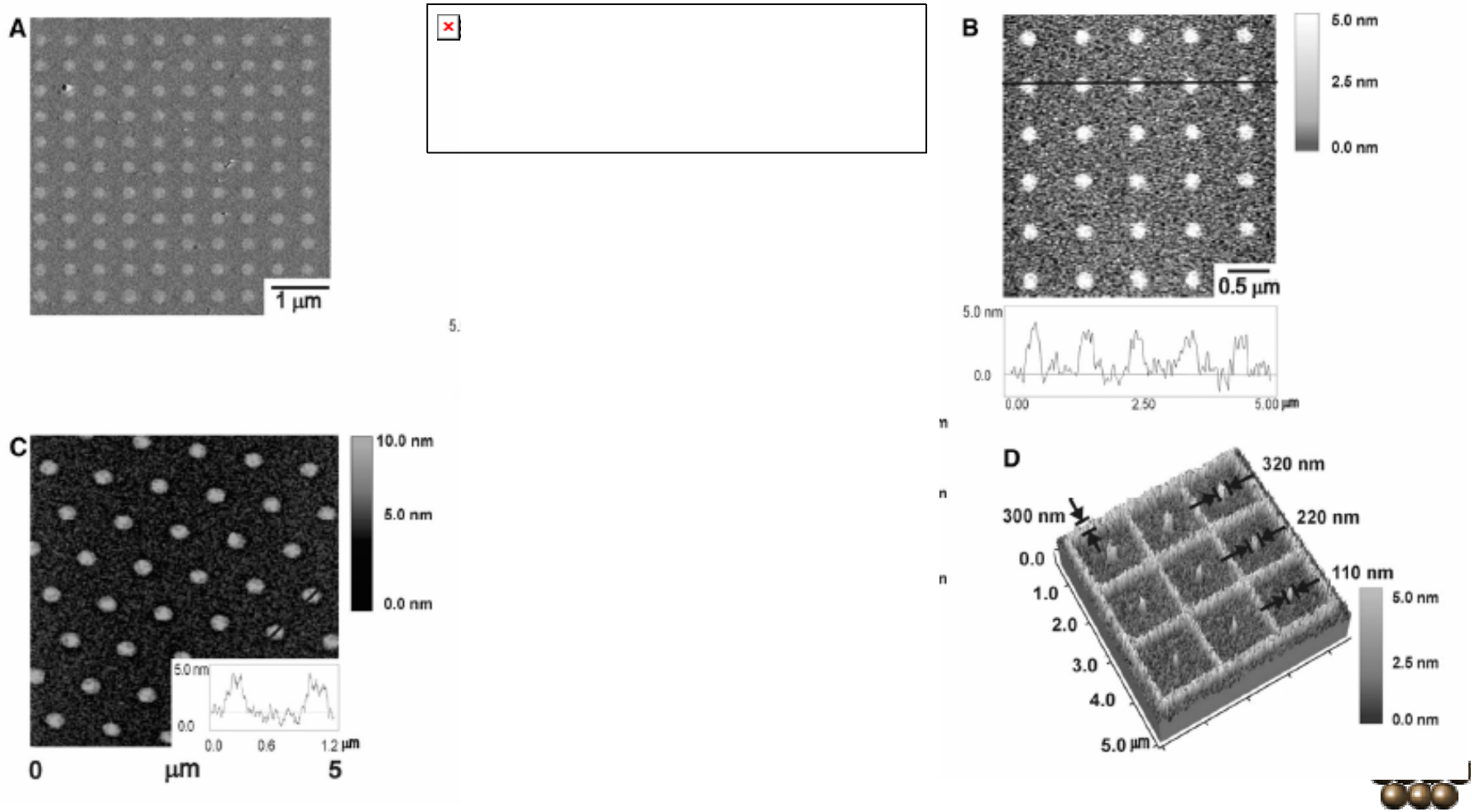

Protein Nanoarrays Generated By Dip-Pen Nanolithography

Ki-Bum Lee,[1] So-Jung Park,[1] Chad A. Mirkin,[1]* Jennifer C. Smith,[2] Milan Mrksich[2]*

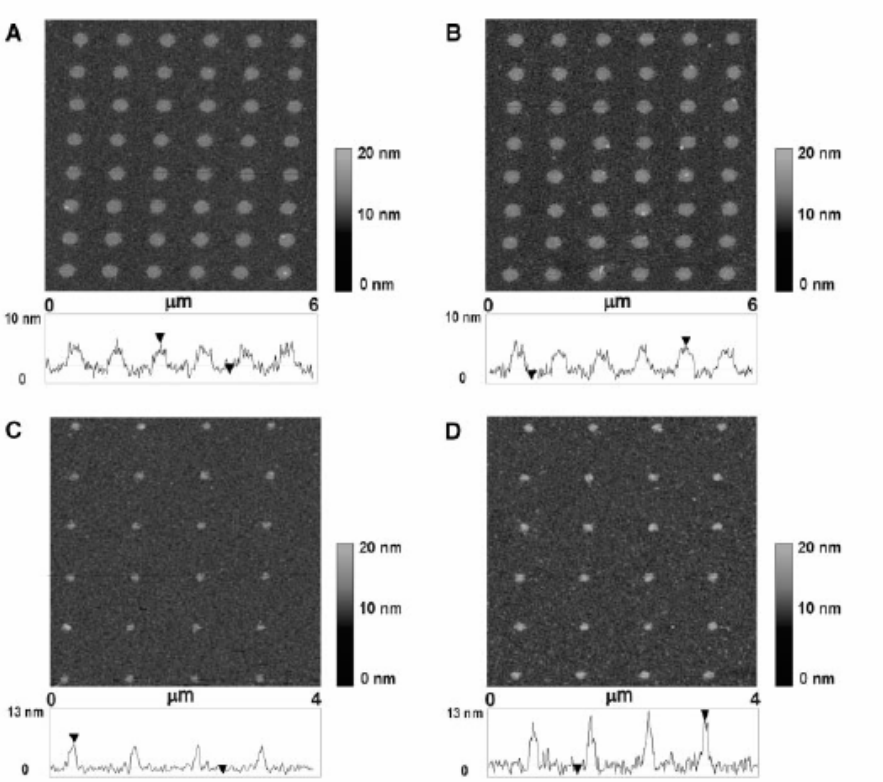

Fig. 3. AFM tapping mode image and height profile of rabbit IgG assembled onto an MHA dot array generated by DPN before (**A**) and after (**B**) exposure to a solution containing lysozyme, Retronectin, goat/sheep anti-IgG, and human anti-IgG. An IgG nanoarray before (**C**) and after (**D**) treatment with a solution containing lysozyme, goat/sheep anti-IgG, human anti-IgG, and rabbit anti-IgG. All images were taken at a 0.5-Hz scan rate in tapping mode.

Protein Nanoarrays Generated By Dip-Pen Nanolithography

Ki-Bum Lee,[1] So-Jung Park,[1] Chad A. Mirkin,[1]* Jennifer C. Smith,[2] Milan Mrksich[2]*

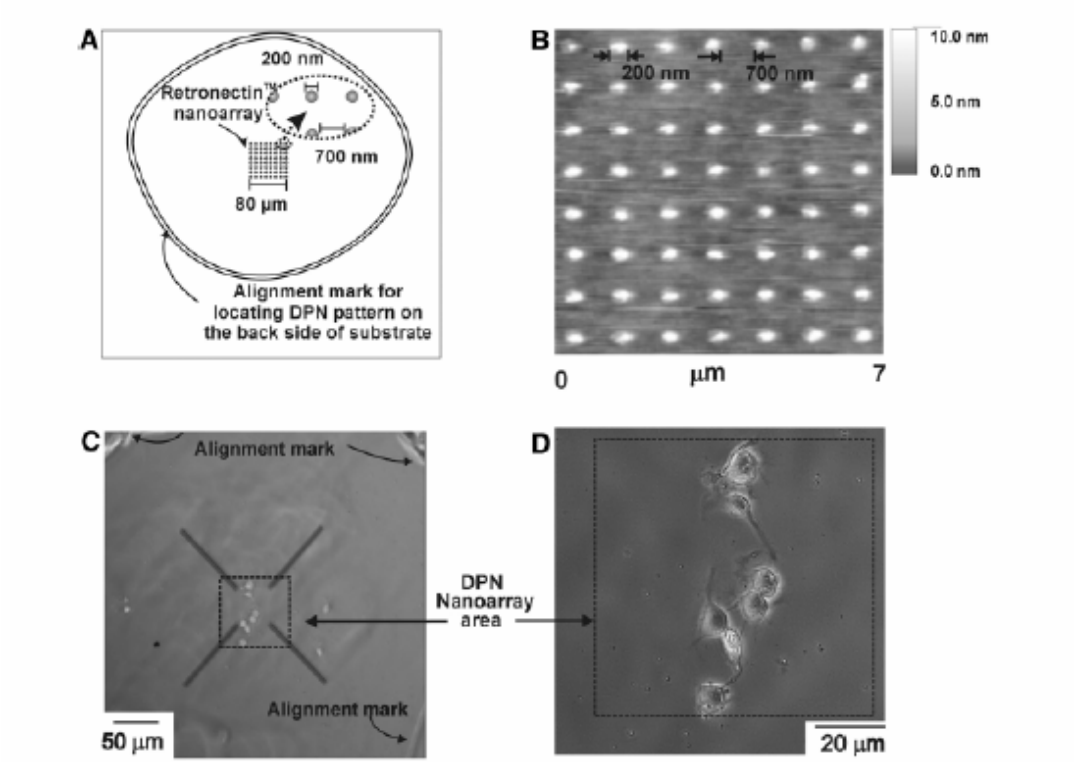

Fig. 4. (A) Diagram describing the cell adhesion experiment on the DPN-generated pattern. The total patterned area is 6400 μm^2. The alignment marks were generated by scratching a circle into the backside of the Au-coated glass substrate. (B) Topography image (contact mode) of the Retronectin protein array. Imaging conditions were the same as in Fig. 1B. (C) Large-scale optical microscope image showing the localization of cells in the nanopatterned area. (D) Higher resolution optical image of the nanopatterned area, showing intact cells.

Dip-Pen Array

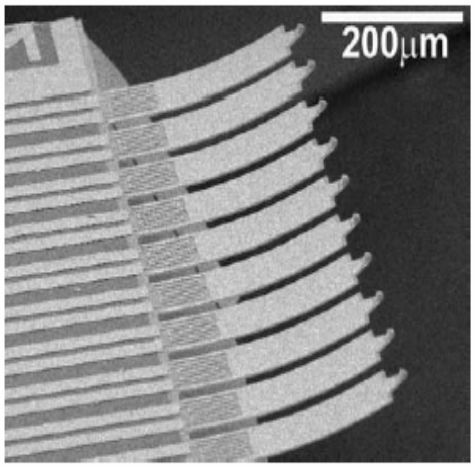

FIG. 2. An array of ten thermally actuated DPN probes showing the power lead and heater layout. Each probe is 300 μm long, 80 μm wide, and 1.3 μm thick.

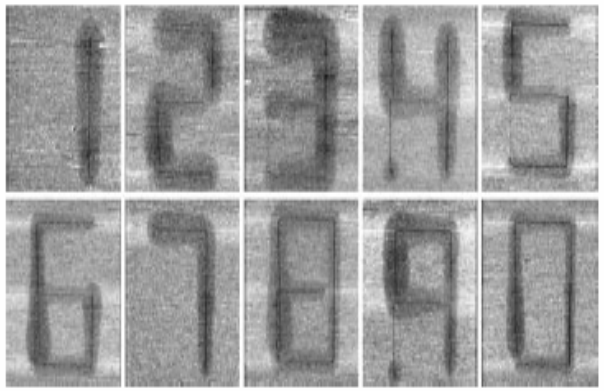

FIG. 4. LFM scans, 8 μm square, of ten simultaneously generated ODT patters on a gold surface. Each numeral is 6 μm tall, 4 μm wide, and was written at 1 μm/s.

Ultimate STM Lithography

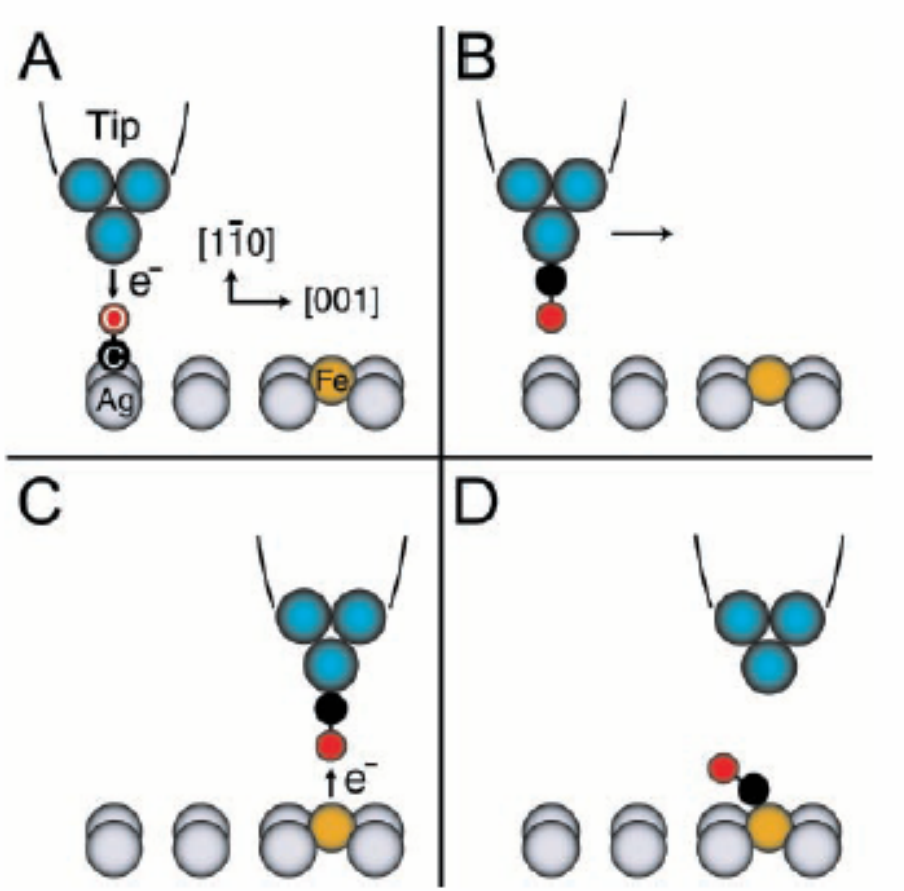

Single Atomic Manipulation

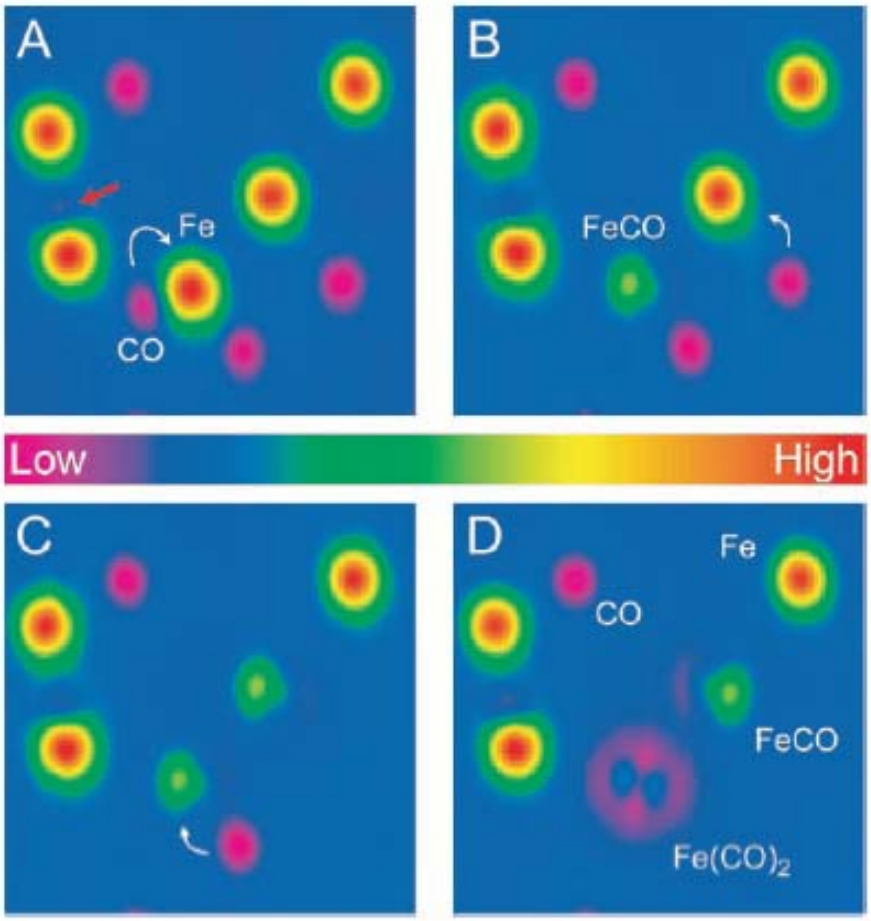

Single Molecular Vibrational Spectra by STM

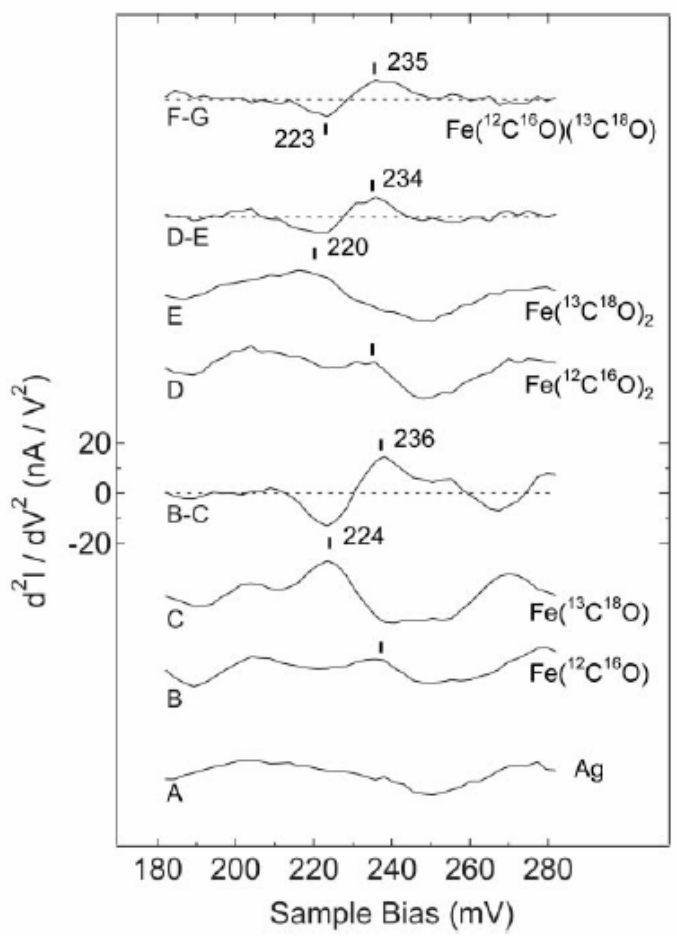

Building Molecule Step by Step

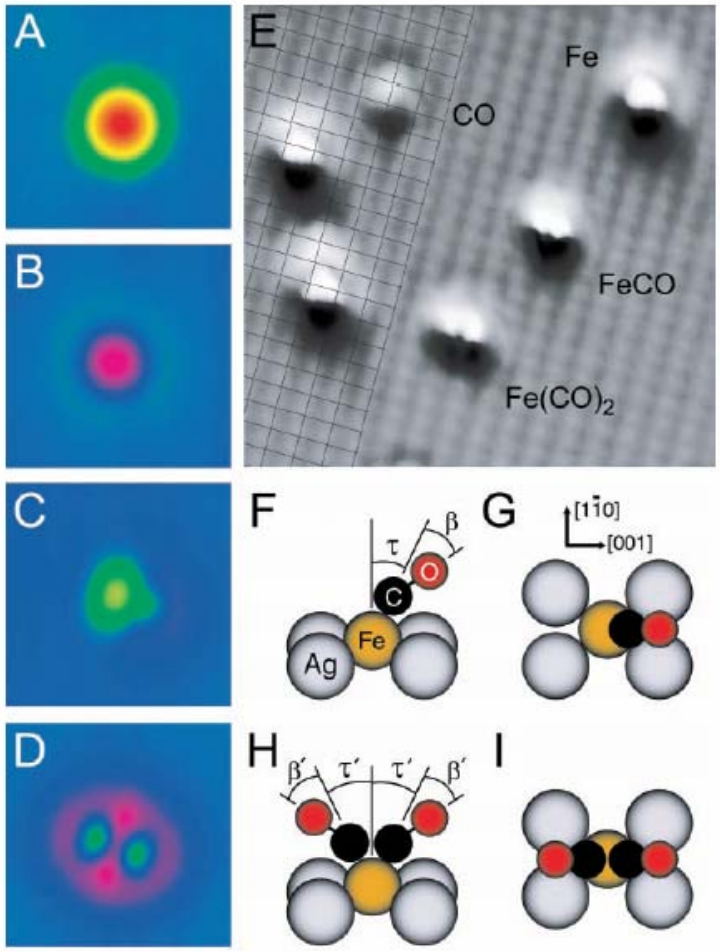

Atomic Manipulation

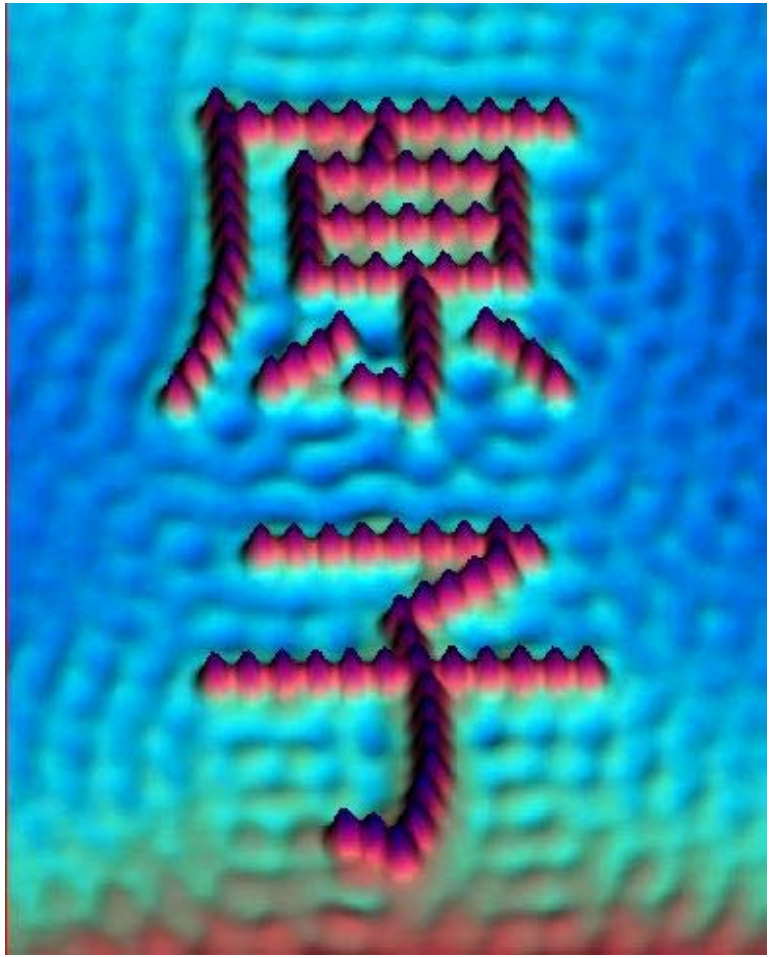

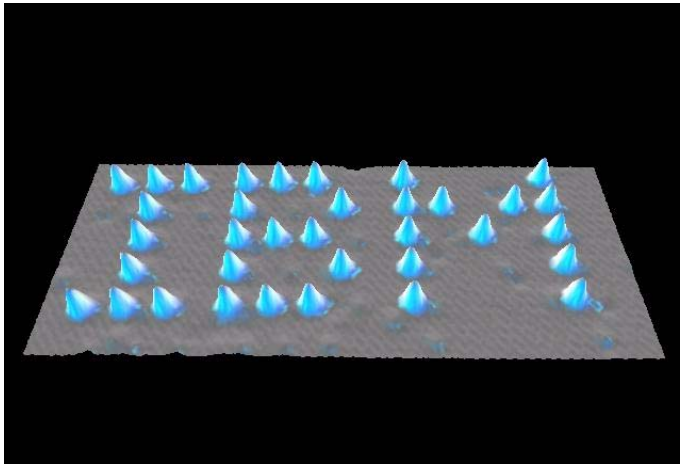

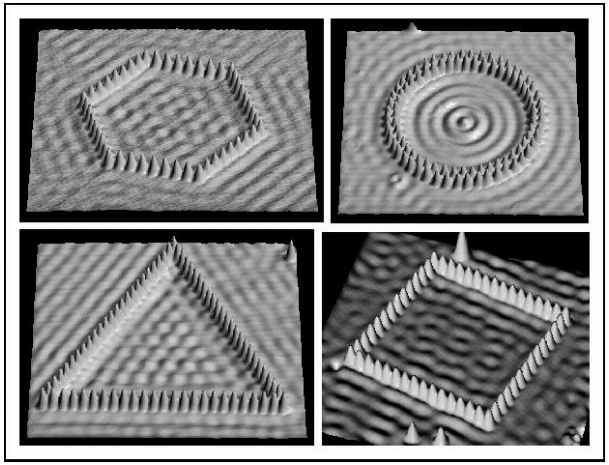

Near-Field Microscope

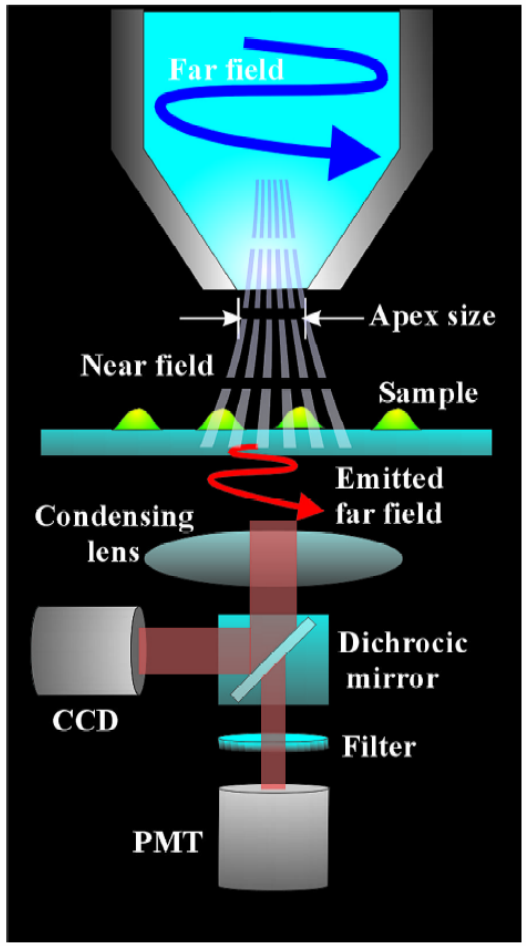

Near-Field Images

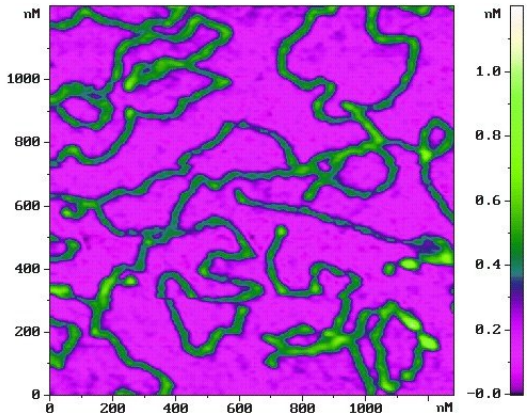

DNA

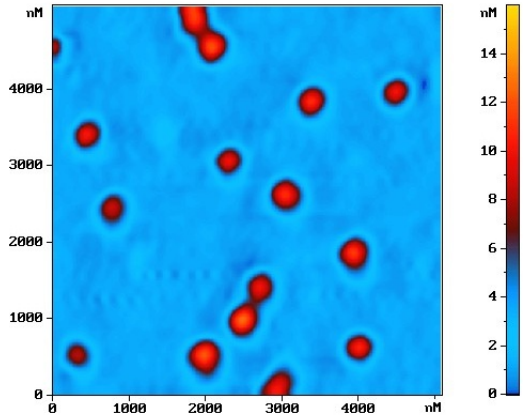

Nanosphere

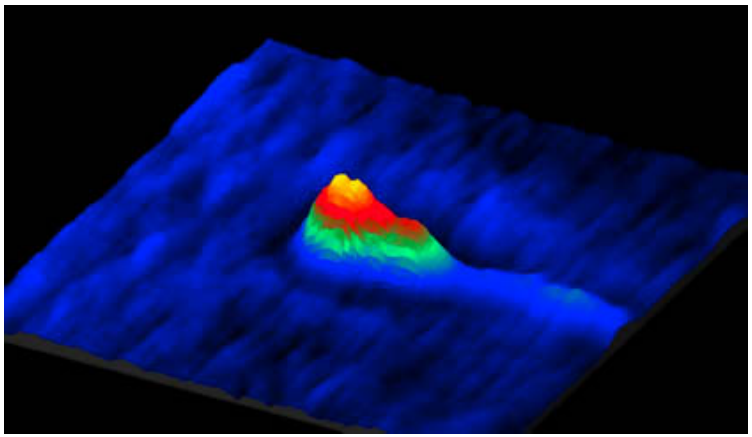

Sperm

Near-Field Lithography

Figure 2. TappingMode image of a lithography test pattern. The Aurora-3 used nanolithography software to write into S1805 photoresist. 25μm scan.

Replication

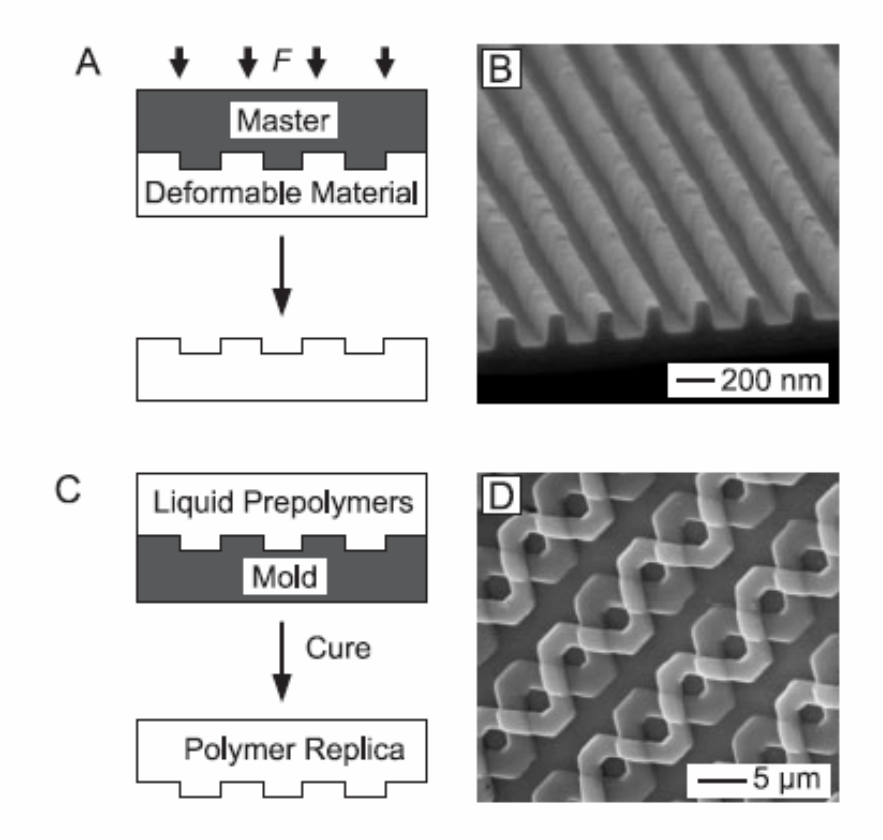

Align the pattern and Exposure

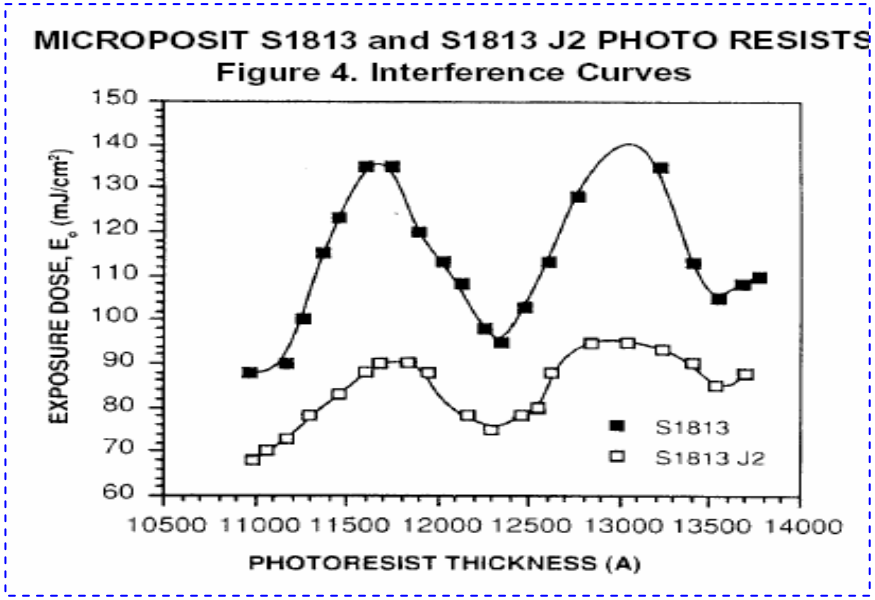

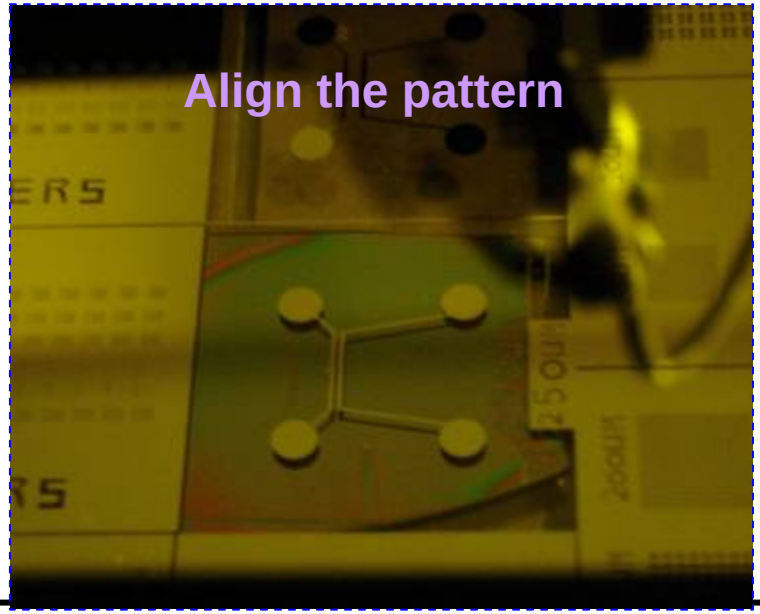

Stepper

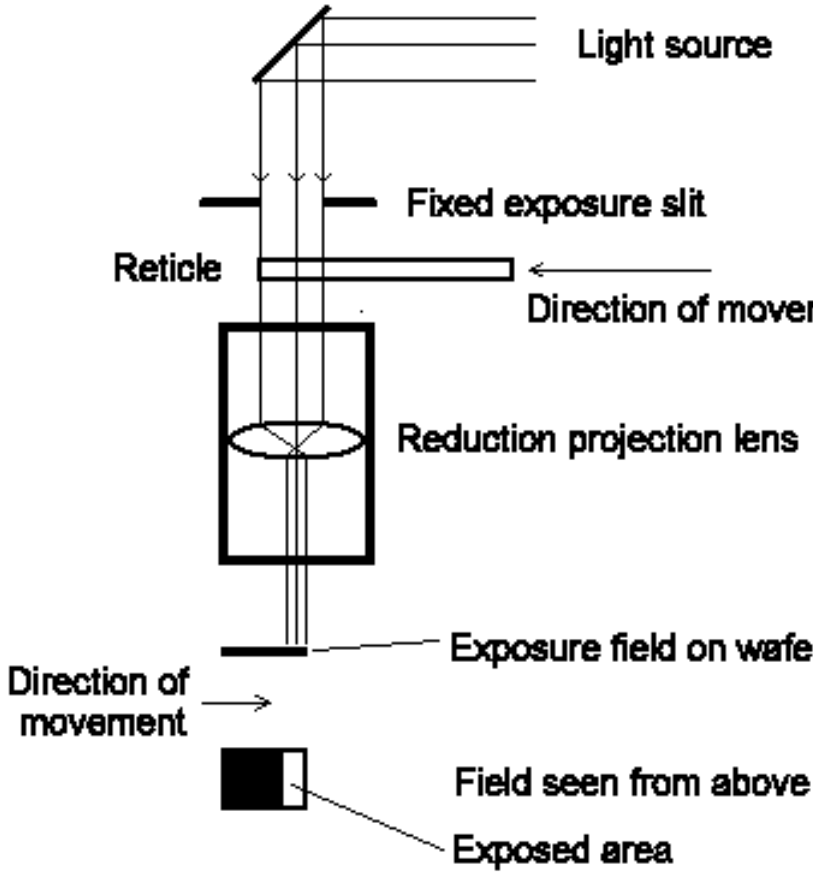
Light source
Fixed exposure slit
Reticle
Direction of move
Reduction projection lens
Exposure field on wafe
Direction of movement
Field seen from above
Exposed area

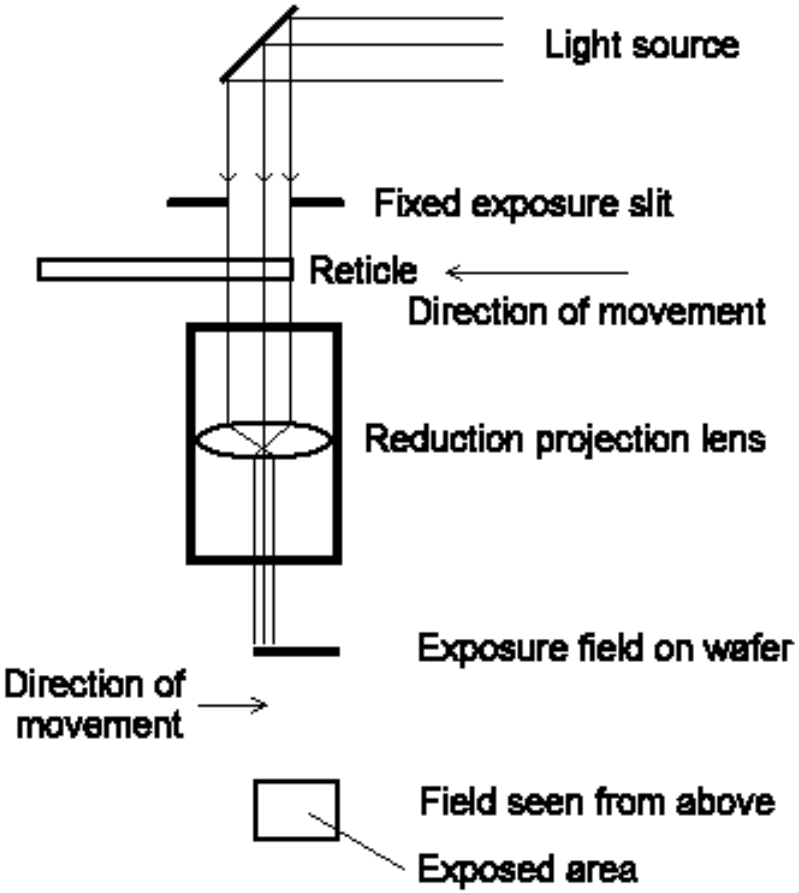
Light source
Fixed exposure slit
Reticle
Direction of movement
Reduction projection lens
Exposure field on wafer
Direction of movement
Field seen from above
Exposed area

E-beam Projection

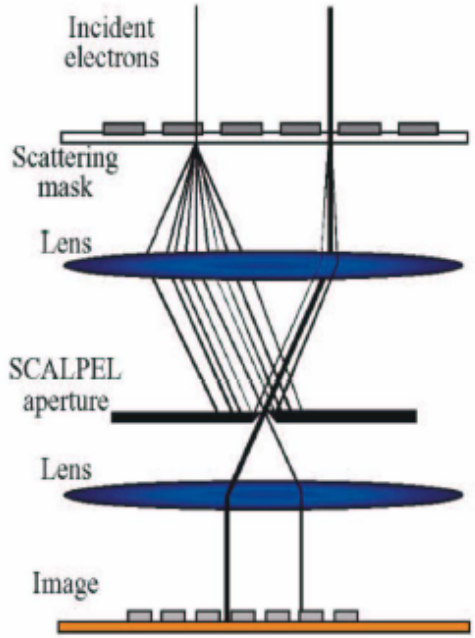

Bell Lab (1999)
There 'was' a consortium including Applied Materials, Inc. and ASM Lithography Holding N.V.; Lucent Technologies Inc.; Motorola, Semiconductor Products Sector; Samsung Electronics Co., Ltd.; and Texas Instruments Incorporated (TI).

Imprint Lithography with 25-Nanometer Resolution

Stephen Y. Chou; Peter R. Krauss; Preston J. Renstrom

Science, New Series, Volume 272, Issue 5258 (Apr. 5, 1996), 85-87.

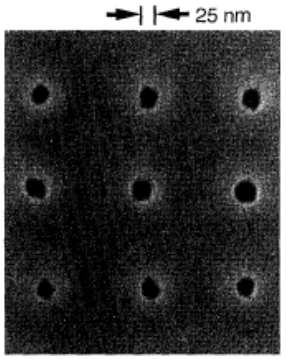

Fig. 2. SEM micrograph of a top view of holes 25 nm in diameter with a period of 120 nm, formed by compression molding into a PMMA film.

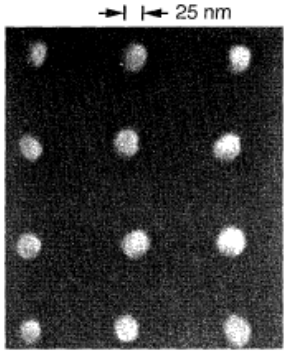

Fig. 5. SEM micrograph of the substrate in Fig. 2, after deposition of metal and a lift-off process. The diameter of the metal dots is 25 nm, the same as that of the original holes created in the PMMA.

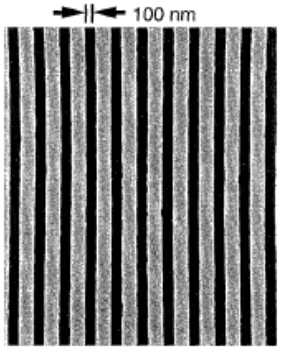

Fig. 3. SEM micrograph of a top view of trenches 100 nm wide with a period of 250 nm, formed by compression molding into a PMMA film.

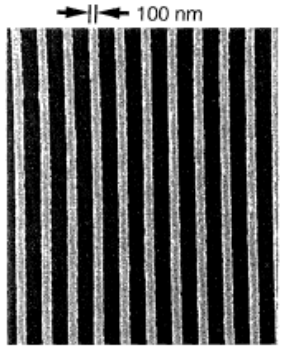

Fig. 6. SEM micrograph of the substrate in Fig. 3, after deposition of metal and a lift-off process. The metal linewidth is 100 nm, the same as the width of the original PMMA trenches.

Nanoimprint Lithography

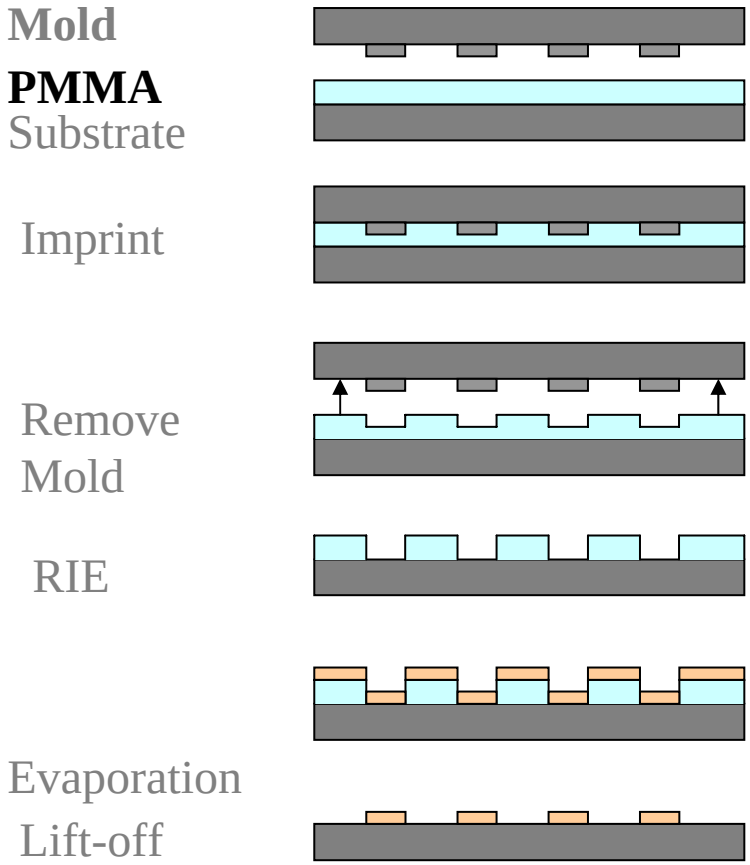

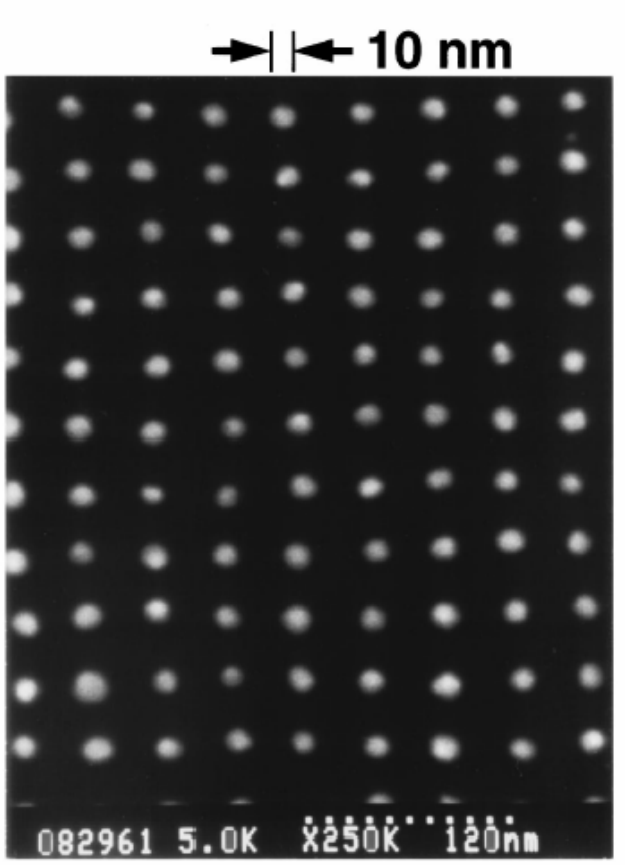

Ultrafast and direct imprint of nanostructures in silicon

NATURE | VOL 417 | 20 JUNE 2002 |

Stephen Y. Chou*, Chris Keimel & Jian Gu

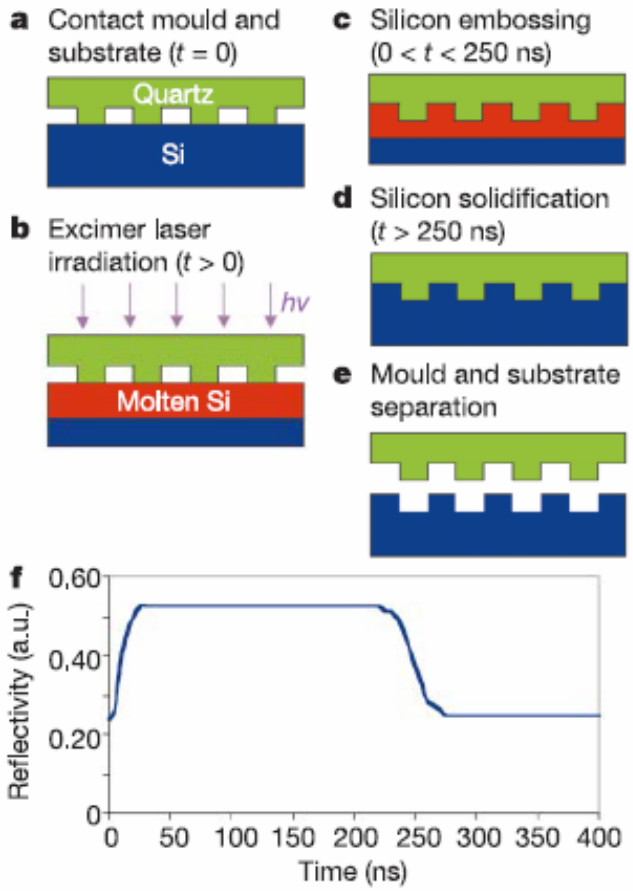

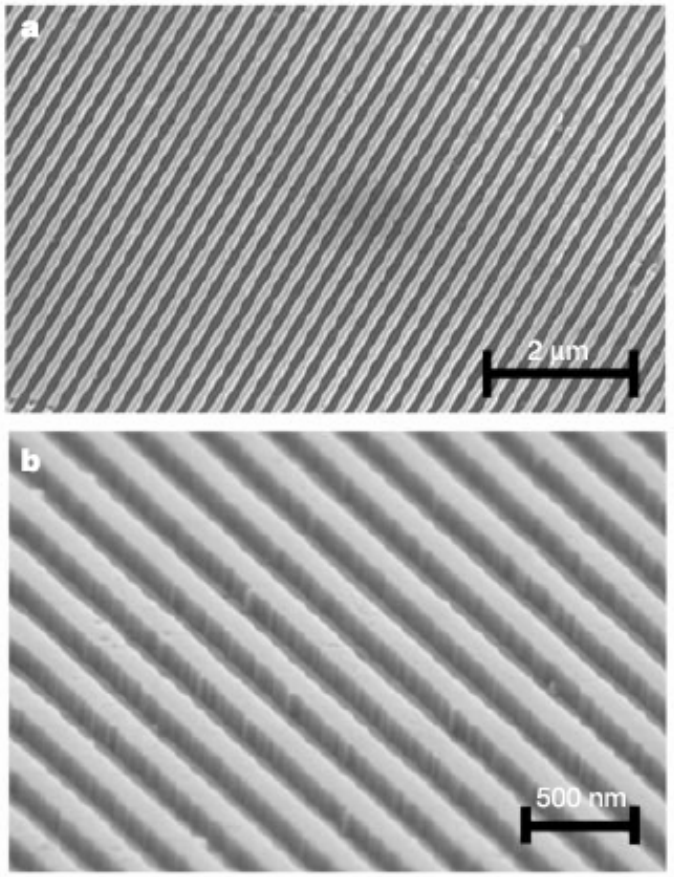

Step and Flash Imprint Lithography

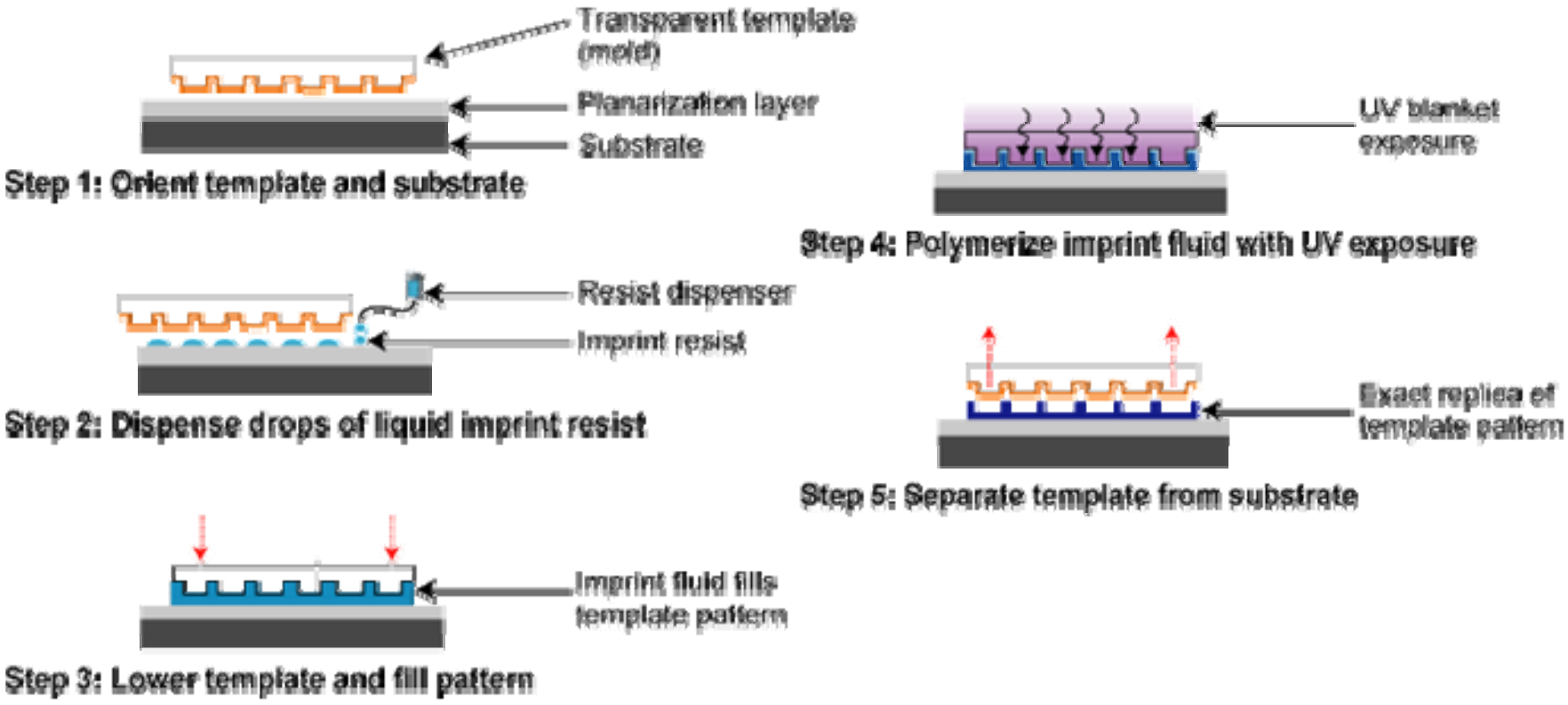

Nanoimprintors

NX-2000, Nanoimprintor, Nanonex

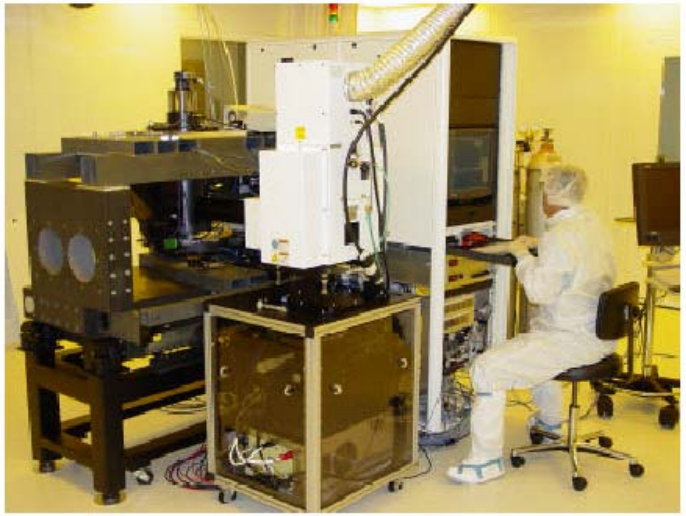

IMPRIO 100

Molecular Imprints, Inc.™

- Resolution: Sub-50 nanometers, imprint template (mold) limited.
- Alignment: < 500 nm, 3σ (X, Y, and Rotation).
- Flexibility: Handles up to 8 inch wafers, including fragile substrates.
- Field size: 25 x 25 mm full active print area, 100 μm street width.

Imprinting Result

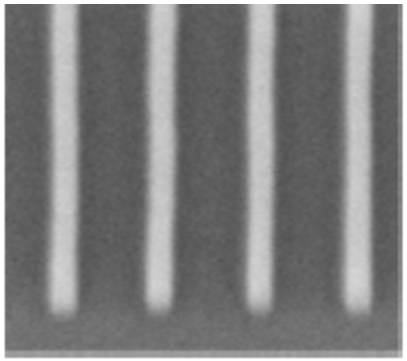

Imprinted 20 nm isolated lines

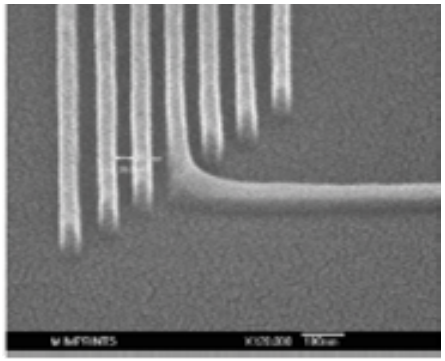

Imprinted 30 nm dense lines

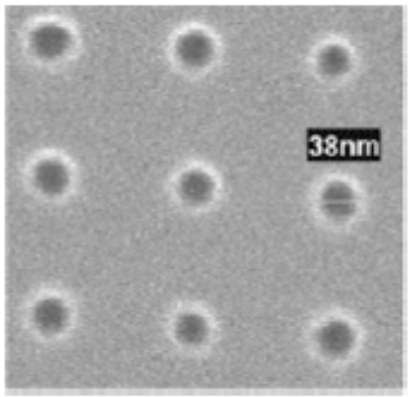

Imprinted sub-40 nm contacts

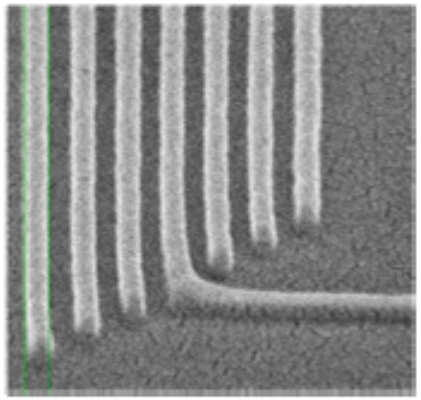

Imprinted 50 nm dense lines

Challenges

- Mask Fabrication (1:1)
- Lift-off process
- Resist
- Mask Design

Nanosphere Lithography

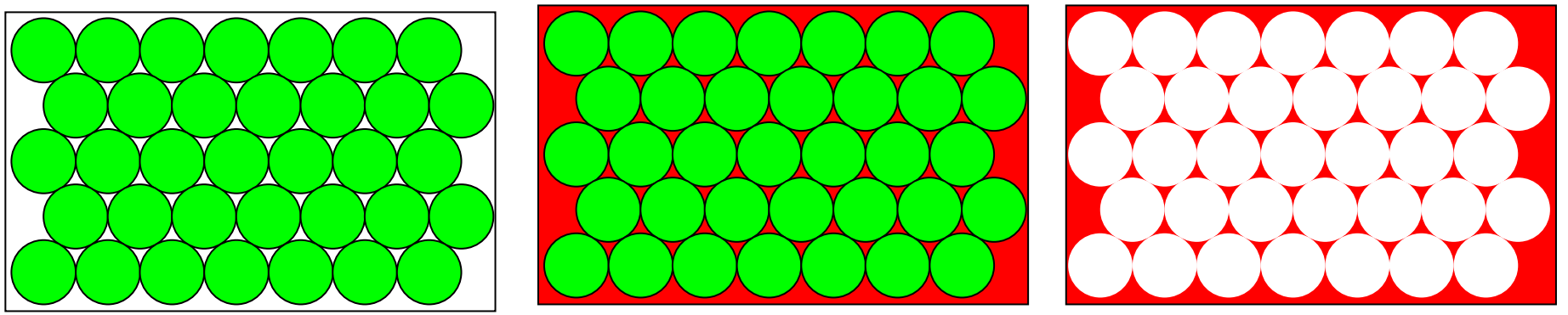

Single layer → Metal deposition → Lift-off

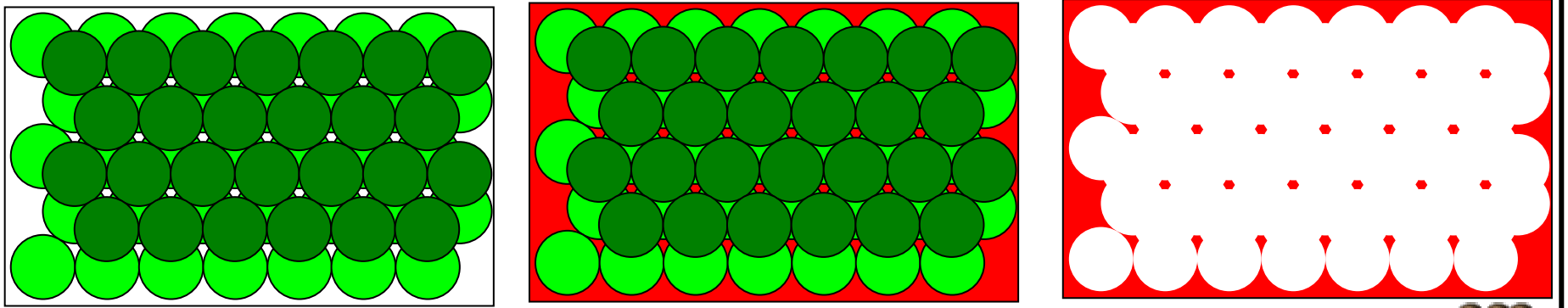

Double layer Metal deposition Lift-off

Array Dimension

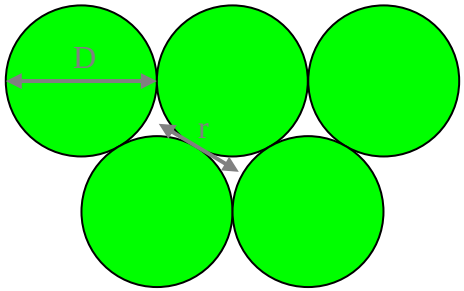

$$r = \frac{1}{\sqrt{3}} D$$

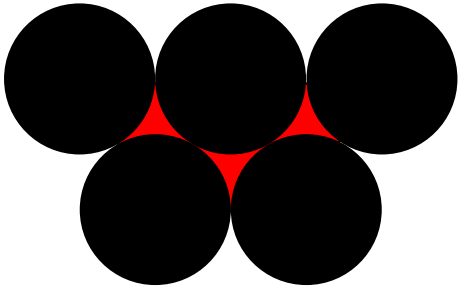

$$a = \frac{3}{2}\left(\sqrt{3} - 1 - \frac{1}{\sqrt{3}}\right) D$$

~1/4 D

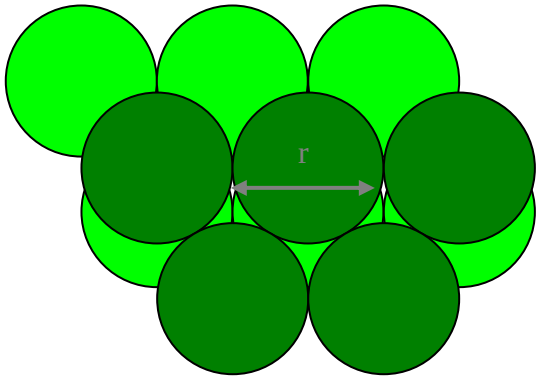

$$r = D$$

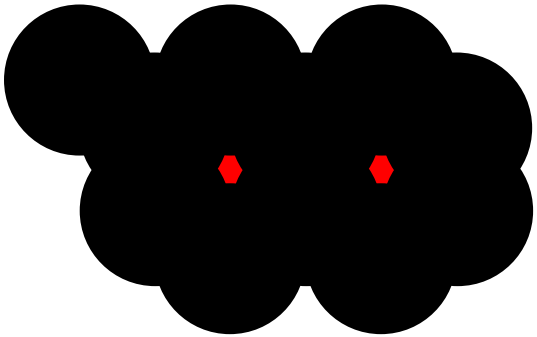

$$a = \left(\sqrt{3} - 1 - \frac{1}{\sqrt{3}}\right) D$$

~1/7 D

Optical Image of PS Template

800 nm PS

Nanosphere Lithography

350 nm

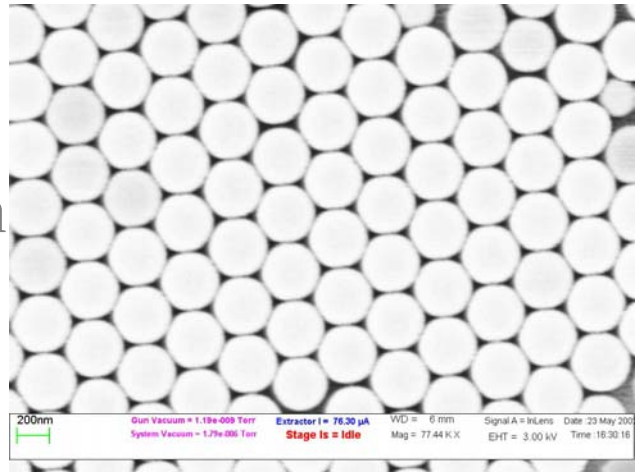

550 nm

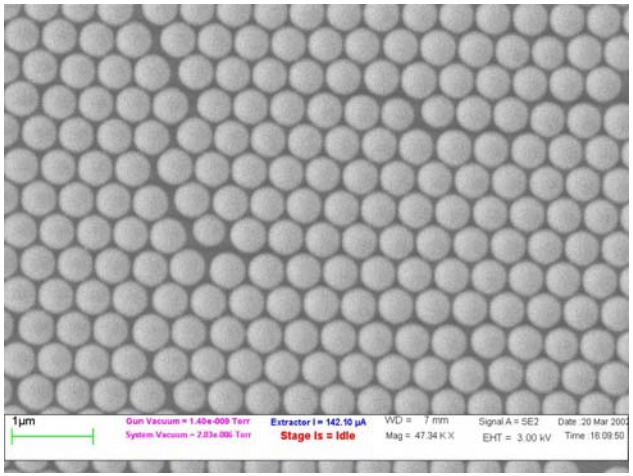

400 nm

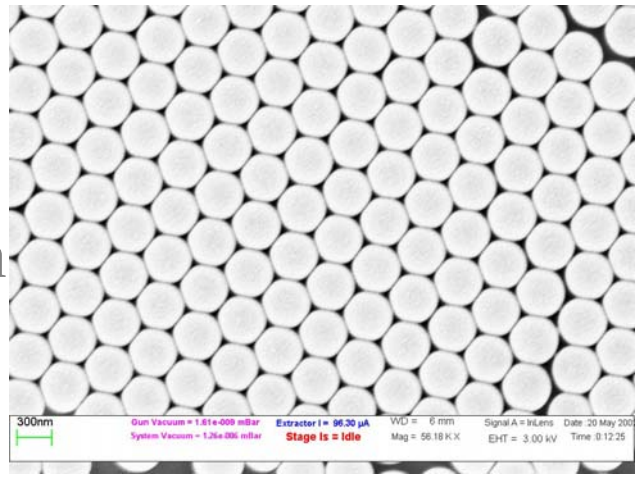

880 nm

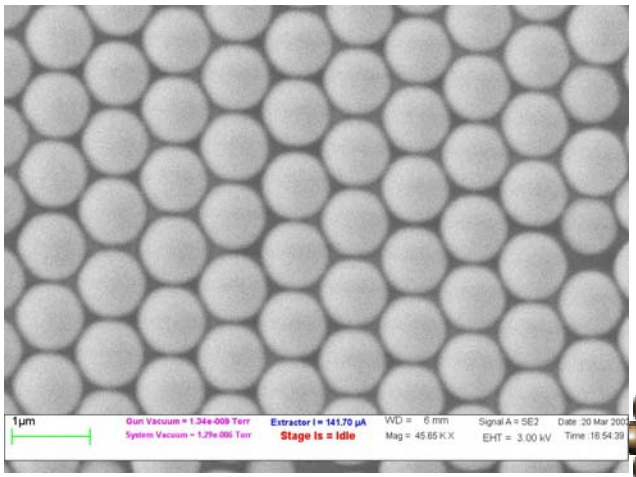

Single Layer Templates

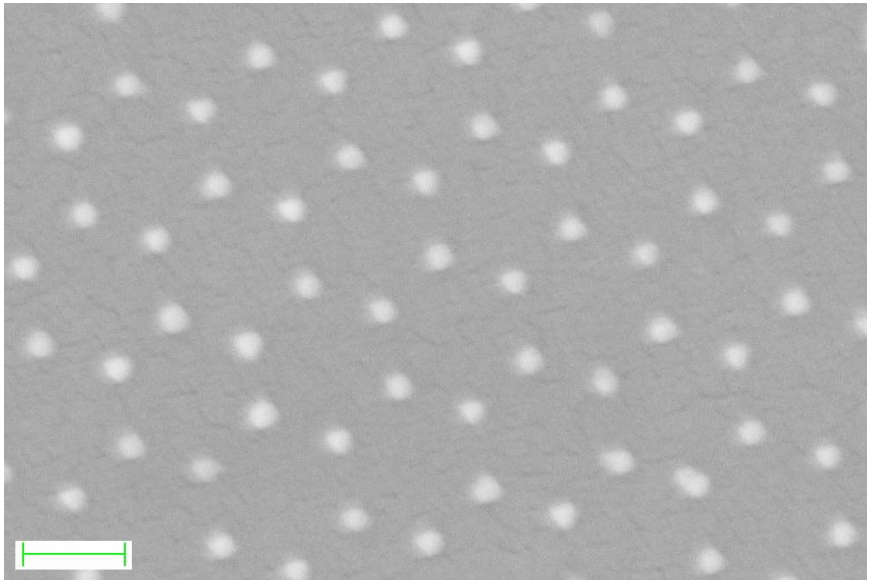

280 nm

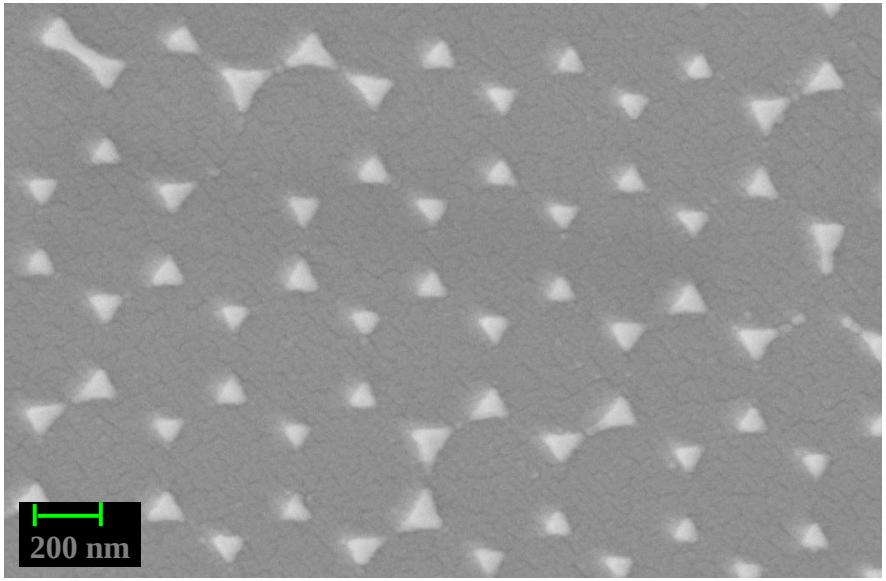

550 nm

Double Layer Templates

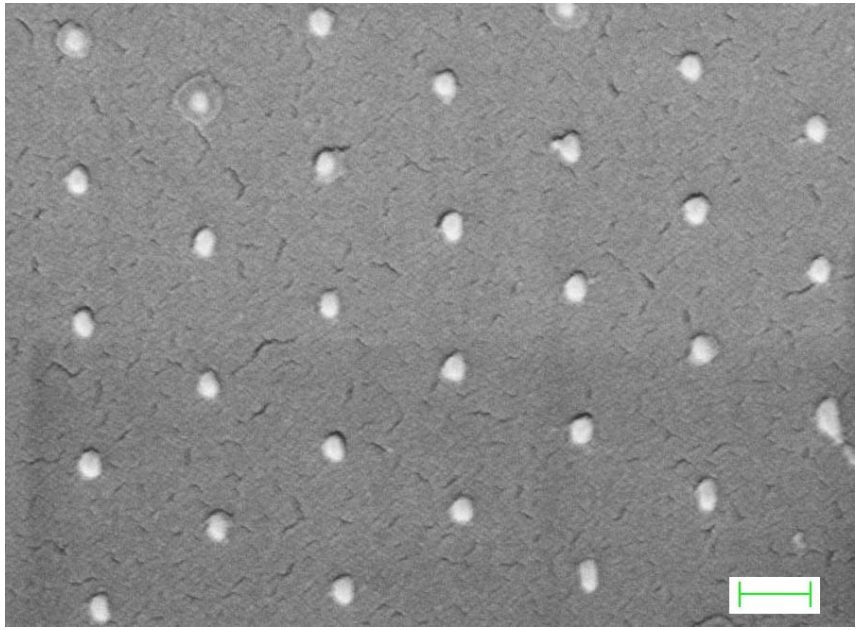

400 nm

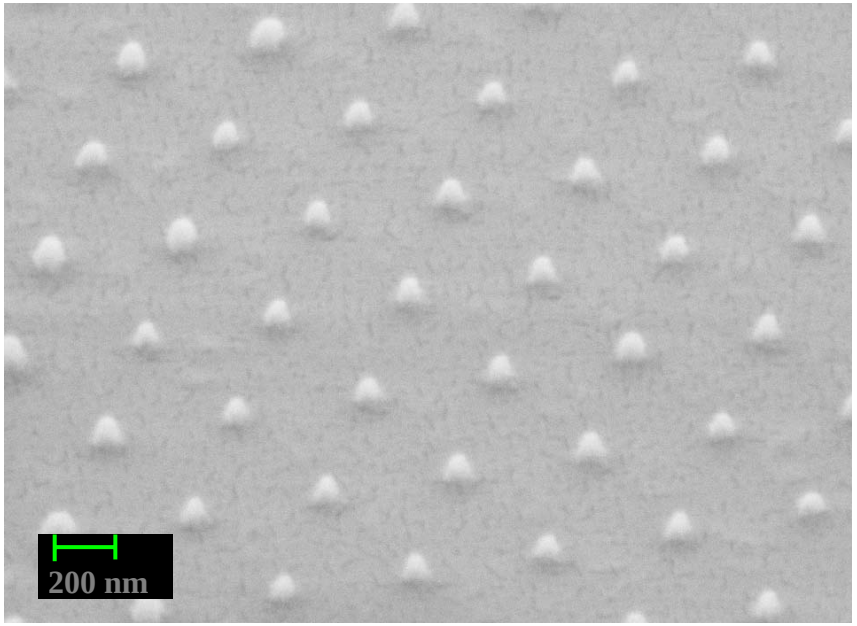

550 nm

Soft Lithography

Annu. Rev. Mater. Sci. 1998. 28:153–84

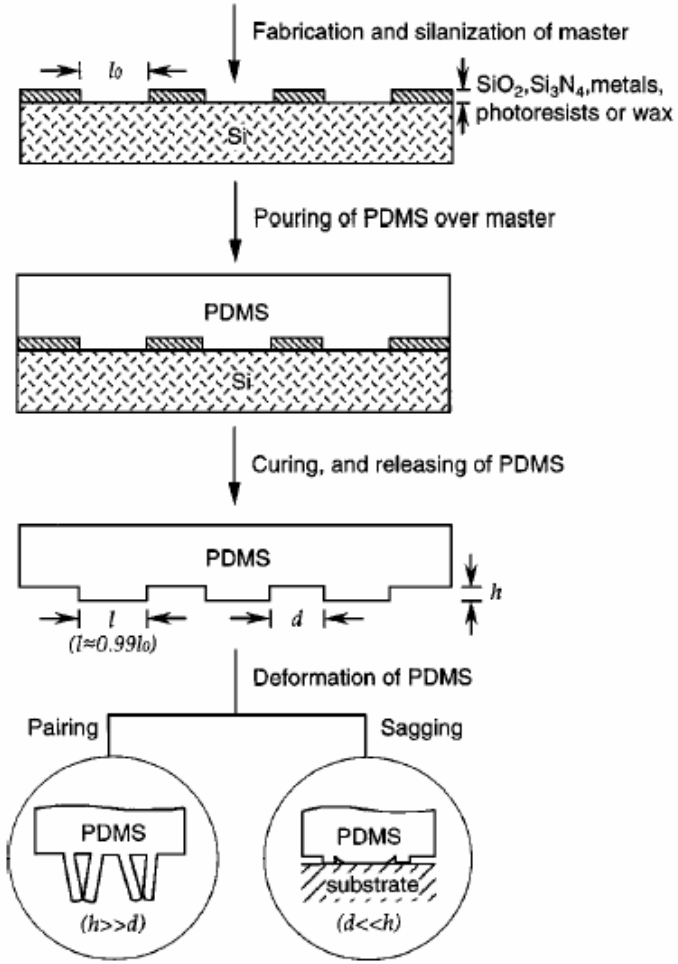

Soft Lithography

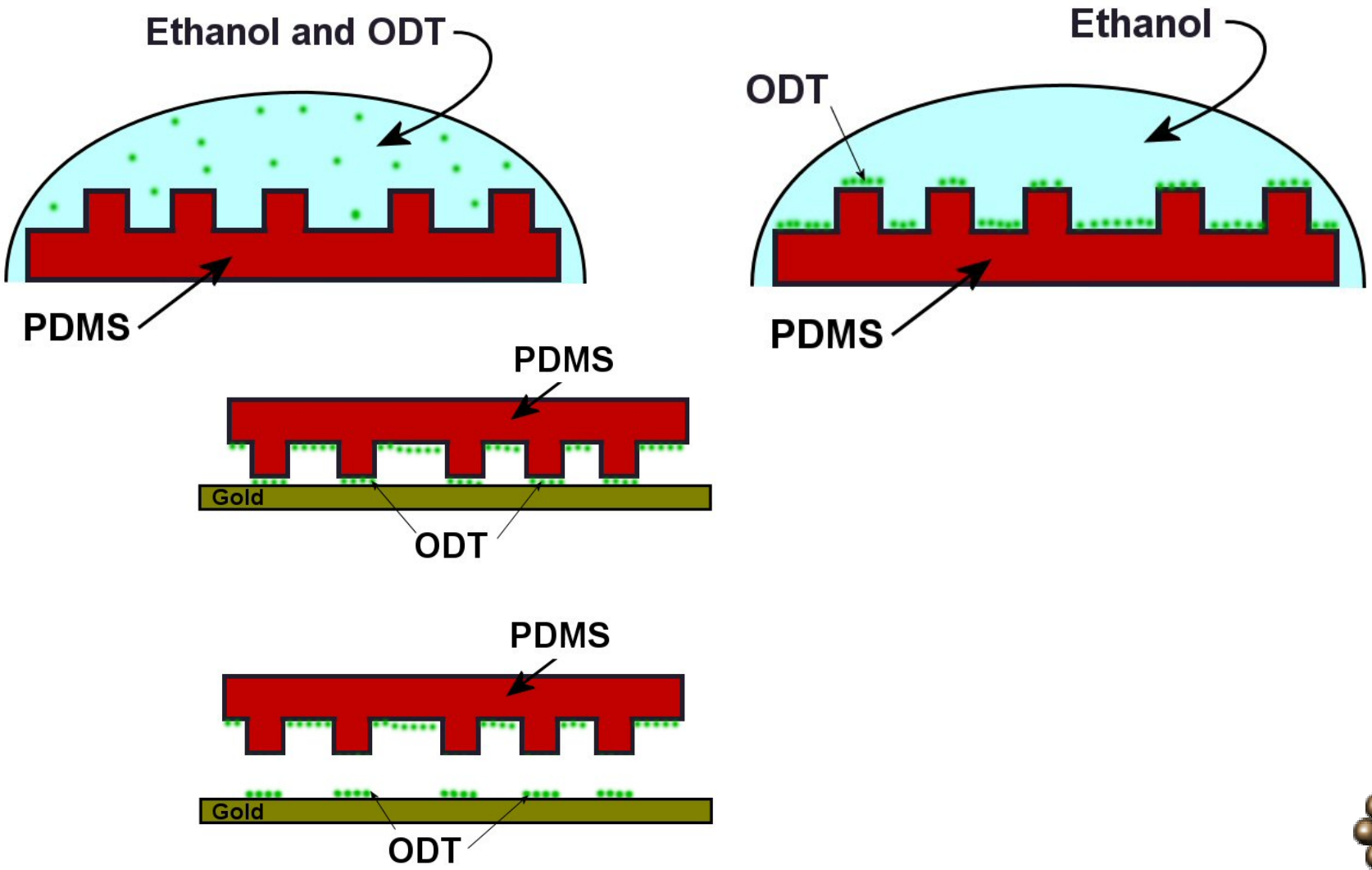

Table 1 Comparison between photolithography and soft lithography

	Photolithography	Soft lithography
Definition of patterns	Rigid photomask (patterned Cr supported on a quartz plate)	Elastomeric stamp or mold (a PDMS block patterned with relief features)
Materials that can be patterned directly	Photoresists (polymers with photo-sensitive additives)	Photoresists[a,e]
	SAMs on Au and SiO_2	SAMs on Au, Ag, Cu, GaAs, Al, Pd, and SiO_2[a] Unsensitized polymers[b–e] (epoxy, PU, PMMA, ABS, CA, PS, PE, PVC) Precursor polymers[c,d] (to carbons and ceramics) Polymer beads[d] Conducting polymers[d] Colloidal materials[a,d] Sol-gel materials[c,d] Organic and inorganic salts[d] Biological macromolecules[d]
Surfaces and structures that can be patterned	Planar surfaces 2-D structures	Both planar and nonplanar Both 2-D and 3-D structures
Current limits to resolution	~250 nm (projection) ~100 nm (laboratory)	~30 nm[a,b], ~60 nm[e], ~1 μm[d,e] (laboratory)
Minimum feature size	~100 nm (?)	10 (?) - 100 nm

[a–e]Made by (a) μCP, (b) REM, (c) μTM, (d) MIMIC, (e) SAMIM. PU:polyurethane; PMMA: poly(methyl methacrylate); ABS: poly(acrylonitrile-butadiene-styrene); CA: cellulose acetate; PS: polystyrene; PE: polyethylene; and PVC: poly(vinyl chloride)

Micro-contact Printing

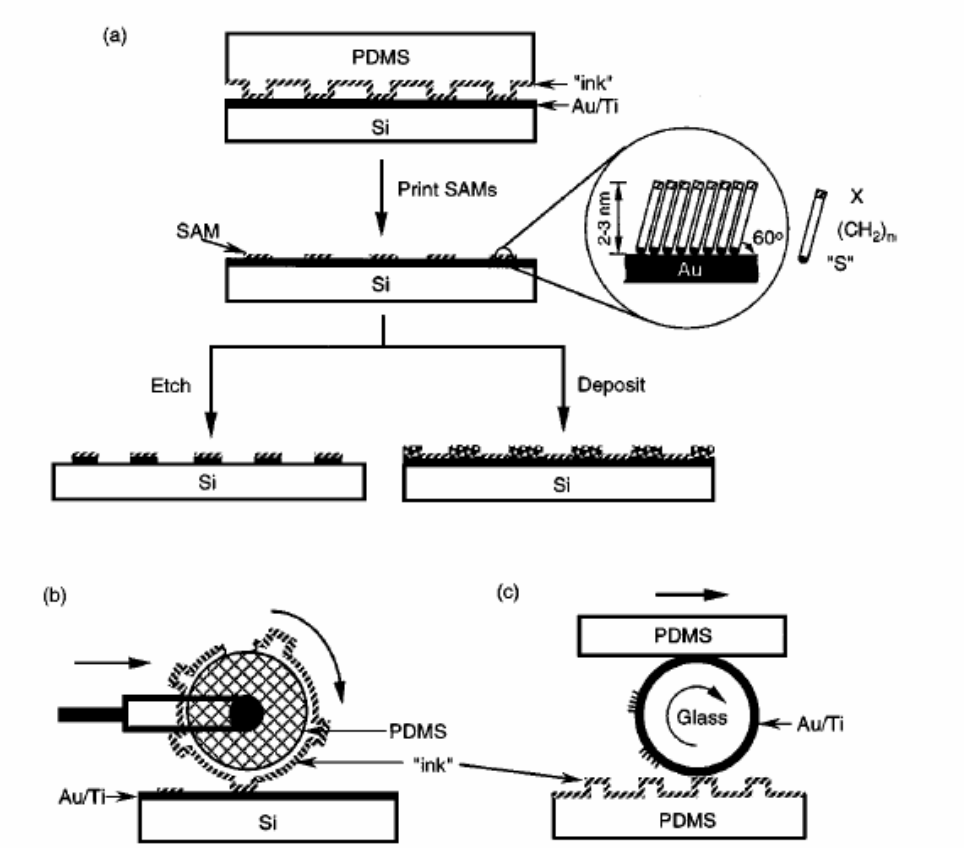

Figure 2 Schematic procedures for μCP of hexadecanethiol (HDT) on the surface of gold: (*a*) printing on a planar surface with a planar stamp (21), (*b*) printing on a planar surface over large areas with a rolling stamp (128), and (*c*) printing on a nonplanar surface with a planar stamp (174).

Micro-contact Printing

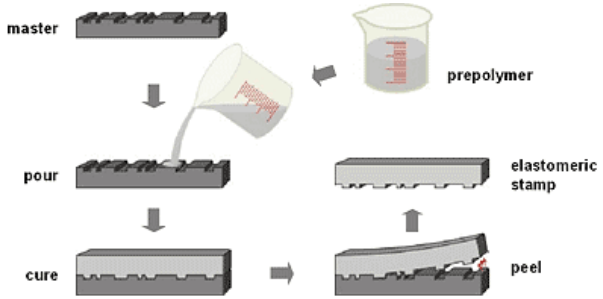

Fig.2 The stamp replication process: A master with a negative of the desired pattern is cast with a pre-polymer. After curing the polymer, the elastomeric stamp is peeled off the master and ready for microcontact printing.

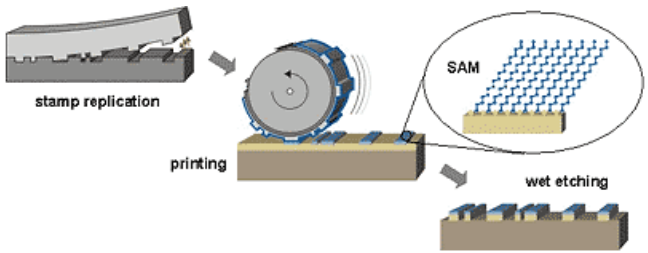

Fig.1 The microcontact printing (μCP) process: An elastomeric stamp is replicated from a master. After inking of the stamp with a suitable ink, it is fixated on a printing machine with help of which it is brought into conformal contact with a substrate. There the ink forms a self-assembled monolayer (SAM) which can be used as a resist in a subsequent wet etching step.

Micro-contact Printing

http://mrsec.wisc.edu/Edetc/nanolab/print/text.html

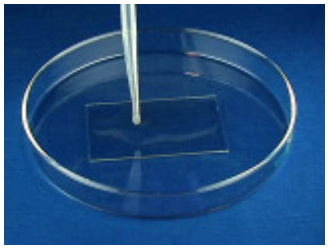

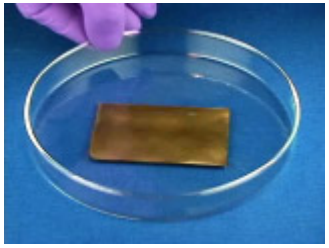

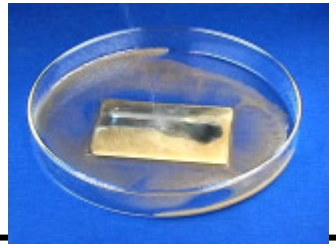

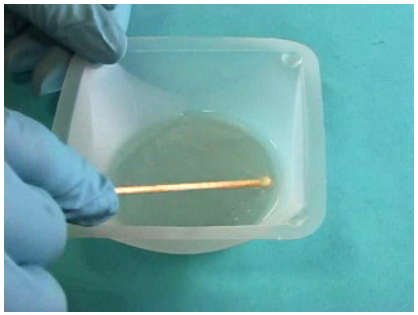

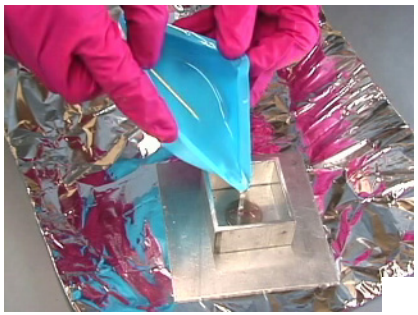

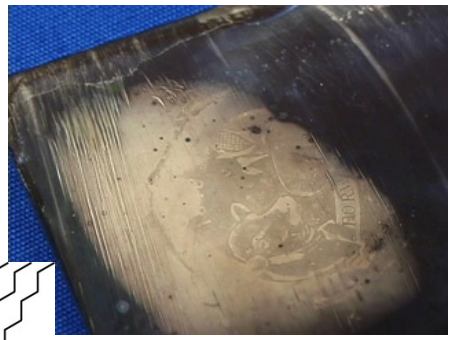

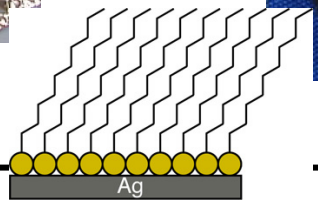

Micro-contact Printing

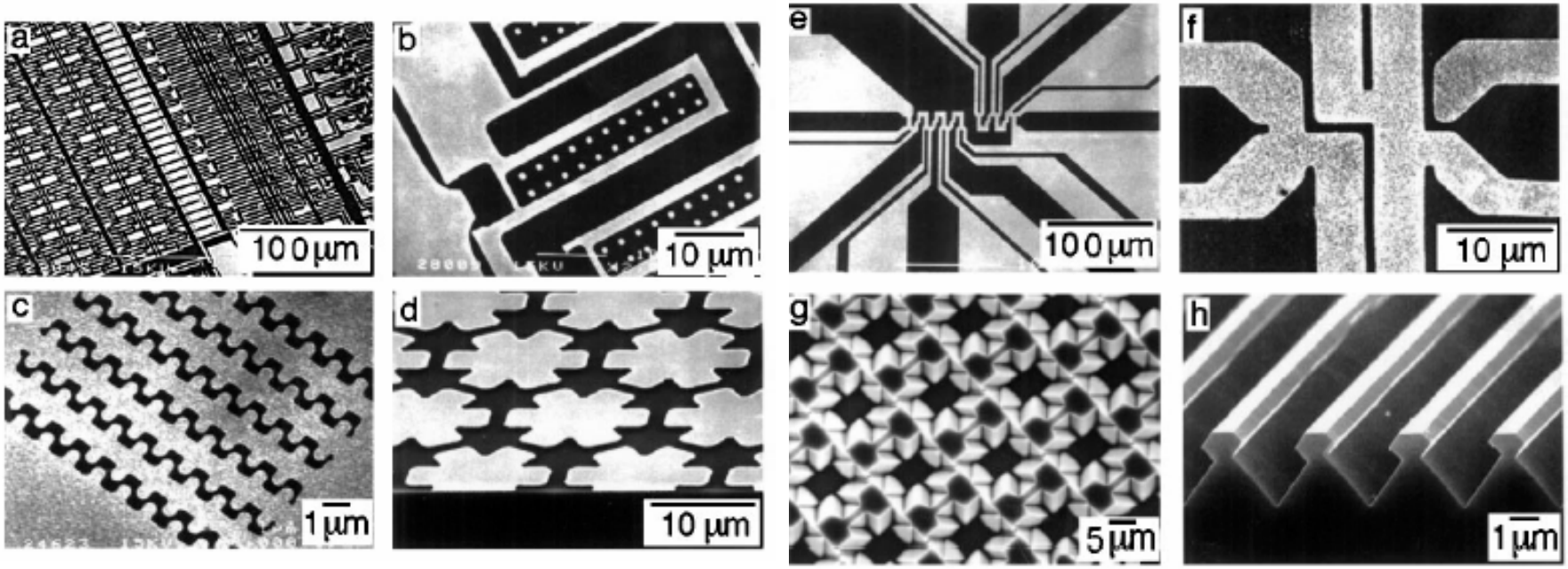

Self-Assemble Monolayer (SAM)

Chem. Rev. **2005**, *105*, 1103–1169

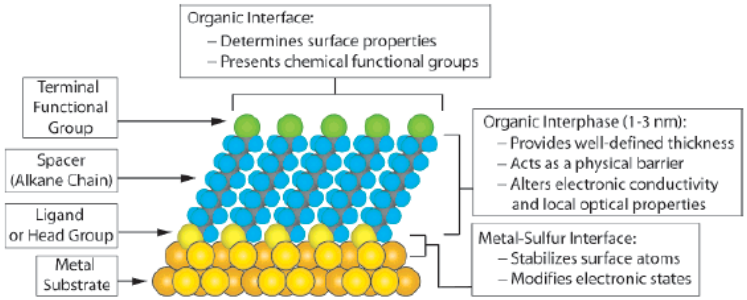

Ligand	Substrates	Morphology of Substrate: Thin Films or Bulk Material	Morphology of Substrate: Nanoparticles or Other Nanostructures
ROH	Fe_xO_y		35
	Si-H	36	
	Si	37	
RCOO-/RCOOH	α-Al_2O_3	38,39	
	Fe_xO_y		40
	Ni		41,42
	Ti/TiO_2	43	
RCOO–OOCR	Si(111):H	44	
	Si(100):H		
Ene-diol	Fe_2O_3		45
RNH_2	FeS_2	46	
	Mica	47	
	Stainless Steel 316L	48	
	$YBa_2Cu_3O_{7-\delta}$	49	
	CdSe		50
RC≡N	Ag	51	
	Au		
R-N≡N$^+$(BF_4^-)	GaAs(100)	52	
	Pd	52	
	Si(111):H	52	
RSH	Ag	26	53,54
	$Ag_{90}Ni_{10}$	55	
	AgS		56
	Au	26	57
	AuAg		58
	AuCu		58
	Au_xPd_{1-x}		58
	CdTe		59
	CdSe		60
	CdS		61,62
	Cu	26	58
	FePt		63-66
	GaAs	67	
	Ge	68	
	Hg	69-71	
	HgTe		72
	InP	73	
	Ir		74
	Ni	75	
	PbS		76-78
	Pd	30	74,79
	PdAg		58
	Pt	32	80
	Ru		81
	Stainless Steel 316L	48	
	$YBa_2Cu_3O_{7-\delta}$	82	
	Zn	83	
	ZnSe	84	
	ZnS		85
RSAc	Au	86	
R–S	Au		87
RSR'	Au	88	
RSSR'	Ag	89	90
	Au	20	90-92
	CdS		61
	Pd	30	
R–S–S	Au	93	
RCSSH	Au	94	
	CdSe		95
$RS_2O_3^-Na^+$	Au	96	98
	Cu	97	
RSeH	Ag	99	
	Au	100,101	
	CdS		60
	CdSe		102
RSeSeR'	Au	101	
R_3P	Au		103
	FeS_2	46	
	CdS		104
	CdSe		104
	CdTe		104
$R_3P=O$	Co		105,106
	CdS		104
	CdSe		104
	CdTe		104
$RPO_3^{2-}/RP(O)(OH)_2$	Al	107	
	Al-OH	108	
	$Ca_{10}(PO_4,CO_3)_6(OH)_2$	109	
	GaAs	110	
	GaN	110	
	Indium tin oxide (ITO)	111	
	Mica	112	
	TiO_2	113,114	
	ZrO_2	114,115	
	CdSe		116-118
	CdTe		118,119
RPO_4^{2-}	Al_2O_3	120	
	Nb_2O_5	120	
	Ta_2O_3	121	
	TiO_2	120,122	
RN≡C	Pt	123	124
$RHC=CH_2$	Si	37	
RC≡CH	Si(111):H	125	
$RSiX_3$ X = H, Cl, OCH_2CH_3	HfO_2	126	
	ITO	127	
	PtO	128	
	TiO_2	113,126,129	
	ZrO_2	126,129	

S-Au 25-30 Kcal/mole
Si-O 190 kcal/mole

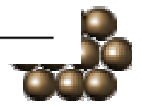

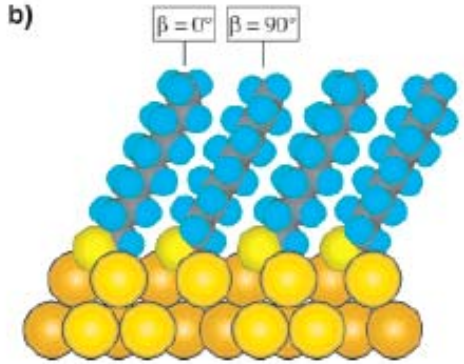

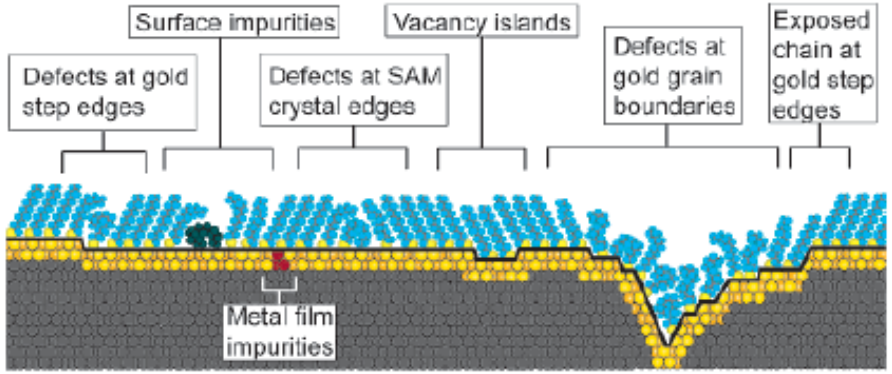

Figure 7. Schematic illustration of some of the intrinsic and extrinsic defects found in SAMs formed on polycrystalline substrates. The dark line at the metal−sulfur interface is a visual guide for the reader and indicates the changing topography of the substrate itself.

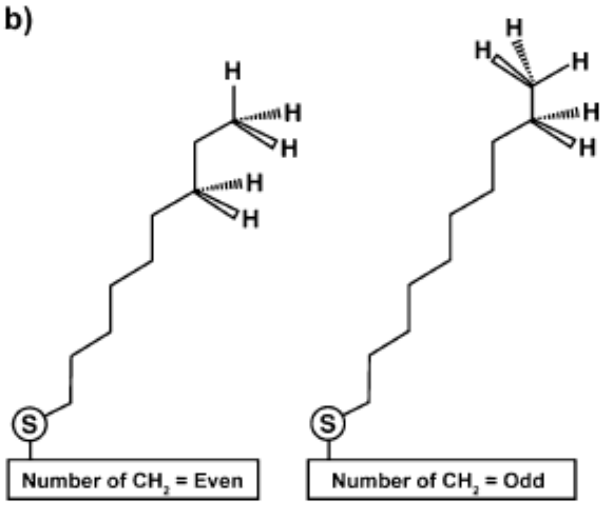

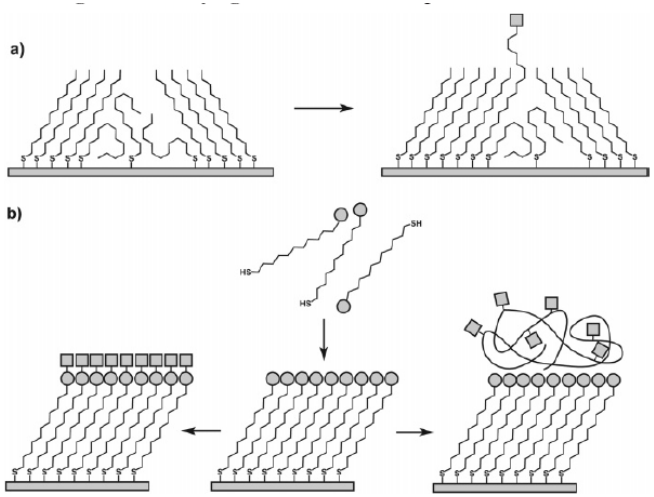

[c] (a) Insertion of a functional adsorbate at a defect site in a preformed SAM. (b) Transformation of a SAM with exposed functional groups (circles) by either chemical reaction or adsorption of another material.

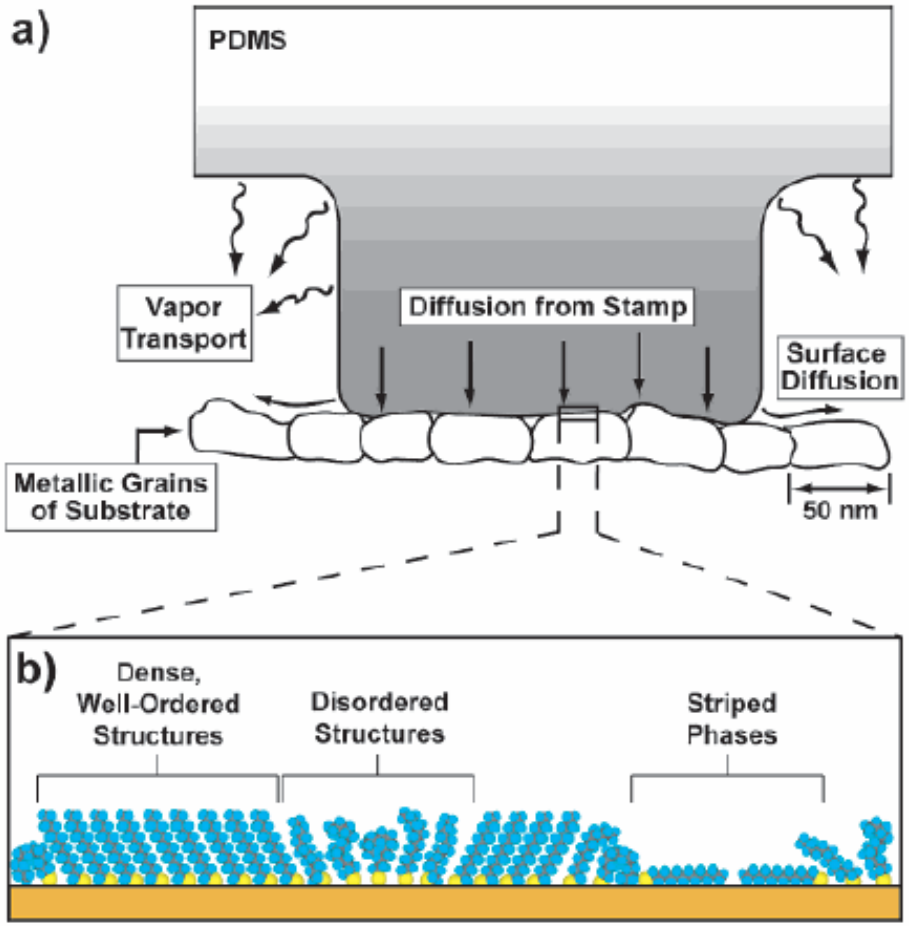

Figure 12. (a) Schematic illustration depicting the application of a PDMS stamp containing thiols to a polycrystalline metal film. The primary mechanisms of mass transport from the stamp to the surface are shown. The grayscale gradient approximates the concentration of thiols adsorbed in the stamp itself. (b) Magnified schematic view that illustrates the variety of structural arrangements found in SAMs prepared by μCP when the stamp is wetted with a 1−10 mM solution and applied to the substrate for 1−10 s.

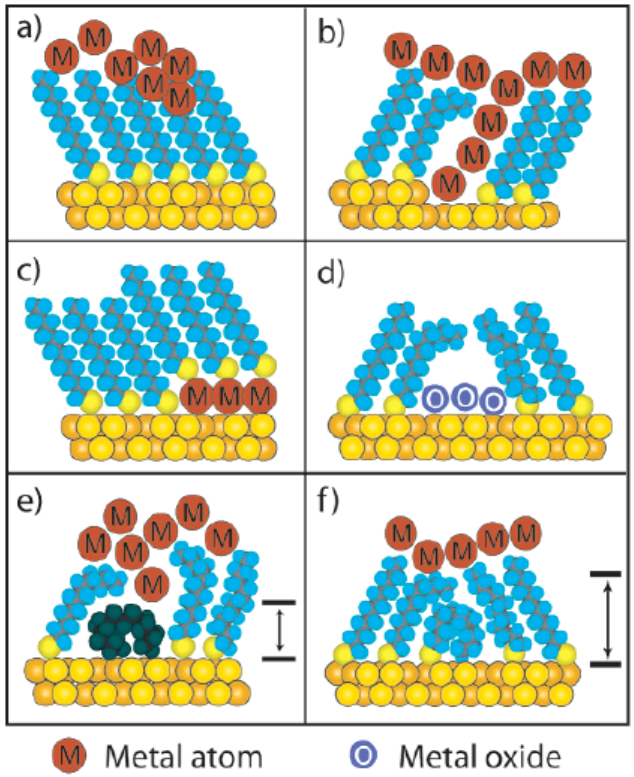

Figure 17. Schematic illustration of the types of defects in SAMs that can influence the rate of electron transfer in two-terminal (or three-terminal) devices. (a) Chemical reaction with the organic component of SAMs during evaporation of metal films. (b) Formation of metallic filaments during evaporation or operation of the device. (c) Deposition of adlayers of metal on the surface of the substrate supporting the SAM. (d) Formation of oxide impurities on the surface. (e) Organic (or organometallic) impurities in the SAM. (f) Thin regions in the SAM resulting from conformational and structural defects. In e and f the dimension normal to the surface that is denoted by the black arrows indicates the approximate shortest distance between the two metal surfaces; note that these distances are less than the nominal thickness of the ordered SAM.

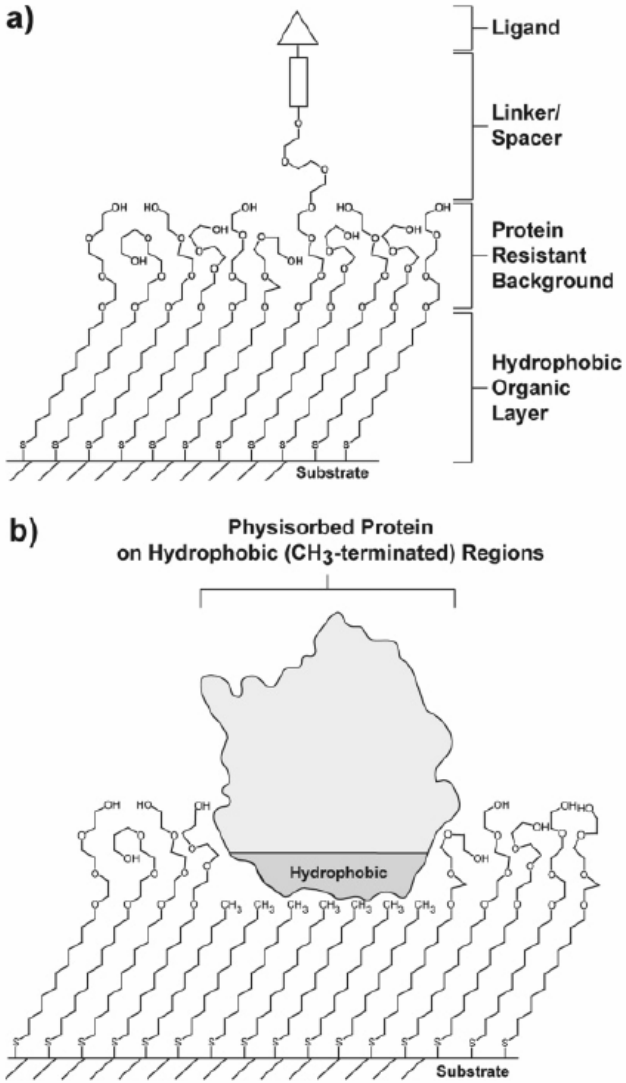

Figure 21. Schematic illustrations of (a) a mixed SAM and (b) a patterned SAM. Both types are used for applications in biology and biochemistry.

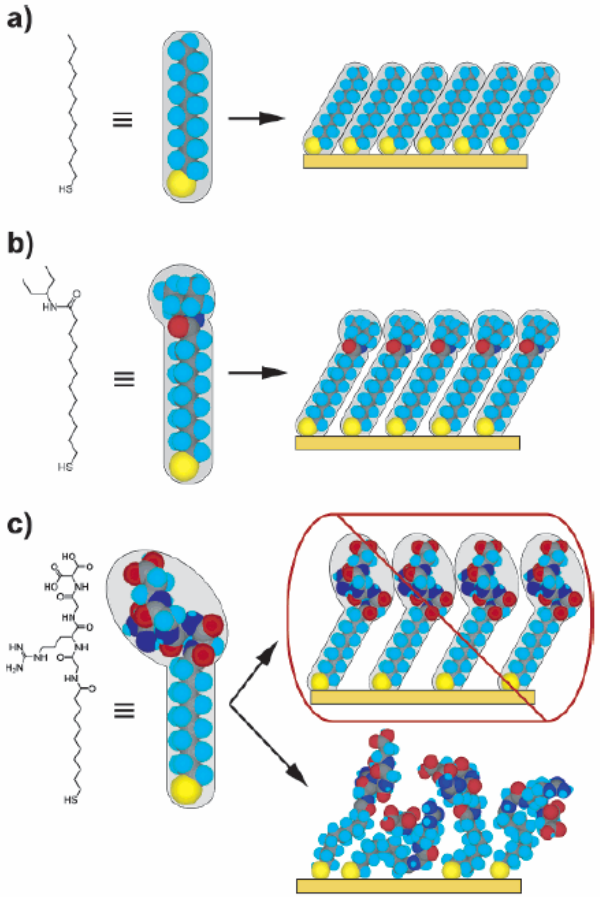

Figure 22. Schematic diagram illustrating the effects that large terminal groups have on the packing density and organization of SAMs. (a) Small terminal groups such as $-CH_3$, $-CN$, etc., do not distort the secondary organization of the organic layer and have no effect on the sulfur arrangement. (b) Slightly larger groups (like the branched amide shown here) begin to distort the organization of the organic layer, but the strongly favorable energetics of metal−sulfur binding drive a highly dense arrangement of adsorbates. (c) Large terminal groups (peptides, proteins, antibodies) sterically are unable to adopt a secondary organization similar to that for alkanethiols with small terminal groups. The resulting structures probably are more disordered and less dense than those formed with the types of molecules in a and b.

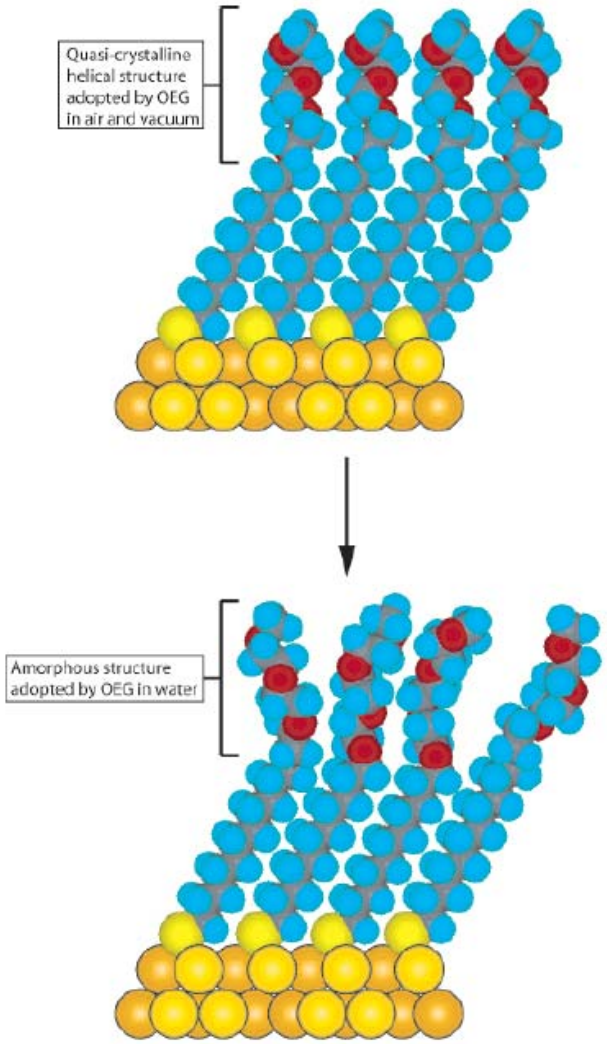

Figure 23. Schematic illustration of the order−disorder transition evidenced by SAMs of alkanethiolates terminated with triethylene glycol. The EG_3 group loses conformational ordering upon solvation in water.

Control of crystal nucleation by patterned self-assembled monolayers

NATURE | VOL 398 | 8 APRIL 1999

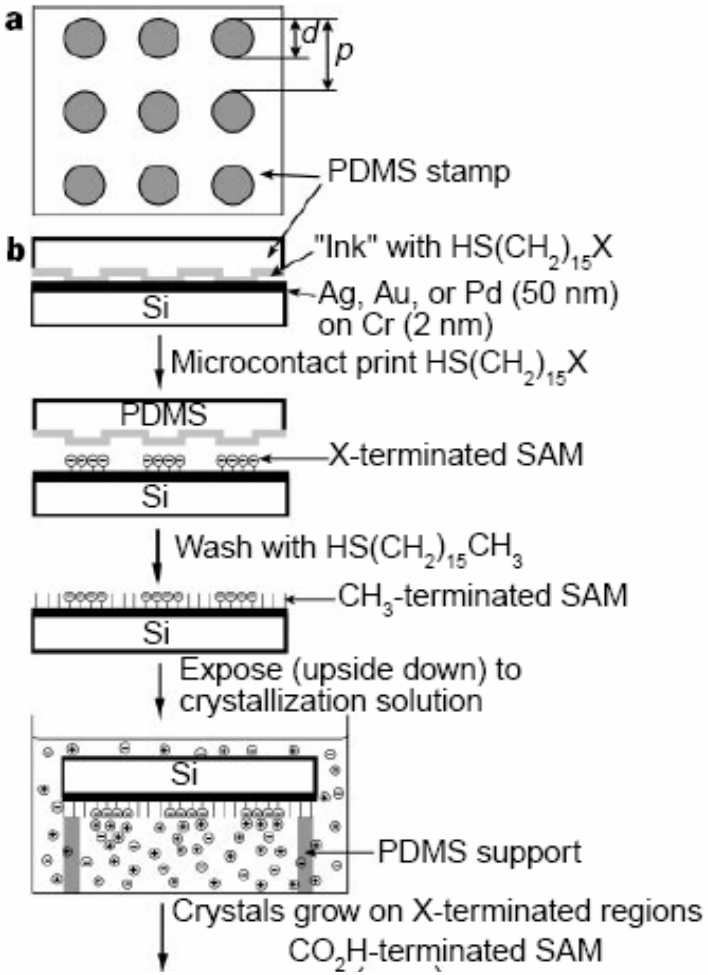

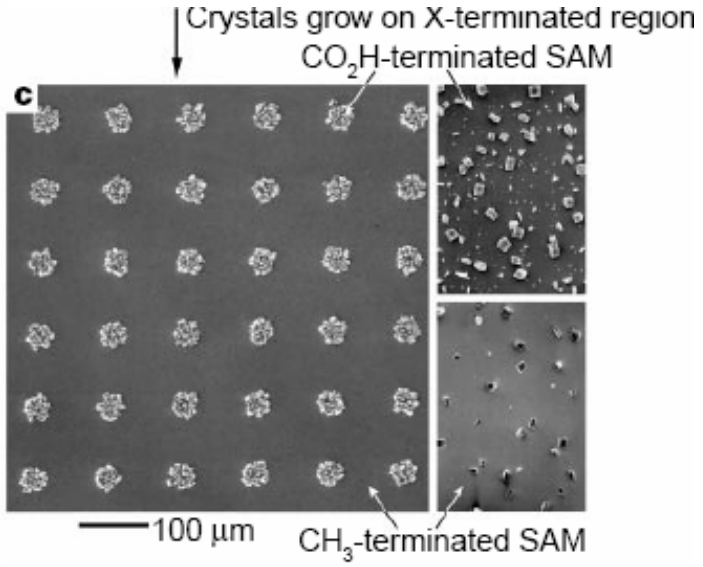

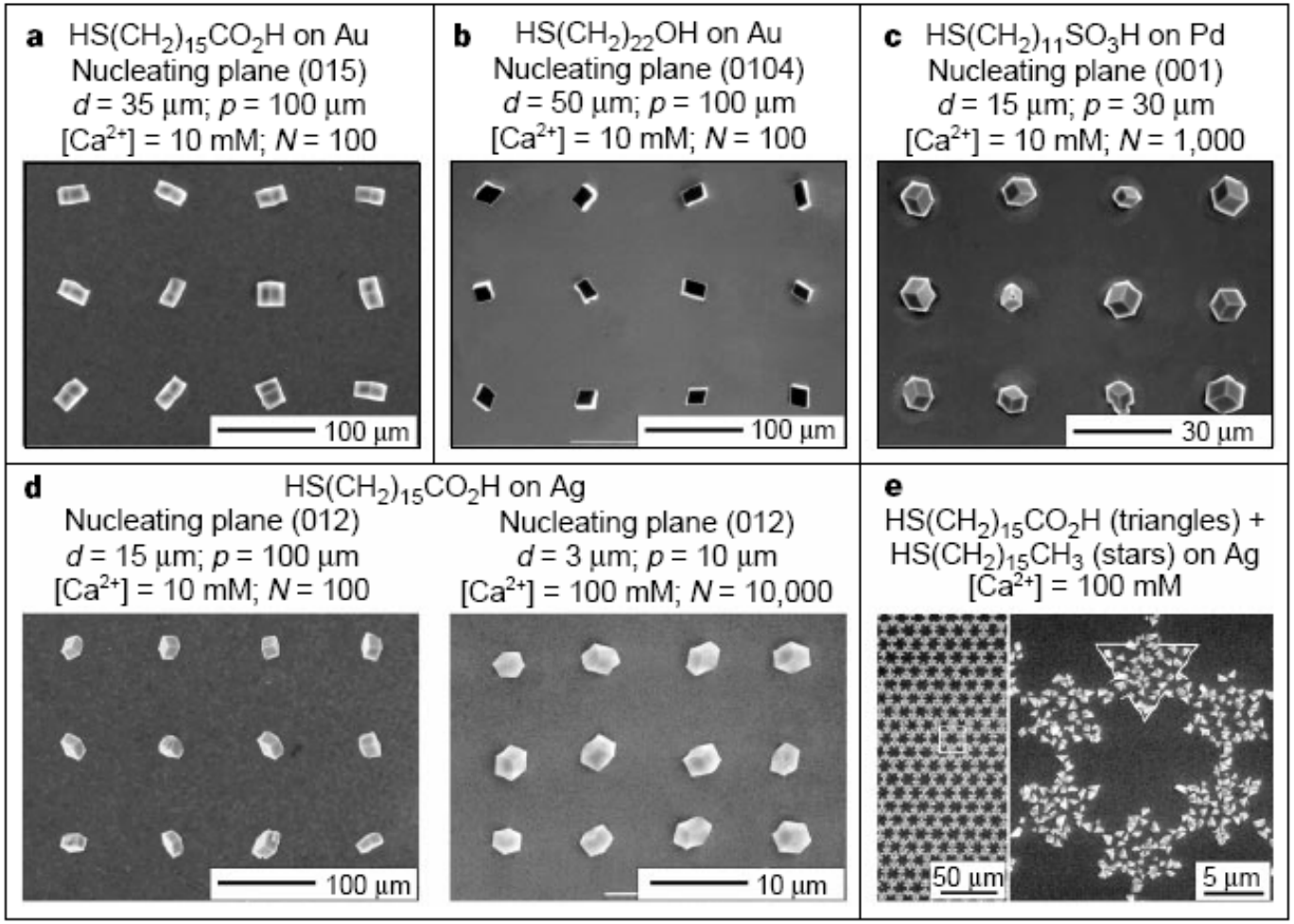
a
HS(CH2)15CO2H on Au
Nucleating plane (015)
d = 35 μm; p = 100 μm
[Ca2+] = 10 mM; N = 100
100 μm
b
HS(CH2)22OH on Au
Nucleating plane (0104)
d = 50 μm; p = 100 μm
[Ca2+] = 10 mM; N = 100
100 μm
c
HS(CH2)11SO3H on Pd
Nucleating plane (001)
d = 15 μm; p = 30 μm
[Ca2+] = 10 mM; N = 1,000
30 μm
d
HS(CH2)15CO2H on Ag
Nucleating plane (012)
d = 15 μm; p = 100 μm
[Ca2+] = 10 mM; N = 100
100 μm
Nucleating plane (012)
d = 3 μm; p = 10 μm
[Ca2+] = 100 mM; N = 10,000
10 μm
e
HS(CH2)15CO2H (triangles) +
HS(CH2)15CH3 (stars) on Ag
[Ca2+] = 100 mM
50 μm
5 μm

Patterning of organic single crystals

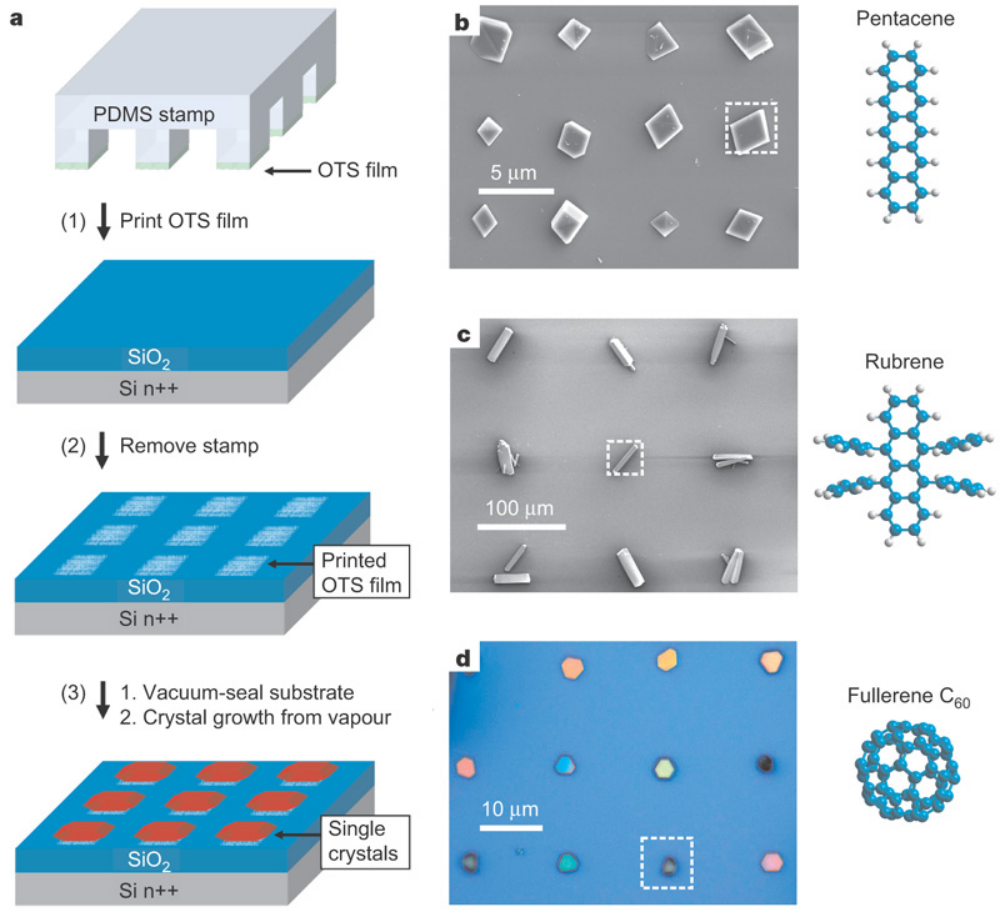

Nature 444, 913-917(14 December 2006)

Large On-Off Ratios and Negative Differential Resistance in a Molecular Electronic Device

J. Chen,[1] M. A. Reed,[1]* A. M. Rawlett,[2] J. M. Tour[2]*

19 NOVEMBER 1999 VOL 286 SCIENCE

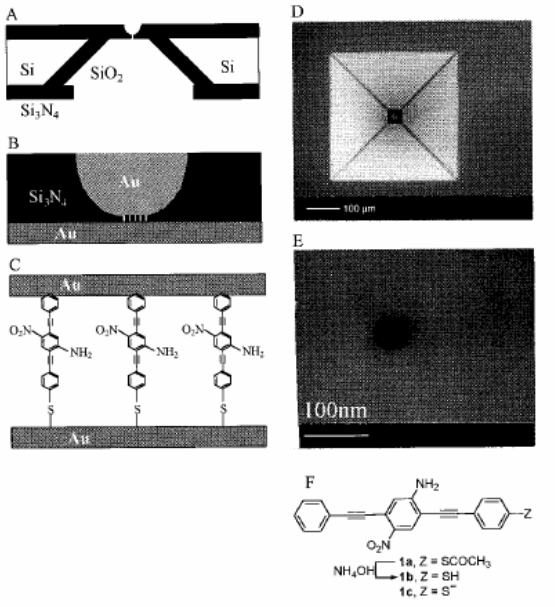

Fig. 1. Schematics of device fabrication. **(A)** Cross section of a silicon wafer with a nanopore etched through a suspended silicon nitride membrane. **(B)** Au-SAM-Au junction in the pore area. **(C)** Blowup of (B) with **1c** sandwiched in the junction. **(D)** Scanning electron micrograph (SEM) of pyramid Si structure after unisotropic Si etching [that is, the bottom view of (A)]. **(E)** SEM of an etched nanopore through the silicon nitride membrane. **(F)** The active molecular compound **1c** and its precursors the free thiol **1b** and the thiol-protected system **1a**.

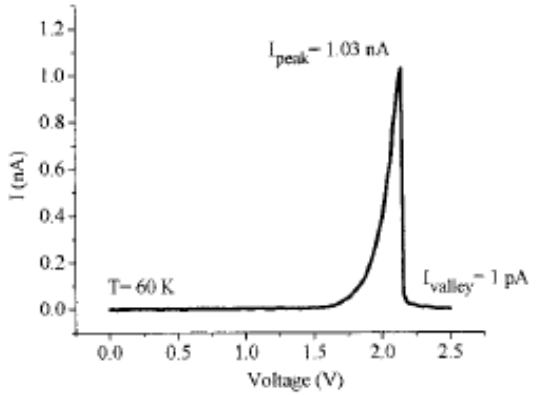

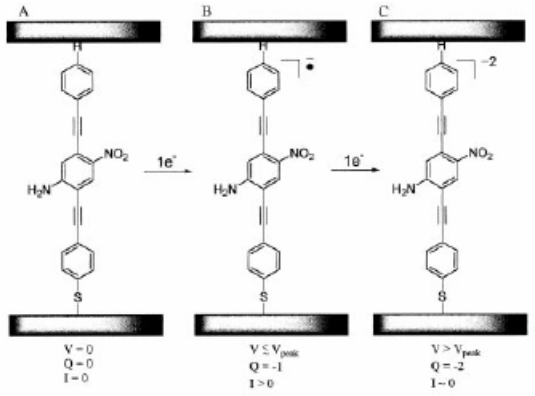

Fig. 4. Potential mechanism for the NDR effect. As voltage is applied, the molecules in the SAM (**A**) undergo a one-electron reduction to form the radical anion (**B**) that provides a conductive state. Further increase of the voltage causes another one-electron reduction to form the dianion insulating state (**C**). Q is the charge.

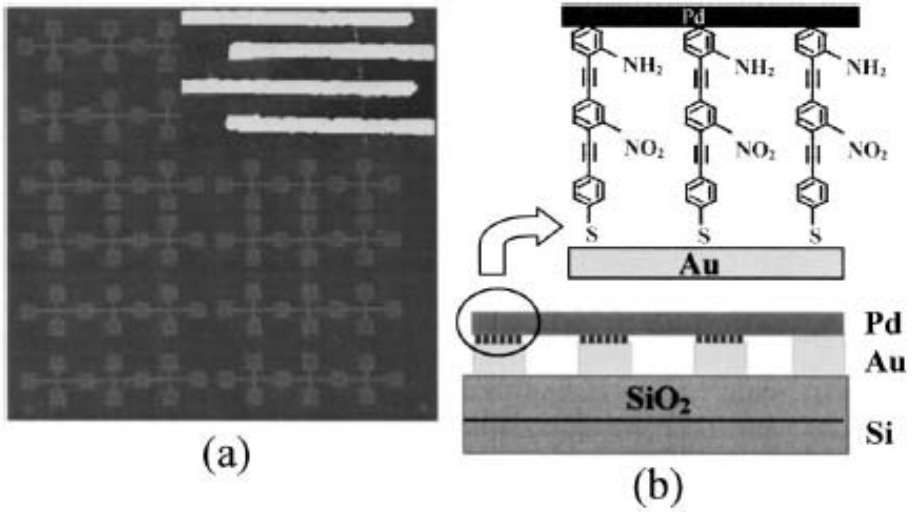

FIG. 1. (a) Optical micrograph of the nanoelectrode array. Inset: AFM image of four Au nanoelectrodes with a Pd nanowire lying across. (b) Schematic diagram of the Pd/molecular wires/Au junctions on a Si/SiO_2 substrate.

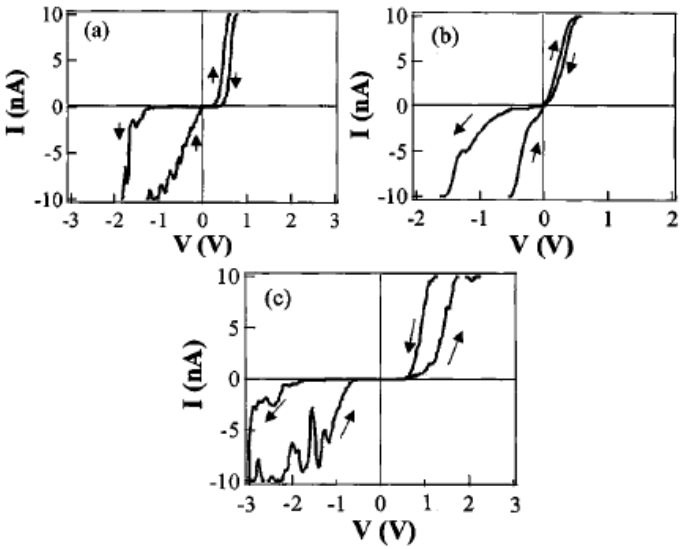

FIG. 3. Typical $I-V$ curves of molecular devices. (a), (b), and (c) correspond to molecules **a**, **b**, and **c** shown in Fig. 2, respectively.

Geometric Control of Cell Life and Death

SCIENCE • VOL. 276 • 30 MAY 1997

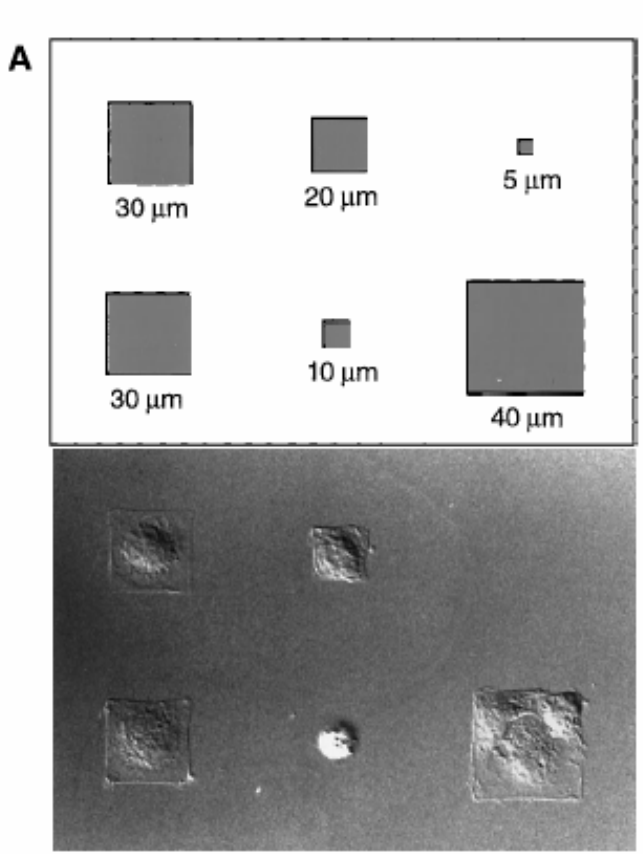

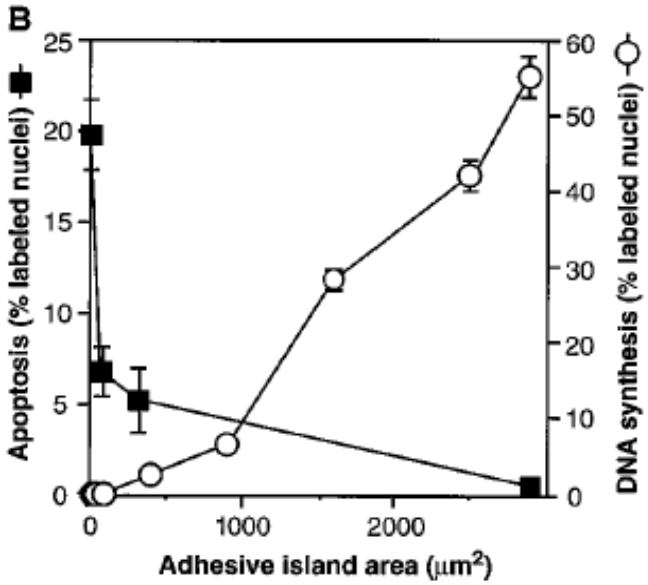

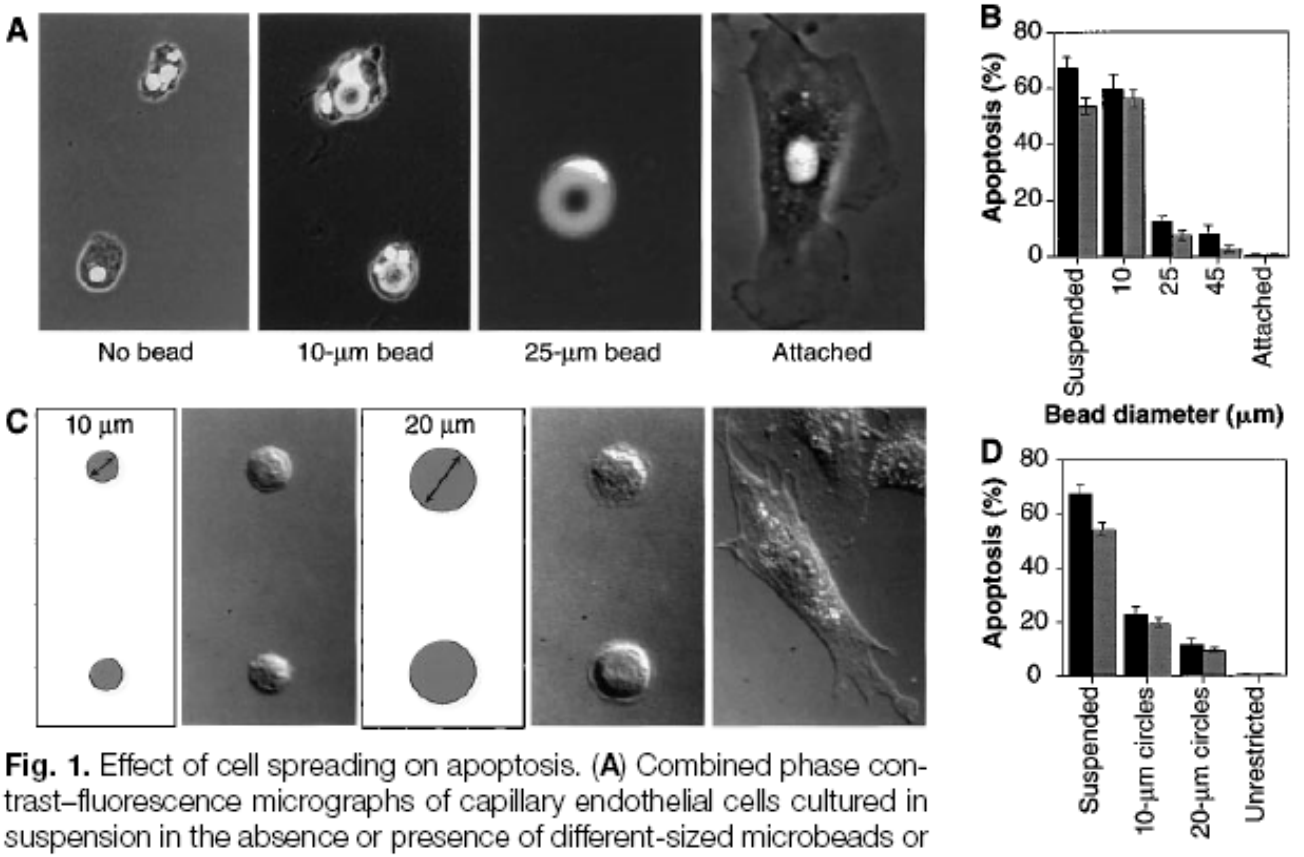

Fig. 1. Effect of cell spreading on apoptosis. (**A**) Combined phase contrast–fluorescence micrographs of capillary endothelial cells cultured in suspension in the absence or presence of different-sized microbeads or attached to a planar culture dish coated with FN for 24 hours (*28*). In the highly spread cell on the 25-μm bead, only the flattened 4′,6′-diamidino-2-phenylindole (DAPI)–stained nucleus is clearly visible. (**B**) Apoptosis in cells attached to different-sized beads, in suspension, or attached to a dish. The apoptotic index was quantitated by measuring the percentage of cells exhibiting positive TUNEL staining (black bars) (Boehringer Mannheim), which detects DNA fragmentation; similar results were obtained by analyzing changes in nuclear condensation and fragmentation in cells stained with DAPI at 24 hours (gray bars). Apoptotic indices were determined only within single cells bound to single beads. Error bars indicate SEM. (**C**) Differential interference-contrast micrographs of cells plated on substrates micropatterned with 10- or 20-μm-diameter circles coated with FN (left), by a microcontact printing method (*29*) or on a similarly coated unpatterned substrate (right). (**D**) Apoptotic index of cells attached to different-sized adhesive islands coated with a constant density of FN for 24 hours; similar results were obtained with human and bovine capillary endothelial cells (*28*). Bars same as in (B).

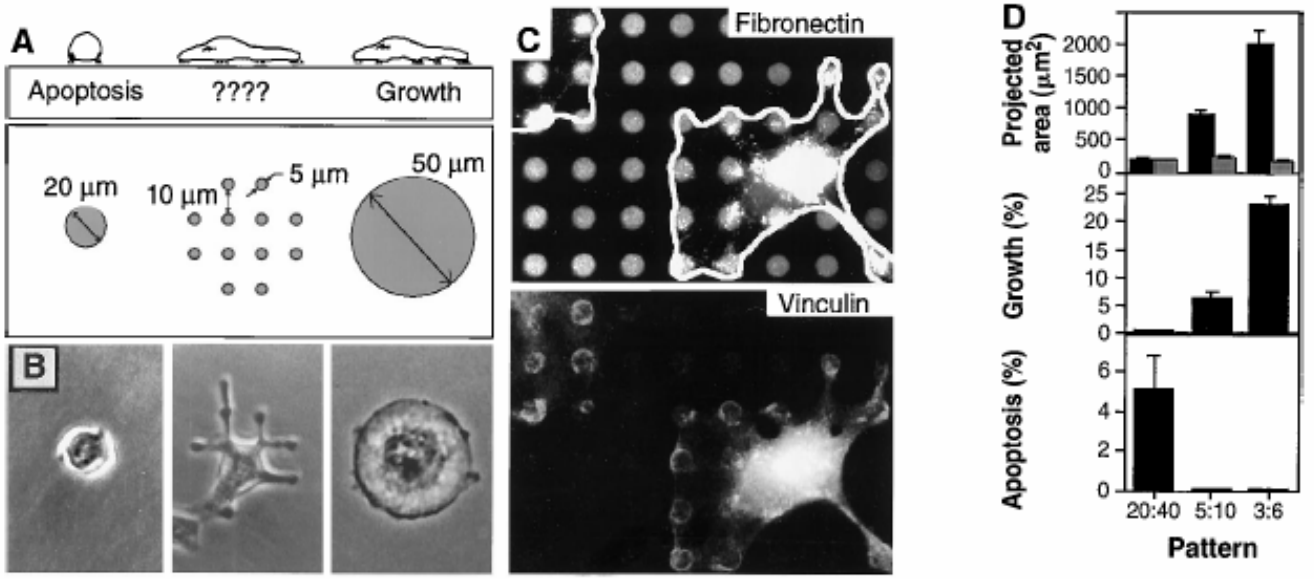

Fig. 3. Cell-ECM contact area versus cell spreading as a regulator of cell fate. (**A**) Diagram of substrates used to vary cell shape independently of the cell-ECM contact area. Substrates were patterned with small, closely spaced circular islands (center) so that cell spreading could be promoted as in cells on larger, single round islands, but the ECM contact area would be low as in cells on the small islands. (**B**) Phase-contrast micrographs of cells spread on single 20- or 50-μm-diameter circles or multiple 5-μm circles patterned as shown in (A). (**C**) Immunofluorescence micrographs of cells on a micropatterned substrate stained for FN (top) and vinculin (bottom). White outline indicates cell borders; note circular rings of vinculin staining, which coincide precisely with edges of the FN-coated adhesive islands. (**D**) Plots of projected cell area (black bars) and total ECM contact area (gray bars) per cell (top), growth index (middle), and apoptotic index (bottom) when cells were cultured on single 20-μm circles or on multiple circles 5 or 3 μm in diameter separated by 40, 10, and 6 μm, respectively.

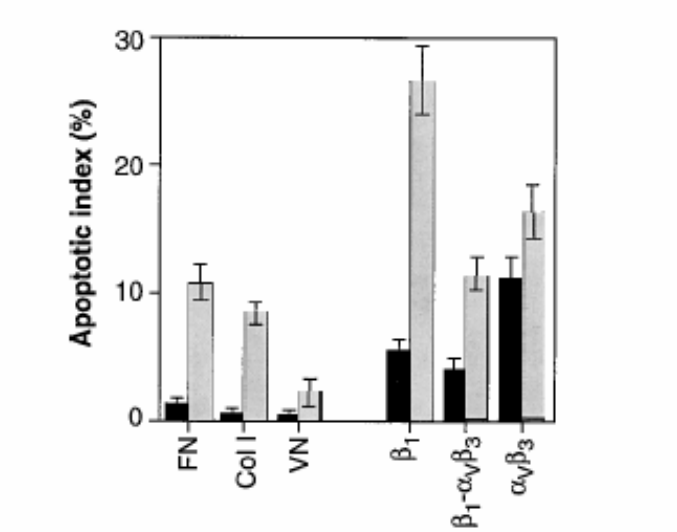

Fig. 4. Role of different integrin ligands in cell shape–regulated apoptosis. Apoptotic indices (percentage positive TUNEL staining) for cells cultured for 24 hours on unpatterned substrates (black bars) or on 20-μm circles (gray bars) coated with FN, type I collagen (Col I), vitronectin (VN), anti-β_1, anti-$\alpha_V\beta_3$, or antibodies to both integrin β_1 and integrin $\alpha_V\beta_3$ (*29*).

hexadecanethiol [$HS(CH_2)_{15}CH_3$] was printed onto gold-coated substrates with a flexible stamp containing a relief of the desired pattern. The substrate was immersed immediately in 2 mM tri(ethylene glycol)-terminated alkanethiol [$HS(CH_2)_{11}(OCH_2CH_2)_3OH$ in ethanol], which coated the remaining bare regions of gold. When these substrates were immersed in a solution of FN, vitronectin, or type I collagen (50 μg/ml in phos-

Electrochemical Desorption of Self-Assembled Monolayers Noninvasively Releases Patterned Cells from Geometrical Confinements

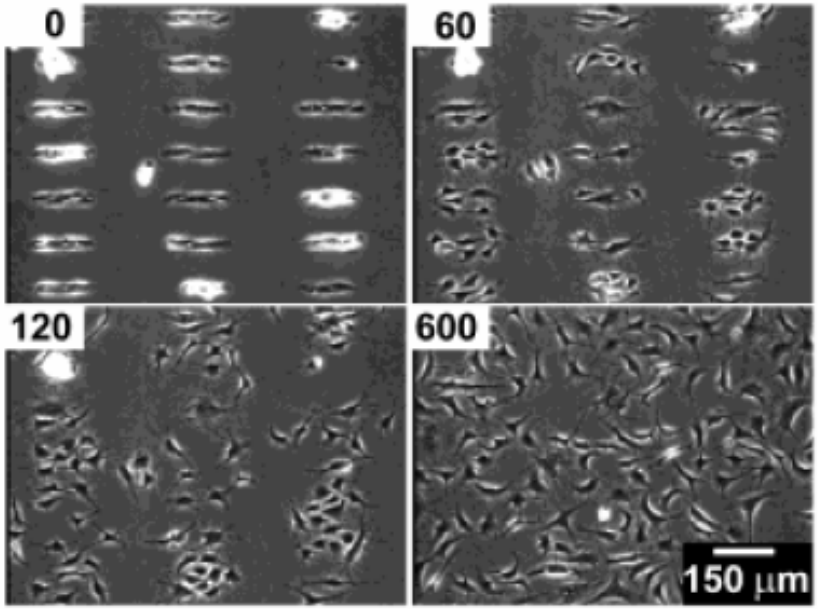

Figure 1. BCE cells were allowed to attach to a surface patterned with $C_{11}EG_3$ and C_{18}. Application of a cathodic voltage pulse (−1.2 V for 30 s in this case) released the cells from the microislands. The numbers indicate the time elapsed (in minutes) after the voltage pulse.

■ **J. AM. CHEM. SOC. 2003**, *125*, 2366−2367

Directing cell migration with asymmetric micropatterns

http://www.pnas.org/cgi/reprint/102/4/9

PNAS | January 25, 2005 | vol. 102 | no. 4 | 975

Xingyu Jiang*, Derek A. Bruzewicz*, Amy P. Wong*, Matthieu Piel†, and George M. Whitesides*‡

*Department of Chemistry and Chemical Biology, Harvard University, 12 Oxford Street, Cambridge, MA 02138; and †Department of Molecular and Cellu Biology, Harvard University, 16 Divinity Avenue, Cambridge, MA 02138

Contributed by George M. Whitesides, December 2, 2004

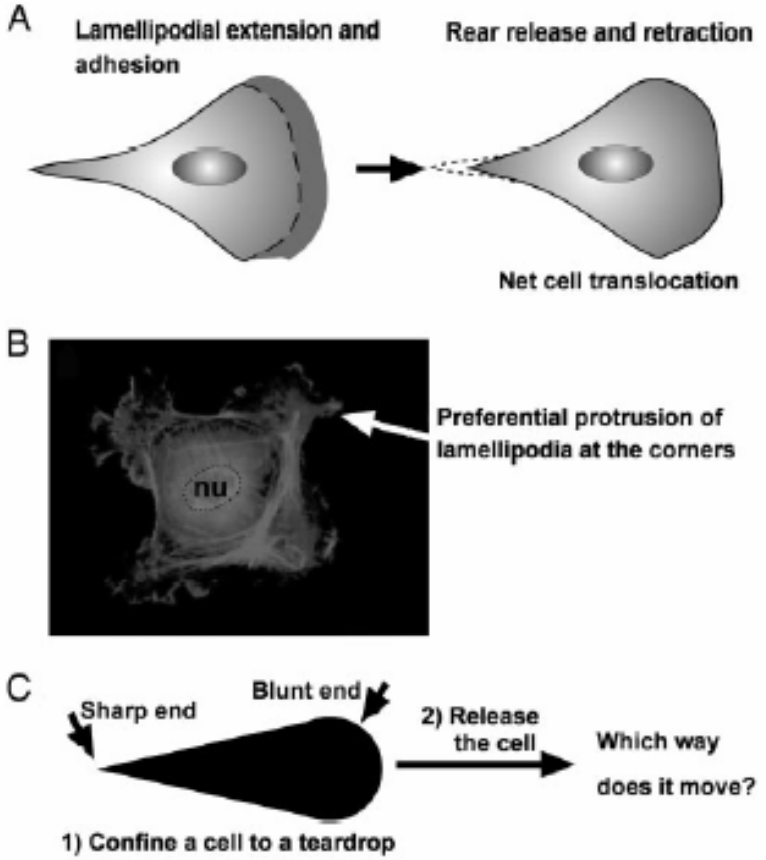

Fig. 1. A problem on cell motility. (*A*) A cartoon illustration of the migration of a typical mammalian cell on a flat surface. This teardrop shape is found in many types of cells. (*B*) Cells confined to squares preferentially extend their lamellipodia from the corners. nu, nucleus. (*C*) If a cell is confined to a shape of teardrop, will the cell preferentially extend its lamellipodia from the sharp end or from the blunt end? If released from confinement, in which direction will it likely move?

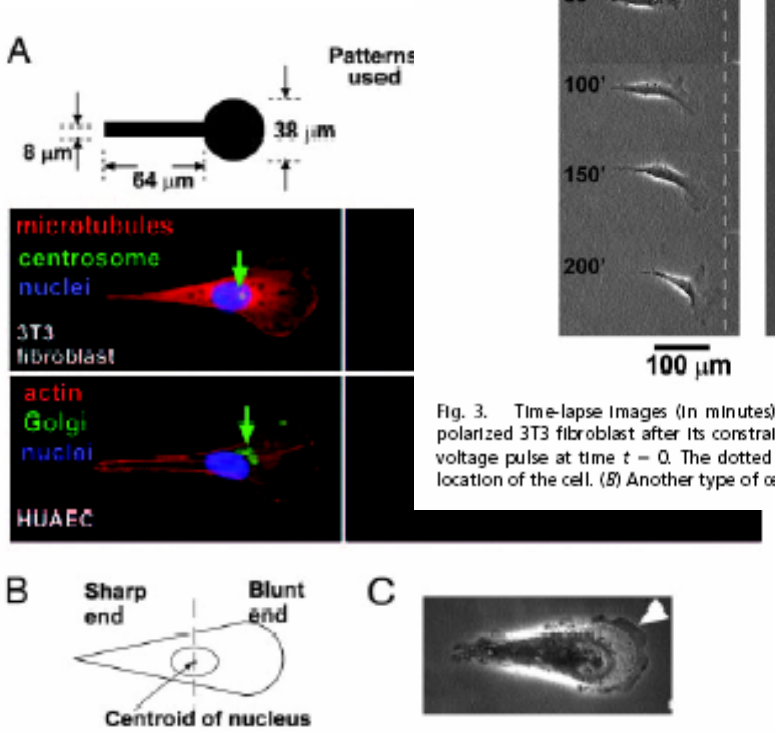

Fig. 2. Asymmetric patterns polarize immobilized cells. (*A*) The Golgi and the centrosome are located closer to the half of a cell with the blunt end. We used phallodin, antigolgin, DAPI, antitubulin, and antipericentrin to identify actin (red), the Golgi (green), the nucleus (blue), microtubules (red), and the centrosome (green), respectively. The green arrows indicate the location of centrosomes in 3T3 cells and Golgi in human umbilical artery endothelial cells (HUAEC). (*B*) We divided the cell into a half with the sharp end and a half with the blunt end by a vertical line drawn at the centroid of the nucleus; >80% ($n = 30$) of the centrosomes and Golgi were localized in the region of the wide end. (*C*) The lamellipodia of immobilized 3T3 cells tended to extend more from the blunt end as well (arrowhead). The dotted line indicates the edges of the adhesive pattern.

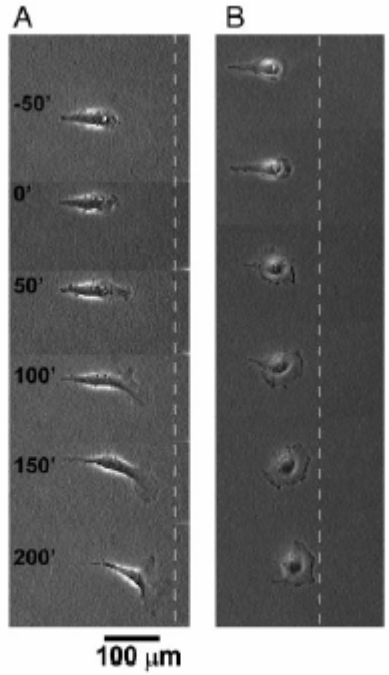

Fig. 3. Time-lapse images (in minutes) show the motility of an initially polarized 3T3 fibroblast after its constraint is released. (*A*) We applied the voltage pulse at time $t = 0$. The dotted line serves as a reference for the location of the cell. (*B*) Another type of cell, COS-7, shows similar behavior.

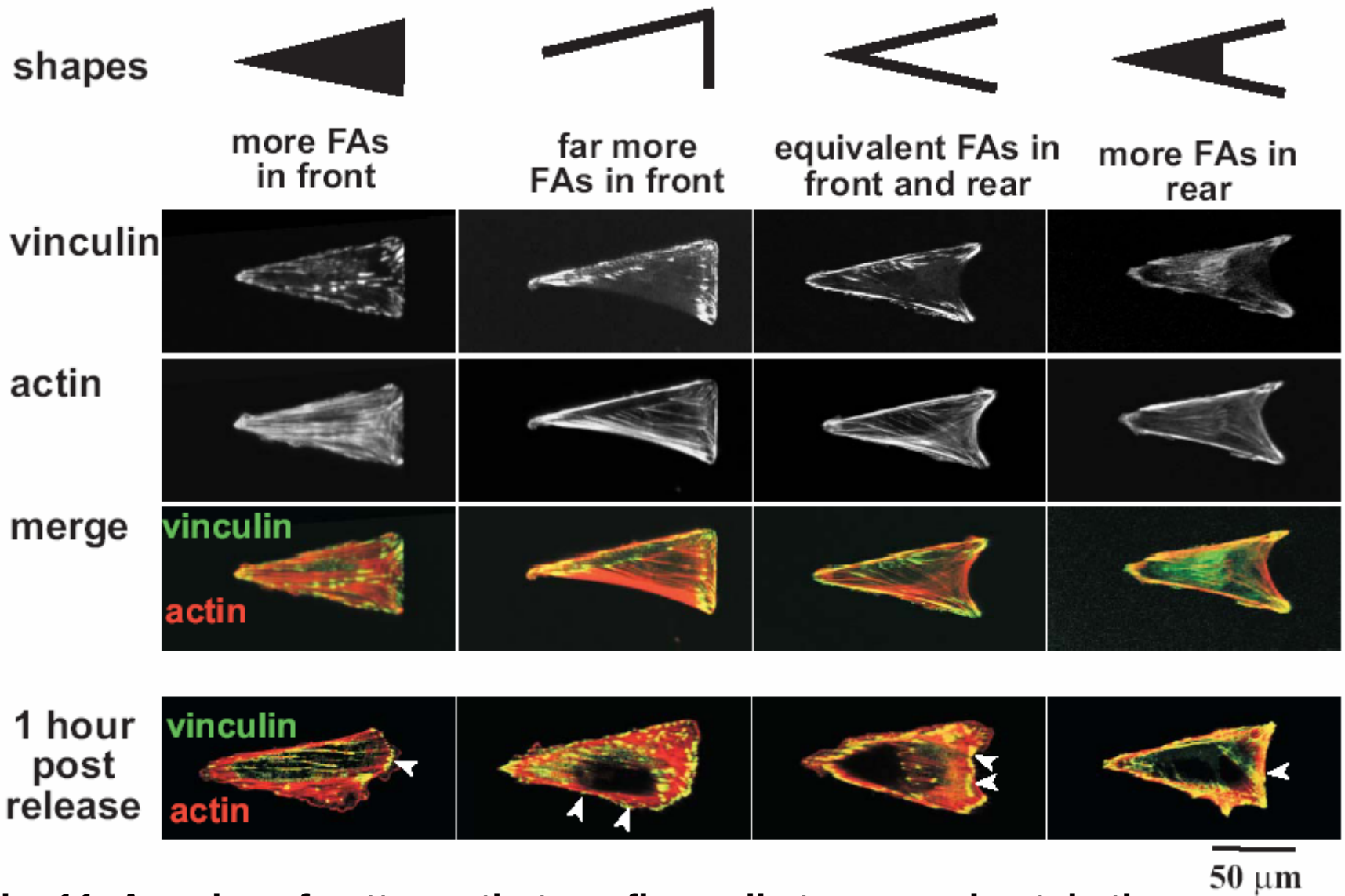

Fig. 11. A series of patterns that confine cells to approximately the same projected geometry (visualized by the actin cytoskeleton) but distribute the focal adhesions (FAs; visualized by immunostaining for vinculin) differently. The bottom row shows that new focal adhesions formed 1 h after release in areas that were inert to attachment of cells prior to release (arrowheads).

Soft-Lithography

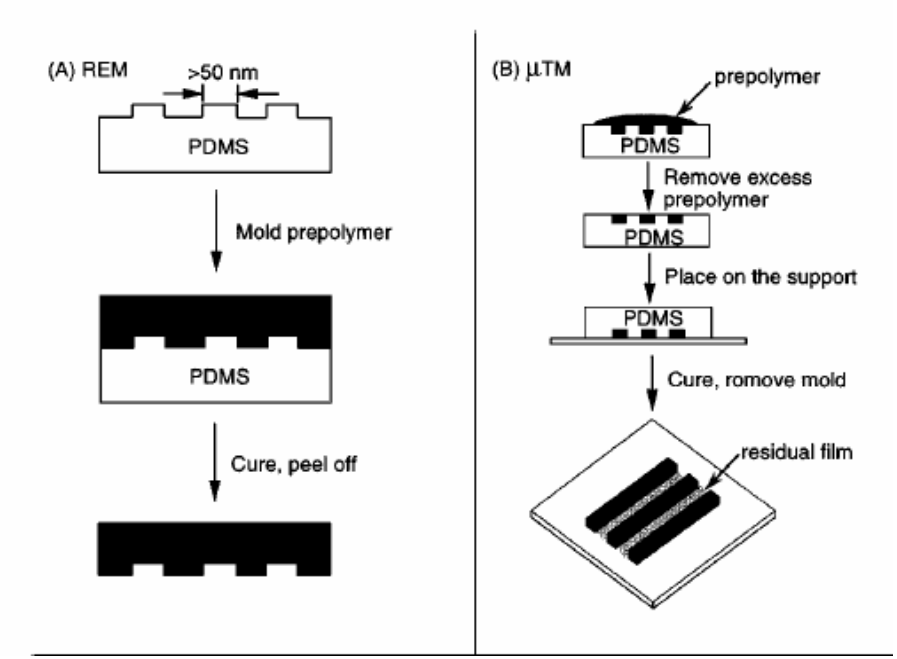

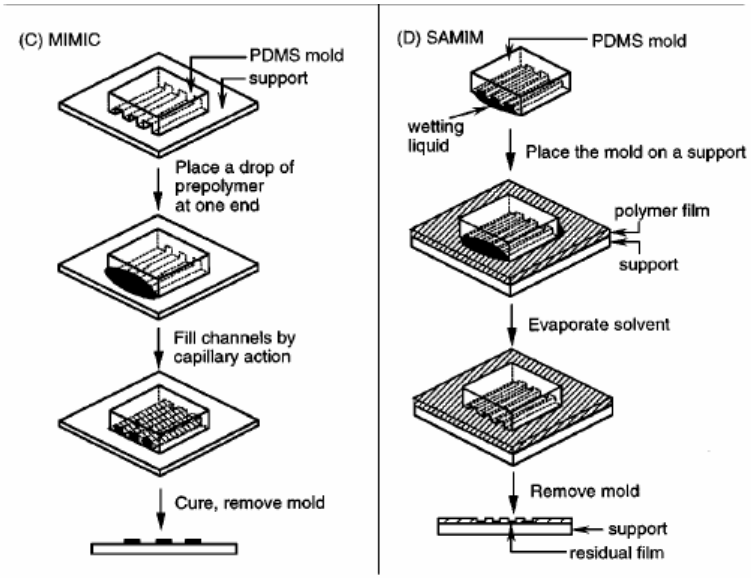

Figure 5 Schematic illustration of procedures for (*a*) replica molding (REM), (*b*) microtransfer molding (μTM), (*c*) micromolding in capillaries (MIMIC), and (*d*) solvent-assisted micromolding (SAMIM).

Electrophoresis 2002, 23, 3461–3473

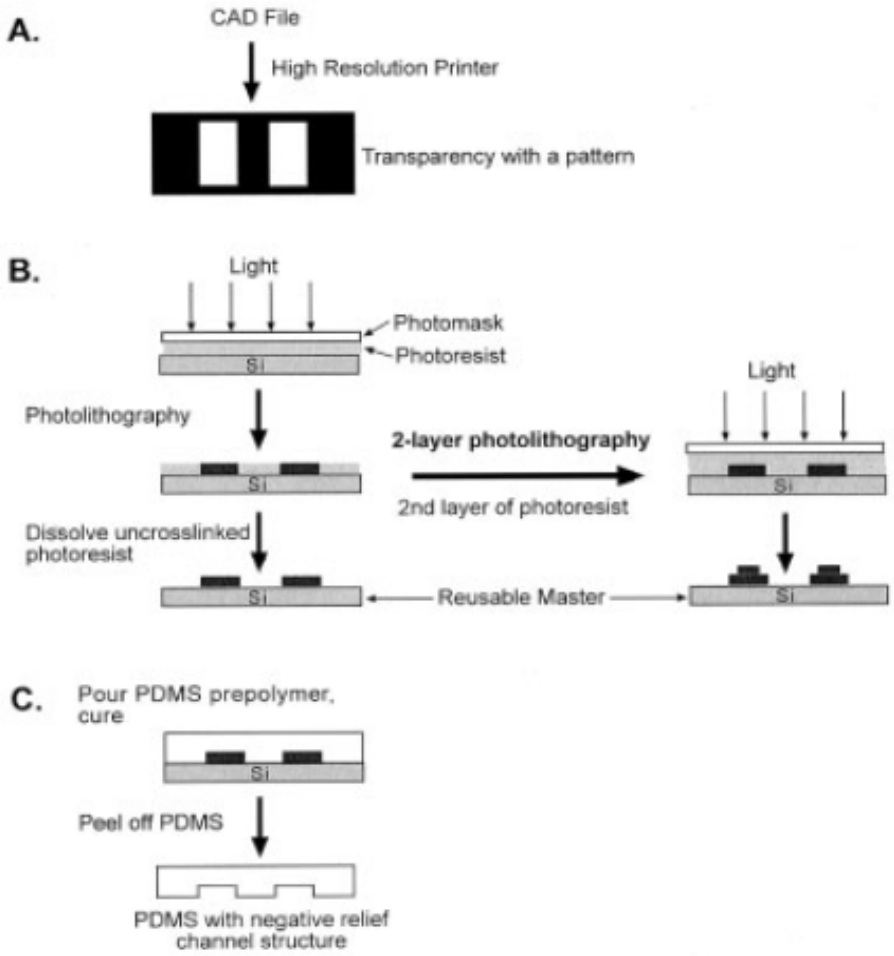

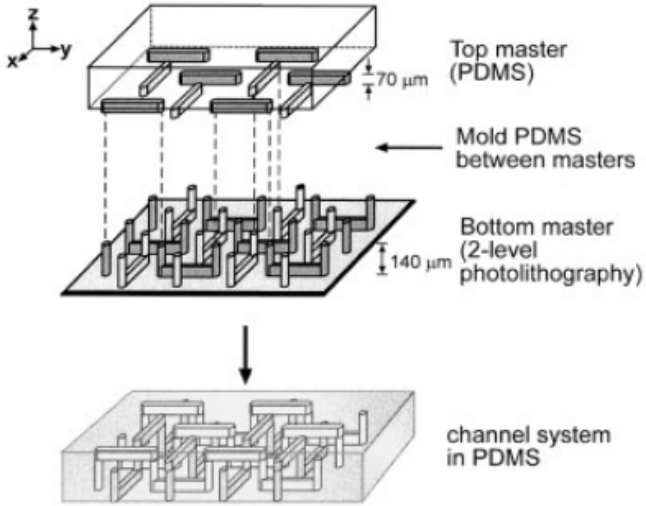

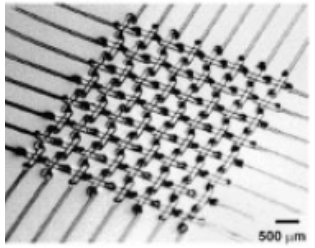

D.

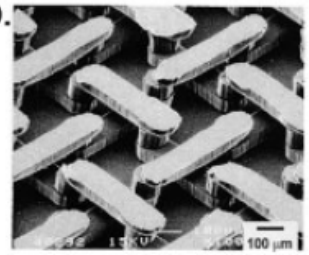

Replication Result

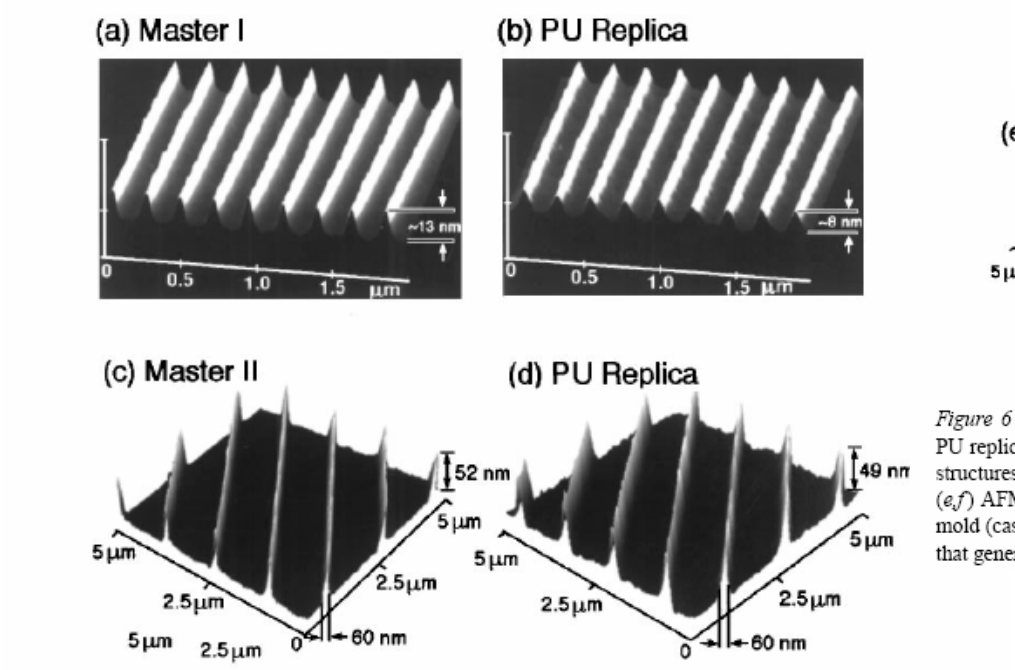

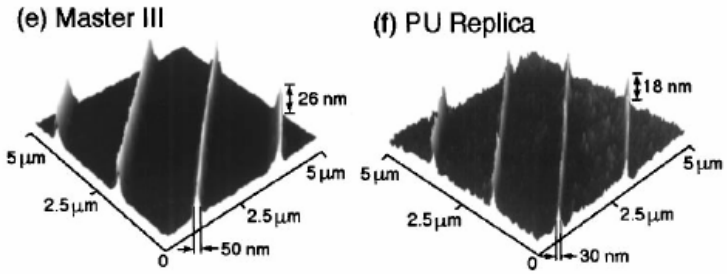

Figure 6 (*a,b*) Atomic force microscopy (AFM) images of Cr structures on a master, and a PU replica prepared from a PDMS mold cast from this master (153). (*c,d*) AFM images of Au structures on another master, and a PU replica produced from a PDMS mold cast from this master. (*e,f*) AFM images of Au structures on a third master, and a PU replica fabricated from a PDMS mold (cast from this master) while this mold was mechanically deformed by bending in a manner that generated narrower lines.